MATHEMATICAL MODELING OF WHEAT DRYING WITH INPUT FROM MOISTURE MOVEMENT STUDIES USING MAGNETIC RESONANCE IMAGING

BY
PRABAL KUMAR GHOSH

A Thesis
Submitted to the Faculty of Graduate Studies
The University of Manitoba
in Partial Fulfillment of the Requirements
for the Degree of

DOCTOR OF PHILOSOPHY

Department of Biosystems Engineering
University of Manitoba
Winnipeg, Manitoba

THE UNIVERSITY OF MANITOBA

FACULTY OF GRADUATE STUDIES

*****

COPYRIGHT PERMISSION

MATHEMATICAL MODELING OF WHEAT DRYING WITH INPUT FROM MOISTURE MOVEMENT STUDIES USING MAGNETIC RESONANCE IMAGING

BY

PRABAL KUMAR GHOSH

A Thesis/Practicum submitted to the Faculty of Graduate Studies of The University of Manitoba in partial fulfillment of the requirement of the degree

DOCTOR OF PHILOSOPHY

Dedicated

To

Dr. D.S. Jayas

ABSTRACT

Canada annually produces around 50 Mt (million tonnes) of grains and oilseeds worth about 6 billion dollars. Drying is the most important method for preservation of grains. Wheat was selected because it is a major crop in Western Canada and is staple food for most of the world population. An MR imaging probe (Helmholtz configuration, 7 mm internal diameter) was designed and constructed to specifically fit a single wheat kernel for drying studies at temperatures ranging from ambient to about 60°C. Prior to MRI, wheat kernels were preconditioned to a known moisture level. Individual kernels were placed into the imaging probe to be placed into the bore of the vertical MRI magnet and drying was started and continued for 4 h at 30, 40, and 50°C at a constant nitrogen gas flow (~0.23 m s^{-1}). Two-dimensional MRI data were acquired continuously using a Hahn spin-echo pulse sequence and saved at equal time intervals (about 10 min based on the set-up parameters) without interrupting the drying process. Samples of intact kernels (with all three components: pericarp, germ, and endosperm), mechanically scarified kernels with incisions in the pericarp, and kernels with the germ removed were dried at the above-stated temperatures. A calibration curve of MRI image intensity versus the actual moisture content of the grain was also obtained, using NMR spectra of grains at different, known, moisture contents. Mathematical models based on the real-time conditions from the present research were developed to simulate simultaneous heat and mass transfer during wheat drying.

The MR images clearly showed a non-uniform moisture distribution inside the intact-wheat kernel before and during drying. Further analysis of the MR images revealed that moisture loss from the seed parts differed significantly during drying and was dependent upon the grain components. The rates of moisture change in the pericarp, endosperm, and germ during drying were clearly different. The rate of moisture loss was slower from the endosperm region, whereas the pericarp region dried faster at the initial stages of drying. Furthermore, water had the tendency to move from the endosperm towards the germ to finally move out from the grain. These observations are an important consideration to develop accurate grain drying models with well-defined initial and boundary conditions. In case of the mechanically-scarified kernels, water was released relatively faster from the scarified regions of the pericarp, as compared to the intact kernels. This is expected because the intact pericarp behaves as a moisture barrier after the initial drying and hinders the movement of water from the kernel. In the case of germ-removed kernels, water moved out in a uniform manner from the kernel. A proper synthesis of the results from these analyses led to the development and validation of a mathematical model to follow the moisture distribution inside a grain kernel as a function of drying time and initial moisture content. The model was developed based on non-uniform moisture distribution in the wheat components at the beginning of drying. The new grain drying model is expected to significantly advance the control of mass transfer during drying to maintain both the quality of the product and the economy of the process.

ACKNOWLEDGEMENTS

It is my proud privilege to express my profound sense of gratitude and sincere thanks to my advisor, Dr. Digvir S. Jayas, P.Eng., P.Ag., FASABE, FCSBE, FAIC, Distinguished Professor, Department of Biosystems Engineering; Associate Vice President (Research) and Canada Research Chair in Stored Grain Ecosystems, University of Manitoba for his inspiring guidance, invaluable advice, constructive criticism, painstaking efforts, unfailing support, keen interest and encouragement throughout the course of this study.

I am aware of my debt to the members of my advisory committee, Dr. Noel D.G. White, Research Scientist, Cereal Research Centre, Agriculture and Agri-Food Canada, and Adjunct Professor, Departments of Biosystems Engineering and Entomology, University of Manitoba; and Dr. Marco L.H. Gruwel, Research Council Officer, Institute for Biodiagnostics (Winnipeg), National Research Council of Canada, and Adjunct Professor, Department of Chemistry, University of Manitoba for their timely suggestions, encouragement and help extended during the entire tenure of this investigation. No less is my gratitude due to Dr. Edward A. Smith, Senior Lecturer, Department of Mathematics and Statistics, University of Paisley, Scotland, UK, for his valuable advice, encouragement and timely help rendered during the mathematical modelling component of my research work. I am greatly indebted to Dr. Peter A. Zhilkin, Institute for Biodiagnostics (Winnipeg), for his valuable assistance partly during the MR image processing for my research work. Many thanks to Dr. Dirk Maier, Professor and Associate Head, Department of Agricultural and Biological Engineering, Purdue University, USA, for serving as my external examiner and reviewing this thesis.

'Canada Graduate Scholarship' awarded by the Natural Sciences and Engineering Research Council of Canada (NSERC), University of Manitoba Graduate Fellowship, W.E. Muir Award for outstanding achievement in Biosystems Engineering, American Society of Agricultural Engineers Information and Electrical Technologies Division's 2004 'Select Meeting Paper Award' for my Doctoral program are thankfully acknowledged. My special thanks to Dr. Jayas's Discovery Grant from NSERC and Canada Research Chairs Program for providing me financial assistance during the course of my study from the very beginning.

My sincere thanks to AACC International, Canadian Society for Bioengineering, and American Society of Agricultural and Biological Engineers for permitting me to use their copyrighted materials.

I owe thanks to the technicians of the Institute for Biodiagnostics (Winnipeg), Mr. Matt Macdonald of the Biosystems Engineering, and Mr. David Treble of the Faculty of Agricultural and Food Sciences, University of Manitoba, for their technical co-operation and help during this study.

A special word of appreciation is due to my colleagues for their friendly help, support, and valuable suggestion during this study. I do thank every person who directly or indirectly aided the cause of preparing my thesis.

Words fail me to express my deep sense of emotions and gratitude for my family members, and my wife Swati, whose love, affection, forbearance, encouragement and good wish have made this study possible.

Prabal Kumar Ghosh

TABLE OF CONTENTS

LIST OF FIGURES

LIST OF TABLES

CHAPTER 1

INTRODUCTION

Globally, about 2 billion tonnes (Gt) of grains, oilseeds, and legumes (hereinafter referred to as grains) are produced annually and stored at different stages in the grain distribution chain between the producer and the consumer. Grains are usually harvested at a moisture content higher than that is safe for storage to reduce field losses resulting from weather conditions, wildlife damage, or shattering loss due to overdrying. Cereal grains are usually harvested at more than 17% w.b. (wet mass basis) moisture content (m.c.) (Friesen 1980). Grains are seasonal and perishable, and technologies and practices are available to store them properly until consumed. In general, high moisture levels can lead to spoilage of grains during storage. Proper moisture conditions are, therefore, important for safe grain storage and handling. Grain drying is a common method to artificially remove the moisture from the harvested grain to attain a safe storage moisture content. Drying of grains prevents the occurrence of hot spots caused by mould growth, slows enzymatic changes, and considerably increases the storage life. It also reduces grain mass, thereby facilitating transportation and handling. For example, wheat is usually harvested at 18-20% m.c. and dried to 14% m.c. for short-term storage (6-12 mo) and 13% m.c. for long term storage (over 1 y) (Brooker et al. 1992). Drying of grains is commonly performed by forcing air through the bulk grain at different temperatures: natural (ambient) temperature, near-ambient temperature, low temperature, or high temperature.

Most commercial high capacity grain dryer units are interfaced with a computer control system which maintains the residence time of the grain in the dryer to give improved grain quality and achieve the target moisture content without over-drying (wasted energy and reduced dry grain mass) or under-drying (less than optimal weight grain). The proper functioning of the computer control system can be done by mathematical models that can accurately predict the variations of moisture contents in grains during drying to achieve the target moisture content.

There is general agreement that drying behavior of grains is largely influenced by the temperature and moisture distribution in the grains when dried using forced air at different temperatures. Furthermore, grains are heterogeneous in structure. Thus, grain drying is a complex process of simultaneous heat and mass transfer. To use the drying techniques at farm or industry levels and to develop accurate mathematical models, it is necessary to understand the underlying mechanisms of drying inside grain kernels.

Magnetic resonance imaging (MRI) is a technique for observing moisture movement and distribution inside intact kernels in a non-destructive and non-invasive way. Magnetic resonance imaging uses radio waves and powerful magnets to generate images of tissue. A strong magnetic field partially aligns the hydrogen atoms of water molecules in the tissue. A radio wave then disturbs the built-up magnetization, and radio waves are in turn emitted as the magnetization returns to its starting location. These radio waves are detected and used to construct an image. Several books provide details on MRI principles (Bushong 1988; Stark and Bradley 1992; Ruan and Chen 1998). Ghosh and Jayas (2004)

have extensively reviewed the recent research developments of MRI techniques and its potential use in solving various grain related research problems.

Magnetic resonance imaging can be used to obtain two or three-dimensional moisture transfer profiles inside a single grain kernel during drying. Little work has been carried out to determine transient moisture distributions inside the grain kernels during the drying process. The first experiment of this kind was reported by Song and Litchfield (1990) who determined the transient moisture profile in ear corn during hot-air drying at 60°C with an air velocity of 1.83 m s^{-1} for 5 h. Trends in moisture loss for different parts of corn kernels were visually investigated from MR images, since brightness of the image is directly proportional to the proton density and hence the moisture content. One-dimensional transient moisture profiles across the center of an ear of corn were obtained based on image pixel intensities at different drying times. Moisture distribution and changes inside the corn cobs were distinctly different, and non-uniform, during the drying process. Song et al. (1992) investigated moisture transfer from sequential three-dimensional MR images of corn kernels obtained during drying at 27°C and 49°C at an air velocity of 5 m s^{-1} for 3 h and 1 h, respectively. A series of proton density images of one central slice was evaluated. It was determined that moisture distribution in the kernels was non-uniform. Moisture loss also differed significantly during drying through two primary routes: the glandular layer of the scutellum, and the pericarp. Kovács and Neményi (1999) used a standard Hahn spin-echo imaging pulse sequence to obtain MR images of yellow dent corn (Helga variety) kernels during drying at 46°C with an air velocity of 1.4 m s^{-1} for 4.5 h and performed moisture gradient vector analysis to

demonstrate the pathways of moisture loss from the kernel during drying. Moisture distribution inside the whole kernel was not uniform before and during drying. Moisture loss was faster and higher from the endosperm than the pericarp. However, moisture loss was the lowest from the scutellum. Common observation from all these studies is an anisotropic and non-uniform nature of moisture distribution and migration during drying of corn kernels.

Magnetic resonance imaging has also been used to successfully determine grain moisture content in different grains (from 4% to 40% w.b.) (barley: Miller et al. 1980; corn: Miller et al. 1980, Tollner and Hung 1992; and wheat: Miller et al. 1980, Brusewitz and Stone 1987, Chambers et al. 1989, Tollner and Hung 1992). Brooker et al. (1992) gravimetrically determined that the initial moisture content distribution in a freshly harvested corn kernel is non-uniform (whole kernel 36% m.c., w.b.; germ 48% m.c., w.b.; endosperm 31% m.c., w.b.; and pericarp 53% m.c., w.b.). This feature was further evidenced in most of the cereal grains including corn by several researchers using MRI (barley: McEntyre et al. 1998, Gruwel et al. 2001, Gruwel et al. 2002, Glidewell 2006; corn: Ratković 1987, Song and Litchfield 1990, Bačić et al. 1992, Song et al. 1992, Ruan et al. 1992, Ruan and Litchfield 1992, Song et al. 1998, Kovács and Neményi 1999; rice: Takeuchi et al. 1997, Horigane 2001, Frìas et al. 2002, Ishida et al. 2004, Mohorič et al. 2004, Kasai et al. 2005; and wheat: Jenner et al. 1988, Stapley et al. 1997, Song et al. 1998, Fukuoka et al. 2000, Turhan et al. 2001, Gruwel et al. 2004).

Simulation studies of grain drying rely on the solution of equations for simultaneous heat and moisture distribution inside the grain mass. Several semi-theoretical and empirical models describing the thin-layer (a single grain kernel or one layer of grain kernels or a polylayer of many grain thickness) as well as the deep-bed (more than 20 cm deep) drying process for specific grains have already been reviewed and compared (Jayas et al. 1991; Cenkowski et al. 1993; Pabis et al. 1998; Parde et al. 2003; Ghosh et al. 2004). These models can predict the moisture loss from the grain bulk during drying but cannot predict the internal moisture and temperature variations and their distribution within individual grain kernels with drying time. Since cereal grains are hygroscopic capillary porous materials and drying can generate considerable temperature and moisture gradients in the grains, hydro-thermal stress can develop which deteriorates the grain quality in many ways. Improper drying due to lack of knowledge about internal moisture and temperature distribution inside the grain kernels can adversely affect the test weight, milling and baking characteristics, and head-rice yield and cause physical damage and increase stress-crack susceptibility. For example, wheat drying is usually accomplished with near-ambient air or hot air with a recommended drying temperature preferably below 60°C to maintain its milling and baking characteristics (e.g., loaf volume). However, stress-cracking is not prevalent in wheat (Nellist and Bruce 1995).

Internal mass (moisture) transfer in wheat or other cereal grains during drying is caused by concentration gradients resulting from liquid or vapour diffusion or their combination (corn: Hall and Rodrigues-Arias 1958, Hustrulid and Flikke 1959, Allen 1960, Pabis and Henderson 1961, Chittenden and Hustrulid 1966, Chu and Hustrulid 1968a,b, Fortes and

Okos 1978, Sokhansanj and Gustafson 1980, Walton et al. 1988, Czaba and Neményi 1997, Neményi et al. 2000; rice: Allen 1960, Husain et al. 1973, Sokhansanj and Gustafson 1980, Steffe and Singh 1982, Yang et al. 2002; and wheat: Babbitt 1949, Simmonds et al. 1953, Becker and Sallans 1955, Becker 1959, Watson and Bhargava 1974, Fortes et al. 1981, Jia et al. 2000). Simmonds et al. (1953) indicated that capillary forces play a very minor role in the mass transfer during wheat drying.

In recent years, with the advent of powerful computers, single grain kernel drying has been simulated by simultaneous heat and mass transfer models considering various moisture transfer phenomena (one or more of diffusion, capillary flow, or evaporation-condensation mechanisms) and geometrical shape (barley: Haghighi et al. 1990, Irudayaraj et al. 1992, Miketinac et al. 1992; corn: Sokhansanj and Gustafson 1980, Irudayaraj et al. 1992, Czaba and Neményi 1997, Neményi et al. 2000; rice: Husain et al. 1973, Sokhansanj and Gustafson 1980, Yang et al. 2002, Wu et al. 2004; and wheat: Jia et al. 2000). All of these models were solved numerically mostly involving the finite element method, in which moisture distribution was approximated by a discrete model composed of a set of piecewise continuous functions defined over a finite number of sub-domains or elements (Segerlind 1984). A summary of these models is discussed in Miketinac et al. (1992). Further, all of these studies used an invasive method to measure the kernel moisture level, destroying the sample. Moreover, all of the published grain-drying models were derived assuming that moisture distribution is uniform in a grain at the beginning of drying and that the moisture removal from the grains is uniform during drying to simplify these models for computation. However, these simplifications do not

represent the reality as has been demonstrated by published studies of moisture distribution using MRI and therefore may reduce the accuracy of the model predictions. There is a need to develop and solve mathematical models of coupled heat and moisture transfer in grain that take into consideration the non-uniform distribution of moisture before the start of drying and non-uniform movement of moisture from grain during drying. However, no efforts have been made so far to determine moisture removal pattern for wheat kernels and the effects of grain structural components on the movement of moisture from the grain kernels during drying using MRI.

Wheat (*Triticum aestivum* L.) was selected in this study because it is a world leading cereal grain in terms of production and consumption. The internal structure and composition of a wheat kernel is very complicated (MacMasters et al. 1964; Brooker et al. 1992; Pomeranz and Bechtel 1978; Evers and Bechtel 1988) and therefore the anatomy of the entire kernel is of importance in determining the movement of moisture during drying. Since the structure of wheat is heterogeneous, the prediction of kernel drying becomes very complicated as it involves both heat and mass transfer.

Therefore, the objectives of this research were:

1. To investigate the patterns of moisture movement and distribution inside wheat kernels during drying from the magnetic resonance (MR) images.
2. To study the influence of grain structural components on the internal moisture removal and distribution pattern during drying using MR images.

3. To study the movement of moisture inside the wheat kernel from the moisture gradient vectors calculated from each pixel of the subtraction of MR images.
4. To study wheat drying kinetics using MR to be able to identify the real time conditions during drying for developing accurate grain drying models which can be solved with well-defined initial and boundary conditions.
5. To develop and validate mathematical models of two-dimensional (2D) simultaneous heat and moisture transfer during drying of wheat using information obtained from the MRI experiments.

The material presented in this thesis is organized into eight chapters. The first chapter provides preamble of this research by addressing the problem, hypothesis and objectives. The second chapter begins with the description of the morphology of a wheat kernel. It then continues with an explanation of the basic principles of Magnetic Resonance Imaging technique with its application in different agricultural and food processing operations including cereal grains, oilseeds, fruits and vegetables. It further describes the theory of grain drying and explains the available grain drying models. It then provides the comments on the existing models and the need for developing the new grain drying model. The third chapter addresses parts of these research findings which covers objectives 1 to 3. The fourth chapter also covers research findings from objectives 1 to 3. Chapters 3 and 4 were reprinted from publications based on research for this thesis in two peer-reviewed international journals. The fifth and sixth chapters address objectives 4 and 5 of this research, respectively. Both of these chapters are based on research from this thesis. The fifth chapter has been accepted for publication and the sixth chapter is

currently in the review process for publication in international peer-reviewed journals. Chapter seven provides the conclusions drawn from the present research. Chapter eight gives some recommendations for future research. Since this thesis is prepared according to the paper-based form, no separate section on the materials and methods is given as the details have been covered in the individual chapters (papers). All the data for constructing the chapters are provided in Appendices.

REVIEW OF LITERATURE

2.1 Wheat Morphology

Wheat is a staple grain which is consumed in various forms around the world. Global wheat production was about 629 million tonnes (Mt) in the year 2005 from a total harvested area of about 217 Mha (FAOSTAT 2006). An increased wheat production of about 85 Mt over the last decade indicates an increasing demand due to the world's growing population. Therefore, safer and proper storage of wheat has become a major concern for farmers and storage managers. The recommended harvesting moisture content for wheat is usually 18-20% w.b. (wet mass basis), whereas the safe storage moisture content is recommended to be 14% w.b. for short-term (6-12 mo) and 13% w.b. for long-term storage (over 1 y) (Brooker et al. 1992). Drying of wheat is globally practiced to reduce moisture of grain for safe storage. Wheat is usually dried using near-ambient air or hot air with a condition that wheat is not heated above 60°C to maintain its germination, milling and baking qualities (e.g., loaf volume).

A kernel of wheat consists of three major components, the endosperm (85-90% by mass), the germ or embryo (2-3% by mass), and the pericarp (7-8% by mass) (Simmonds et al. 1953). This type of cereal grain is also called a kernel or caryopsis. Figure 2.1 shows a detailed wheat kernel structure. The entire structure of a wheat kernel can influence the movement of moisture inside the kernel during drying. The complex anatomy of a wheat kernel makes drying a complicated process of simultaneous heat and mass transfer. Detailed description on the wheat structure is explained elsewhere (MacMasters et al.

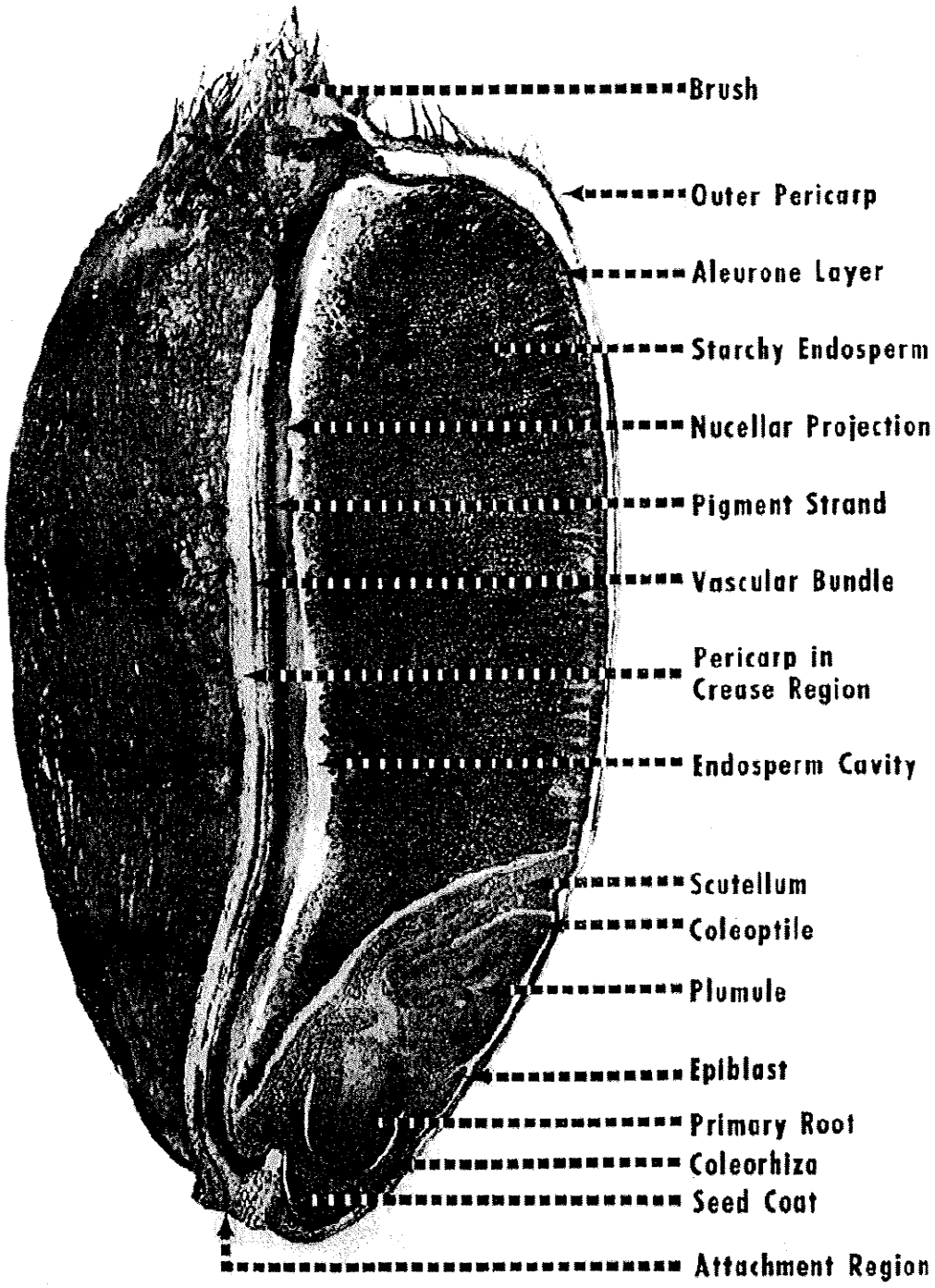

Figure 2.1 Wheat kernel structure (longitudinal section) (Source: MacMasters et al. 1964). [Reproduced with permission from AACC International]

1964; Pomeranz and Bechtel 1978; Evers and Bechtel 1988; Brooker et al. 1992). The following paragraphs explain, in brief, the structural details of a wheat kernel.

2.1.1 Germ (Embryo)

Germ is composed of two parts: the embryonic axis, which is responsible for seed germination, and the scutellum, which is responsible for food storage, digestion and absorption of food from the endosperm during seed germination. The attachment region of the scutellum to the endosperm is composed of scutellar epithelium, which is a layer of secreting cells. The scutellum and embryonic axis are connected by provascular bundles formed by conducting tissues. The scutellum contains more oil and protein but less starch. The germ is a separate and distinct component of the seed. Therefore, it is easy to remove from the whole kernel. There is a thin layer of empty cells, which works as a cementing layer between the germ and endosperm.

2.1.2 Pericarp

Pericarp is a protective layer for the entire seed. Thickness of pericarp is usually 45-50 μ. The pericarp consists of several layers, from outside to inside: epidermis, hypodermis, cross cells, and tube cells. The epidermis and hypodermis are considered to be the outer pericarp; both have mostly single-layer thick-walled cells. The cells of these two layers are closely adhered to each other without intercellular spacing. Further, the innermost portion of the hypodermis contains thin-walled cells, which divide the outer pericarp from the inner region. Water can move faster due to this division since the area lacks in continuous cellular structure. The cross cells and tube cells inward from the hypodermis

form the inner pericarp. These cells are so named because the long axes of the cross cells lie perpendicular and that of the tube cells lie parallel to the long axis of the kernel. The cross cells are connected in rows without leaving any intercellular spaces near the endosperm region, whereas the cells are irregular in shape close to the germ causing numerous intercellular spaces. On the other hand, the tube cells are connected by projections and therefore, the layer contains intercellular spaces.

A longitudinal crease, opposite to the germ, runs from the very base to the tip of the pigment strand of the kernel, contains a vascular bundle which runs through the pericarp tissue. A seed coat, joined to the cross and tube cells on the outside and to the nucellar epidermis on the inside, forms a complete coat around the endosperm and the germ. The thickness of the seed coat varies. The thickest region appears towards the crease and the thinest region is over the germ for an easy movement of water. A nucellar epidermis, a compressed thick-walled cellular layer, lies between the seed coat and the aleurone layer with less intercellular spaces.

2.1.3 Endosperm

The outer layer of endosperm is the aleurone layer, which is a single cell-layer thick. The aleurone layer, on its exterior, is attached to the nucellar epidermis, and on its interior, is attached to the endosperm. The cells are aligned perpendicular to the surface of the kernel. However, the cells are cellulosic and thick, but are joined together with noncellulosic material, therefore create less intercellular space. Minute canals or delicate protoplasmic cells adjoin the endosperm to the aleurone layer. The endosperm contains

cells containing protein and starch. The endosperm cells are different in shape and size and their thickness varies at different regions. Thinner cells are found near the aleurone layer, which contain highly water-insoluble hemicellulose but the thicker cells are found near the crease or at the centre of the kernel with less hemicellulose indicating high water mobility.

2.2 Nuclear Magnetic Resonance (NMR)

Nuclear magnetic resonance (NMR) technology, commonly used for NMR spectroscopy and magnetic resonance imaging (MRI), is one of the most powerful non-invasive and non-destructive methods currently available for research. Magnetic resonance phenomenon was first discovered under the leadership of Felix Bloch from Stanford University and Edward Purcell from Harvard University in 1946 for which both of them won the Nobel Prize in Physics in 1952. Since then several investigations have been carried out to explore the application and advancement of the MR technique. The MR technique has been adopted quickly in the medical field for its unique non-invasive and non-destructive features. Nuclear magnetic resonance spectrometers became popular during 1960-70 and were widely used. In 1972, Paul C. Lauterbur of the University of Illinois first generated a two-dimensional proton MR image of a water sample. In 1974, Lauterbur produced the first image of a live animal using non-uniform magnetic fields. This innovation made significant changes in the medical sciences in terms of research and clinical diagnostics on soft tissues, tumor, brain, and cardiovascular diseases. In 1991, Richard Ernst of Eldgenössische Technische Hochschule Zürich (Swiss Federal Institute of Technology Zurich), was awarded the Nobel Prize in Chemistry and in 2003,

Paul Lauterbur and Sir Peter Mansfield of the University of Nottingham were awarded the Nobel Prize in Medicine for their unique discoveries in magnetic resonance imaging.

2.2.1 Principle of Nuclear Magnetic Resonance

The principle of NMR is based on the spinning mechanism of specific nuclei present in the molecules of biological tissues. Molecules are assemblies of atoms consisting of nuclei containing positively-charged protons and chargeless neutrons surrounded by orbiting negatively-charged electrons. Some nucleus behaves like a tiny magnet, exhibits strong magnetism and generates a small magnetic moment, $\vec{\mu}$, due to a characteristic spin (I). Nuclei of isotopes of some elements in the Periodic Table have integral spins (e.g., I = 1, 2, 3), some have fractional spins (e.g., I = 1/2, 3/2, 5/2), and a few have no spin, I = 0 (e.g., ^{12}C, ^{16}O, ^{32}S). Isotopes of particular interest found in most biological systems are ^{1}H, ^{13}C, ^{19}F and ^{31}P, all of which possess I = 1/2 and ^{23}Na possesses I =3/2. Atoms consisting of different nuclei, possess different spin values, which are given in Table 2.1.

In the absence of an external magnetic field (B_o), nuclei are randomly distributed inside the biomaterials resulting in a zero net magnetization (M_o). Orientation of each and every nuclei follows the quantum mechanics theory where nuclear spin quantum number $I = \pm n/2$ where n = 0, 1, 2, ... When a nucleus with $I = \pm 1/2$ (e.g., ^{1}H or proton) is exposed to a strong magnetic field (B_o), polarization results into a measurable net magnetization (2I + 1), parallel to the field. The net magnetization precesses around the magnetic field at a well defined rate, called the Larmor frequency (ν):

Table 2.1 Magnetic resonance properties of major nuclei found in biological tissues (Pope and Sarafis 1990; Stark and Bradley 1992).

Nucleus	^{1}H	^{31}P	^{23}Na	^{13}C	^{19}F
Spin (I)	1/2	1/2	3/2	1/2	1/2
Gyromagnetic ratio (MHz T^{-1})	42.6	17.2	11.3	10.7	40.0
Natural abundance, %	100	100	100	1	100
Relative sensitivity	1.0	6.6×10^{-2}	9.25×10^{-2}	1.8×10^{-4}	0.83

$$\omega = 2\pi\nu = \gamma B_o \qquad (2.1)$$

where ω is the angular frequency (rad s^{-1}); γ is the gyromagnetic ratio, i.e., ratio of the magnetic moment to the angular moment of the particle (rad T^{-1} s^{-1}); and B_o is the magnetic field strength (T).

Further, the magnetic moment of the lower energy (+1/2 state) aligns with the field but that of the higher energy (-1/2 state) aligns in the opposite direction to the field. The energy difference (ΔE) between the lower and higher energy levels is very small which develops mainly due to the concentration of more nuclei at the stable lower energy level. When there is no external magnetic field (B_o), the spin states have the same energy but they change in the presence of an external field. The energy difference, ΔE is proportional to the magnetic field strength by the following relationship:

$$\Delta E = \frac{\mu B_o}{I} \qquad (2.2)$$

2.2.2 Nuclear Magnetic Resonance Spectroscopy

NMR spectroscopy uses a strong magnetic field. Modern equipment is available which is capable of generating magnetic field strength of 1 Tesla (T) to 20 T with the use of powerful magnets (the earth's magnetic field strength is approximately 0.00005 T). In this case, small energy difference (ΔE) between low and high energy levels is considered as the frequency (MHz), which depends upon the magnetic field strength, and the specific nuclei being studied. By convention, in NMR, the z-axis of the Cartesian coordinate system coincides with the axis of the main magnetic field (B_o) inside the bore of a magnet, while the xy-plane lies perpendicular to it. To perturb the equilibrium

magnetization from its original orientation to create a resonant effect, a radio-frequency (RF) pulse (B_1), is applied to tip the magnetization into the xy-plane, perpendicular to B_o. This process is most efficient at resonance which occurs when the RF frequency equals the Larmor frequency with energy equal to ΔE. The tip-angle of the magnetization depends upon the strength and duration of the RF field, which is applied perpendicular to B_o. This resonance effect is termed nuclear magnetic resonance (NMR). Most NMR applications focus on detecting hydrogen or proton (^1H) nucleus because of its relatively large abundance in both water and oil in biological materials, and it has the highest gyromagnetic ratio (γ) and sensitivity of all isotopes to produce a strong NMR signal (Table 2.1).

After the RF is turned off, the nuclei are again subjected to the effects of the static magnetic field, realign themselves to return or relax back to their original equilibrium state, parallel to B_o, by losing energy in the form of RF-wave. This process is called the relaxation process. The RF wave is characterized by the Larmor frequency and is received by the detection coil of an NMR instrument. This process can be characterized by two relaxation constants: T_1 and T_2. The longitudinal or spin-lattice relaxation time, T_1, describes the time required for the z-component of the magnetization (M_z) to return to its equilibrium value. The transverse or spin-spin relaxation time, T_2, describes the time required for the transverse magnetization (M_{xy}) to return to its equilibrium state. Relaxation times (T_1 and T_2) are a function of chemical composition, mobility, temperature, solute and moisture concentration, and structure (Schrader et al. 1992). Long T_1 or T_2 values indicate slow relaxation whereas short T_1 or T_2 values indicate fast

relaxation. T_1 and T_2 are equal in case of water and some dilute solutions (Schimdt et al. 1996). Difference in the relaxation times is exploited to highlight different sections within a particular biological material. The T_1 relaxation time is usually longer than T_2 relaxation time. Relaxation rates (R_1 or R_2) are the inverse of the relaxation times (T_1 or T_2).

2.2.3 T_1 and T_2 Measurement Techniques

Since T_1 and T_2 denote the fundamental property of a sample, it is necessary to discuss the methodology of their measurement procedure. Various pulse sequences are adopted to measure T_1 and T_2. The signals or intensities are recorded after application of pulse sequence to the spins. T_1 is usually measured by the 'inversion-recovery' technique. In this technique, a 180^o-τ-90^o sequence is run with varying time (τ). Time, τ, is called inversion delay. Single 90^o RF pulse is not helpful to measure T_1 because it is hard to detect magnetization along the z-axis. The inverse-recovery pulse sequence applies the 180^o pulse before the application of a 90^o pulse to invert the magnetization in the – z direction with a magnitude of - M_o. The time gap of τ before the application of a 90^o pulse helps the magnetization to decay due to T_1 relaxation. The equation for measuring T_1 is:

$$M_z(\tau) = M_o(1 - 2e^{-\frac{\tau}{T_1}}) \qquad (2.3)$$

T_1 can also be measured by a 'T_1 saturation recovery' pulse sequence (TISR). In this sequence, a series of 90^o pulses is applied followed by a time gap of τ before acquisition of the signal. The application of first 90^o pulse flips the magnetization to the xy-plane

instead of 180° to the – z axis. Thus, the equation for measuring T_1 in TISR sequence is slightly modified as:

$$M_z(\tau) = M_o(1 - e^{-\frac{\tau}{T_1}}) \qquad (2.4)$$

However, accuracy in measuring T_1 is less in the TISR sequence compared to the inverse-recovery pulse sequence.

When a 90° RF pulse is applied, transverse or xy-plane magnetization, M_{xy}, reaches its peak value equal to M_o and then it decays exponentially. This decay curve is termed as 'free induction decay' (FID). T_2 is measured from the following equation:

$$M_{xy} = M_o\, e^{-\frac{\tau}{T_2}} \qquad (2.5)$$

However, the actual T_2 is sometimes difficult to measure using a single 90° RF pulse due to magnetic field inhomogeneties. A common method for measuring actual or true T_2 is the 'Hahn spin-echo pulse sequence' (Hahn 1950). This sequence involves a 90° pulse followed by a 180° pulse after a certain time gap, τ (90°-τ-180°- τ- acq) in which the spin magnetization is rephased or refocused some time after the initial pulse. This rephasing of the spins develops a free induction decay signal, termed as spin-echo amplitude, which becomes the highest at time 2τ. Thus decay in the spin-echo amplitude can be observed by applying the 180° pulse at different times. This decay pattern of the spin-echo amplitude can be used to measure the T_2. Again T_2 determination can be wrong with spin-echo sequence due to the effect of molecular diffusion. When diffusion occurs, nuclei move in the magnetic field during the time of the refocusing experiment (2τ) and therefore the spin-echo amplitude reduces in addition to T_2 decay. The 'Carr-Purcell-

Meiboom-Gill pulse sequence' (CPMG) follows the 90^{o}-τ-180^{o}-3τ-180^{o}-5τ-180^{o}-... pulse scheme to produce echoes at times 2τ, 4τ, 6τ,... The T_2 is measured from the envelope from the decay of multiple echo amplitudes.

2.2.4 Nuclear Magnetic Resonance Spectrometer

NMR spectroscopy can be used to obtain information about the microscopic chemical and physical components in the molecules. An NMR spectrometer typically comprises of a sample holder surrounded by a superconducting magnet, an RF transmitter and receiver coil, and a computer for pulse programming, data acquisition and analysis.

Nuclear magnetic resonance (NMR) spectroscopy can be used to determine the structure of organic compounds since it is possible to analyze the entire spectrum using this technique. Although protons have the same magnetic moment they resonate at different frequencies for different chemical components. Thus different proton signals can be achieved at the same magnetic field strength from different organic compounds. Location of different NMR signals from different compounds in a spectrum depends upon the external magnetic field strength and the RF frequency (Fig. 2.2). Calibration of the NMR spectrum is commonly carried out based on a reference signal obtained from a chemically non-reactive standard compound. Further, NMR signals are separated by chemical shift, which is used to characterize differences in resonance frequencies at different field strengths. Various NMR spectrometers are currently available on the market targeting different application areas.

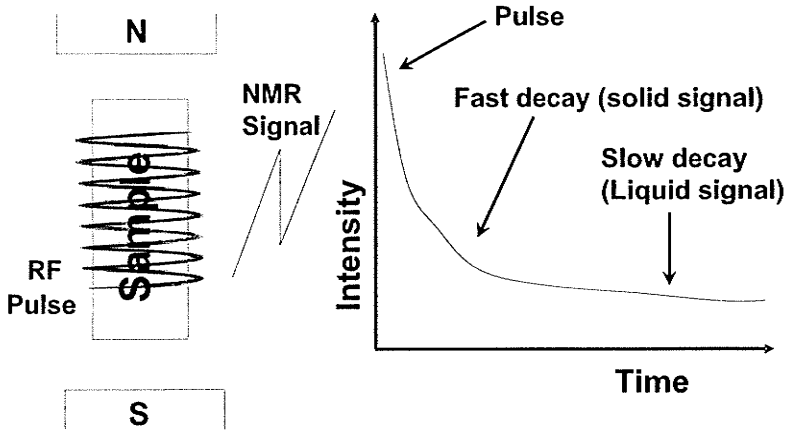

Figure 2.2 Schematic of nuclear magnetic resonance signal formation.

Since the present work is based on Magnetic Resonance Imaging (MRI), emphasis is given to the description of the MRI technique.

2.3 Magnetic Resonance Imaging (MRI)

Magnetic resonance imaging is based on the principles of nuclear magnetic resonance (NMR). Nuclear magnetic resonance is a spectroscopic technique through which physical and chemical information about the molecules from an object are obtained. Magnetic resonance imaging technique can produce image of the NMR signal in the presence of magnetic field gradient. A magnetic field gradient is a variation in the magnetic field with respect to the position of the object. In MRI, usually one-dimensional magnetic field gradient is used where the magnetic field is increased with respect to its direction. Magnetic field at the magnetic isocentre (x,y,z = 0,0,0) is B_o with resonance frequency ω_o. When an object containing different proton density regions is placed within the magnet, the regions experience different magnetic fields. This results in an NMR spectrum with different signal intensities. The NMR signal amplitudes are proportional to the number of regions perpendicular to the field gradient. This is called 'frequency encoding'. Since the Larmor or resonance frequency, λ, is proportional to the magnetic field strength, i.e. $\lambda = \gamma B_o$, and magnetic field strength is a function of position; the resonance frequency and the spatial position of proton density regions are related as:

$$\omega = \gamma (B_o + x G_x) = \omega_o + \gamma x G_x \qquad (2.6)$$

where G_x is the magnetic field gradient in the x-direction.

Back projection imaging was first discovered by Paul Lauterbur to produce an MR image. In this method, an one-dimensional magnetic field gradient was applied on the object placed in the magnetic field at many angles between 0^{o} and 359^{o} to obtain different NMR spectrum at every angle. Once the spectrum data were obtained, the data were back projected through space to produce a reconstructed image.

Hornak (2006) stated that "the back projection imaging technique is highly educational but hardly used in state of the art imagers. Instead, Fourier transform imaging techniques are used". In Fourier transform imaging, the FID signals are Fourier transformed to obtain an image. Images are obtained using double Fourier transformation from the collected dataset of frequency encoded data and for each k-space. When a 1-D magnetic field gradient is applied, the transverse magnetization vectors precess with the resonance frequency (Eq. 2.6) along the direction of the magnetic field gradient. A phase encoding gradient is usually applied before the frequency encoding gradient is turned on. The phase encoding gradient is applied at a right angle to the frequency encoding gradient to obtain a 2D image. When the phase encoding gradient is turned on, the transverse magnetization vectors at different regions start rotating at phase angle (φ) with the direction of phase encoding gradient with unique precessional frequencies. The phase angle, φ, can be written as:

$$\varphi = \gamma \, Y \int_{0}^{t} G_{y}(t) \, dt \qquad (2.7)$$

where Y is the phase encoding gradient direction and G_y is the phase encoding gradient strength. The sequence of turning on and off of gradients is repeated until all FID data are collected to form an image. The steps of an MR image formation can be found elsewhere

(Stark and Bradley 1992; Ruan and Chen 1998; Hornak 2006). The time between the repetitions of the sequence is called the repetition time (TR). The image acquisition time, therefore, is equal to the product of the TR value and the number of phase encoding steps.

In MRI, slice selection is possible. A slice is a plane through an object with certain thickness. The protons in a slice can be excited by means of a combination of a 90° RF pulse and a magnetic field gradient. The bandwidth of the RF pulse ($\Delta\omega$) and the magnitude of the magnetic field gradient (slice selective gradient) (G_z) determine the thickness of the slice. The slice thickness (ΔZ) is determined by the following relationship:

$$\Delta Z = \frac{\Delta \omega}{2 \pi \gamma G_z} \tag{2.8}$$

for protons γ = 42.67 Hz G^{-1}. Thus the slice thickness is reduced by increasing the gradient strength (G cm^{-1}) or by decreasing the RF bandwidth (Hz). Usually during Fourier transform imaging, if slice selection is necessary, the slice selection gradient is applied prior to the application of the phase encoding gradient and the frequency encoding gradient.

Usually in MRI, imaging planes of slices are not defined as xy, xz or yz planes but an anatomic coordinate system is used. These are: 'axial', which is perpendicular to the z axis of the magnet; 'coronal', which is x axis of the magnet; and 'sagittal', which is object axis of the magnet. A mathematical description of the MRI image formation is given by Ruan and Chen (1998).

Different pulse sequences are used to produce MRI images to explore specific information. Since the present work is based on spin-echo imaging, I will only discuss the working principles for spin-echo imaging sequence.

2.3.1 Spin-Echo Pulse Sequence

A spin echo uses a 90° excitation pulse followed by one or more 180° RF pulse to generate a spin-echo. Each 180° pulse generates a separate spin echo that can be used to generate the image. The time gap between the 90° and 180° RF pulses is TE/2, where TE is the echo time when an echo is formed. A phase encoding gradient is applied between the 90° and the 180° pulse to minimize the echo time. The frequency encoding gradient is applied after the 180° pulse during the collection of the signal or echo. The echo is usually centered in the middle of the frequency encoding gradient so that the gradient is switched on during the rephasing and dephasing part of the echo as well as the peak. The time from application of the first RF pulse to the peak of the echo formation is called the echo time (TE). Once an echo is generated, another RF pulse is applied after a relaxation time (TR) to generate the next echo. During each TR, the signal from each slice is phase encoded and frequency encoded, and then the information is stored in the array processor of the computer. The FID is initially measured as RF intensity versus time. Fourier transformation converts this into signal amplitude versus frequency and is used to generate an image. The frequency domain spectrum has two important parameters associated with it, the spectrometer frequency (SF) and the spectral width or sweep width (SW). Shaped pulses are used to obtain uniform frequency-domain excitation of spins in the presence of static magnetic field gradient. A conventional rectangular shaped pulse

produces a characteristic sine-shaped [sin(x)/x] excitation profile. A typical spin-echo pulse sequence is shown in Fig. 2.3. The horizontal direction represents the time line, with time progressing from left to right. The first line shows the timing of the frequency-encoding (or read) gradient, which is turned on during signal measurement. The second line shows the timing of the phase-encoding gradient. This is turned on during signal excitation (90^{o} RF pulse) and signal measurement. Horizontal stacked-lines indicate different strengths of phase-encoding for acquisitions. The third line shows the timing of the slice-selection gradient. The fourth line indicates when the RF pulses were sent into the object and when the signal was coming out from the object. Vertical dotted lines separate different duration lines with arrow heads show loops, rectangular drawn broken lines denote the echo formation area. The MR signal intensity, I, of each volume element (pixel) using Hahn spin-echo pulse sequence (90^{o}-TE/2-180^{o}- acquisition) is:

$$I = \rho \left[1 - 2\exp\left(\frac{-TR - \frac{TE}{2}}{T_1} \right) + \exp\left(\frac{-TR}{T_1} \right) \right] \exp\left(\frac{-TE}{T_2} \right) \qquad (2.9)$$

where ρ is the proton density, which represents the apparent water content.

2.3.2 Magnetic Resonance Imaging Hardware

A typical MRI system comprises of a superconducting magnet, shim coils, gradient coils, RF coils and a computer system. A typical set up for MRI experiment is shown in Fig. 2.4. The permanent magnets are usually cylindrical in shape with a bore inside to place an object of interest for imaging. The shape, size and orientation (horizontal or vertical) of the magnets vary based on the applications. Magnetic field strengths (B_o) produced by these magnets vary between 0.1 and 20 T. Within the magnet are the shim coils

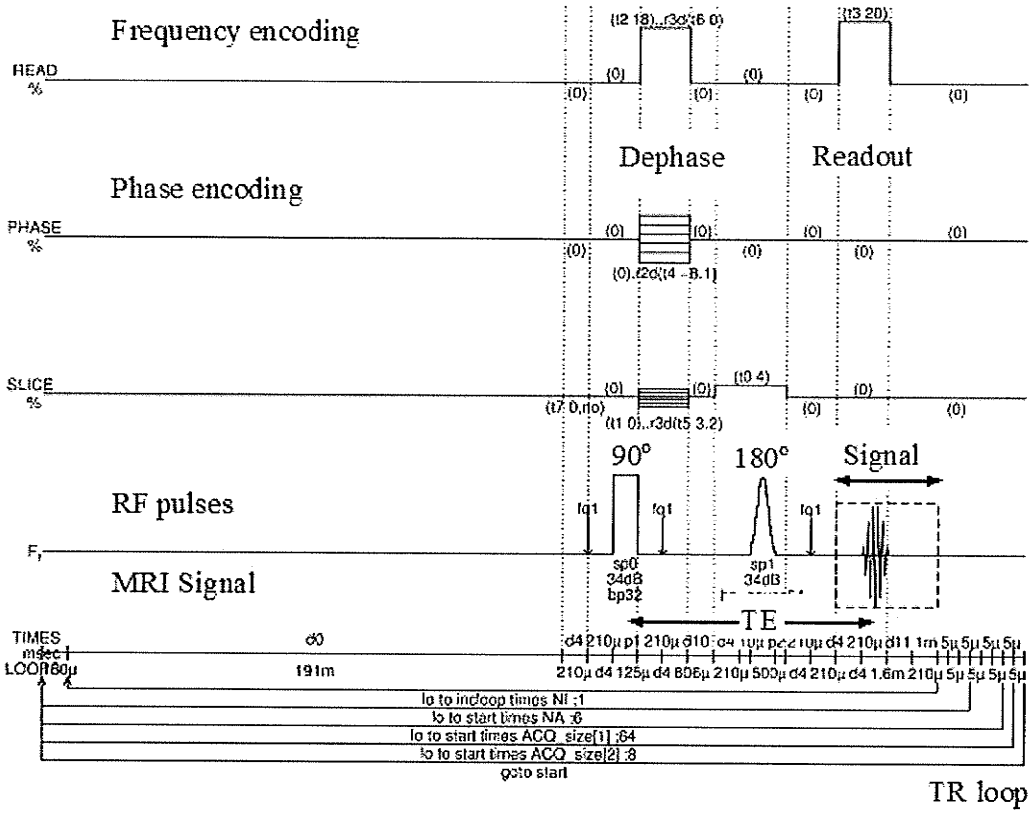

Figure 2.3 Hahn spin-echo pulse program used in this study.

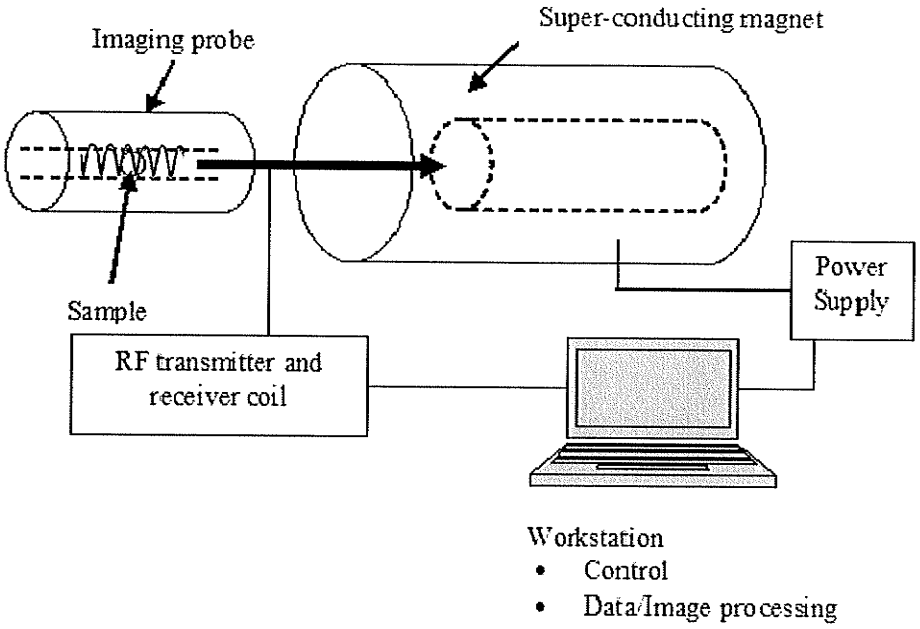

Figure 2.4 Schematic diagram of a typical magnetic resonance imaging set-up.

(electromagnetic coils) through which electric current is supplied to produce a homogeneous B_o field. Specially designed gradient coils are responsible for generating linear magnetic field gradients across the object (in 3D). Within the gradient coils is the RF coil, commonly known as imaging or sample probe, which produces the B_1 magnetic field necessary to excite the protons. The RF coil also detect signal produced due to the excitation of the protons inside the object. The imaging probe and the gradient coils are critical components for MRI imaging and often they are custom-built targeting specific applications. In my experiment, since I am dealing with a single grain kernel drying process (grain dimension is very small as compared to a human being), I needed to develop a specific MR-probe for grain imaging. More details of the grain-imaging probe are given in Appendix-A. The main components of the imaging probe are capacitors and inductor. The capacitors are used for adjusting the frequency and impedance of the circuit for maximum efficiency and the inductor is used for transmitting the RF energy to pick up the induced MR signal from the sample. In general, a variety of probe designs are used, e.g., solenoid or saddle shaped (Helmholtz coils), circular loop wire shaped, birdcage tunnel-shaped. The computer system with software programs is used to control the desired RF frequency; proper pulse sequence; shape, amplitude and timing of field gradients needed to conduct an MR imaging experiment through the selected region of interest (ROI). The computer system is an integral part which is interfaced between the operator and the MRI system to record the signals passing through the receiver, the signal is then amplified, filtered, demodulated, and digitized for storage and display as digital images. Most MRI experiments provide 7 bits (128 gray levels) or 8 bits (256 gray levels)

images. Image acquisition time for a 2-dimensional image is proportional to the repetition time (TR). The acquisition time is usually expressed as:

$$\text{Image acquisition time}_{2D} = TR \times STEPS \times NEX \quad (2.10)$$

where STEPS is the number of phase encoding gradient steps, and NEX is the number of excitations or acquisitions or averages. If TR = 3000 ms, STEPS = 256, and NEX =1, then the image acquisition time would be 12.8 min. An increase in the image acquisition time is directly proportional to the number of acquisitions. However, the more MR signals are acquired, the better would be the image, because the signal-to-noise ratio (SNR) increases with the square root of the number of acquisitions. The image acquisition time should be short enough so that large dynamic changes do not occur during acquisition, but it should be long enough to obtain an acceptable SNR for good image contrast. Image acquisition time for 3-dimensional MRI is expressed as:

$$\text{Image acquisition time}_{3D} = TR \times STEPS \times NEX \times SLICES \quad (2.11)$$

where SLICES is the number of slices in the 3D image. Suppose that a 3D image has 128 slices and that each slice has 256 × 256 pixels in the image, this 3D image consists of a 128 × 256 × 256 voxels. If TR = 20 ms, STEPS = 256, and NEX =1, then the image acquisition time would be 11 min. Reducing the field of view (FOV) will increase the spatial resolution but may require more signal acquisition time to maintain an adequate SNR.

2.3.3 Comparison of Magnetic Resonance Imaging with Different Non-Destructive Methods

Many agri-food industries are relying on the use of machine vision systems to solve various problems related to the post-harvest processing of agricultural products. Various

imaging techniques are currently available with their unique capabilities to study internal and external characteristics of agri-food materials. These include visible imaging, X-ray, X-ray computed tomography (CT), near-infrared (NIR) hyperspectral imaging, thermal imaging, and magnetic resonance imaging (MRI). All of these imaging techniques are based on different working principles. Of them, visible imaging, X-ray CT, NIR hyperspectral, and thermal imaging are based on working at specific wavelength ranges of the electromagnetic spectrum.

The visible imaging system consisting of cameras (monochrome or color) generates reflectance or transmittance characteristics from an object illuminated by a visible light source (typically 400-700 nm spectral range). The reflectance and transmittance light sources are used for extracting external and internal features, respectively. However, visible imaging is not efficient for determining intrinsic details. Comparatively more intrinsic details can be available by using an X-ray imaging system. An X-ray image is formed by penetrating high energy photons having 0.1-100 nm wavelength through an object. Two types of X-ray imaging are generally practiced in the agri-food industry; soft X-rays with 1 to 100 nm wavelength with less penetration power and hard X-rays (or X-ray CT) with 0.1-1 nm wavelength with more penetration power. The X-ray imaging technique provides images based on object density differences. However, X-ray imaging gives relatively little information compared to other techniques and also proper care should be exercised to avoid its harmful radiation effect.

Near-infrared (NIR) imaging is generated based on transmittance or reflectance characteristics of near-infrared light (700-2500 nm wavelength) propagated through an object. In NIR spectroscopy, concentration of NIR light absorbed molecules can be estimated. NIR imaging is a non-destructive and non-invasive method which not only quantifies chemical constituents but also gives intrinsic information of an object. However, for the proper functioning of the NIR system, large amounts of reference data are needed for calibration.

Thermal imaging is generated from the infrared radiation (700-1 nm) pattern of an object due to different thermal conductivity or thermal diffusivity values of the constituents. In other words, thermal imaging provides a surface temperature map of an object. Although this imaging technique is non-contact type, it requires the creation of a temperature difference in an object either by heating or cooling to get an indirect internal information. This requirement limits the use of this technique for studying biological products and process information.

MRI imaging is a non-invasive and non-destructive method which gives a map of an MR-active nucleus in an object when subjected to a magnetic field. Therefore, this technique can generate more intrinsic details of an object. Gonzalez et al. (2001) indicated that soft biological tissues are transparent to X-rays and opaque to radiation in NIR or visible spectra whereas MRI can visualize internal structural features. Comparison of image information received by adopting different machine vision technologies is shown in Fig. 2.5 for a wheat kernel.

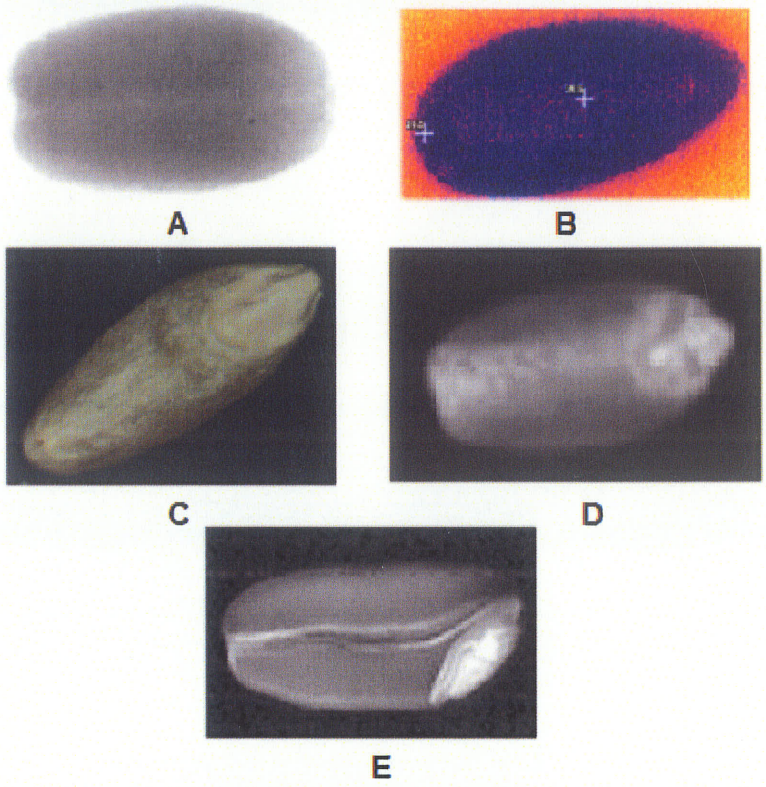

Figure 2.5 Images of a Canada Western Red Spring (CWRS) wheat kernel (cv. A.C. Barrie) acquired using different machine vision technologies, A – soft X-ray image (Karunakaran et al. 2004), B – thermal image (Manickavasagan et al. 2005), C – visible image, D – NIR image, E – MR image (Ghosh et al. 2006).

2.4 Applications of Magnetic Resonance Imaging in Agri-Food Operations

Agricultural products such as cereal grains, oilseeds, fruits and vegetables are susceptible to various biological and physiochemical changes during their harvesting, storage, and processing until they are consumed. A common goal of all the agricultural producers and food processing industries is to reduce the product loss and to maintain the product quality. Variability in growth and maturity of agricultural produce and development of internal defects can significantly affect their end use characteristics. Further, improper processing without knowledge of intrinsic mechanisms can result in poor quality end products and can cause economic loss. Often times agricultural and food industries experience significant economic loss due to improper handling and processing of agricultural commodities. Many destructive and non-destructive techniques are recently adopted by several agricultural and food industries in their processing operations to make a high quality product and to reduce the economic loss. Of all the techniques, machine vision is currently getting more attention for its potential to reveal intrinsic details. Working principles of some of the major machine vision techniques have been discussed in Section 2.3.4. Each technique has unique characteristics to solve specific problems. In agricultural products water and/or oil (or lipids) are the major constituents which are responsible for changes that occur at the growth or development stage or during processing operations. Of all the imaging techniques, Magnetic Resonance Imaging (MRI) is a unique tool which provides spatial information of the intrinsic phenomena in a biological product. Actual and accurate information derived from the MR imaging helps to solve various problems related to production, harvesting, storage, processing, grading and packaging of agricultural products. Although costs associated with this technique are

very high and the operation is complex compared to other imaging techniques, information available from MRI is very useful to determine correct processing parameters, to validate the existing models, and to develop accurate process models. Results of these studies can eventually help maintain both the quality of the product and the economy of the process. There is tremendous potential of using MRI as a tool to solve various problems associated with agricultural products and their processing operations. The following paragraphs briefly describe the published research related to agricultural products where MRI has been used.

2.4.1 Fruits and Vegetables

2.4.1.1 Evaluation of Internal Disorders

MRI has been used to observe internal physical structure and quality of some fruits and vegetables non-invasively. It has been used to assess internal bruises and storage disorders over time (apple: Chen et al. 1989, Zion et al. 1995, McCarthy et al. 1995; onion: Chen et al. 1989; peach: Chen et al. 1989; and pear: Chen et al. 1989), amount of water-core present (apple: Wang et al. 1988; and pear: Wang and Wang 1989, Lammertyn et al. 2003a,b), internal browning development during air-storage or controlled atmosphere (CA) storage (apple: Clark and Burmeister 1999, Gonzalez et al. 2001), void space or cavity formation (watermelon: Saito et al. 1996), mealiness assessment (apple: Barreiro et al. 1999, 2000; nectarine: Sonego et al. 1995; and peach: Barreiro et al. 2000), post harvest water loss (kiwifruit: Burdon and Clark 2001), ripening (avocado: Chen et al. 1989; grape: Andaur et al. 2004; kiwifruit: Ruan and Chen 1998, Clark et al. 1998; pineapple: Chen et al. 1989; raspberry: Williamson et al. 1991;

strawberry: Ruan and Chen 1998; and tomato: Chen et al. 1989, Ishida et al. 1989), worm damage and dry regions (orange: Chen et al. 1989; and pear: Chen et al. 1989) and freeze injury (peach: McCarthy and Kauten 1990; persimmon: Clark and Forbes 1994; potato: Sun et al. 1993; and zucchini squash: Wang and Wang 1992). Since all these quality parameters are associated with the concentration and state of water or oil to a certain extent, MRI has been successfully applied to localize water or oil distributions by varying different parameters within the imaging pulse sequences. The affected and unaffected tissues were easily detected qualitatively and quantitatively using image processing algorithms from the contrast of the MR images since proton density is directly proportional to signal or image intensity (brightness). For example, bruising tissues or tissues with water-core breakdown show high intensity due to high free water content or mobile protons; ripened or matured tissues show high intensity due to high water content; void spaces or cavities show zero intensity due to the absence of liquid water; brown tissues show low signal intensity corresponding to the regions with low free water content. A gray-scale MR image of a browning affected apple slice would display dark brown, normal and light brown tissues as black, dark grey and light grey, respectively.

2.4.1.2 Product Quality Determination

Measurement of deterioration in the quality factors of fruits and vegetables such as color, shape, size, texture, flavor, and vitamins prior-to and during processing is essential for maintaining marketability of the products. Drying of fruits and vegetables is one of such processing techniques, which is done normally to create dehydrated products to enhance the shelf life, to make them available during off-seasons and to use them in rehydrated

forms. Knowledge of actual moisture and temperature distribution as a function of drying time and accurate measurement of associated parameters (such as diffusion coefficient, convective heat- and mass-transfer coefficient, thermal conductivity etc.) is essential for modeling and process control. Perez et al. (1989) used MRI to determine the moisture transfer profiles during drying of an apple. McCarthy et al. (1991) estimated an effective moisture diffusion coefficient during the drying of apple by use of transient moisture profiles obtained from MRI. The diffusivity value was based on an agreement between the MRI-generated moisture profiles and mass transfer model-simulated moisture profile. Ruan et al. (1991) and Verstreken et al. (1998) followed the similar approach to estimate moisture diffusivity in potato and flesh and skin of an apple during drying using MRI. Freezing is another method of food preservation. Sugar in fruit tissues is an important constituent which is responsible for the alteration in food quality during maturation or processing. Gamble (1994) used MRI to study water and sugar distribution in blueberries before and after freezing. It was found that the freezing process can significantly alter the distribution of sugars in a fruit which affects the fruit quality. Fruit firmness is another important quality parameter which is usually measured from force-deformation data obtained by compressing the product. However, this technique is highly mechanical and is not able to provide information about the internal structural integrity of the product. MRI is shown to have potential to quantify force-deformation data from the firmness study of tomato using a compression technique (Gonzalez et al. 1998).

2.4.1.3 Temperature Mapping

Thermal processing of food materials is commonly practiced to control spoilage due to bacteria or micro-organisms. Variation in heating and development of hot and cold spots in food materials mostly occur due to non-uniform internal composition, shape and size of the product. Many different techniques have been adopted to determine the temperature distribution pattern during heating. These include the use of thermocouple or fibre optic probes which are destructive methods or the use of infra-red thermal imaging which can measure only the surface temperature. MRI has the potential to map the temperature distribution in three dimensions non-destructively during thermal processing of foods. Since the resonance frequency of water protons can be correlated with the temperature, the chemical shift of the water molecules can be used to map the temperature distribution. Sun et al. (1993) used half Fourier transform MRI of diffusion for temperature mapping of potato. Hulbert et al. (1995, 1997) tested T_1-weighted MR images to map temperature distributions and to determine a convective heat transfer coefficient during cooking of carrot. They reported that this technique is useful for accurate measurement of thermal properties and for thermal processing simulation studies but is highly dependent on the structure of the material.

Comprehensive literature reviews on the applications of MRI in the food related research with description of various imaging techniques is available from various excellent sources (Chen et al. 1989; McCarthy and Kauten 1990; Schrader et al. 1992; Simoneau et al. 1993; McCarthy and McCarthy 1994; Hills 1995; Schimdt et al. 1996; Ruan and Chen 1998; Koptyug and Sagdeev 2002).

2.4.2 Cereal Grains and Oilseeds

The MRI technique is getting increasing popularity as an alternative to other imaging techniques (visible images using line or area scan cameras, X-ray computed tomography, near infra-red, thermal imaging etc.) to solve various problems related to grains, oilseeds, and pulses (hereinafter collectively referred to as grains). This include studying dynamic phenomena that occur during processing and storage, water or oil mobility and distribution, diffusion, measurement of water, insect infestation. There is an ever increasing demand for grains to feed the growing world population. The grain industry would like to reduce the processing and storage losses to increase available grains for consumption. MRI has the potential for giving non-destructive and non-invasive continuous on-line images in two- or three- dimensions during grain handling, drying and storing. With recent technological advances in MRI, single grain kernels can be studied with the use of small probe with high sensitivity and resolution. The following paragraphs focus on the extensive research dealing with moisture measurement and transient moisture profiles of grains during drying and other processes that have been reported in the published literature. Table 2.2 provides a summary of the MRI techniques and associated parameters used to solve a variety of problems in grains and oilseeds.

2.4.2.1 Moisture Content Measurement

Conventionally grain moisture content is determined by the standard air oven method (ASAE 2003). This method is gravimetric and destructive that gives an average value of whole grain whose component parts have variable moisture content. Proper knowledge of moisture contents in individual grain components can improve the assessment of

Table 2.2 Summary of magnetic resonance imaging parameters in different techniques used in research related to grains and oilseeds.

Grain	Process	Technique	MRI parameters	Magnetic field (T)	Moisture level (% w.b.)	Source
Corn	Steeping at RT*	3D Gradient-focused echo or fast low-angle shot (FLASH)	TR: 0.05-0.20 s TE: 2.8-7.0 ms θ: 45°	4.7 (200 MHz)	35-39	Ruan and Litchfield (1992)
	Steeping at RT	3D Gradient-focused echo or fast low-angle shot (FLASH)	TR: 0.1 s TE: 1 ms θ: 40° Image acquisition time: 15 min	4.7 (200 MHz)	35-37	Ruan et al. (1992)
	Drying	3D Spin-Echo	TR: 36-73 ms TE: 2.9-3.2 ms Image acquisition time: 5 min	4.7 (200 MHz)	33-36	Song and Litchfield (1994)
	Drying	Spin-Echo	TR: 10 s TE: 28 ms Image acquisition time: 10 min 40 s	4.7 (200 MHz)	--	Song and Litchfield (1990)
	Drying	Spin-Echo	TR: 73 ms TE: 8 ms	4.7	36	Song et al. (1992)
	Drying	Spin-Echo	TR: 200 ms TE: 2.1 ms Image acquisition time: 7 min 48 s	(300 MHz)	53	Kovacs and Neményi (1999)
Wheat	Boiling and Steaming	Spin-echo	TR: 2 s TE: 2.2 ms	--	28-48	Stapley et al. (1997)
	No processing	3D Projection-reconstruction with Spin-Echo	TR: 500 ms TE: 2.66 ms Image acquisition time: 29.5 min	9.4	12	Song et al. (1998)
	No processing	Spin-Echo	TR: 2 s TE: 2.1 ms	(300 MHz)	--	Chua et al. (2004)
	Drying	Spin-Echo	TR: 50 ms TE: 11.4 ms	9.4	56-58	Turhan et al. (2001)
	No processing	Single Point Imaging (SPI)	TR: 10 ms TE: 2.7 ms	11.7 (500 MHz)	11-40	Gruwel et al. (2004)

Rice	Boiling	Multi-Spin-Echo CPMG	TE: 14-24 ms Image acquisition time: 40 min	4.7 (200 MHz)	42-76	Takeuchi et al. (1997)
	Cooking	3D RARE or Turbo-Spin-Echo	TR: 500 μs First TE: 6.6 Subsequent TE: 4.2 ms Image acquisition time: 1 min 4 s	0.7	--	Mohoric et al. (2004)
	Seed growth	Spin-Echo	TR: 0.5 s TE: 3.9 ms	7.1	--	Horigane et al. (2001)
	Drying	Constant Time Imaging (CTI)	TR: 50 ms θ: 16° Image acquisition time: 13 min 41 s	9.4 (400 MHz)	16	Frias et al. (2002)
	Drying	Single Point Imaging (SPI)	TR: 20 ms Image acquisition time: 10 min	(300 MHz)	17	Ishida et al. (2004)
	Cooking	Multi-Spin-Multi-Echo (MSME)	TR: 16 s TE: 4.5 ms	8.4 (360 MHz)	--	Kasai et al. (2005)
Barley	Seed growth	Spin-Echo	TR: 500 ms TE: 6.56 ms	7.1	--	Glidewell (2006)
	Imbibition	Spin-Echo	TE: 6.35 ms Image acquisition time: 17 min	(360.13 MHz)	--	Gruwel et al. (2002)
Oat	Imbibition	--	TR: 14.9 ms TE: 8.48 ms Image acquisition time: 6.4 min	8.45	--	Hou et al. (1997)

*RT: room temperature.

parameters associated with the processing operations and develop accurate models to maintain quality during grain storage and handling. Miller et al. (1980) found a good correlation of pulsed nuclear magnetic resonance (NMR) output with the standard air oven moisture content in the range of 15 to 40% (w.b.) for barley, corn, grain sorghum, and wheat. Brusewitz and Stone (1987) successfully measured moisture content of hard red winter wheat using a pulsed NMR-FID technique. In the FID technique, a short 90° RF pulse was applied to the sample. For this pulse, the NMR output signal decayed according to the binding state of water. The peak amplitude of the FID was proportional to the total hydrogen or water content in the sample. For moisture content (m, % w.b.) determination the equation considered is:

$$m = K \frac{V_2}{V_1} \tag{2.12}$$

where V_2 is the FID voltage at a selected time (V); V_1 the FID peak voltage (V); and K the calibration constant. The FID ratio V_2/V_1, at 58 μs was linearly correlated (R = 0.98) to wheat moisture content (7.9 to 16.4% w.b.) determined by the standard air oven method by the following equation:

$$\text{FID ratio} = 9.1 + 2.4\ m \tag{2.13}$$

NMR output was unaffected by grain mass bulk density and dockage content. In terms of repeatability and stability, the NMR method was more sensitive to moisture than currently used dielectric techniques. However, it was observed that NMR could not be used to determine moisture content below 7.5% w.b. because most of that moisture was presumed to be tightly bound water (Miller et al. 1980; Brusewitz and Stone 1987).

Chambers et al. (1989) determined moisture content of the component parts of individual wheat grains of two UK grown varieties, Maris Huntsman and Flanders. Moisture content was described by the following calibration model of typical NMR spectra to standard air oven moisture content (m = 3.3 to 19.6% w.b.):

$$m = -2.79\,X^2 + 14.13\,X + 1.88 \qquad (2.14)$$

where X = (NMR signal area)/(wet mass).

The NMR technique can produce signals from both liquid and solid components. As wheat consists mainly of both water and starch molecules, the NMR spectra obtained from the wheat kernels is asymmetric in nature and peaks of these signals shift to a higher magnetic field with the decreasing water content.

Tollner and Hung (1992) followed techniques used by Brusewitz and Stone (1987) to evaluate moisture content in wheat (Stacey), corn (DK677), soybean (Thomas), pecan (Stuart), and peanut (Florunner) by using a pulsed NMR-FID technique. Table 2.3 shows the equations developed to predict the moisture contents. They reported that the FID ratio compensated the variations in sample size, effect of electronic components and drift, and temperature changes in the magnet. Moisture prediction equations were linear for the cereal grains and second-order for the oilseeds since oilseeds have more oil content than cereals. High oil content in pecans (about 43% oil compared to about 20% moisture) and peanuts (about 29% oil compared to about 50% moisture) reduced the FID shape sensitivity to moisture content and therefore the coefficient of determination (R^2) for the

Table 2.3 Equations for moisture predictions (Tollner and Hung 1992).

Cereal grains	Moisture prediction equation	R^2	Oilseeds	Moisture prediction equation	R^2
Wheat	$4.31 + 52.75\frac{V_2}{V_1}$	0.91	Soybean	$31.82 - 17.5\frac{V_2}{V_1} + 222.6\left(\frac{V_2}{V_1}\right)^2$	0.89
Corn	$5.201 + 42.44\frac{V_2}{V_1}$	0.81	Pecan	$1.96 - 593.4\frac{V_2}{V_1} + 446.3\left(\frac{V_2}{V_1}\right)^2$	0.29
			Peanut	$5.937 - 1716.8\frac{V_2}{V_1} + 1231\left(\frac{V_2}{V_1}\right)$	0.73

V_2/V_1 is the FID ratio.

relationship between moisture and NMR variables describing FID shape were low for these two oilseeds.

2.4.2.2 Moisture Absorption Study

Different grains are processed differently for various end use purposes. Some of the processing techniques involve a significant absorption of moisture by the grains. For example, wet milling of corn, cooking or boiling of rice or wheat, steeping for malting barley. Knowledge of actual mechanics of moisture distribution during these operations and the effect of governing factors can improve the performance of the processing operations with increased production and reduced cost.

2.4.2.2.1 Corn

Ruan and Litchfield (1992) studied water mobility and distribution inside the corn kernel during room temperature steeping using three-dimensional MRI. Since the structure of a corn kernel is complex, values of spin-lattice relaxation time (T_1) and apparent spin-spin relaxation time (T_2^*) were different in the parts of the kernel (Table 2.4). The value of T_2^* depends on spin-spin interactions as well as the homogeneity of the external magnetic field. The value of T_2^* is always less than spin-spin relaxation time (T_2). Higher water mobility was observed in pericarp and germ, while the water in the endosperm showed the lowest mobility. It was also found that the moisture distribution was non-uniform and lower in the endosperm compared to the germ. Ruan et al. (1992) revealed a variation in apparent water content in corn components after measuring T_1 and T_2^* values (Table 2.5) and studied the effect of corn kernel components on the resistance of moisture movement

Table 2.4 Average values of T_1 and T_2^* of different parts of corn kernel during steeping (Ruan and Litchfield 1992).

Component	T_1(ms)	T_2^*(ms)
Germ	250	3.0
Endosperm	100	1.5
Pericarp	400	10.0

Table 2.5 T_1 and T_2^* of different parts of corn kernel (Ruan et al. 1992).

Component	T_1(s)	T_2^*(ms)
Germ	450	17
Endosperm	350	6.0

during steeping. They studied the moisture profiles obtained from the 2D MR images during steeping at 25°C and 53°C and observed that water diffused more slowly into the endosperm than into the germ, and that moisture transfer was non-uniform during the entire steeping process. Water absorption was slow at low steeping temperature. They indicated that the effective water diffusivity in corn increased with temperature.

2.4.2.2.2 Wheat

Stapley et al. (1997, 1998) used MRI to study and model the water ingress pattern during boiling and steaming of wheat (UK-grown Riband variety) from the moisture profiles of transverse cross sections. They mentioned a range of bulk T_1 times for raw wheat as 390-440 ms and provided the following relationship to measure T_2 in ms at different moisture content (m, % w.b.):

$$T_2 = -1.76 + 21.80\ m \qquad (2.5)$$

They also provided the following relationship between the average pixel intensity (I, arbitrary units) and the moisture content (w, decimal w.b.) as determined by a gravimetric method:

$$w = 0.11 + 0.09\ I \qquad (2.6)$$

Further, they compared T_2 measured by Eq. 2.5 with the T_2 measured by taking a series of images using different echo times and performing least square method using the equation:

$$I = I_o \exp\left(-\frac{TE}{T_2}\right) \quad (2.7)$$

where I_o is the pixel intensity at echo time (TE) = 0.

The values of T_2 in the inner region ranged from 3.5 ms to 4 ms whereas in the outer region T_2 was relatively high (between 7 ms and 8 ms). During boiling, water moved slowly towards the centre of the grain but steaming showed a homogenous distribution of water ingress. Further, the lowest signal was observed above 10% w.b. and T_2 of 2.2 ms. An activation energy for the steaming process was reported to be 40 kJ mol^{-1}. Song et al. (1998) studied the moisture distribution pattern in a mature wheat kernel containing 12% w.b. moisture content using 3D MR images. They observed that the moisture distribution was not uniform in the starchy endosperm and the moisture content of endosperm varied between 7.3% to 16.4% w.b. They reported bulk T_1 and T_2 of the wheat grain as 100 ms and 1.99 ms, respectively. However, T_2 of an intact wheat kernel was previously reported to be about 30 ms (Eccles et al. 1988; Jenner and Jones 1990).

2.4.2.2.3 Rice

Moisture distribution during rice boiling was visualized and modeled by Takeuchi et al. (1997) using 2D MRI. Their model was based on a simple diffusion phenomenon. Moisture ingress was asymmetrical during boiling and assumed to be influenced by starch gelatinization. The following equation was provided to measure T_2 in ms with respect to the moisture content (w, decimal w.b.):

$$T_2 = \exp(0.60 + 4.39\ w) \quad (2.8)$$

No MRI signal was detected below T_2 of 12 ms.

Horigane et al. (2001) performed MRI to study water distribution during the cooking of rice kernels. They described the reason of hollow or crack development inside the rice kernels during boiling. These hollows were generated due to a combined effect of concentrated gelatinized starch and volume expansion of rice kernels during boiling. This study showed the potential of MRI to evaluate cooked rice quality. Mohorič et al. (2004) also monitored moisture ingress patterns during rice boiling using a 3D RARE or Turbo-spin-echo MRI technique. They used Eq. 2.8 for T_2 determination and provided the following relationship between the NMR signal and moisture content (w, decimal w.b.):

$$\frac{I}{I_o} = w \exp\left(\frac{TE_{eff}}{T_2}\right) \tag{2.9}$$

where I_o is the initial signal intensity, arbitrary units; and TE_{eff} is the effective echo time for signals collected in RARE imaging.

Quantification of water content and its distribution during rice cooking was studied by Kasai et al. (2005) using MRI. Water content was measured from the following relationship with T_2 value in each pixel of T_2 images:

$$M = 0.25 \ln (0.68\, T_2) \tag{2.10}$$

where M is the water content in decimal, dry basis. Undercooked (32-37% w.b. moisture content), optimum cooked (37-44% w.b.), and overcooked (38-63% w.b.) rice kernels showed T_2 values of 10-17, 17-38 and 38-63 ms, respectively.

2.4.2.2.4 Barley

Steeping of barley in water is an essential initial step for the malting process. Barley hydration can be affected by its physical structure and enzymatic activities. MRI was used by McEntyre et al. (1998) to study the path of water ingress and its distribution during steeping of barley. An asymmetric nature of moisture absorption patterns was reported. Initial water uptake was found in the outer layers after which it was distributed in the germ, scutellum, and crushed cell and endosperm cavity regions. Gruwel et al. (2001) used proton NMR to study the pathways and dynamics of water uptake during the initial 7 h barley steeping process and reported that water uptake is proportional to $\sqrt{D\,t}$, where D is the water diffusivity and t is time. Variability in water uptake by the kernel was described by a viscosity model.

2.4.2.2.5 Oat

Hou et al. (1997) studied the imbibition of oat and indicated that during the initial period of imbibition (first 8 h), water uptake was more dominant in the germ-scutellar region. Water then penetrated into the endosperm region. They also tried mechanical scarification of the kernel to determine if the site of cutting enhanced the imbibition. Cutting closer to the germ resulted in rapid germ hydration.

2.4.2.2.6 Soybean

Water distribution in soybean seeds during 24 h of imbibition was observed by Pietrzak et al. (2002) using MRI. It has been observed that water penetration into the soybean is a

multistage process where it first fills the micropyle and hilum and then cotyledons, seed coat and embryonic axis.

2.4.2.3 Grain Drying Analysis

Drying of grains is an important operation for grain handling and storage. Researchers are working with the heat and mass transfer phenomena during grain drying with a view of increasing efficiency, in other words, reducing drying costs in full-scale dryers. However, for modeling the drying phenomena, one needs to understand the underlying mechanisms. MRI can be used to obtain two- or three-dimensional moisture transfer patterns inside a single grain kernel during drying. Little work has been carried out to determine transient moisture transfer inside the grain kernels during the drying process.

2.4.2.3.1 Corn

The first experiment of this kind was reported by Song and Litchfield (1990) who used MRI to quantify mass transfer such as the transient moisture movement in the ears of corn based on image pixel intensities during hot air drying at 60°C with an air velocity of 1.8 m s^{-1} for 5 h. Trends of moisture loss from different parts of corn kernels were visually investigated from MR image sequences since brightness of the image is directly proportional to the proton density and hence the moisture content. One-dimensional transient moisture profiles were plotted from the MRI data, and changes in moisture distribution (with respect to both time and space) were quantified from the sequential images. The values of T_1 for endosperm and germ were 1.9 s and 0.7 s, respectively, and the values of T_2 for endosperm and germ were 11 ms and 8 ms, respectively. Moisture

distribution and changes inside the corn cobs were distinctly different and non-uniform during the drying process. Initial moisture content in the germ was reported higher than that in the endosperm. Song et al. (1992) visually examined a series of MR images to investigate moisture transfer and distribution from and within a corn kernel during drying at 27°C and 49°C at an air velocity of 5 m s^{-1} for 3 h and 1 h, respectively. A series of proton density images of one central slice was evaluated. It was determined that the moisture distribution in the kernels was non-uniform. Moisture loss also differed significantly during drying through two primary routes: the glandular layer of the scutellum and the pericarp. T_1 and T_2 were 0.4-0.6 ms and 4-5 ms, respectively. Kovács and Neményi (1999) collected MR images of corn kernels during drying at 46°C with an air velocity of 1.4 m s^{-1} for 4.5 h. They performed a moisture gradient vector analysis to demonstrate the pathways of moisture loss from the corn kernel. T_2 of scutellum, pericarp and endosperm were measured as 21.9 ms, 13.9 ms, and 9.1 ms, respectively using Eq. 2.9. An image subtraction method was used to study the real moisture loss from the whole kernel using sequential images. Moisture distribution inside the whole kernel was not uniform prior-to and during drying. Moisture loss was faster from the endosperm than that from the pericarp and it was the slowest from the scutellum.

2.4.2.3.2 Wheat

Turhan et al. (2001) used MRI to differentiate the moisture movement patterns during drying of gelatinized soft and hard wheat kernels at 40 to 100°C with an air velocity of 2.5-3 m s^{-1}. They reported that the moisture distribution was non-uniform at the beginning of drying and actual water transport did not follow Fick's diffusion theory due

to their inherent composition and micro-structural differences. Hard wheat kernels dried relatively slower than the soft wheat kernels because the hard wheat kernels contain a strong protein and starch matrix which offers more resistance to water movement.

2.4.2.3.3 Barley

Gruwel et al. (2002) showed that MRI could be a valuable tool to study kilning, the final stage of barley malting process, when the seed moisture is dried quickly from 43 to 4% w.b. Quick drying can result in an uneven drying with disperse moisture concentration in the seed. MRI gave an insight into the actual water distribution within the kernel during kilning.

2.4.2.3.4 Rice

Moisture distribution pattern during rice (16% w.b. moisture content) drying at 30°C and 60°C at an air velocity of 0.9 m s^{-1} was modeled by Frías et al. (2002) from the moisture profiles obtained with a 'constant time imaging' (CTI) technique. This technique allows the acquisition of images from low moisture content and mobility samples. Their model was based on the simple diffusion phenomena in an infinite cylinder considering shrinkage during drying. Since the model considered a simple geometry and the effect of lipid was neglected, certain limitations in the model predictions were visible. Loss of moisture from harvested rough rice seeds (17% w.b. moisture content) at various drying temperatures (40-70°C) was visualized by Ishida et al. (2004). They used a 'single point imaging' (SPI) technique to obtain images from low moisture seeds having short T_2 (in this case, T_2 was less than 1 ms). Moisture transfer during drying was non-uniform inside

the rice grain, where germ and endosperm contained more moisture than the husk. Further, during drying the rate of water loss was faster from the outer region than from the central region of a rice kernel. Moisture loss agreed with the following well-known equation for the spherical model of drying materials:

$$\frac{M - M_e}{M_o - M_e} = \left(\frac{6}{\pi^2}\right)\sum_{n=1}^{\infty}\left(\frac{1}{n^2}\right)\exp(-Kn^2t) \qquad (2.11)$$

where M is the dry basis moisture content (decimal); M_o is the initial dry basis moisture content (decimal); M_e is the equilibrium dry basis moisture content (decimal); K is the rate constant (min^{-1}); and t is the drying time (min). It was further observed from their study that MRI can also detect the time, location, and nature of structural changes such as the stress-cracks during drying. In this case, stress-cracks were visualized at 70°C, which is an important consideration for grain quality control. They reported an overall activation energy of the drying process as 63 kJ mol^{-1}.

2.4.2.4 Drying Induced Stress Crack Development

Stress cracks in grains are usually developed during drying. During drying, grains containing a high moisture content typically develop stress cracks due to a high moisture or temperature gradient. Corn and rice are highly susceptible to stress cracks compared to wheat. However, stress crack development should not occur to ensure high product quality. Development of stress cracks has several disadvantages: grains show poor germination rate, become highly susceptible to insect or microbial attack, yield less starch, and create hazardous dust which can cause explosions.

2.4.2.4.1 Maize

Song and Litchfield (1990) studied drying induced stress cracks in maize kernels by MRI. They studied the effect of moisture and temperature gradients as well as varietal influence on the formation of stress cracks. Stress cracks developed in the vitreous endosperm regions with high moisture gradients during high temperature drying.

2.4.2.4.2 Soybean

Zeng et al. (1996) indicated from their MRI study that during soybean drying high moisture gradients are produced in the seedcoat resulting in more cracks than in the cotyledons.

2.4.2.5 Grain Kernel Characterization

Knowledge of moisture and oil content and their distribution inside the kernels is important for process optimization and quality preservation. For example, moisture and oil contents influence grain germination rate, storage life, and milling processes. Observation of moisture or oil movement, distribution, and their localization in a structurally complex grain kernel is, therefore, necessary.

2.4.2.5.1 Wheat

Jenner et al. (1988) first reported *in-vivo* water movement in developing wheat using MR micro-imaging. The bulk T_2 value reported was 20 ms. They reported an overall water diffusion coefficient of 8.3×10^{-10} m^2 s^{-1}. Chua et al. (2004) used MRI to study the distribution of water and oil in wheat kernels. They reported that oil is mainly

concentrated in germ whereas water dominates overall liquid composition of the wheat grain. Gruwel et al. (2004) have recently shown the advantage of using SPI to obtain an image of the water distribution of both a highly hydrated (40% w.b.) and very dry wheat kernel (11% w.b.). They described this technique as "a pure phase encoding technique in which a single point of the magnetic resonance signal is acquired after a short encoding time in the presence of a gradient" which can produce images from rapidly decaying signals. They further mentioned that 3D reconstruction of the MR image data can provide information on any structural-imperfections.

2.4.2.5.2 Maize

Ratković (1987) studied the state of water in maize at various moisture contents (5-50% w.b.) from proton NMR T_1 relaxation time calculations. They observed that T_1 was more influenced by signal coming from endosperm water than that from the germ which contains both oil and water. However, T_1 could not be measured below 5-7% w.b. moisture content due to the absence of 'free' water.

2.4.2.5.3 Barley

MRI has also been used to study the morphological development of grains from the moisture distribution patterns in barley (Glidewell 2006). Gruwel et al. (2002) used MRI to distinguish viable and non-viable malting barley kernels and identified that low levels of sprouting before or after harvesting is responsible for the loss of viability during storage.

2.4.2.5.4 Rice

Moisture distribution in developing rice caryopses was visualized by Horigane et al. (2001).

2.4.2.6 Water and Oil Diffusion

2.4.2.6.1 Wheat

Diffusion of water in wheat endosperm has been studied by Callaghan et al. (1979). They used a 'pulsed field gradient NMR' (PFG-NMR) technique and reported that the water diffusivity is function of the water content levels in the grain. The PFG-NMR method involves the formation of a spin-echo using two field-gradient pulses separated by a 180° RF pulse. Water diffusivity in wheat endosperm was reported to be varying from 2×10^{-10} m^2 s^{-1} to 12×10^{-10} m^2 s^{-1} for moisture content in the range of 88-98% relative humidity. Eccles et al. (1988) used the same technique to study the localized water diffusivity in wheat kernel components. They observed a linear trend of decreasing MR signal amplitude with increasing strength of pulsed field gradient for a fairly wet wheat kernel (53% w.b.). The rate of decrease in signal amplitude is related to the water diffusivity. The diffusivity (diffusion time 5 ms) of different regions of the endosperm varied between 5×10^{-10} m^2 s^{-1} to 10×10^{-10} m^2 s^{-1}, the endosperm cavity or the pigment strand area was 11×10^{-10} m^2 s^{-1}, and the pericarp and aleurone layer was 9×10^{-10} m^2 s^{-1}. Jenner and Jones (1990) compared water diffusivity of an untreated wheat kernel with that of a frozen and thawed kernel using PFG-NMR. They reported that water diffusivity of untreated wheat ranged between 7×10^{-10} m^2 s^{-1} and 9×10^{-10} m^2 s^{-1} whereas that of frozen and then thawed grains was much higher which ranged between 14×10^{-10} m^2 s^{-1}

to 16×10^{-10} m^2 s^{-1}. The higher diffusivity in frozen and then thawed grains was due to ruptured cell membranes, plastids and other cytoplasmic organelles that hindered the diffusive motion of water. However, they did not report on the moisture movement pattern in the germ. Stapley et al. (1998) determined the diffusivity (diffusion times 20, 100, and 400 ms) during soaking and cooking of wheat using PFG-NMR. They reported a faster diffusivity in the outer layers (a maximum of 3×10^{-10} m^2 s^{-1}) and slower diffusivity in the inner portion (an average of 0.001×10^{-10} m^2 s^{-1} during soaking and 3×10^{-10} m^2 s^{-1} during cooking).

2.4.2.6.2 Maize

Bačić et al. (1992) measured diffusivity of oil in dry maize kernels using PFG-NMR. They reported that oil diffusivity in maize can vary between 0.01×10^{-10} m^2 s^{-1} and 0.04×10^{-10} m^2 s^{-1}. The diffusivity was measured at 5 ms and 20 ms.

A comprehensive literature review about the measurement of moisture diffusion in foods using PFG-NMR method is given by Watanabe and Fukuoka (1992).

2.4.2.7 Insect Infestation

Protecting grains from spoilage due to insect infestation is essential for the survival of mankind. Insect and mite-infested crops in storage quickly lose weight and quality resulting in farmers losing income and reduction in the available grains for consumption.

2.4.2.7.1 Wheat

Chambers et al. (1984) studied the development and detection of the grain weevil, *Sitophilus granarius* (L.) hidden within individual wheat grains using NMR spectroscopy. Although the method could not detect the insects until in its third-larval instar, it measured the water content of wheat which is relevant to the survival of stored-product insects. This method can identify ten kernels infested with *S. granarius* larvae in a bulk wheat sample of 500 kernels.

2.5 Grain Drying

Globally around 2.4 billion tonnes (Gt) of grains, oilseeds, and legumes (hereinafter referred to as grains) are produced annually (FAOSTAT 2006). The grains need to be stored safely until consumed. Safe storage of grains can be accomplished by manipulating two important physical factors: temperature and moisture content (Fig. 2.6), provided the grains are not invaded by insects, mites, rodents, or birds (Jayas et al. 1995). Grains stored at high moisture and high temperature spoil fast (Fig. 2.6). The spoilage can be measured by several factors including the end use of the grain. But a drop in germination, presence of visible mould, increase in free fatty acids, amount of carbon dioxide produced, or a combination of two or more of these factors are commonly used as spoilage indices. A drop in germination seems to occur first and therefore, is considered as the most sensitive parameter. The width of the short-term storage zone and values for the axes labels for temperature and moisture content in Figure 2.6 are dependent on the type of grain and the factor being used to measure spoilage. For example, the moisture

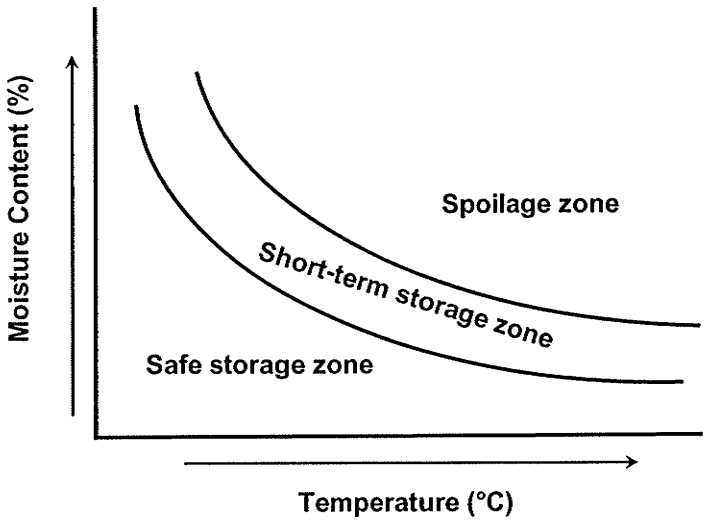

Figure 2.6 Relationship between temperature and moisture content for safe storage of grain (Source: Jayas and Ghosh 2006).

content for storing wheat safely for more than a year under a temperate climate is 12-13% w.b. but for canola (an oilseed crop) it is 8-9% w.b.

Grains are usually harvested at a high moisture level to avoid shattering losses and to reduce the growing season in order to grow two or more crops in a year. Sometimes, undesirable rain also forces the farmers to harvest the grains at a high moisture level. Therefore, drying is a common practice to artificially remove moisture from the harvested grain by forcing air at different temperatures to attain moisture content for safe storage. Thus quality of the stored grain is maintained. A list of safe storage moisture contents for storing grains up to one year on the Canadian prairies is given in Table 2.6 (CGC 1993). Drying of grains prevents microbial growth and slows enzymatic changes and considerably increases the storage life. It also reduces grain mass; thus, facilitating its transportation, and handling. In most years and in most countries drying of grains is commonly accomplished by forcing air through the bulk grain at different temperatures: natural (ambient) temperature, near-ambient temperature, low temperature, or high temperature and by using the dryeration technique. During the natural-air drying, ambient air is used without heating to remove the excess moisture from the grain. In near-ambient drying, the temperature of the ambient air is raised by 1 to 5°C from frictional losses of the fan and motor assembly. In low temperature drying, the ambient air is heated by 5 to15°C using external sources of energy (e.g., electricity, fossil fuels, solar energy). In high temperature drying, air is usually heated to about 50 to 200°C based on the initial moisture content of the grain, the end use of the dried grains, and the type of dryer. Maximum temperatures of grain during drying for different end uses are given in Table

Table 2.6 Upper limit of safe moisture contents for storing grain up to one year under Canadian prairies (Compiled from CGC 1993).

Crop	Moisture Content[a] (% w.b.)
Wheat	14.5
Oats	14.0
Barley	14.8
Rye	14.0
Flaxseed	10.0
Canola and rapeseed	10.0
Mustard seed	9.5
Peas	16.0
Lentils	14.0
Fava Beans	16.0
Buckwheat	16.0
Triticale	14.0
Corn	15.5
Soybeans	14.0
Sunflower seed	9.5
Safflower seed	9.5

[a]For long-term storage (>1 year) in well-engineered structures, the moisture content should be 1 to 3 percentage points less than the values listed in this table.

2.7 (Hall 1980). In all high temperature dryers which use hot air to dry grain heat is mainly transferred by convection from air to grain and by conduction within grain. Air is also used to carry the removed moisture. The dryeration process or combination drying consisting of high-temperature drying and aeration, is an advantageous process since grains can be exposed to the high temperature drying followed by tempering and then cooling using aeration. Stress-cracks development is reduced due to the tempering process (Cnossen and Siebenmorgen 2000). Aeration allows the maintenance of a uniform grain temperature which helps in reducing the moisture migration inside the grain bulk due to temperature differences. It further helps in removing unpleasant odors and in venting fumigants. The dryeration process is thermally more efficient than conventional drying and rapid cooling and results in better quality grain than high temperature drying for the removal of the same amount of moisture.

2.5.1 Control

Grain drying has significant effects on the quality of grains (e.g., head yield of rice, cracking of corn, milling and baking qualities of wheat, and oil content from oilseeds). To maintain the grain quality after drying and to maximize throughput at optimal energy efficiency, different control strategies have to be adopted for the operation of different dryers. During natural air and near-ambient drying detrimental effects on grain quality can be avoided if drying can be completed within the allowable safe storage time which depends on the initial moisture content of grain and weather conditions. Further, in near-ambient air drying, the amount of airflow needed to dry grain depends on the grain type, the grain volume, harvest date and initial moisture content of the grain. The airflow can

Table 2.7 Maximum safe temperature (°C) of grain during drying for various end uses (Hall 1980).

Crop	End Use		
	Seed	Sold for Commercial Use	Animal Feed
Ear Corn	43	54	82
Shelled corn	43	54	82
Wheat	43	60	82
Oats	43	60	82
Barley	41	41	82
Sorghum	43	60	82
Soybeans	43	49	
Rice	43	43	
Peanuts	32	32	

be controlled using a simple on-off switch based on the time of the day to more sophisticated systems taking into consideration the progress of drying and the changing weather conditions (Ryniecki et al. 1993a,b; Epp et al. 1997). Since intermittent airflow can cause severe increase in the dry matter loss, continuous airflow is recommended until the drying front reaches the surface of the grain bed after which airflow can be controlled to maintain the grain moisture content. During high temperature drying detrimental effects on grain quality can be avoided if grain is not heated beyond a critical temperature. If grain is heated beyond its critical temperature due to dryer type or improper functioning of the dryer then end use characteristics of grain can be severely affected. In high-temperature dryers, several parameters such as grain discharge rate, drying air temperature, airflow rate, and grain temperature at the dryer discharge affect the target moisture content. Altering the grain discharge rate is a commonly used practice to effectively control the moisture content of the grain. Measurement of discharge grain temperature is also used for controlling grain dryers. Care, however, must be exercised so that the temperature sensor is not exposed to wind or to solar radiation. Exposure of the sensor to wind will decrease the sensed temperature and could result in over drying of grain whereas exposure of the sensor to solar radiation could halt the drying too early. In-line moisture sensors which can accurately sense the moisture of hot grain would be the best way to control the dryers but such sensors are not yet available. Therefore, in high temperature dryers, effective heater control is an essential design consideration. Different dryer control systems are explained by Brooker et al. (1992). A model predictive controller for industrial cross-flow grain dryers has been developed by Liu and Bakker-Arkema (2001) for better accuracy and stability. There is an increasing demand to

optimize the dryer control strategy to maintain grain quality, uniformity of drying with efficient energy use considering variable environmental conditions.

2.5.2 Effect of Drying on Grain Quality

Grain quality cannot be defined specifically for a particular grain. Several factors such as uniformity and soundness of the kernels, test weight, amount of foreign material in grain, and breakage susceptibility are used to characterize grain quality for a particular end use of a grain type. For example, for bread wheat, milling and baking characteristics are important; for corn yield of grits and flour during dry milling and yield of starch during wet milling are important; for malting barley, germination is important; for paddy, head-rice yield is important; for pulses, quality of protein and cooking time are important; and for oilseeds, yield and quality of oil are important. Test weight, physical damage, stress-crack susceptibility, milling and baking characteristics, oil quality, and head-rice yield can be adversely affected by improper drying using high temperature air, and the expected effect is briefly described below.

The test weight of grain is expressed as the mass of grain required to fill a standard volume and is expressed as kg hL^{-1} (lb bu^{-1}). Although test weight may not be the best indicator of the end use quality, higher test weight usually implies better quality and it is easy to measure, therefore, it is used in grain grading standards. Test weight is a function of grain moisture content. Grain harvested at high moisture and dried properly gives higher test weight than field dried grain of the same moisture content. But damaged grain due to unacceptable heating gives lower test weight (Brooker et al. 1992).

Physical damage, e.g. breakage, discoloration or shrinkage are very important issues associated with the drying of grain to maintain acceptable quality standards. The high speed of drying in the heated-air dryers may cause damage to the grain kernels. Interior or exterior stress cracks develop in the grain kernels due to the creation of temperature and moisture gradients during drying which cause an adverse effect on oil or starch recovery (Watkins and Maier 2001). Head-rice yield is reduced due to an increased number of stress cracks while yellowing of rice is more due to improper drying (Cnossen and Siebenmorgen 2000). Keeping oilseeds at high temperature results in darker oil causing an increase in refining cost. Brooker et al. (1992) classified stress cracks as single, multiple, or checked with two or more intersecting cracks. Montross et al. (1999) showed that the number of these cracks for corn dried in mixed-flow, cross-flow and 3-stage concurrent-flow dryers were different (Table 2.8). In a cross-flow dryer, the breakage susceptibility of corn is high near the air inlet of the grain column (Table 2.9) and increases with a decrease in the average final moisture content to which corn is to be dried (Table 2.10). Stress-cracking is not prevalent in the small grains (e.g, wheat, barley, oats, and rapeseed) (Nellist and Bruce 1995). Removing moisture from grain in small increments, tempering grain or both reduce stress cracks.

Milling processes separate the grain components for further processing into usable products. For example, milled wheat flour is used in baking. Drying at too high temperature of wheat kernels can cause denaturation of the gluten proteins which adversely affects the baking quality. The major quality criterion for wheat is loaf volume which is decreased if wheat is heated beyond its safe temperature.

Table 2.8 Average type of stress cracks and stress cracked percentage of corn dried in three types of dryers (Montross et al. 1999).

Dryer types	Single (%)	Multiple (%)	Checked (%)	Stress-cracked (%)
Cross-flow	3.4	38.6	45.8	87.8
Mixed-flow	8.0	32.5	25.0	65.5
3-Stage Concurrent-flow	5.8	27.1	19.7	52.6

Table 2.9 Grain temperature, moisture content, and breakage susceptibility at different locations in grain columns of a conventional cross-flow dryer after drying corn without cooling from 25.5% to an average of 19% (w.b.) at 110°C (Brooker et al. 1992).

Distance from Air Inlet (cm)	Grain Temperature (°C)	Moisture Content (% w.b.)	Breakage Susceptibility (%)
1.25	102	10	48
7.50	78	20	11
13.75	51	24	10

Table 2.10 Effect of the average final moisture content on breakage susceptibility of 25% moisture content (w.b.) corn dried in a conventional cross flow dryer at 110°C (Brooker et al. 1992).

Final Average Moisture Content (% w.b.)	Breakage Susceptibility (%)
18	11
15	18
13	27
11	39

Excessively high temperature kills the germ and results in reduced germination capacity. Poor germinating seeds have detrimental effects on their end uses (e.g., in malting of barley or for seed purposes). Safe drying temperature can be decided based on the initial moisture content of the grain and the residence time in the dryer. Recommended drying temperature range to maintain seed viability is about 38-43°C (Table 2.7). Seed damage usually occurs when grain temperature exceeds the critical grain temperature. The highly moist kernels can retain their viability when dried in a concurrent-flow dryer even at a higher temperature drying since the kernels do not reach the high temperature.

2.5.3 Need of Grain Drying Models

Most commercial high capacity grain dryer units are interfaced with a computer control system which maintains the residence time of the grain in the dryer to obtain improved grain quality and achieve the target moisture content without over-drying (wasted energy and reduced dry grain weight) or under-drying (unmarketable grain). Computer simulations of different grain drying models play a significant role in optimizing the dryer control strategy with efficient drying to maintain grain quality. Mathematical modeling of grain drying not only helps in understanding the physics of drying but also helps in studying the dryer operations (Sharp et al. 1982). Simulation studies of grain drying depend upon simultaneous heat and moisture distribution inside the grain mass modeling. Grain drying is usually accomplished either in a thin-layer (a single grain kernel or one layer of grain kernels or a polylayer of many grain thickness) or in a deep-bed (more than 20 cm deep). Most of the earlier grain drying models were empirical or semi-empirical in nature mostly considering thin layer drying. These models may not

always accurately give the heat and moisture transfer in deep-bed analysis (Sharp et al. 1982). This problem was solved by the development of complex partial differential equation (p.d.e.) – based models. Sharp et al. (1982) further indicated the use of numerical integration methods to solve the set of p.d.e. for layer by layer for a deep bed of grain in which each layer may be assumed to be of a uniform grain moisture content and temperature. Various semi-theoretical and empirical models describing the thin-layer as well as the deep-bed drying process for specific grains have already been reviewed and compared (Jayas et al. 1991; Cenkowski et al. 1993; Pabis et al. 1998; Parde et al. 2003; Ghosh et al., 2004). A number of equilibrium moisture content (e.m.c.) equations of theoretical, semi-theoretical, and empirical forms to obtain the e.m.c. data needed to solve the drying models have been compiled and compared by Sun and Woods (1993) and Parde et al. (2003). The standard equilibrium moisture content (e.m.c.) - equilibrium relative humidity (e.r.h.) relationships for the particular crops are available from the ASAE Standard D245.5 (ASAE 1995).

Published thin-layer or deep-bed drying models cannot predict the internal moisture and temperature variations and their distribution within individual grain kernels as a function of drying time. Since cereal grains are hygroscopic capillary porous materials and drying can generate considerable temperature and moisture gradients in the grains, hydro-thermal stress can develop which deteriorates the grain quality in many ways. Improper drying due to lack of knowledge about internal moisture and temperature distribution inside the grain kernels can significantly deteriorates the quality of grain.

Internal mass (moisture) transfer in wheat or other cereal grains during drying is driven by concentration gradients resulting from liquid or vapour diffusion or their combination (corn: Hall and Rodrigues-Arias 1958, Hustrulid and Flikke 1959, Allen 1960, Pabis and Henderson 1961, Chittenden and Hustrulid 1966, Chu and Hustrulid 1968a,b, Fortes and Okos 1978, Sokhansanj and Gustafson 1980, Walton et al. 1988, Czaba and Neményi 1997, Neményi et al. 2000; rice: Allen 1960, Husain et al. 1973, Sokhansanj and Gustafson 1980, Steffe and Singh 1982, Yang et al. 2002; and wheat: Babbitt 1949, Simmonds et al. 1953, Becker and Sallans 1955, Becker 1959, Watson and Bhargava 1974, Fortes et al. 1981, Jia et al. 2000). Simmonds et al. (1953) indicated that capillary forces play a minor role in the mass transfer during wheat drying.

2.5.4 Drying Theories and Models

Since grains are heterogeneous in structure, drying process becomes a complex phenomenon of simultaneous heat and mass transfer. In recent years, with the advent of powerful computers, single grain kernel drying has been simulated by simultaneous heat and mass transfer models considering various moisture transfer phenomena and the geometrical shape (barley: Haghighi et al. 1990, Irudayaraj et al. 1992, Miketinac et al. 1992; corn: Sokhansanj and Gustafson 1980, Irudayaraj et al. 1992, Czaba and Neményi 1997, Neményi et al. 2000; rice: Husain et al. 1973, Sokhansanj and Gustafson 1980, Yang et al. 2002, Wu et al. 2004; and wheat: Jia et al. 2000). Published models of this kind were developed based on either constant material properties or a simple one-dimensional or two-dimensional geometry. These models were developed to accurately describe temperature and moisture distributions within a single grain kernel during

drying. All of these models were solved numerically mostly involving the finite element method (FEM), in which the moisture content distribution was approximated by a discrete model composed of a set of piecewise continuous functions defined over a finite number of sub-domains or elements (Segerlind 1984). The following paragraphs discuss some of the published models to determine simultaneous heat and mass transfer during drying of single grain kernels.

2.5.4.1 Simultaneous Heat and Mass Transfer Equations

The earlier approach of Luikov's (1966) coupled system of partial differential equations for predicting the interaction between heat and mass transfer in capillary porous bodies is:

$$\frac{\partial M}{\partial t} = K_{11} \nabla^2 M + K_{12} \nabla^2 T \qquad (2.12a)$$

$$\frac{\partial T}{\partial t} = K_{21} \nabla^2 M + K_{22} \nabla^2 T \qquad (2.12b)$$

where M is the moisture content, decimal, d.b.; t is the time, h ; T is the temperature, °C; K_{11} and K_{22} are phenomenological coefficients; and the other K values (i.e., K_{12} or K_{21}) are coupling coefficients.

Husain et al. (1973) proposed a system of non-linear coupled heat and moisture transfer model very similar to the Luikov's equations based on variable diffusion coefficient. The system of equations is as follows:

$$\frac{\partial M}{\partial t} = D \nabla^2 M + \frac{\partial D}{\partial M} (\text{grad } M)^2 + D \delta \nabla^2 T + \frac{\partial D}{\partial M} (\nabla M) \nabla (T) \qquad (2.13a)$$

$$\frac{\partial T}{\partial t} = \alpha \nabla^2 T + K \frac{\partial M}{\partial t} \qquad (2.13b)$$

where D is the variable diffusion coefficient ($m^2 s^{-1}$); δ is the thermo-gradient coefficient ($^oC^{-1}$); α is the thermal diffusivity ($m^2 s^{-1}$); and $K = L\varepsilon C^{-1}$, where, L is the latent heat of vaporization of water (kJ kg^{-1}); ε is the coefficient of internal evaporation; and C is the specific heat (kJ kg^{-1} $^oC^{-1}$). The model was numerically solved to predicting thin-layer drying behavior of rough rice.

Sokhansanj and Gustafson (1980) have assumed that cereal grain drying is an isothermal process (Bakker-Arkema et al. 1977) and moisture movement inside a grain kernel occurs due to vapour diffusion. The following two-dimensional coupled heat and mass transfer equations (Cartesian coordinates) were solved using the finite element method to describe moisture and temperature distributions within a single corn and rice kernel during drying:

Mass transfer equation:

$$\frac{\partial M}{\partial t} = D\left(\frac{\partial^2 M}{\partial x^2} + \frac{\partial^2 M}{\partial y^2}\right) \qquad (2.14)$$

Heat transfer equation:

$$C_g \frac{\partial T}{\partial t} = K\left(\frac{\partial^2 T}{\partial x^2} + \frac{\partial^2 T}{\partial y^2}\right) + L\rho_g \frac{\partial M}{\partial t} \qquad (2.15)$$

Initial conditions:

$$M(x, y, t = 0) = M_o \qquad (2.16)$$

$$T(x, y, t = 0) = T_o \qquad (2.17)$$

Boundary conditions:

$$\left(l_x \frac{\partial M}{\partial x} + l_y \frac{\partial M}{\partial y} \right)\Bigg|_s = h_m (M_s - M_e) \tag{2.18}$$

$$\left(l_x \frac{\partial T}{\partial x} + l_y \frac{\partial T}{\partial y} \right)\Bigg|_s = h_t (T_s - T_a) \tag{2.19}$$

where M is the dry basis moisture content (decimal); t is the time (h); D is the diffusivity ($m^2\ s^{-1}$); C_g is the specific heat of grain (kJ kg^{-1} $^oC^{-1}$); T is the temperature (^oC); K is the thermal conductivity (W m^{-1} K^{-1}); L is the latent heat of vaporization of water (kJ kg^{-1}); l_x and l_y are the direction cosines; s is the surface; ρ_g is the grain density (kg m^{-3}); h_m is the mass transfer coefficient (m s^{-1}); h_t is the heat transfer coefficient (W m^{-2} K^{-1}); T_s is the surface temperature (^oC); and T_a is the ambient temperature (^oC).

The grain kernels (corn or rice) were divided into two-dimensional triangular elements and the moisture and temperature distributions were approximated for each element following Segerlind's approach (1984). The mass distribution pattern indicated that the diffusion coefficient is a function of moisture and temperature and it has dependency on the grain structural components, e.g., pericarp, endosperm, and germ or embryo. The presence of the coupling factor $\left(\frac{\partial M}{\partial t} \right)$ on the heat transfer equation (or, the vapour diffusion effect) was analyzed in view of its effect on the heat distribution inside the kernel. This factor was more pronounced at the later stages of drying (for large moisture gradient) compared to the early stages. For rice drying, maximum heat and mass transfer gradients were found at the interface of the pericarp and the endosperm of the kernel thus suggesting a maximum hydro-thermal stress at that location.

Misra and Young (1980) have investigated the effect of density and concentration on the mass diffusivity including the effect of linear shrinkage in order to study the moisture distribution pattern during the soybean drying. They hypothesized that the moisture difference, which was a function of the liquid concentration gradient, increases exponentially with the increase in the concentration gradient and uniform moisture flow resistance inside the kernel. They used the finite element technique to solve the following set of equations considering the soybean a spherical body:

Moisture transfer equation:

$$\frac{\partial M}{\partial t} = \frac{1}{r^2}\frac{\partial}{\partial r}\left(r^2 D \frac{\partial M}{\partial r}\right) \tag{2.20}$$

Initial condition: $(0 \le r \le R)$

$$\text{at } t = 0, M = M_o(r) \tag{2.21}$$

Boundary condition:

$$-\left(D\frac{\partial M}{\partial r}\right)\Big|_R = h_m (M_s - M_o) \tag{2.22}$$

where r is the radius of grain (m); M_s is the dry basis moisture at the surface (decimal); M_o is the initial dry basis moisture content (decimal).

Fortes et al. (1981) reported that heat and moisture transfer in a hygroscopic capillary-porous medium (a wheat kernel) during drying and rewetting is a complex process due to various factors. These factors are: variety, maturity, field conditions, geometry, and anisotropy. Although many researchers have assumed liquid diffusion with isothermal conditions to be a predominant factor for grain drying, Fortes et al. (1981) suggested considering three major factors in combination: moving evaporation front towards the

surface of the grain, a vaporization-condensation process, and a coupling between heat and mass transfer. They have proposed a model for the combined drying and wetting based on irreversible thermodynamics and mechanistic approach assuming wheat as an isotropic, spherical body with negligible shrinkage and no preferential path of moisture migration. The model predicted the drying characteristics of mature wheat very well and moisture movement was found to be a function of both liquid and vapour diffusion. However, isothermal conditions were evident after the initial stage of drying.

Sokhansanj and Bruce (1987) proposed a conduction model for grain drying which assumed liquid diffusion of moisture to the outer boundaries of the kernel and evaporation only at the surface of the grain. They considered a grain kernel as a spherical shape and have given the following two equations for coupled heat and mass transfer phenomena:

$$\frac{\partial M}{\partial t} = D\left(\frac{\partial^2 M}{\partial r^2} + \frac{2}{r}\frac{\partial M}{\partial r}\right) + \left(\frac{\partial M}{\partial r}\right)^2 \frac{\partial D}{\partial M} \tag{2.23}$$

$$\rho C \frac{\partial T}{\partial t} = K\left(\frac{\partial^2 T}{\partial r^2} + \frac{2}{r}\frac{\partial T}{\partial r}\right) \tag{2.24}$$

where ρ is the density of the grain (kg m^{-3}); K is the thermal conductivity (W m^{-1} K^{-1}); r is the radial coordinate (m).

Haghighi and Segerlind (1988) have used a variational approach of the finite element method to study the simultaneous moisture removal and heat intake process inside a soybean kernel considering it as an axisymmetric and isotropic sphere. They have used

the following form of equations using cylindrical coordinates so that the models can also be applied to the axisymmetric non-spherical models:

Mass transfer equation:

$$\frac{\partial M}{\partial t} = D\frac{\partial^2 M}{\partial r^2} + D\left(\frac{1}{r}\frac{\partial M}{\partial r}\right) + D\left(\frac{\partial^2 M}{\partial z^2}\right) \tag{2.25}$$

Heat transfer equation:

$$\rho_g C_g \frac{\partial T}{\partial t} = K\left(\frac{\partial^2 T}{\partial r^2}\right) + K\left(\frac{1}{r}\frac{\partial T}{\partial r}\right) + K\left(\frac{\partial^2 T}{\partial z^2}\right) + L\rho_g \frac{\partial M}{\partial t} \tag{2.26}$$

Initial conditions:

$$M(t=0) = M_o \tag{2.27}$$

$$T(t=0) = T_o \tag{2.28}$$

Boundary conditions: $t > 0, r = R$ (surface)

$$-D\left(\frac{\partial M}{\partial r} + \frac{\partial M}{\partial z}\right) = h_m (M_s - M_e) \tag{2.29}$$

$$-K\left(\frac{\partial T}{\partial r} + \frac{\partial T}{\partial z}\right) = h_t (T_s - T_a) \tag{2.30}$$

The models were solved considering constant material properties (diffusion coefficient, thermal conductivity, and specific heat) and assuming convective moisture removal and heat intake at the surface of the kernel. The major focus of this work was to describe the finite element method to solve the coupled equations in detail. It was observed that the early stage of drying is crucial due to the development of hydro-thermal stress as a result of high values of moisture and temperature gradients. A similar effect was reported by other researchers (Sokhansanj and Bruce 1987; corn: Ekstrom et al. 1966; rice: Arora et al. 1973; and soybeans: Misra and Young 1980).

Haghighi et al. (1990) formulated and solved a set of coupled conductive heat and diffusive moisture transfer equations for drying of a barley kernel using the finite element method. They have modeled the barley kernel considering it both as an isotropic prolate spheroid as well as an isotropic sphere of equal volume. The barley kernels were divided into two-dimensional axisymmetric Lagrangian elements and the moisture and temperature distributions were approximated for each element in cylindrical coordinates following Galerkin's weighted residual method. Their models and the corresponding boundary conditions were based on the equations proposed by Bruce (1985) and Sokhansanj and Bruce (1987) of the following forms:

Mass transfer equation (same as Haghighi and Segerlind 1988):

$$\frac{\partial M}{\partial t} = D\frac{\partial^2 M}{\partial r^2} + D\left(\frac{1}{r}\frac{\partial M}{\partial r}\right) + D\left(\frac{\partial^2 M}{\partial z^2}\right) \tag{2.31}$$

Heat transfer equation (same as Haghighi and Segerlind 1988 but with the last term taken out):

$$\rho_g C_g \frac{\partial T}{\partial t} = K\left(\frac{\partial^2 T}{\partial r^2}\right) + K\left(\frac{1}{r}\frac{\partial T}{\partial r}\right) + K\left(\frac{\partial^2 T}{\partial z^2}\right) \tag{2.32}$$

Initial conditions:

$$M\,(t \le 0) = M_o \tag{2.33}$$

$$T\,(t \le 0) = T_o \tag{2.34}$$

Boundary condition:

$t > 0$, on surface

$$M_s = e^{-\gamma t}\,(M_o - M_e) + M_e \tag{2.35}$$

$$KA\left(\frac{\partial T}{\partial r}+\frac{\partial T}{\partial z}\right)=A\,h_t\,(T_a-T_s)=V\,\rho\,\left[L+C_v\,(T_a-T_s)\right]\frac{\partial M}{\partial t} \qquad (2.36)$$

where M_s is the surface moisture content (d.b.); γ is the drying parameter; A is the surface area of the single grain (m^2); h_t is the convective heat transfer coefficient (W m^{-2} K^{-1}); V is the volume of the grain (m^3); and C_v is the specific heat of vapor (J kg^{-1} K^{-1}).

The above model and boundary conditions considered all the material properties as constant except the diffusivity, thermal conductivity, and specific heat, which were dependent on the temperature and moisture content of the grain. Further, they have considered convective heat transfer at the surface of the kernel and a conductive transfer at the inner layers. However, the moisture was assumed to move towards the surface by liquid diffusion and then evaporated at the surface of the kernel. The prolate spheroidal model described the experimental data very well compared to the spherical model as it is close to the shape of a barley kernel.

Czaba and Neményi (1997) investigated simultaneous heat and moisture distributions as a function of drying time inside a corn kernel considering the real geometrical shape of the kernel. They have used a finite-element approach for the same set of equations (Sokhansanj and Gustafson 1980) in their simulation study where they included the effect of moisture evaporation as the coupling factor in place of the heat source factor of the heat transfer equation. They have used the COSMOS/M (Structural Research & Analysis Corp., Santa Monica, CA) general finite element package for their simulation study. Their model was complex as they considered the specific heat for the germ and endosperm as a function of average moisture content of the germ and endosperm. In addition, the diffusivity was also taken as a function of the average moisture content and

the average temperature. They have modified the heat transfer equation a little keeping the mass transfer equation and the initial and boundary conditions (Sokhansanj and Gustafson 1980) the same. The heat transfer equation was in the following form:

$$\rho\ C\ \frac{\partial T}{\partial t} = K\left(\frac{\partial^2 T}{\partial x^2} + \frac{\partial^2 T}{\partial y^2}\right) + L\,\rho\ \frac{\partial M}{\partial t} \tag{2.37}$$

Jia et al. (2000) simulated two-dimensional coupled heat and mass transfer within a wheat kernel during drying considering wheat as an isotropic material. They have used the variational calculus method of the finite element analysis considering ellipsoidal-shaped wheat kernel as cylindrical coordinate system and a negligible shrinkage. For the following set of equations and boundary conditions, they have assumed heat conduction inside the kernel and convection at the surface and a combination of liquid diffusion and evaporation causing moisture movement inside the kernel and the moisture evaporation at the surface:

Mass transfer equation:

$$\frac{\partial M}{\partial t} = D\left(\frac{\partial^2 M}{\partial x^2} + \frac{\partial^2 M}{\partial y^2}\right) \tag{2.38}$$

Heat transfer equation:

$$\rho\ C\ \frac{\partial T}{\partial t} = K\left(\frac{\partial^2 T}{\partial x^2} + \frac{\partial^2 T}{\partial y^2}\right) + L\,\rho\ \frac{\partial M}{\partial t} \tag{2.39}$$

Initial conditions:

$$M\ (x, y, t = 0) = M_o \tag{2.40}$$

$$T\ (x, y, t = 0) = T_o \tag{2.41}$$

Boundary conditions:

$$-D\left(\frac{\partial M}{\partial x}+\frac{\partial M}{\partial y}\right)=h_m\,(M_s-M_e) \tag{2.42}$$

$$KA\left(\frac{\partial T}{\partial x}+\frac{\partial T}{\partial y}\right)=A\,h_t\,(T_a-T_s)=V\,\rho\,\left[L+C_v\,(T_a-T_s)\right]\frac{\partial M}{\partial t} \tag{2.43}$$

It is clearly evident that the boundary condition for the heat transfer equation is similar to that used by Haghighi et al. (1990). The major focus of this study was on the quality prediction of the dried wheat grains based on the stress-crack analysis. Like the previous studies, it was found that the maximum temperature gradient occurs at the initial stage of drying causing high thermal stress development. The moisture gradient continued to increase with drying time with a very sharp increase in moisture gradient at the initial stages of drying causing higher stress in the kernel. Thus it is important to study the temperature and moisture distributions inside a grain kernel at the initial stages of a drying process. Moisture intensity was found more inside the kernel than at the surface because the direction of the temperature gradient becomes opposite to that of the moisture gradient at the initial drying stage and thereby obstructing moisture diffusion towards the surface of the grain kernel. They have suggested tempering or intermittent drying to be followed in order to avoid stress-crack development and to achieve high quality grains after drying.

Ranjan et al. (2001) used a three-dimensional control volume approach to solve coupled heat and mass transfer equations to improve the drying of barley and soybean. They have used Fourier's law of heat conduction and Fick's law of moisture diffusion to study the combined heat and mass transfer within the grains. In the case of mass transfer equation, they have assumed only liquid diffusion towards the surface and evaporation on the

surface. However, a coupled convective-evaporative boundary condition has been assumed in case of the heat transfer equation. Constant material properties have been used to solve the equations. The moisture profile analysis indicated that moisture loss was fast due to the effect of a high moisture gradient at the initial stages of drying. Temperature was increased only during the very early stage of drying and then remained in a steady-state. Further, they observed that during drying the moisture content was very high in the center of the grain kernel compared to the outer regions whereas the temperature showed a reverse trend. The equations and their boundary conditions are indicated below:

Mass transfer equation:

$$\frac{\partial M}{\partial t} = D\left(\frac{\partial^2 M}{\partial x^2} + \frac{\partial^2 M}{\partial y^2} + \frac{\partial^2 M}{\partial z^2}\right) \tag{2.44}$$

Heat transfer equation:

$$\rho \ C \ \frac{\partial T}{\partial t} = K\left(\frac{\partial^2 T}{\partial x^2} + \frac{\partial^2 T}{\partial y^2} + \frac{\partial^2 T}{\partial z^2}\right) \tag{2.45}$$

Boundary conditions:

$$-D\left(\frac{\partial M}{\partial x} + \frac{\partial M}{\partial y} + \frac{\partial M}{\partial z}\right) = h_m\,(M_s - M_e) \tag{2.46}$$

$$KA\left(\frac{\partial T}{\partial x} + \frac{\partial T}{\partial y} + \frac{\partial T}{\partial z}\right) = A\ h_t\,(T_a - T_s) + V\,\rho\ \left[L + C_v\,(T_a - T_s)\right]\ \frac{\partial M}{\partial t} \tag{2.47}$$

Yang et al. (2002) studied two-dimensional temperature and moisture distributions within a single rice kernel during drying and tempering to determine the effect of moisture

content gradient on rice fissure formation. They used the following heat and mass transfer equations considering a rice kernel as an axisymmetric cylindrical:

Mass transfer equation:

$$\frac{\partial M}{\partial t} = D\frac{\partial^2 M}{\partial r^2} + D\left(\frac{1}{r}\frac{\partial M}{\partial r}\right) + D\left(\frac{\partial^2 M}{\partial z^2}\right) \tag{2.48}$$

Heat transfer equation:

$$\rho\ C\ \frac{\partial T}{\partial t} = K\left(\frac{\partial^2 T}{\partial r^2}\right) + K\left(\frac{1}{r}\frac{\partial T}{\partial r}\right) + K\left(\frac{\partial^2 T}{\partial z^2}\right) + L\,\rho\ \left(\frac{1}{1+M}\right)\frac{\partial M}{\partial t} \tag{2.49}$$

Initial conditions:

$$M\ (t = 0) = M_o \tag{2.50}$$

$$T\ (t = 0) = T_o \tag{2.51}$$

Boundary conditions:

$$-D\left(\frac{\partial M}{\partial r} + \frac{\partial M}{\partial z}\right) = h_m\ (M_s - M_e) \tag{2.52}$$

$$KA\left(\frac{\partial T}{\partial r} + \frac{\partial T}{\partial z}\right) = A\ h_t\ (T_a - T_s) + \frac{V}{1+M}\rho\ \left[L + C_v\ (T_a - T_s)\right]\frac{\partial M}{\partial t} \tag{2.53}$$

In the above equations, they considered convective heat transfer at the surface and heat conduction in the inner parts of a rice kernel. The moisture transfer was assumed to be a cumulative effect of both the liquid and vapour diffusion towards the surface and evaporation on the surface and inside the kernel. They reported a diminishing temperature gradient at the very early stages of rice drying whereas the moisture gradient remained almost constant throughout the whole drying process since it reached its peak. Thus they found that at the initial stages of drying the rice kernel was more durable and unbreakable due to high thermal expansion coefficient and small modulus of elasticity.

Therefore, they concluded that the constant high moisture gradient is responsible for stress crack development.

2.5.5 Comments on Published Grain Drying Theories and Models

Most of the previous works on drying models have assumed one or more of the following mechanisms: capillary flow, liquid diffusion, surface diffusion, vapor diffusion, thermal diffusion, hydrodynamic flow to analyze simultaneous heat and mass transfer phenomena. A summary of these models is described in Miketinac et al. (1992). Moreover, all of these grain drying models were derived under a number of assumptions made to simplify these models for computation. All of the published models have assumed that the moisture content distribution is uniform in a grain at the beginning of drying and that the moisture removal from the grains is uniform during drying. However, these simplifications do not represent the reality as has been demonstrated by published studies of moisture distribution using MRI and therefore may reduce the accuracy of the model prediction. Brooker et al. (1992) reported a non-uniform initial moisture distribution in a freshly harvested corn kernel (whole kernel 36% w.b., germ 48% w.b., endosperm 31% w.b., and pericarp 53% w.b.). This feature was further evidenced in most of the cereal grains, including corn, by using the non-invasive and non-destructive magnetic resonance imaging (MRI) technique by several researchers as indicated in Section 2.4 (barley: McEntyre et al. 1998; corn: Ratković 1987, Song and Litchfield 1990, Bačić et al. 1992, Song et al. 1992, Ruan et al. 1992, Ruan and Litchfield 1992, Kovács and Neményi 1999; rice: Takeuchi et al. 1997, Ishida et al. 2004; and wheat: Jenner et al. 1988, Stapley et al. 1997, Song et al. 1998). There is a need to develop and solve a mathematical model of coupled heat and mass transfer in grain that takes into

consideration the non-uniform distribution of moisture before the start of drying and the non-uniform movement of moisture from the grain kernel during drying. Such a model will have to incorporate different flow mechanisms for moisture in different parts of the grain. In this present study such a model was developed, solved and validated for wheat drying.

MAGNETIC RESONANCE IMAGE ANALYSIS TO EXPLAIN MOISTURE MOVEMENT DURING WHEAT DRYING[1]

Prabal K. Ghosh[1], Digvir S. Jayas[1], Marco L.H. Gruwel[2, 3], Noel D.G. White[1, 4, 5]

[1]Department of Biosystems Engineering, University of Manitoba, Winnipeg, Manitoba, Canada, R3T 5V6

[2]NRC Institute for Biodiagnostics, 435 Ellice Avenue, Winnipeg, Manitoba, Canada, R3B 1Y6

[3]Department of Chemistry, University of Manitoba, Winnipeg, Manitoba, Canada, R3T 2N2

[4]Cereal Research Centre, Agriculture and Agri-Food Canada, 195 Dafoe Road, Winnipeg, Manitoba, Canada, R3T 2M9

[5]Department of Entomology, University of Manitoba, Winnipeg, Manitoba, Canada, R3T 2N2

Abstract

Two-dimensional (2D) spin-echo magnetic resonance imaging (MRI) was used to explain the moisture movement in single wheat kernels prior to and during drying. Drying was performed at temperatures of 40°C and 50°C using heated N_2 gas at a velocity of 0.23 m s^{-1}. Individual wheat kernels of 20% to 64% moisture content (wet mass basis) were dried to study the moisture movement inside the kernel during drying. MR images were recorded at equal time intervals during drying. Moisture distribution and transfer were analyzed from MR images of wheat kernels obtained before and during drying. Moisture distribution was non-uniform at an equilibrium state prior to drying. Further, moisture loss from the seed parts differed significantly during drying. The MR images were used to obtain the drying rates and patterns of water in wheat kernels during the drying

[1] This paper was published in the ***Transactions of the ASABE*** **49(4): 1181-1191 (2006).**

process. Influence of grain parts on the moisture distribution was also studied using mechanically scarified kernels and germ-removed kernels.

Keywords: *Drying, Magnetic resonance imaging, Moisture movement, Wheat.*

3.1 Introduction

Globally, about 2 billion tonnes of grains, oilseeds, and legumes (hereinafter referred to as grains) are produced annually and stored at different stages in the grain distribution chain between the producer and the consumer. Grains are seasonal and perishable, and efforts have been made to store them properly until consumed. Drying of grains is the most important method for preservation because the removal of water from kernels prevents microbial growth, slows enzymatic changes, and considerably increases the storage life. It also reduces grain mass, thereby facilitating transportation and handling. There is a general agreement that drying behavior of grains is largely influenced by the temperature and moisture distribution in the grains when dried using near-ambient temperature air or hot air. Furthermore, grains are heterogeneous in structure. Thus, grain drying is a complex process of simultaneous heat and mass transfer. To use the drying techniques at farm or industry level and to develop accurate mathematical models, it is necessary to understand the underlying mechanisms of drying inside grain kernels.

Magnetic resonance imaging (MRI) is a technique for observing moisture movement and distribution inside intact kernels in a non-destructive and non-invasive way, and MRI can be used to explain the moisture pattern during the drying process. An MR image provides a map of the spatial distribution of an MR-active nucleus subjected to a very strong magnetic field (11.7 T for our study; the Earth's magnetic field is approx. 5×10^{-5} T). The

nucleus of interest in our study is hydrogen (^{1}H, spin 1/2), which was used to map the water (H_2O) distribution within a grain. Each ^{1}H nucleus can be considered to behave as a tiny magnet with a small magnetic moment, $\vec{\mu}$. In the absence of an external magnetic field (B_o), the nuclei are randomly distributed inside the biomaterials, resulting in zero net magnetization (M_o). However, when a magnetic field (B_o) is applied, the polarization results in a measurable net magnetization, parallel to the field. The net magnetization precesses around the magnetic field at a well-defined rate, called the Larmor frequency (ν):

$$\omega = 2\pi\nu = \gamma B_o \tag{3.1}$$

where ω is the angular frequency (rad s^{-1}); γ is the gyromagnetic ratio (42.6 MHz T^{-1} for ^{1}H); and B_o is the magnetic field strength (T).

By convention in MRI, the z-axis coincides with the axis of the main magnetic field (B_o). To perturb the equilibrium magnetization from its original orientation, a radio-frequency (RF) pulse is applied to tip the magnetization into the xy plane, perpendicular to B_o. This process occurs most efficiently at resonance that occurs at an RF frequency equal to the Larmor frequency. The tip angle of the magnetization depends on the strength and duration of the RF-B_1 field, which is applied perpendicular to B_o. After the RF is turned off, the nuclei relax back to their equilibrium state, parallel to B_o. This process can be characterized by two relaxation constants, T_1 and T_2. The longitudinal or spin-lattice relaxation time, T_1, describes the time required for the z-component of the magnetization (M_z) to return to its equilibrium value. The transverse or spin-spin relaxation time, T_2, describes the time required for the transverse magnetization (M_{xy}) to return to its

equilibrium state. During this return to equilibrium, a free induction decay (FID) can be observed caused by the decaying precession of magnetization, which induces an alternating voltage in the receiver. The FID or time domain MR signal is then Fourier transformed to provide a relationship between intensity and frequency. MR images are obtained by simultaneously turning on the magnetic field gradients. The time required for the FID to relax back to equilibrium is directly related to T_2. Several books provide details on MRI principles (Bushong 1988; Stark and Bradley 1992; Ruan and Chen 1998).

Magnetic resonance imaging has been used successfully by several researchers for non-destructive determination of the average moisture content in different grains (from 4% to 40% wet mass basis), such as wheat, maize, barley, grain sorghum, soybeans, and peanuts (Miller et al. 1980; Brusewitz and Stone 1987; Chambers et al. 1989; Tollner and Hung 1992). MRI has the potential to determine the moisture transfer profile of wheat, rice, and maize kernels during cooking, boiling, and steeping (soaking) (Ruan and Litchfield 1992; Ruan et al. 1992; Takeuchi et al. 1997; Stapley et al. 1998; Song et al. 1998; Fukuoka et al. 2000; Watanabe et al. 2001).

Magnetic resonance imaging has also been used to determine transient moisture transfer inside grain kernels during the drying process. Song and Litchfield (1990) initiated this work by measuring the transient moisture profile in ear corn during hot-air drying at 60°C with an air velocity of 1.83 m s^{-1} for 5 h. Trends in moisture loss for different parts of corn kernels were visually investigated from MR images, since brightness of the image

is directly proportional to the proton density and hence the moisture content. One-dimensional transient moisture profiles across the center of an ear of corn were obtained based on image pixel intensities at different drying times. Moisture distribution and changes inside the corn cobs were distinctly different, and non-uniform, during the drying process. Song et al. (1992) investigated moisture transfer from sequential three-dimensional MR images of corn kernels obtained during drying at 27°C and 49°C at an air velocity of 5 m s^{-1} for 3 h and 1 h, respectively. A series of proton density images of one central slice were evaluated. It was determined that moisture distribution in the kernels was non-uniform. Moisture loss also differed significantly during drying through two primary routes: the glandular layer of the scutellum, and the pericarp. Kovács and Neményi (1999) used a standard Hahn spin-echo imaging pulse sequence to demonstrate the pathways where water rapidly passed through whole yellow dent corn (Helga variety) kernels during drying at 46°C with an air velocity of 1.4 m s^{-1} for 4.5 h. Moisture distribution inside the whole kernel was not uniform before and during drying. Moisture loss was faster and higher from the endosperm than the pericarp. However, moisture loss was the lowest from the scutellum.

The grain drying models presented in the literature were derived under a number of assumptions made to simplify these models for computation. All of the published models have assumed that the moisture content distribution is uniform in a grain at the beginning of drying and that the moisture removal from the grains is uniform during drying. However, results from the published literature of moisture distribution using MRI revealed an anisotropic and non-uniform nature of moisture distribution and migration at

the beginning or during drying of grains. To develop accurate grain drying models, these conditions must be taken into consideration. Therefore, this study was undertaken to investigate the moisture patterns in wheat during drying from MRI images and to study the influence of grain structure on the moisture removal pattern.

3.2 Materials and Methods

3.2.1 Materials and Sample Preparation

Wheat was selected for this study because it is a major crop in western Canada and it is a staple food for a large portion of the world population. The wheat kernels (*Triticum aestivum* L., cv. AC Barrie) used in this study were obtained from the Cereal Research Centre of Agriculture and Agri-Food Canada in Winnipeg, Manitoba. The wheat kernels containing 14% moisture content (m.c.) (wet mass basis) were stored at 4°C prior to the experiments. For the purpose of MR relaxation time measurements and drying experiments, small batches of approximately 15 kernels were imbibed for 18 h at room temperature in distilled water using a 50 mL beaker while shielded from air and light. Before the experiments, imbibed kernels were blotted with a paper towel to remove excess water attached to the surface. For some drying experiments, intact kernels were equilibrated in a closed plastic container for 10 days to achieve 20% m.c. (w.b.) above a KOH solution of a specified concentration at room temperature (Solomon 1951). Wheat kernels with a high moisture level (>20%) were used in this study to acquire bright MR images, which helped in studying the intrinsic details. For every MRI experiment, a new wheat kernel was glued onto the inner surface of a small glass tube (7 mm outer diameter), which could be inserted into the MR imaging probe. The moisture content of

the wheat kernels was determined by the standard air-oven method at the beginning of every MR imaging experiment (ASAE Standards 2003). To test the influence of kernel parts on moisture movement within the grain, mechanical scarification was achieved by either making an incision in the pericarp with a scalpel before starting each experiment or by removing the germ end from the kernel before moisture equilibration (Fig. 3.1). The germ-removed kernels were at lower moisture content (37%) than the whole kernels (64%).

3.2.2 Magnetic Resonance Imaging System, Probe, and Gradient Coils

All MRI experiments were performed on a 11.7 T (500 MHz) Magnex (Magnex Scientific, Ltd., Yarnton, UK) super-conducting vertical bore magnet equipped with a Magnex SGRAD 123/72/S 72 mm self-shielded, water-cooled, gradient set capable of producing a maximum gradient strength of 550 mT m^{-1} located at the Institute for Biodiagnostics, National Research Council of Canada, Winnipeg, Manitoba. A Bruker (Milton, ON) Avance DRX console with a ParaVision v. 2.1.1 operating system was interfaced to the magnet to record and analyze the images on an SGI O_2 computer. The MR imaging probe, consisting of a holder including the thermostat system, thermocouple, and a Helmholtz RF coil, was specially designed and constructed for the present study to specifically fit a single wheat grain (Fig. 3.2). Total length of the apparatus was about 650 mm, and the inner diameter of the resonator was approximately 7 mm. An individual preconditioned kernel (approx. ellipsoidal shape, 6 mm long and 3 mm diameter) was glued inside the small glass tube (12 mm long and 7 mm outer diameter), which was

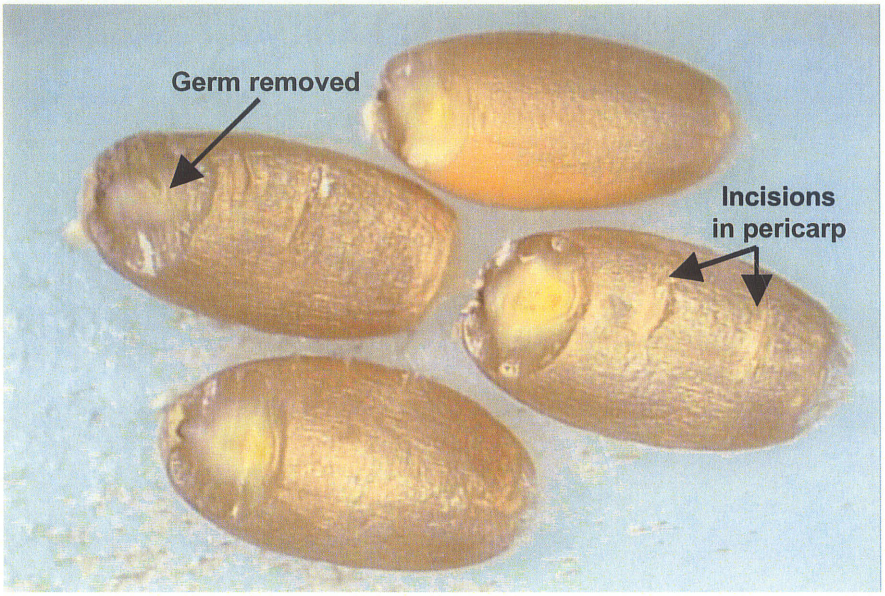

Figure 3.1 Mechanically scarified wheat kernels before taking magnetic resonance images.

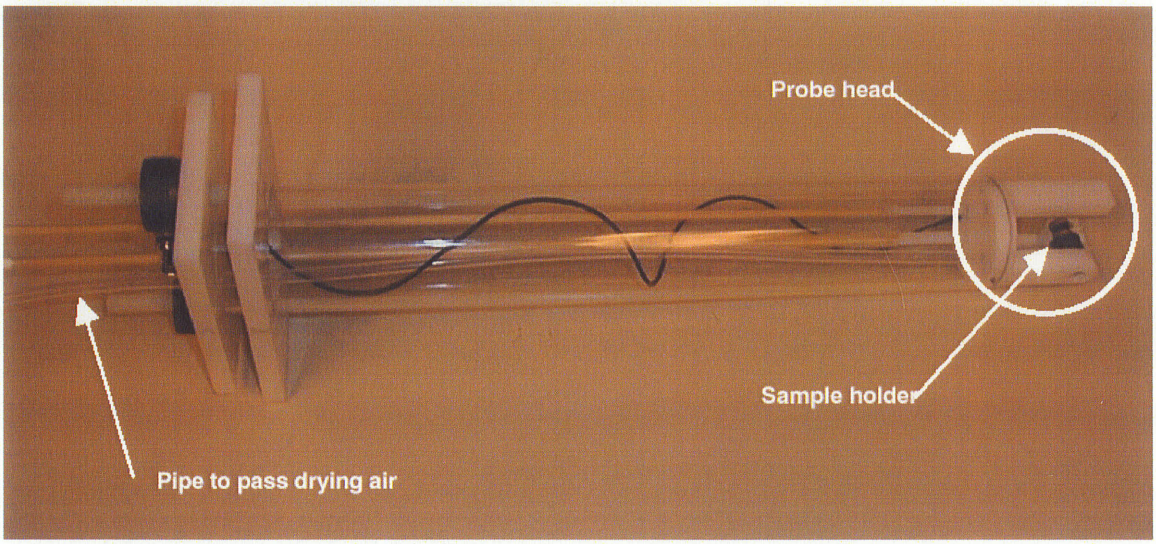

Figure 3.2 Custom-made magnetic resonance imaging probe to acquire images of single wheat kernels. The probe incorporates a holder including the thermostat system, thermocouple, and a Helmholtz radio-frequency (RF) coil.

inserted into the probe, and then the probe was placed into the bore of the MRI magnet. The probe was used to transmit the radio frequency energy and to acquire the resulting decay from the sample. The magnetic field was briefly shimmed for scout images. Transmitter gain was adjusted when a sample was placed in the magnetic field because the impedance of the transmitter coil varied from sample to sample and with the sample's position in the probe. The receiver gain was also adjusted to optimize both the signal-to-noise ratio (SNR) and the dynamic range of the analog-to-digital converter for each scan. Finally, the spectrometer (transmitter) frequency was properly adjusted by acquiring the time-domain signal and observing its deviation from the resonance. This entire procedure (setting up the instrument for adjustments and imaging) was repeated each time at the start of the MR experiment.

3.2.3 Drying Apparatus

Dry nitrogen gas was supplied using an in-line variable temperature and flow controller unit (Bruker BVT-1000, Milton, ON) to ensure a regulated low flow of N_2 gas with controlled temperature through the heater assembly to the MRI probe. A tube (5 mm in internal diameter) for conducting the heated N_2 was covered by heat-insulating material (Fiber Glass R21) to prevent heat loss. The temperature of the gas supply was measured at a close proximity to the sample. Temperatures greater than 50°C were not used, as drying occurred too fast during the first image acquisition time. N_2 gas was used instead of ambient air because of its relative advantages. N_2 is dry and is non-corrosive to most of the instrument materials.

3.2.4 Drying of Wheat Kernels

Moisture movement within and out of wheat kernels during drying was observed under the following conditions: initial moisture contents of 20% to 64% w.b., and drying temperatures of 40°C and 50°C with an accuracy of ±1°C. The grain kernels were subjected to a regulated flow (0.23 m s^{-1}) of pre-heated nitrogen gas. Each drying experiment was continued for 4 h. MRI data were sampled continuously and saved every 10 min 18 s without interrupting the drying process. We were interested in comparing relative drying rates for different components of wheat; therefore, results from a single treatment are presented in this article. The results from other two replicates were similar.

3.2.5 Magnetic Resonance Image Data Acquisition

Preliminary tests were performed to test the custom-designed imaging probe and to determine the suitable image pulse sequences. A conventional, two-dimensional, multi-slice Hahn spin-echo pulse sequence was used for the data acquisition of all samples (Hahn 1950). It utilized a 90° RF excitation pulse to flip the net magnetization vector into the transverse plane, which could be measured. After being flipped into the transverse plane, the nuclei within the net magnetization vector precessed and decreased in total strength because of the dephasing of magnetic dipoles of the nuclei due to spin-spin relaxation and interactions with the heterogeneous field. A 180° RF pulse was applied after a short time (TE/2) to refocus the dephasing of magnetic dipoles due to interactions with the heterogeneous field, and a signal was then induced in the coil, which is called a "spin echo." The time from application of the RF pulse to the peak of the echo formation

is called echo time (TE). Once an echo was generated, another set of RF pulses was applied after a relaxation or repetition time (TR) to generate the next echo.

Based on a compromise between image contrast and imaging time, the repetition time (TR) and the echo time (TE) were set to 200 ms and 3.375 ms, respectively. The total acquisition time was 10 min 18 s. During this time, six scans were acquired for signal averaging. Images were processed as 8-bit in a 128 × 64 × 8 matrix with a field-of-view of 1.28 × 1.28 × 0.4 cm, resulting in a pixel resolution of 100 × 200 × 500 μm. The MR image size was increased by zero-filling. A total of eight ^{1}H density image slices, each of 0.5 mm thickness, were obtained from each wheat kernel.

3.2.6 Magnetic Resonance Image Data Analysis

The acquired images were gray-scale representations of the number of protons in the water containing parts of the wheat kernels, which in turn represents water distribution. The brighter the image, the greater the concentration of protons. The darker the image, the fewer the number of protons. T_2 values and drying curves were obtained from randomly selected pixels in a region of interest representing a specific part of the kernel. The values reported represent a statistical average of these individual pixel measurements. Multi-slice MR image data were scaled with respect to the first image of the series and displayed using the mD (multidimensional) imaging mode of Marevisi v. 7.1 (Institute for Biodiagnostics, National Research Council Canada, Winnipeg, Manitoba) and NIH's public domain Java image processing program ImageJ (http://rsb.info.nih.gov/ij/). Image analysis (image segmentation and thresholding, pixel

selection, plot profiles) was performed with ImageJ and Matlab v. 7, R14 (The Mathworks, Natick, MA). Data were analyzed using the statistical procedures in Microsoft Excel (v. SP-2 2002) and Sigmaplot v. 6.00 (SPSS 2000).

3.3 Results and Discussion

MRI experiments are sensitive to the rate at which the excited nuclei relax after excitation. The rate of relaxation for a given system is a function of chemical composition, mobility, temperature, solute and moisture concentration, and structure (Schrader et al. 1992). It is, therefore, important to measure the relaxation times (T_1 and T_2) from the MR images. T_1 in wheat samples is generally long (390 to 440 ms, as reported by Stapley et al. 1997) and was used only as a constant weighting factor (Eq. 3.2). Therefore, we measured only the transverse relaxation time (T_2), which was acquired using many different echo delays to accurately measure nuclei densities in parts of kernels.

3.3.1 Determination of T_2

The MR signal intensity (I) of each pixel, obtained using the conventional spin-echo pulse sequence (90°-TE/2-180°-TE/2-acquisition), is given by (Song et al. 1992):

$$I = \rho \left[1 - 2 \exp\left(\frac{-TR - \frac{TE}{2}}{T_1} \right) + \exp\left(\frac{-TR}{T_1} \right) \right] \exp\left(\frac{-TE}{T_2} \right) \qquad (3.2)$$

where ρ is the proton density, which represents the apparent water content. In this study, TR>>TE, then Eq. (3.2) becomes:

$$I = \rho\left[1 - \exp\left(\frac{-TR}{T_1}\right)\right]\exp\left(\frac{-TE}{T_2}\right) \tag{3.3}$$

The weighting factor of exp ($-TE/T_2$) is typical for the spin-echo pulse sequence. Transverse relaxation times (T_2) of the different parts of the wheat kernels were measured to ensure that these values were high enough with respect to TE to acquire proton density images. Wheat kernels were preconditioned to a high average moisture level (typically about 64% w.b.) to obtain bright images with very high signal intensities for T_2 determination. A series of eight images with echo times (TE) of 3.65, 7.3, 10.95, 14.6, 18.25, 21.9, 25.55, and 29.20 ms were taken at room temperature. The obtained spin-echo signal amplitude was fitted to the following form of Eq. 3.3 (Fukuoka et al. 2000) to determine T_2 of different parts of the kernels:

$$I_i = I_o \exp\left(\frac{-TE_i}{T_2}\right) \tag{3.4}$$

where I_i is the image intensity (in arbitrary units) for each echo time TE_i (ms), and I_o is the image intensity at echo time, TE = 0.

The MR image intensity values at the different echo times were fitted well to a single exponential curve, which yielded a T_2 value for each pixel of the image (Fig. 3.3). Table 3.1 summarizes the obtained T_2 values for grain parts. The different T_2 values in a wheat kernel indicate the difference in water distribution in different locations in kernel. Song et al. (1998) found an overall T_2 value of 1.99 ms for a mature soft red winter wheat kernel at 20°C using a more time-consuming 3D projection-reconstruction technique with a Hahn spin-echo pulse sequence.

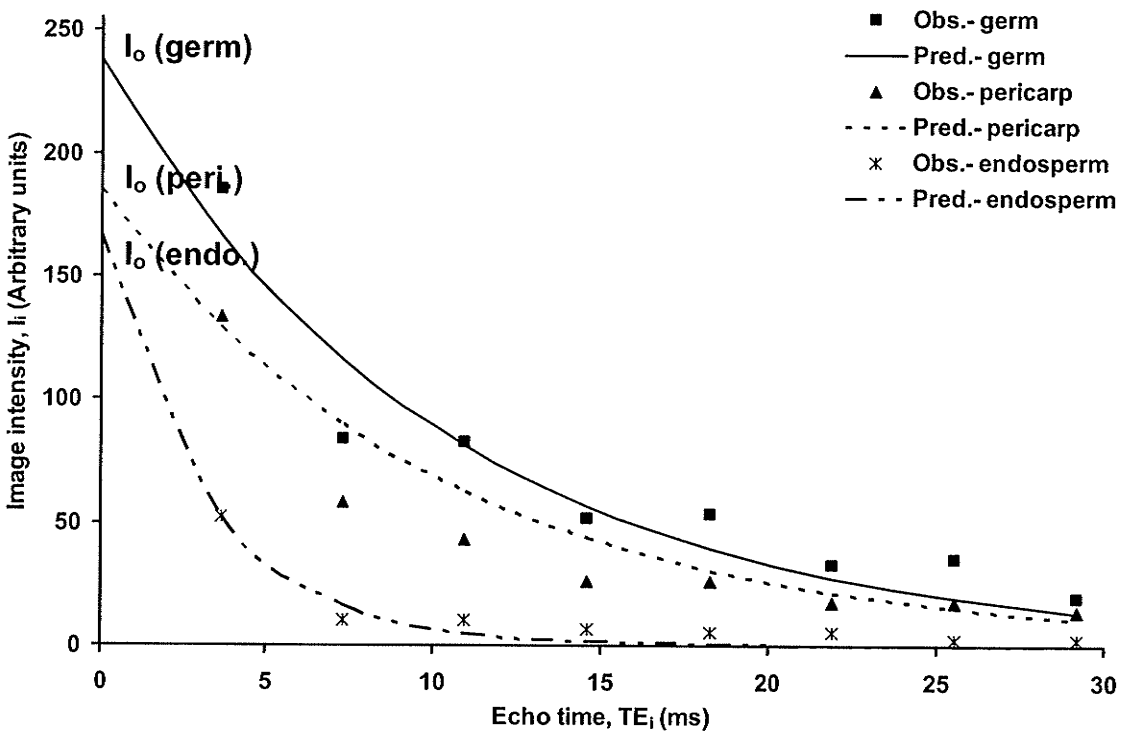

Figure 3.3 Rate of decay of pixel values for calculating T_2 relaxation time of different part of wheat kernel prior to drying.

Table 3.1 T_2 values of different parts of the wheat kernel.

	Wheat Kernel Component		
	Germ	Pericarp	Endosperm
T_2 value (ms)[a]	9.99 ±1.28 (n = 7)	7.16 ±1.37 (n = 7)	3.08 ±0.45 (n = 7)

[a] Mean ±standard deviation, n indicates the number of selected pixel values.

3.3.2 Moisture Distribution inside a Wheat Kernel before Drying

Figures 3.4a and 3.4b show a schematic diagram of the sections of a wheat kernel referenced in the text. Figures 3.5a through 3.5d show the MR images of a preconditioned high-moisture wheat kernel (64% m.c.) and their corresponding intensity profile along the chosen line segments. The regions of the germ, endosperm, and pericarp of the wheat kernel were clearly visible. The brightest high-intensity, irregular-shaped region is the germ (Fig. 3.5a), which corresponds to a high moisture concentration. The endosperm is the gray region with almost uniform intensity surrounded by an even brighter layer, which is the pericarp (Fig. 3.5b). The dark vertical bandwidth, the lowest intensity in the center of the image, represents the crease along the entire longitudinal axis since no water was present (Fig. 3.5d). The straight horizontal lines throughout the images (Figs. 3.5a and 3.5b) were due to RF interference from external signals. The intensity profiles of the images indicated that the moisture distribution within the kernel was non-uniform.

3.3.3 Transient Moisture Profiles during Drying

MRI is an ideal technique to study the heterogeneity of the water distribution inside grain kernels during drying. A representative series of image slices of a single whole wheat kernel (approx. 20% m.c.) out of a 2D data set as a function of drying time at 40°C is shown in Fig. 3.6. A particular transverse slice was selected to best illustrate the moisture distribution in the kernel with the greatest anatomical detail. The SNR of the first image ($t = 0$) in the serial MR images of Fig. 3.6 was 11.8. The SNR was calculated as the ratio

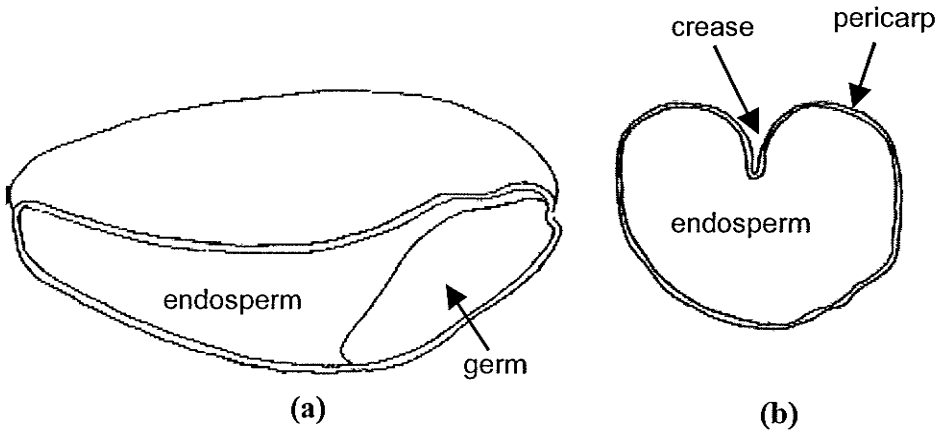

Figure 3.4 Schematic diagram of a wheat kernel: (a) longitudinal cross-section along the crease, and (b) transverse cross-section (Kang and Delwiche 1999).

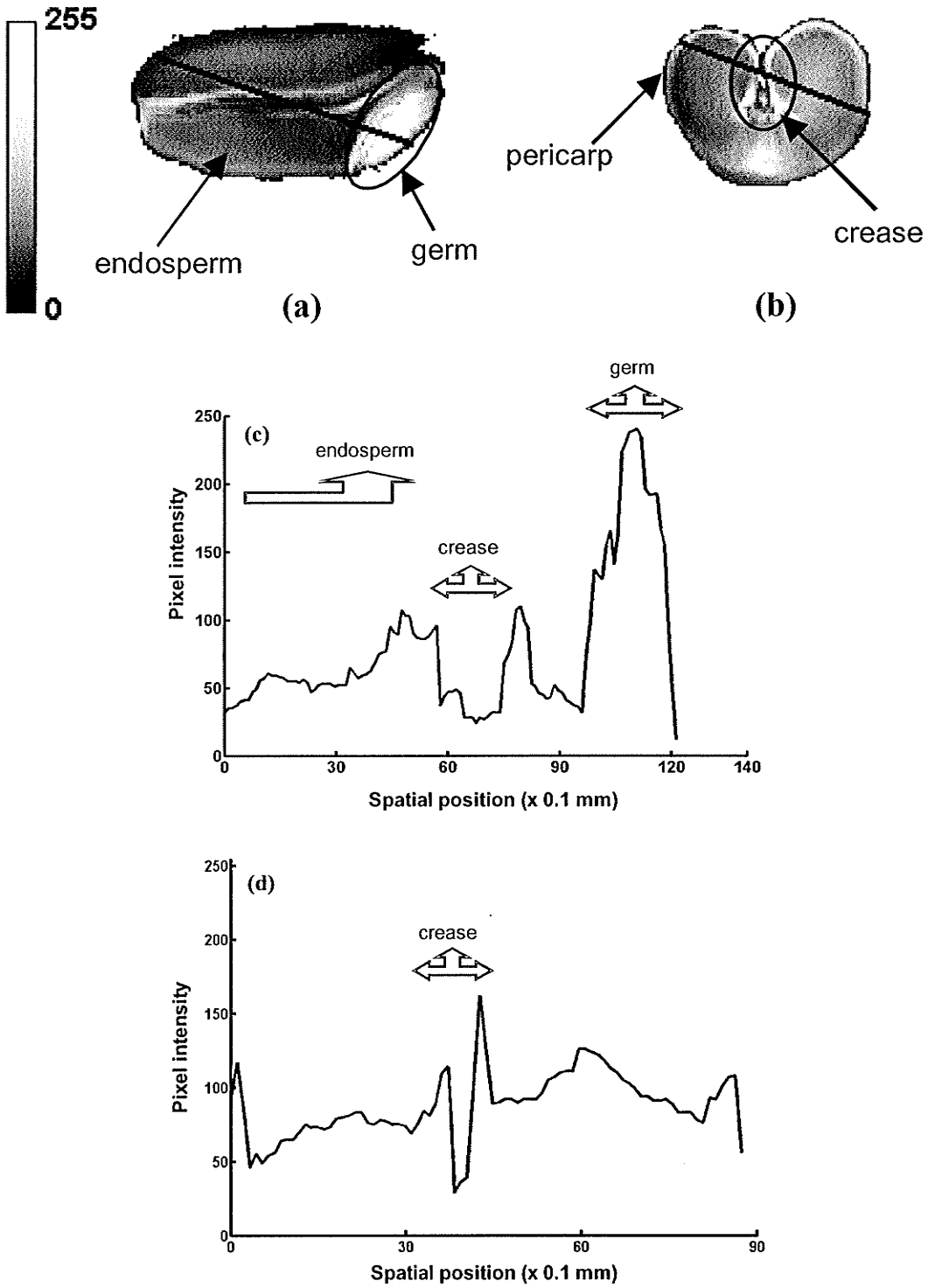

Figure 3.5 Magnetic resonance (MR) images of a wheat kernel (64% w.b.): (a) longitudinal slice, and (b) transverse slice. The sidebar next to the images represents the gray-scale intensity. Black lines indicate the lines selected for the intensity profile. Graphs (c) and (d) represent the MR signal intensity profiles along the line segments.

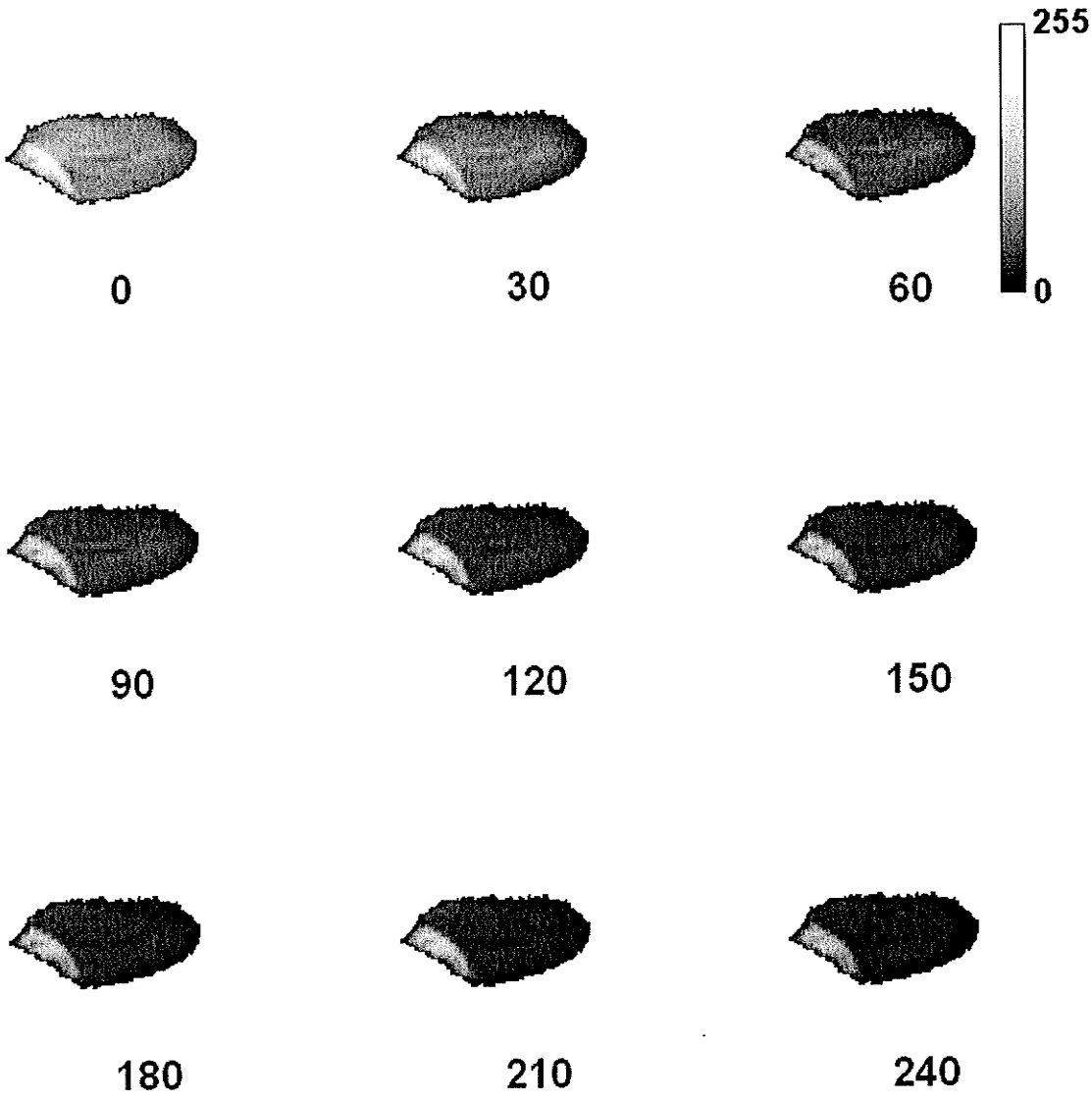

Figure 3.6 Series of two-dimensional magnetic resonance image slices (slice 6) of a whole wheat grain (average moisture content approximately 20% w.b.) during drying at 40°C. Numbers at the bottoms of the scans indicate the time in minutes from the beginning of drying. Sidebar represents the gray-scale intensity of the images.

of the average pixel intensity of a region of interest (ROI) in the whole grain to the average pixel intensity of the same-size area in a region of noise only. The brighter portions represent higher moisture content, and overall signal intensity decreased with time. The images revealed that moisture loss was faster from the pericarp and the endosperm compared to the germ. For the purpose of graphical representation of the moisture movement, MR signal intensities were selected randomly at different points in the endosperm and germ to produce representative drying curves. MR signal intensities in the pericarp region could not be measured, as drying in this area occurred too fast with respect to the time resolution of the experiment. The drying curves in terms of the average MR image intensity for individual pixels versus drying time for the endosperm and germ were plotted for 40°C and 50°C temperatures (Fig. 3.7).

Moisture loss from the endosperm and the germ was found to be uniform with drying time. Decay rate (R_d) of the water amplitude of the drying kernels was measured from a fit of the MRI signal amplitude of the MR images to a 2-parameter single exponential:

$$I(t) = I_0 \exp(-R_d \cdot t) \qquad (3.5)$$

where I(t) is the MRI signal amplitude at time t, and I_0 is the initial MRI signal amplitude at time t = 0.

According to the calculated R_d values, it was further observed that the endosperm released moisture (signal amplitude decreased about 66% at a decay rate of 0.0047 ±0.0002 min^{-1}) faster at 40°C than at 50°C (signal amplitude decreased about 54% at a decay rate of 0.0035 ±0.0003 min^{-1}). However, the germ was able to retain moisture

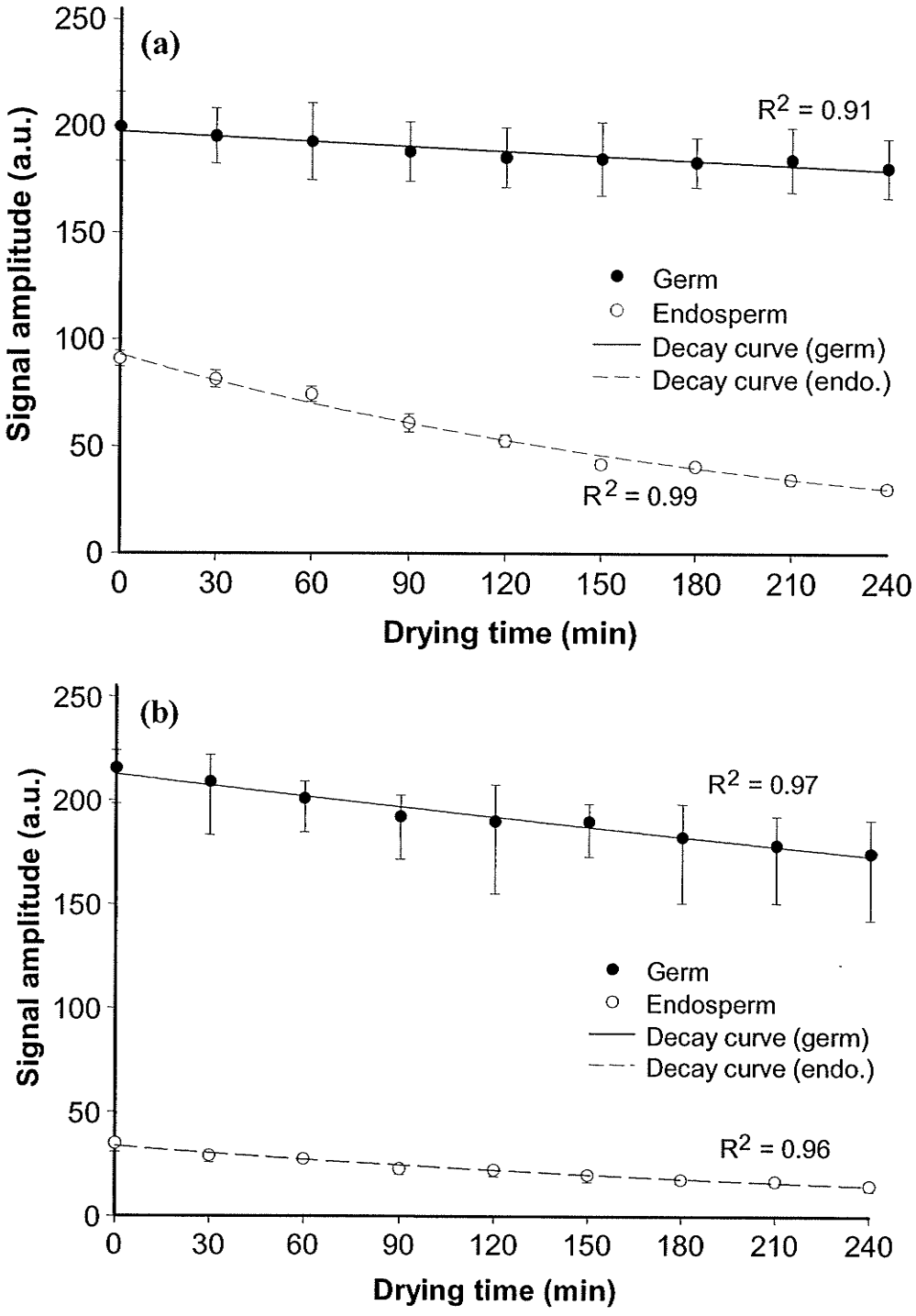

Figure 3.7 Drying curves in terms of magnetic resonance image signal amplitude vs. drying time obtained from a series of two-dimensional magnetic resonance image slices (slice 6) of a whole wheat kernel (average moisture content approximately 20% w.b.) at: (a) 40°C drying temperature, and (b) 50°C drying temperature. The vertical bars show the standard error of the mean of seven randomly selected pixel intensities.

better at 40°C (signal amplitude decreased about 10% at a decay rate of 0.0004 ±0.0003 min^{-1}) than at 50°C (signal amplitude decreased about 19% at a decay rate of 0.0009 ±0.0003 min^{-1}). This drying phenomena of the endosperm contradicts a well-established fact: "the higher the temperature, the faster the drying." Variable capillary effect of the wheat kernel and case-hardening of the outer layer probably caused this variability in moisture movements. Further study is needed to reinforce this statement. The average drying rate data confirmed that there was some case hardening or similar effect at higher temperature for the endosperm. However, the germ did not seem to be affected by the high temperature. It seemed to release moisture at a rate independent (or nearly so) of the temperature. Again, moisture appeared to move through the germ end from the endosperm, whereas the pericarp dried faster and presumably acted as a moisture barrier.

3.3.4 Influence of Grain Components on Moisture Removal during Drying

This anisotropic and non-uniform nature of water migration during the drying of wheat kernels implies that moisture removal from the grain could be dependent on the structural heterogeneities of the grain. Therefore, experiments were performed using mechanically scarified kernels and germ-removed kernels to determine whether the site of superficial cutting of the pericarp and removal of the germ were important for grain moisture movement. Representative sets of two-dimensional sequential MR images of a mechanically scarified and a germ-removed wheat kernel at two different initial moisture contents and at two different drying temperatures are shown in Figs. 3.8 and 3.9. The SNRs of the first images (t = 0) in the serial MR images of Figs. 3.8 and 3.9 were 47.9

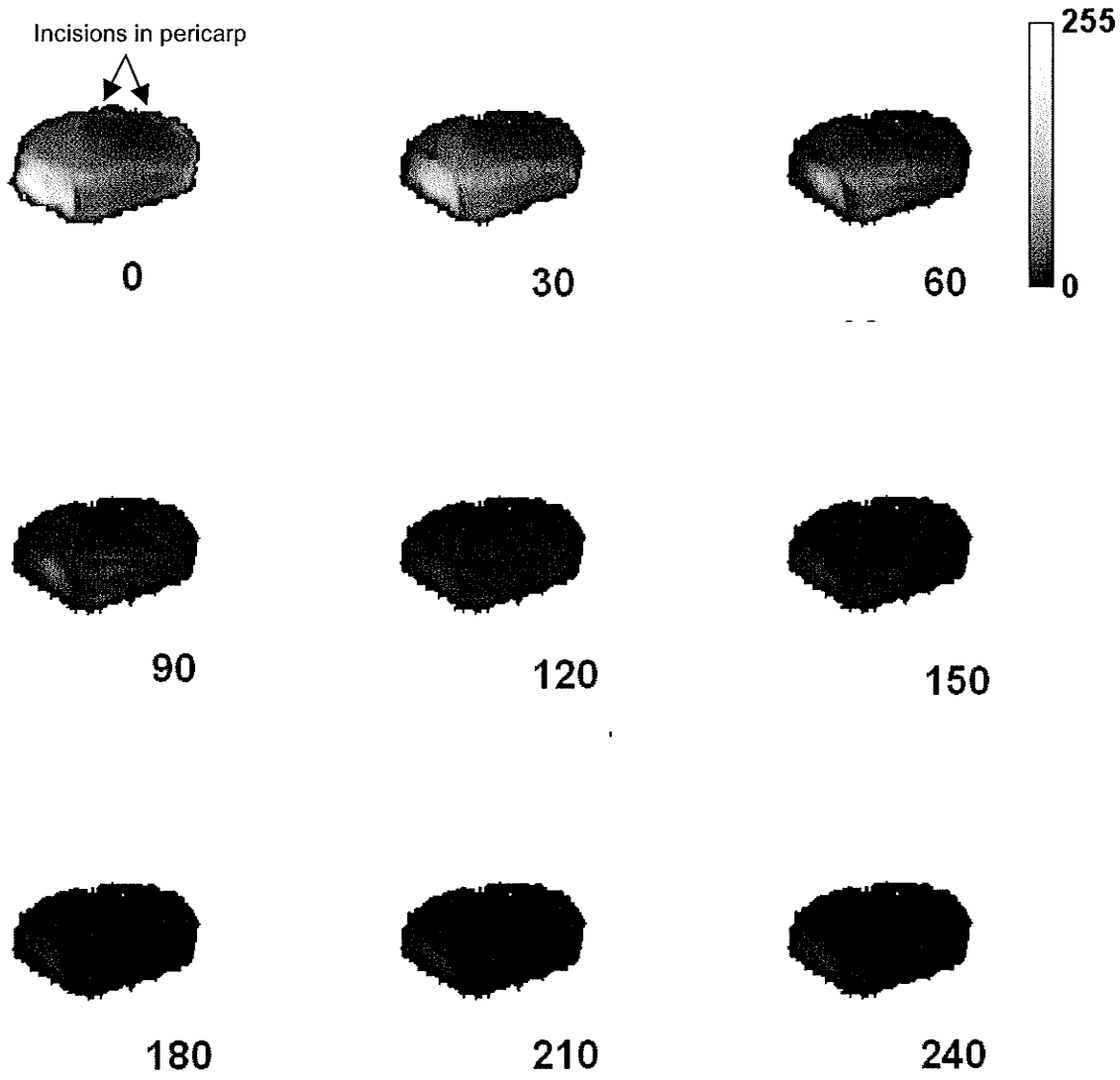

Figure 3.8 Series of two-dimensional magnetic resonance image slices (slice 5) of a mechanically scarified wheat grain (average moisture content approximately 64% w.b.) during drying at 40°C. Numbers at the bottom of the scans indicate the time in minutes from the beginning of drying. Sidebar represents the gray-scale intensity of the images.

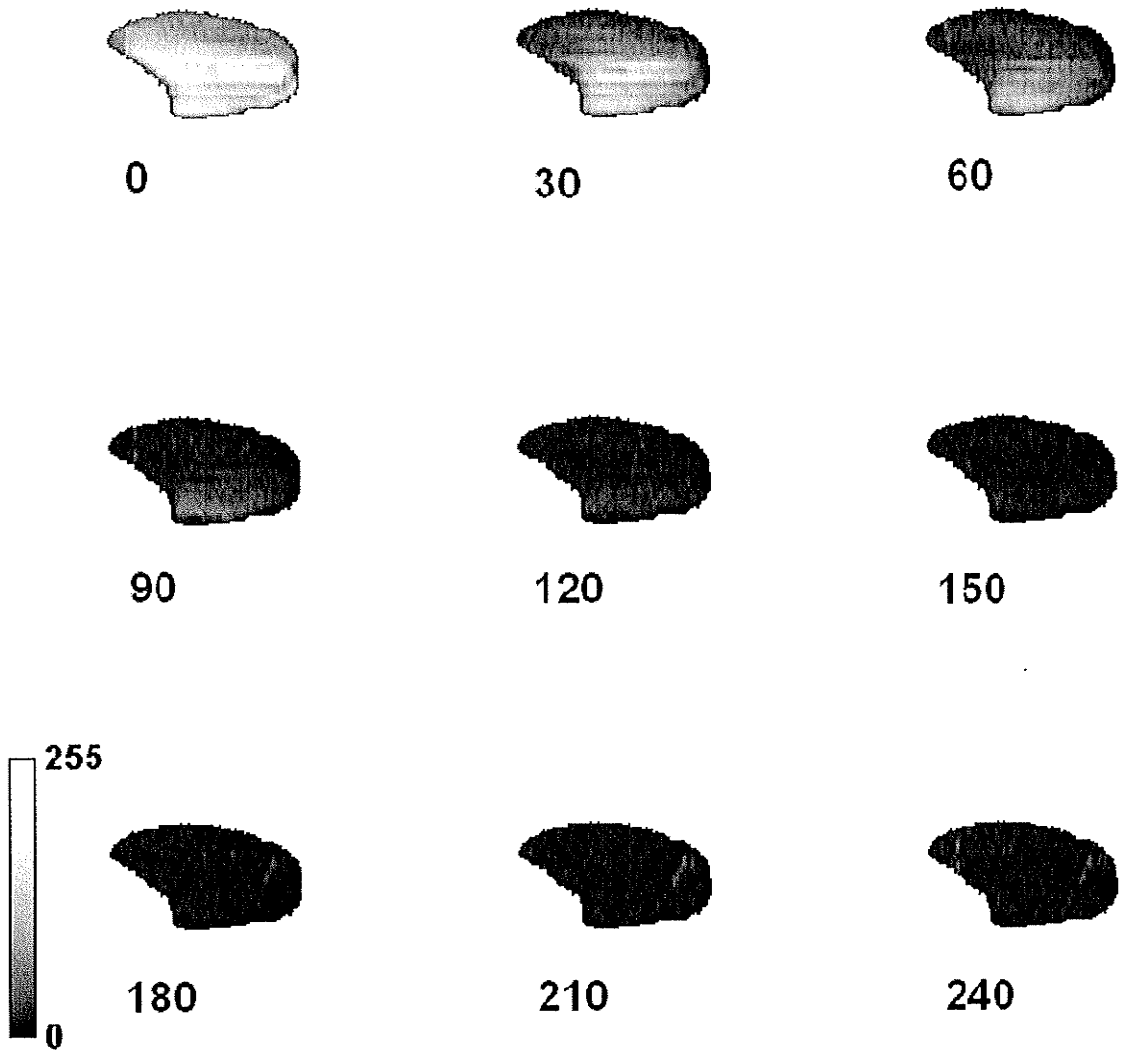

Figure 3.9 Series of two-dimensional magnetic resonance image slices (slice 6) of a germ-removed wheat grain (average moisture content approximately 37% w.b.) during drying at 50°C. Numbers at the bottom of the scans indicate the time in minutes from the beginning of drying. Sidebar represents the gray-scale intensity of the images.

and 18.2, respectively. The moisture transfer and distribution in the wheat kernels during drying was observed from the changes in their transient moisture profiles. The profiles were computed along the centerline of the image slices prior to drying and after every 1 h of drying. The moisture profile is an xy plot of signal intensity (y) versus spatial position (x) and was based on the gray-scale pixel values produced after image processing. Figures 3.10 and 3.11 show the representative plots of moisture profiles obtained from a mechanically scarified wheat kernel dried at 40°C and from a germ-removed wheat kernel dried at 50°C, respectively.

Furthermore, drying curves were plotted to study the influence of individual grain parts on moisture removal. Figures 3.12a and 3.12b show the pattern of moisture removal from the different locations in the kernel (endosperm and germ) of a mechanically scarified wheat kernel during drying at 40°C and 50°C, respectively. The moisture removal pattern in the endosperm and the germ was determined by a 2-point moving average method. In this method, a sequence of averages was computed from a specific number of data points (in our case, the period was set to 2) from a data series. This method smoothed the fluctuations in the data and showed the pattern more clearly. The average of the first two data points was used as the first point in the moving average trend line. The average of the second and third data points was used as the second point in the trend line, and so on. At initial stages of drying (until about 1.5 h), the endosperm accumulated water from the germ end before the water moved out through the incision part of the pericarp (Figs. 3.12a and 3.12b).

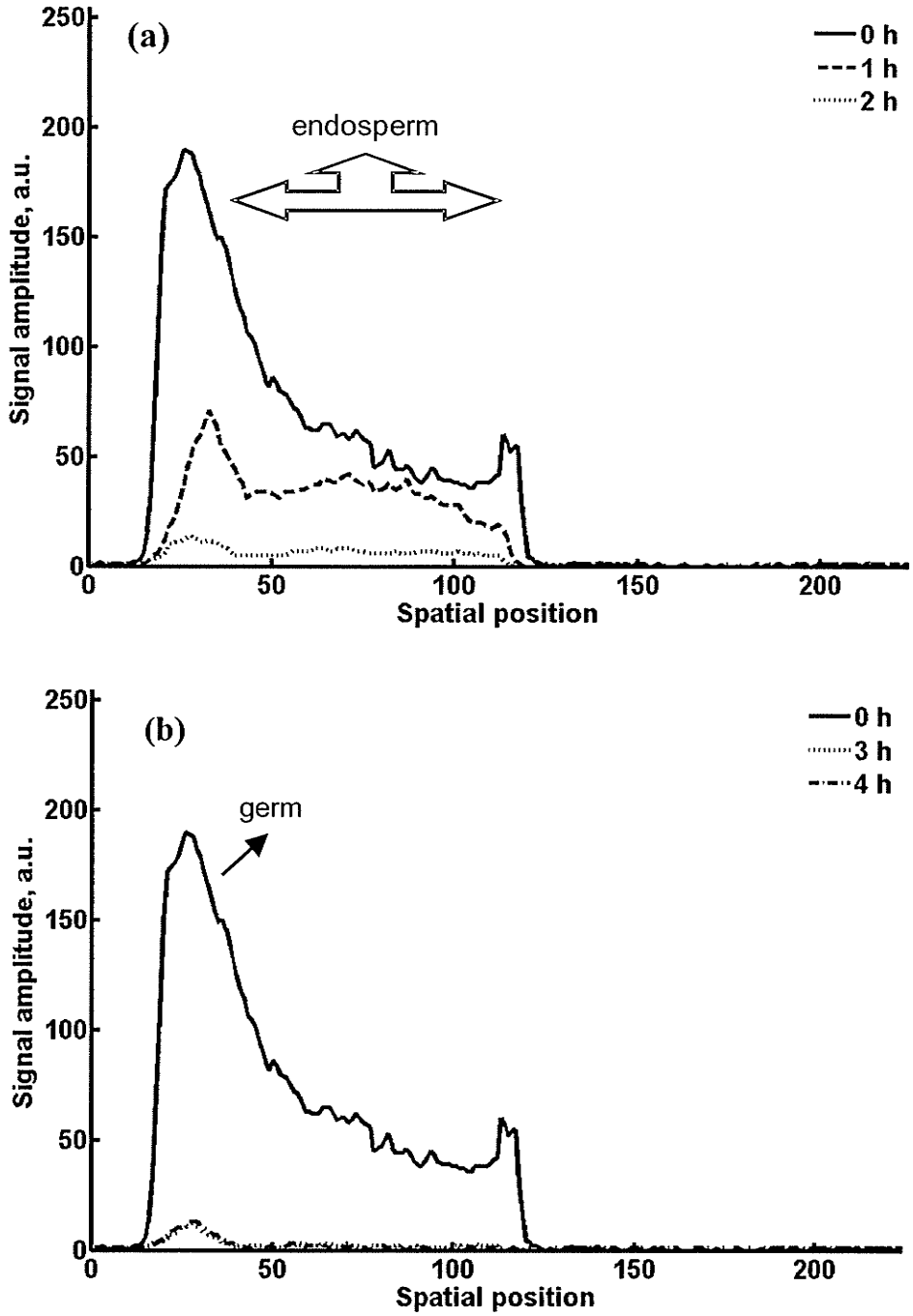

Figure 3.10 Transient moisture profiles obtained through the center of a series of two-dimensional magnetic resonance image slices (slice 5) of a mechanically scarified wheat kernel (initial moisture content approximately 64% w.b.) during drying at 40°C. Moisture profiles after 1 and 2 h and after 3 and 4 h with respect to the initial condition (prior to drying) are shown separately in graphs (a) and (b) for clarity.

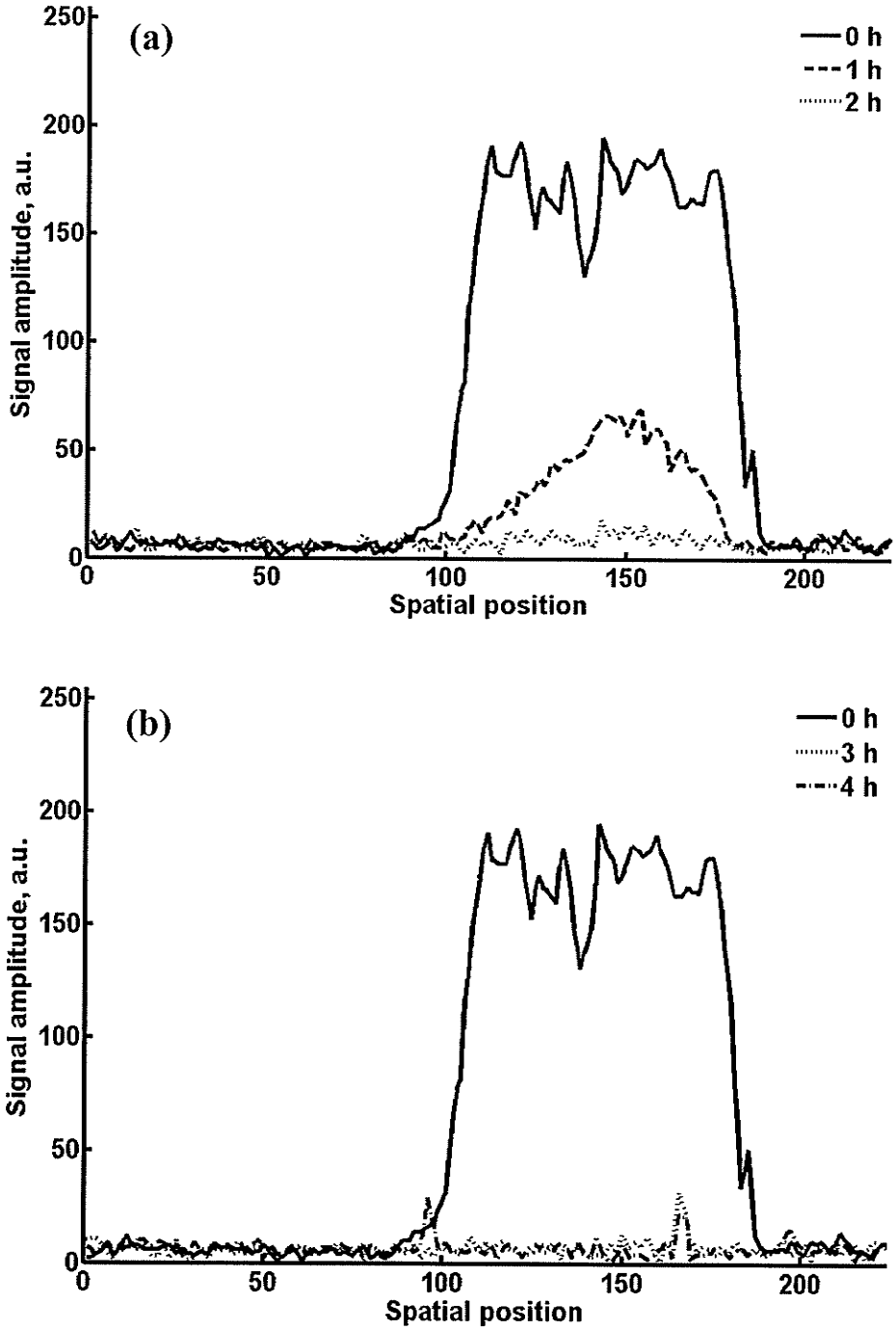

Figure 3.11 Transient moisture profiles obtained through the center of a series of two-dimensional magnetic resonance image slices (slice 6) of a germ-removed wheat kernel (initial moisture content approximately 37% w.b.) during drying at 50°C. Moisture profiles after 1 and 2 h and after 3 and 4 h with respect to the initial condition (prior-to drying) are shown separately in graphs (a) and (b) for clarity.

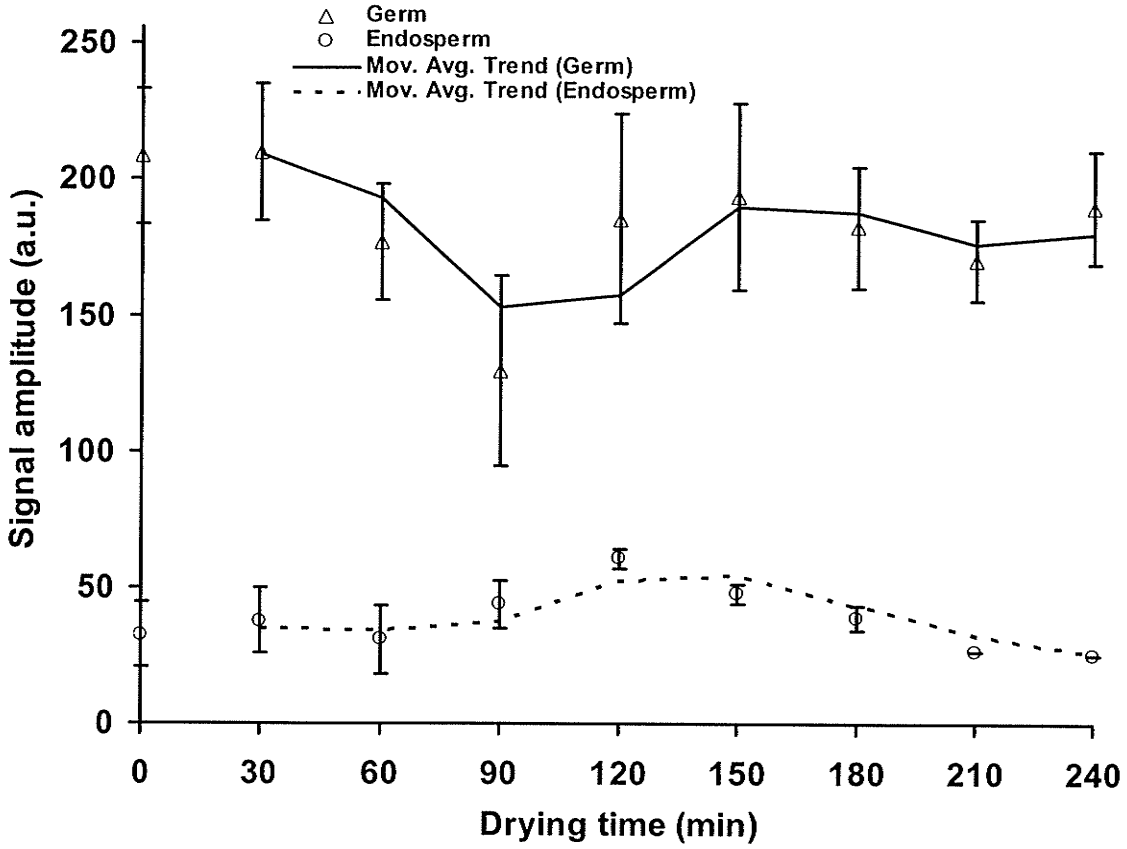

Figure 3.12a Drying curves in terms of magnetic resonance image signal amplitude vs. drying time obtained from series of two-dimensional magnetic resonance image slices (slice 5) of a mechanically scarified wheat kernel (average moisture content approximately 64% w.b.) at 40°C drying temperature. The vertical bars show the standard error of the mean of seven randomly selected pixel intensities.

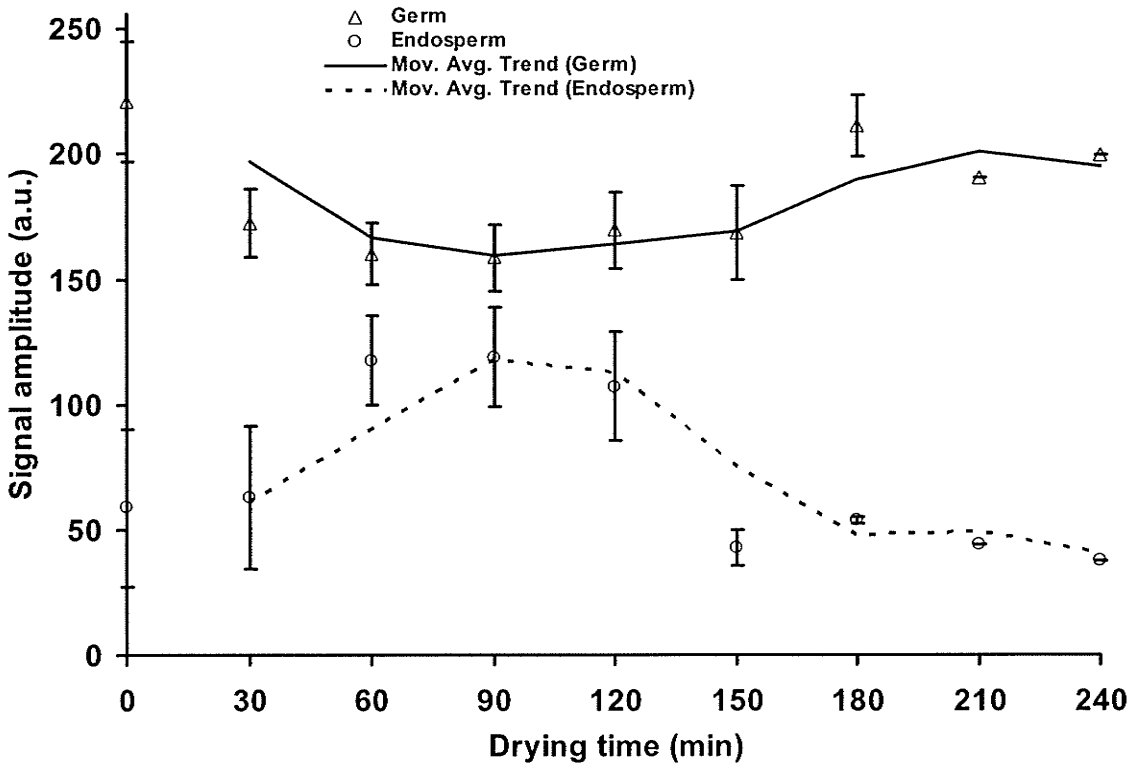

Figure 3.12b Drying curves in terms of magnetic resonance image signal amplitude vs. drying time obtained from series of two-dimensional magnetic resonance image image slices (slice 6) of a mechanically scarified wheat kernel (average moisture content approximately 64% w.b.) at 50°C drying temperature. The vertical bars show the standard error of the mean of seven randomly selected pixel intensities.

It is assumed that when the pericarp was incised, the outer layers (epidermis and hypodermis) as well as the inner layers of the pericarp were broken. Moreover, the inner layers of the pericarp consist of thinner-walled cross-cells and tube-cells containing intercellular spaces through which water could move rapidly. Therefore, at initial stages of drying, water was released relatively faster from the scarified regions of the pericarp. However, after about 1.5 h of water release, the inner bran layers (the aleurone), high in protein, and the outer bran layer (pericarp, seed coats, and nucellus), high in cellulose, hemicellulose, and minerals, had started functioning as a protective coating with the closely adhered thick-walled cells and started to offer more water movement resistance. This observation is in agreement with Hou et al. (1997), who found a relative increase in water content in the endosperm of a wild oat kernel when a mechanical incision was made in the caryopsis. After 1.5 h of drying, the water moved from the endosperm towards the germ through the finger-like cells of the scutellum epithelium (the outer layer of the scutellum located next to the endosperm), which functions as an absorption organ. This water movement could be initiated due to the high osmotic pressure gradient of the germ compared to the endosperm.

Figure 3.13 shows a clear and uniform decay pattern of moisture removal from the drying curves of the germ-removed wheat kernels dried at 40°C and 50°C. As the germ is a separate structure, it could be easily separated from the rest of the wheat kernel. Signal amplitudes were averaged over the different parts of the endosperm. Decay rate (R_d) of the signal amplitude of the kernels dried at 40°C was 0.001 ±0.0003 min^{-1}, whereas at 50°C it was 0.006 ±0.001 min^{-1}. Therefore, when the germ was removed from the wheat

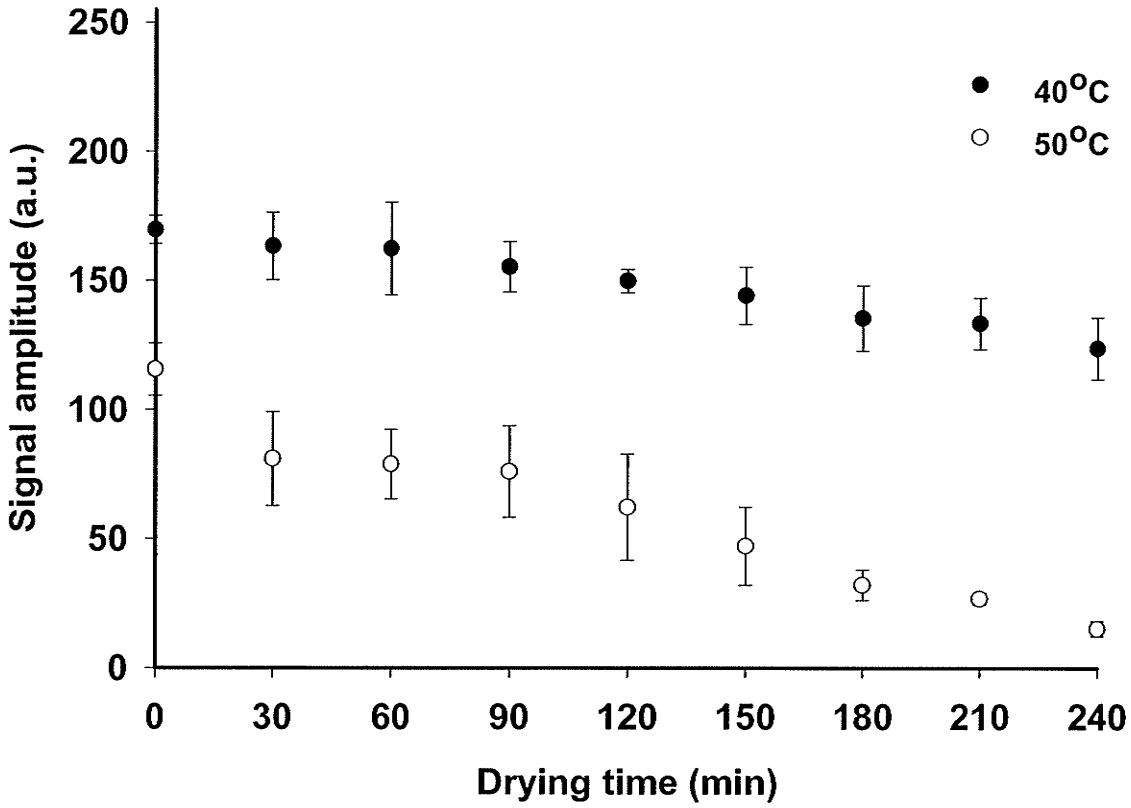

Figure 3.13 Drying curves in terms of magnetic resonance image signal amplitude vs. drying time obtained from series of two-dimensional magnetic resonance image image slices (slice 6) of a germ-removed wheat kernel (average moisture content approximately 37% w.b.) at different drying temperatures. The vertical bars show the standard error of the mean of seven randomly selected pixel intensities.

kernel, the water moved uniformly through the capillaries of the endosperm towards the large rectangular aleurone layer of the endosperm. The aleurone layer is the outermost layer of the endosperm, which is attached to the innermost pericarp layer of the wheat kernel. Once the water reached the aleurone layer of the endosperm, it then moved out from the wheat kernel through the intercellular spaces of the pericarp.

3.4 Conclusions

MRI was found to be an ideal technique to study the heterogeneity of the water distribution inside wheat kernels during drying. The MR images showed that moisture was uniformly distributed in the pericarp region at an equilibrium state prior to drying in a single kernel of wheat. Inside the wheat kernel, the moisture was differentially distributed in the endosperm and germ regions. Water was removed faster from the pericarp than from the endosperm, and the moisture-loss rate during drying was the lowest in the germ. Moisture appeared to move through the germ end of the wheat kernel from the endosperm, whereas the pericarp dried faster and presumably acted as a moisture barrier. Mechanical scarification of the wheat kernel made it easy to visualize the underlying drying phenomena. The results obtained from this study confirmed the general pattern of moisture distribution in grains during drying. Now we can extend these findings to develop and solve mathematical models of coupled heat and mass transfer in grain that take into consideration the non-uniform distribution of moisture before the start of drying and the non-uniform movement of moisture from grain during drying.

Acknowledgements

We thank the University of Manitoba Graduate Fellowship Committee, Canada Research Chairs program, and the Natural Sciences and Engineering Research Council of Canada for providing financial assistance.

References

ASAE Standards. 2003. S352.2: Moisture measurement - Unground grain and seeds. St. Joseph, MI: ASAE.

Brusewitz, G. H., and M. L. Stone. 1987. Wheat moisture and NMR. *Transactions of the ASAE* 30(3): 858-862.

Bushong, S. C. 1988. *Magnetic Resonance Imaging: Physical and Biological Principles.* St. Louis, MO: Mosby-Year Book.

Chambers, J., N. J. McKevitt, K. A. Scudamore, and C. E. Bowman. 1989. Nondestructive determination of the moisture content of individual wheat grains by nuclear magnetic resonance. *Journal of Food Science and Agriculture* 49(2): 211-224.

Fukuoka, M., T. Mihori, and H. Watanabe. 2000. MRI observation and mathematical model simulation of water migration in wheat flour dough during boiling. *Journal of Food Science* 65(8): 1343-1348.

Hahn, E. L. 1950. Spin echoes. *Physical Review* 80(4): 580-594.

Hou, S. Q., E. J. Kendall, and G. M. Simpson. 1997. Water uptake and distribution in non-dormant and dormant wild oat (*Avena fatua* L.) caryopses. *Journal of Experimental Botany* 48(308): 683-692.

Kang, S., and S. R. Delwiche. 1999. Moisture diffusion modeling of wheat kernels during soaking. *Transactions of the ASAE* 42(5): 1359-1365.

Kovács, A. J., and M. Neményi. 1999. Moisture gradient vector calculation as a new method for evaluating NMR images of corn (*Zea mays* L.) kernels during drying. *Magnetic Resonance Imaging* 17(7): 1077-1082.

Miller, B. S., M. S. Lee, J. W. Hughes, and Y. Pomeranz. 1980. Measuring high moisture content of cereal grains by pulsed nuclear magnetic resonance. *Cereal Chemistry* 57(2): 126-129.

Ruan, R. R., and P. L. Chen. 1998. *Water in Foods and Biological Materials: A Nuclear Magnetic Resonance Approach*. Lancaster, PA: Technomic Publishing.

Ruan, R., and J. B. Litchfield. 1992. Determination of water distribution and mobility inside maize kernels during steeping using magnetic resonance imaging. *Cereal Chemistry* 69(1): 13-17.

Ruan, R., J. B. Litchfield, and S. R. Eckhoff. 1992. Simultaneous and nondestructive measurement of transient moisture profiles and structural changes in corn kernels during steeping using microscopic nuclear magnetic resonance imaging. *Cereal Chemistry* 69(6): 600-606.

Schrader, G. W., J. B. Litchfield, and S. J. Schimdt. 1992. Magnetic resonance imaging applications in the food industry. *Food Tech*nology (Dec.): 77-83.

Solomon, M. E. 1951. Control of humidity with potassium hydroxide, sulphuric acid, or other solutions. *Bulletin of Entomological Research* 42: 543-554.

Song, H., and J. B. Litchfield. 1990. Nondestructive measurement of transient moisture profiles in ear corn during drying using NMR imaging. *Transactions of the ASAE* 33(4): 1286-1290.

Song, H. P., J. B. Litchfield, and H. D. Morris. 1992. Three-dimensional microscopic MRI of maize kernels during drying. *Journal of Agricultural Engineering Research* 53(1): 51-69.

Song, H. P., S. R. Delwiche, and M. J. Line. 1998. Moisture distribution in a mature soft wheat grain by three-dimensional magnetic resonance imaging. *Journal of Cereal Science* 27(2): 191-197.

SPSS. 2000. *SigmaPlot for Windows*. Ver. 6.00. Chicago, IL: SPSS, Inc.

Stapley, A. G. F., M. H. Thomas, L. F. Gladden, and P. J. Fryer. 1997. NMR imaging of the wheat grain cooking process. *International Journal of Food Science and Technology* 32(5): 355-375.

Stapley, A. G. F., P. J. Fryer, and L. F. Gladden. 1998. Diffusion and reaction in whole wheat grains during boiling. *AIChE Journal* 44(8): 1777-1789.

Stark, D. D., and W. G. Bradley. 1992. *Magnetic Resonance Imaging*. St. Louis, MO: Mosby-Year Book.

Takeuchi, S., M. Fukuoka, Y. Gomi, M. Maeda, and H. Watanabe. 1997. An application of magnetic resonance imaging to the real-time measurement of the change of moisture profile in a rice grain during boiling. *Journal of Food Engineering* 33(1-2): 181-192.

Tollner, E. W., and Y. C. Hung. 1992. Low-resolution pulse magnetic resonance for measuring moisture in selected grains and kernels. *Journal of Agricultural Engineering Research* 53(3): 195-208.

Watanabe, H., M. Fukuoka, A. Tomiya, and T. Mihori. 2001. A new non-Fickian diffusion model for water migration in starchy food during cooking. *Journal of Food Engineering* 49(1): 1-6.

MAGNETIC RESONANCE IMAGING STUDIES TO DETERMINE THE MOISTURE REMOVAL PATTERNS IN WHEAT DURING DRYING[2]

Prabal K. Ghosh[1], Digvir S. Jayas[1], Marco L.H. Gruwel[2, 3], Noel D.G. White[1, 4, 5]

[1]Department of Biosystems Engineering, University of Manitoba, Winnipeg, Manitoba, Canada, R3T 5V6

[2]NRC Institute for Biodiagnostics, 435 Ellice Avenue, Winnipeg, Manitoba, Canada, R3B 1Y6

[3]Department of Chemistry, University of Manitoba, Winnipeg, Manitoba, Canada, R3T 2N2

[4]Cereal Research Centre, Agriculture and Agri-Food Canada, 195 Dafoe Road, Winnipeg, Manitoba, Canada, R3T 2M9

[5]Department of Entomology, University of Manitoba, Winnipeg, Manitoba, Canada, R3T 2N2

Abstract

Non-invasive Magnetic Resonance Imaging (MRI) was used to study the moisture removal pattern inside a single grain of wheat (cultivar: A.C. Barrie) during drying. Images were obtained using a conventional Spin-Echo pulse sequence on an 11.7 Tesla MR spectrometer equipped with a drying apparatus. Samples of intact kernels (with all three components: pericarp, embryo, and endosperm), mechanically scarified kernels, and kernels with the embryo-removed were dried at different temperatures to study the influence of kernel components on the internal moisture removal and distribution pattern. MR images were recorded at equal time intervals and moisture patterns were analyzed from the MR images of wheat kernels. Analysis of the images revealed that moisture loss

[2] This paper was published in ***Canadian Biosystems Engineering*** **48: 7.13-7.18 (2006).**

from the seed parts differed significantly during drying and was dependent upon the grain components.

Keywords: *Drying, MRI, Wheat, Moisture distribution, Gradient vector.*

4.1 Introduction

Proper moisture conditions are important for safe grain storage and handling. Movement of the water inside the grain kernels plays an important role during drying. Drying is a complex process of simultaneous heat and moisture (mass) transfer. Most of the previous works on drying models (Luikov 1966; Husain et al. 1973; Sokhansanj and Gustafson 1980; Sokhansanj and Bruce 1987; Haghighi and Segerlind 1988; Haghighi et al. 1990; Czaba and Neményi 1997) have assumed one or more of the following mechanisms: capillary flow, liquid diffusion, surface diffusion, vapor diffusion, thermal diffusion, or hydrodynamic flow to analyze simultaneous heat and mass transfer phenomena. The grain drying models presented in the literature were derived under a number of assumptions made to simplify these models for computation. All of the published models have assumed that the moisture content distribution is uniform in a grain at the beginning of drying and that the moisture removal from the grains is uniform during drying. However, these simplifications do not represent the reality as has been demonstrated by published studies of moisture distribution using magnetic resonance imaging (MRI) and therefore may reduce the accuracy of the model prediction. Magnetic resonance imaging is a non-destructive and non-invasive technique that is used to determine the moisture distribution inside intact kernels. The MRI method can enhance understanding of the underlying mechanism of the grain drying process on a single kernel, which would help

in developing accurate grain drying models with well-defined initial and boundary conditions.

Magnetic resonance imaging uses radio waves and powerful magnets to generate images of tissue. A strong magnetic field partially aligns the hydrogen atoms of water molecules in the tissue. A radio wave then disturbs the built-up magnetization, and radio waves are in turn emitted as the magnetization returns to its starting location. These radio waves are detected and used to construct an image. Ghosh and Jayas (2004) have extensively reviewed the recent research developments of MRI techniques and its potential in solving various grain related research problems. Magnetic resonance imaging can be used to obtain two or three-dimensional moisture transfer profiles inside a single grain kernel during drying. Little work has been carried out to determine transient moisture distribution inside the grain kernels during the drying process. The first experiment of this kind was reported by Song and Litchfield (1990) who determined the transient moisture profiles of ears of corn based on image pixel intensities at different drying times. Moisture distribution and changes inside the corn were distinctly different, and non-uniform during the drying process. Song et al. (1992) visually examined a series of MR image sequences to investigate moisture transfer and distribution from and within a corn kernel during drying at 27°C and 49°C. It was determined that moisture distribution in the kernels was non-uniform. Moisture loss also differed significantly during drying through two primary routes; the glandular layer of the scutellum and the pericarp. Kovács and Neményi (1999) used MR images of corn kernels during drying at 46°C and performed moisture gradient vector analysis to demonstrate the pathways of the moisture

loss from the intact kernel during drying. They also found non-uniform distribution of moisture inside the intact kernel before and during drying. Moisture was lost faster from the endosperm than the pericarp and it was the slowest from the scutellum. Ghosh et al. (2004) have first reported an explanation of moisture movement from the MR images of wheat kernels during drying. This study revealed the anisotropic and non-uniform nature of moisture distribution and migration prior-to or during drying of intact-wheat kernels. They observed that moisture loss was faster from the pericarp and endosperm compared to the germ with an increase in drying time. These conditions are an important consideration to develop accurate grain drying models. However, no efforts have been made so far to determine the effects of grain structural components on the movement of moisture from the grain kernels during drying using MRI. Therefore, the objectives of this study were to assess the effect of the structural components of wheat on the movement of moisture during drying using MRI and to study the movement of moisture inside the wheat kernel from the moisture gradient vectors calculated from each pixel of the subtraction of MRI images.

4.2 Materials and Methods

4.2.1 Drying Experiments

The wheat kernels (*Triticum aestivum* L., cv. A.C. Barrie) used in this study were procured from the Cereal Research Centre of Agriculture and Agri-Food Canada, Winnipeg. Individual kernels (approximately ellipsoidal shaped, 6 mm long and 3 mm diameter) were glued inside a small glass tube (12 mm long and 7 mm outer diameter) which was inserted into the probe (Helmholtz configuration) and then the probe was

placed into the bore of the MRI magnet. The grain kernels were subjected to a regulated low flow (0.23 m s^{-1}) of pre-heated N_2 (40 and 50°C ±1°C) during the intact drying process while MR images were obtained. Each drying experiment was continued for 4 h. For each temperature, three different kernels were used for measurements that gave similar results but these could not be averaged because of different kernel sizes. Therefore, a representative image for each treatment was analyzed and discussed. The selected low flow rate of nitrogen was high enough to ensure internally controlled drying. Nitrogen flow was parallel to the long axis of the wheat kernel. The wheat kernels were preconditioned to a selected moisture content (20 to 64% w.b.) by the static equilibrium moisture content method (Solomon 1951) or by imbibition in distilled water for 12-18 h at the beginning of every MR imaging experiment. The wheat kernels with no trace of germination were selected for this study. The initial moisture content of the wheat kernels was determined by the standard air-oven method (ASAE 2003) at the beginning of every MR imaging experiment. Wheat kernels with a high moisture level (>20%) were used in this study to acquire bright MR images which helped in studying the intrinsic details. To test the influence of kernel parts on moisture movement within the grain, mechanical scarification was achieved by either making an incision in the pericarp before starting each experiment, or removing the germ end from the kernel before moisture equilibration. The germ-removed kernels had a low moisture content (37%) compare to the intact kernels (64%).

4.2.2 Magnetic Resonance Image Data Acquisition

All MR images were obtained using a 11.7 T (500 MHz) Magnex (Magnex Scientific Ltd., Yarnton, UK) super-conducting vertical bore magnet equipped with a Magnex SGRAD 123/72/S 72 mm self-shielded, water-cooled, gradient set capable of producing a maximum gradient strength of 550 mT m^{-1} located at the National Research Council of Canada's Institute for Biodiagnostics, Winnipeg, MB. A Bruker (Milton, ON) Avance spectrometer with a ParaVision v.2.1.1 operating system was interfaced to the magnet to record and analyze the images. A conventional three-dimensional multi-slice Hahn spin-echo pulse sequence (Hahn 1950) was used for the MRI data acquisition. Images were processed as 8-bit, in a 128 × 64 × 8 matrix with a field-of-view of 1.28 × 1.28 × 0.4 cm, resulting in a pixel resolution of 100 μm × 200 μm × 500 μm. The MR Image size was increased by zero filling. Based on a compromise between image contrast and imaging time, the repetition time, TR, and the echo time, TE, were set to 200 ms and 3.375 ms, respectively. MRI data were acquired continuously and saved every 10 min 18 s without interrupting the drying process. During this time, six scans were acquired for signal averaging. A total of eight ^{1}H density image slices, each of 0.5 mm thickness, were obtained from each wheat kernel.

4.2.3 Magnetic Resonance Image Data Processing

The acquired MR images were gray-scale representations of the number of protons in the water-containing parts of the wheat kernels, which in turn represents water distribution. The brighter the image, the greater the number of protons. The darker the image, the fewer the number of protons. Multi-slice MR image data were scaled with respect to the

first image of the series, and displayed using Marevisi v. 7.1 (Institute for Biodiagnostics, National Research Council Canada, Winnipeg, MB) and NIH's public domain Java image processing program ImageJ (http://rsb.info.nih.gov/ij/). Image analysis (image acquisition and subtraction, gradient vector calculation and visualization) was performed with Matlab v. 7, R14 (The Mathworks, Natick, MA).

4.3 Results and Discussion

The representative MR images of sequential slices (2D) from MRI data sets (3D) collected as a function of time of an intact wheat kernel (approx. 20% w.b.) after every 1 h of drying at 50°C is shown in Fig. 4.1. A particular transverse slice was selected (slice number 6) to best illustrate the moisture distribution in the kernel with the greatest anatomical detail. The Signal-to-noise ratio (SNR) of the first image (t = 0) in serial MR images of Fig. 4.1 was 8.32. The SNR was calculated as the ratio of average pixel intensity of a region of interest (ROI) in the whole grain (both endosperm and embryo) to the average pixel intensity of the same size area in a region of noise only. The brighter portion represented higher moisture content, and overall signal intensity decreased with time. The brighter portion represented higher moisture content, and overall signal intensity decreased with time. The moisture movement within the wheat kernel during drying was studied as a function of drying time. The images clearly showed that the non-uniform pattern of moisture distribution inside the intact-wheat kernel was present before drying was started and continued during drying. The lowest moisture content occurred in the endosperm. The highest water content was detected in the embryo. The crease of the kernel also looked

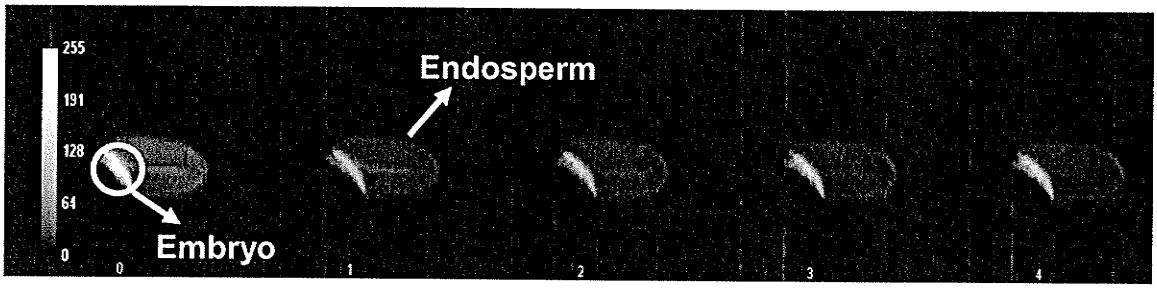

Figure 4.1 Magnetic resonance images of an intact wheat kernel during drying at every hour. Drying conditions: temperature, 50°C; drying time, 4 h. Numbers at the bottom of the images indicate the time, in hours, from the beginning of drying.

bright at the beginning of drying. The probable reason could be that some water molecules adhered to the surface of the crease by the surface tension during wheat conditioning. The images also revealed that moisture loss was faster from the pericarp because MR signal intensities in the pericarp region could not be measured as drying of this area occurred fast with respect to the time resolution of the experiment. The moisture loss from the endosperm was greater when compared to the embryo, which was evident from the inner part of the embryo that remained at high moisture content even after 4 h drying.

We conducted a 2D Gradient Vector analysis, in Matlab, to describe the real moisture loss from each point of the whole-wheat kernel images. The Matlab computed gradient of a function of two variables, I(x,y), is defined as:

$$\nabla I = \frac{\partial I}{\partial x}\hat{i} + \frac{\partial I}{\partial y}\hat{j} \tag{4.1}$$

The gradient can be thought of as a collection of vectors pointing in the direction of increasing values of I. In our case, I is the subtracted image matrix, and x and y are the pixel coordinates. Figure 4.2 shows the subtracted image of the first (before drying) and second (after 1 h of drying) images of an intact wheat kernel shown in Fig. 4.1. The gradient vectors of the moisture loss data for the subtracted image are shown in Fig. 4.3. The longer the vectors the faster the moisture level changes. The rates of moisture change in the pericarp, endosperm, and embryo during drying were clearly different. The rate of moisture loss was slower from the endosperm region, whereas the pericarp region dried faster at the initial stages of drying. The fastest moisture decrease was from the outermost

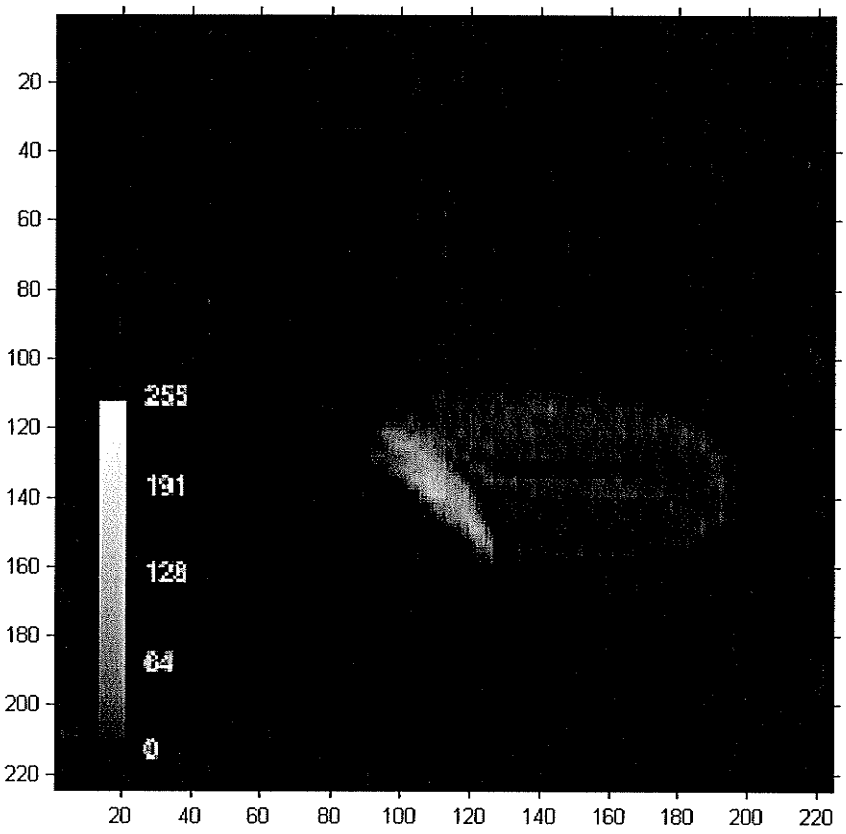

Figure 4.2 Subtracted image of an intact-wheat kernel (after 1 h of drying) obtained from Fig. 4.1. The scales show the pixels and the sidebar in the image represents the moisture contents in terms of the grayscale intensity; high gray values represent high moisture contents.

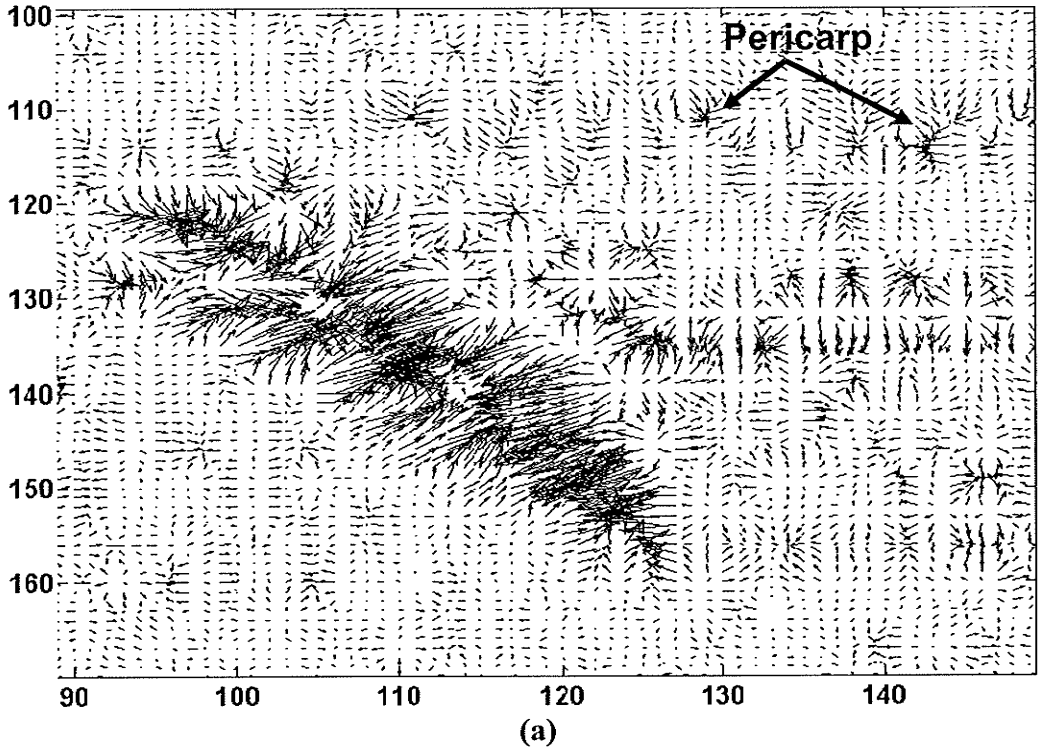

(a)

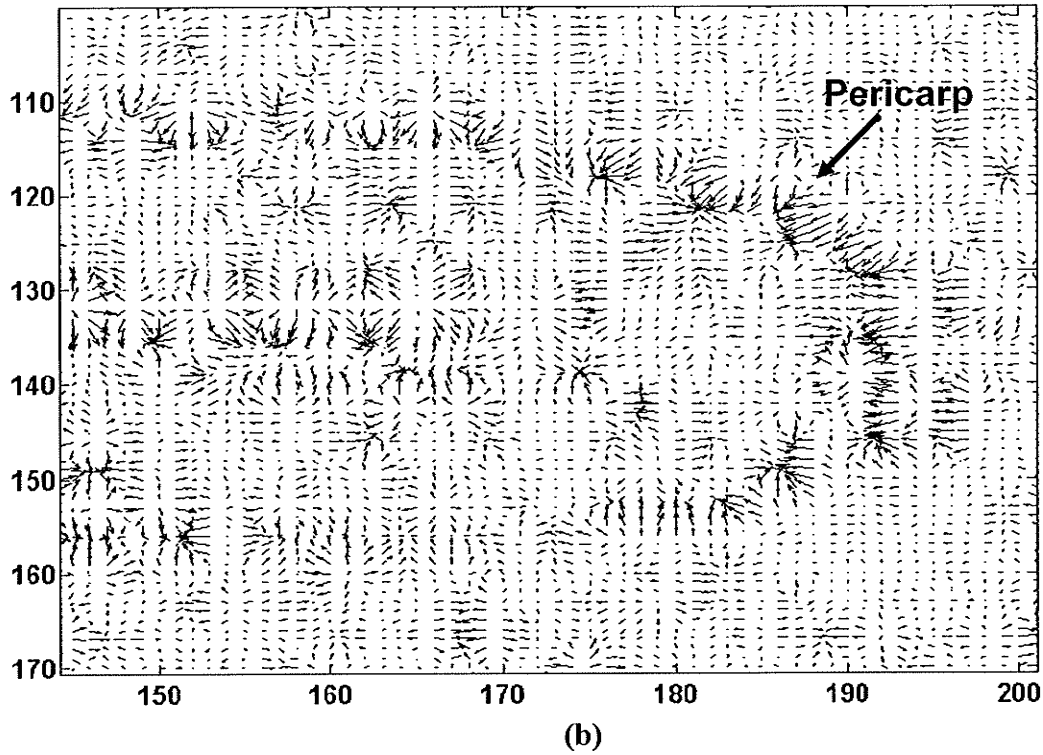

(b)

Figure 4.3 Gradient vectors of the subtracted image matrix of Fig. 4.2: (a) the embryo and part of endosperm region, and (b) the endosperm region. The arrows indicate the moisture movement from each point; the arrow size is proportional to the rate of moisture loss.

layer of the embryo section as its gradient vectors are the largest and pointing outwards from the kernel but the inner vectors show inward movement. The vectors at the transition region of embryo and endosperm show inward movement in the direction of the embryo. This typical direction of arrowheads indicates that the water has the tendency to move from the endosperm towards the germ (embryo) through the fingerlike cells of the scutellum epithelium (the outer layer of the scutellum located next to the endosperm) which functions as an absorption organ. This explains why the embryo was able to retain more moisture even after 4 h of drying. Kovács and Neményi (1999) reported a similar effect on moisture removal in corn kernels during drying.

For the mechanically scarified kernels (approx. 64% w.b.) and embryo-removed kernels (approx. 37% w.b.), the representative images are shown in Figs. 4.4a and 4.4b. The SNRs of the first images (t = 0) in serial MR images of Figs. 4.4a and 4.4b were 47.9 and 18.2, respectively. The 5^{th} and 6^{th} slices were chosen in Figs. 4.4a and 4.4b, respectively, to evaluate the moisture transfer during drying. Gradient vectors were calculated and visualized to determine the moisture removal pattern in both type of grains to test if the site of superficial cutting of pericarp and the removal of embryo influenced the moisture movement in kernels. Figures 4.5 and 4.7 show the subtracted images of the first (before drying) and second (after 1 h of drying) images of a mechanically scarified kernel and an embryo-removed kernel, respectively. Figures 4.6 and 4.8 show the gradient vectors of the 2D moisture movement obtained from Figs. 4.5 and 4.7 for the mechanically damaged kernels and the embryo-removed kernels, respectively. It can be seen from Fig. 4.6 that vectors from the embryo end are directed towards the endosperm section and the

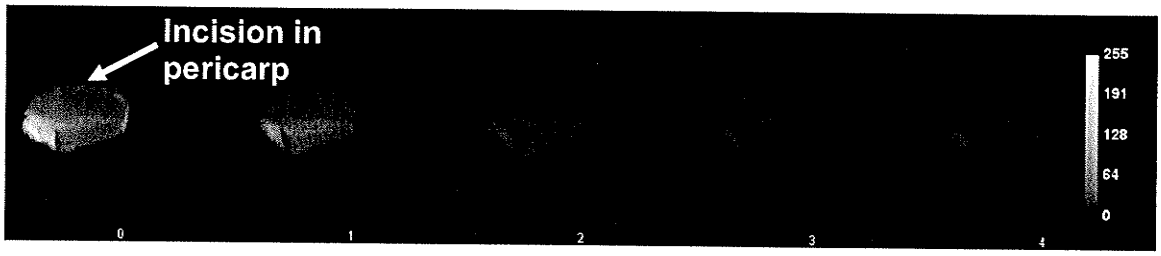

Figure 4.4a Magnetic resonance images of a mechanically scarified wheat kernel during drying at every hour. Drying conditions: temperature, 40°C; drying time, 4 h. Numbers at the bottom of the images indicate the time, in hours, from the beginning of drying.

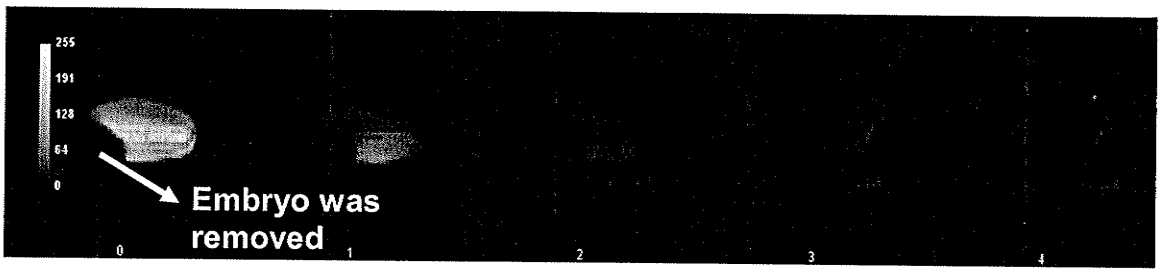

Figure 4.4b Magnetic resonance images of an embryo-removed wheat kernel during drying at every hour. Drying conditions: temperature, 50°C; drying time, 4 h. Numbers at the bottom of the images indicate the time, in hours, from the beginning of drying.

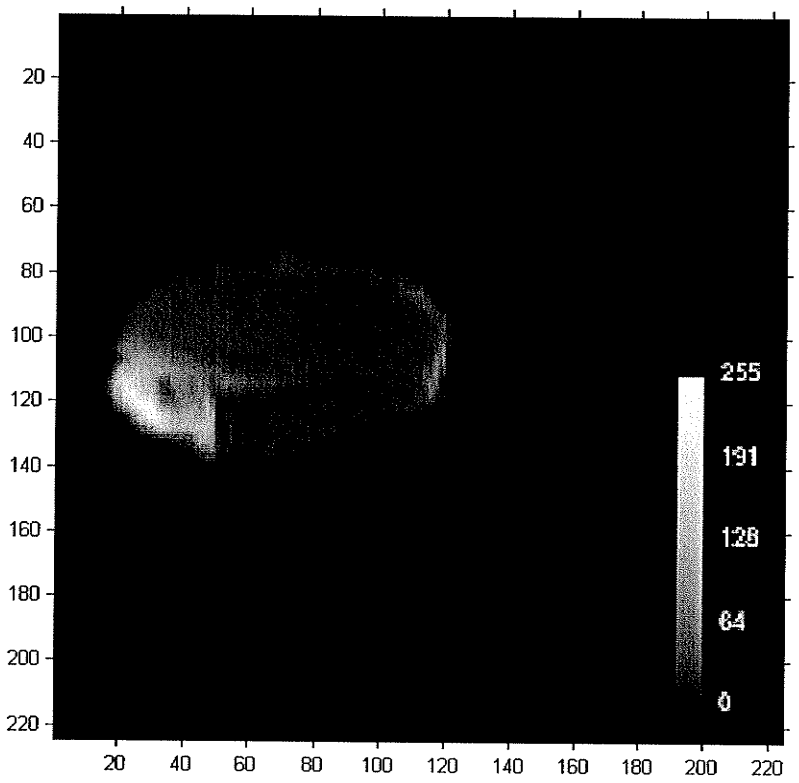

Figure 4.5 Subtracted image of a mechanically scarified kernel (after 1 h of drying) obtained from Fig. 4.4a. The scales show the pixels and the sidebar in the image represents the moisture contents in terms of the grayscale intensity; high gray values represent high moisture contents.

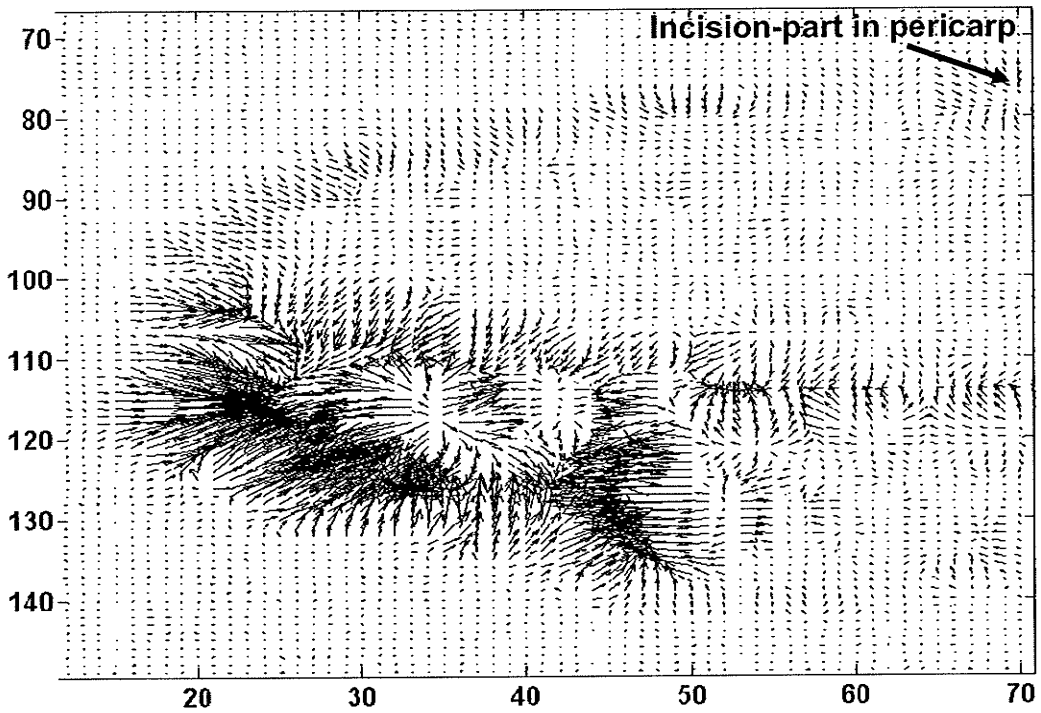

(a)

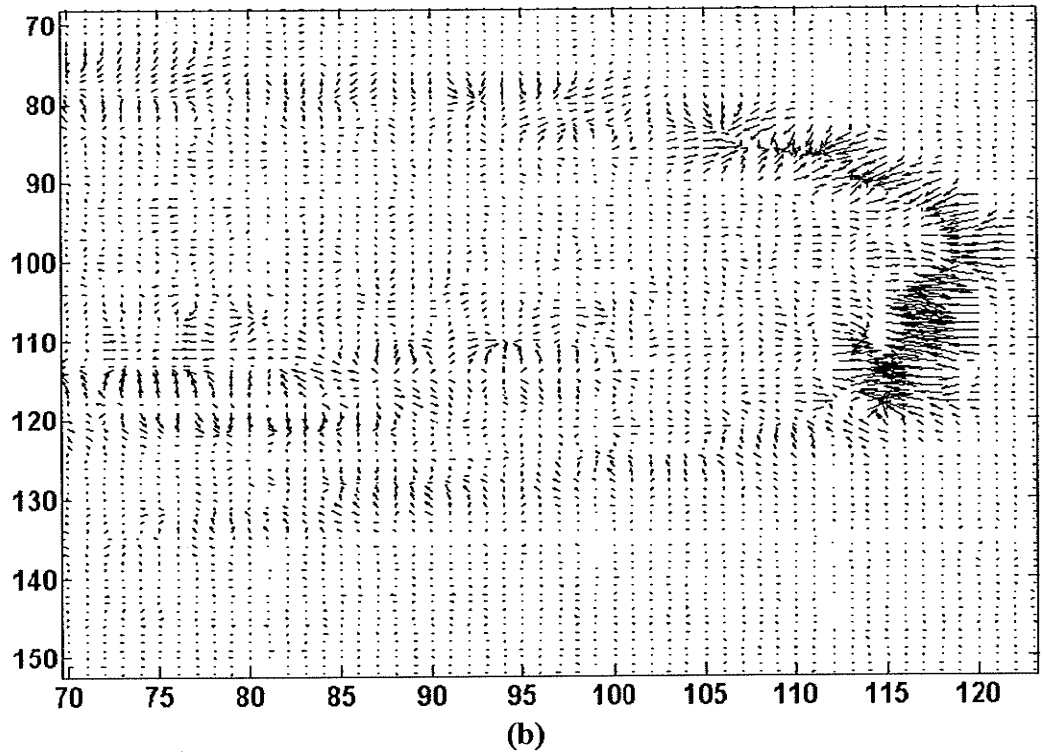

(b)

Figure 4.6 Gradient vectors of the subtracted image matrix of Fig. 4.5: (a) the embryo and part of endosperm region, and (b) the endosperm region.

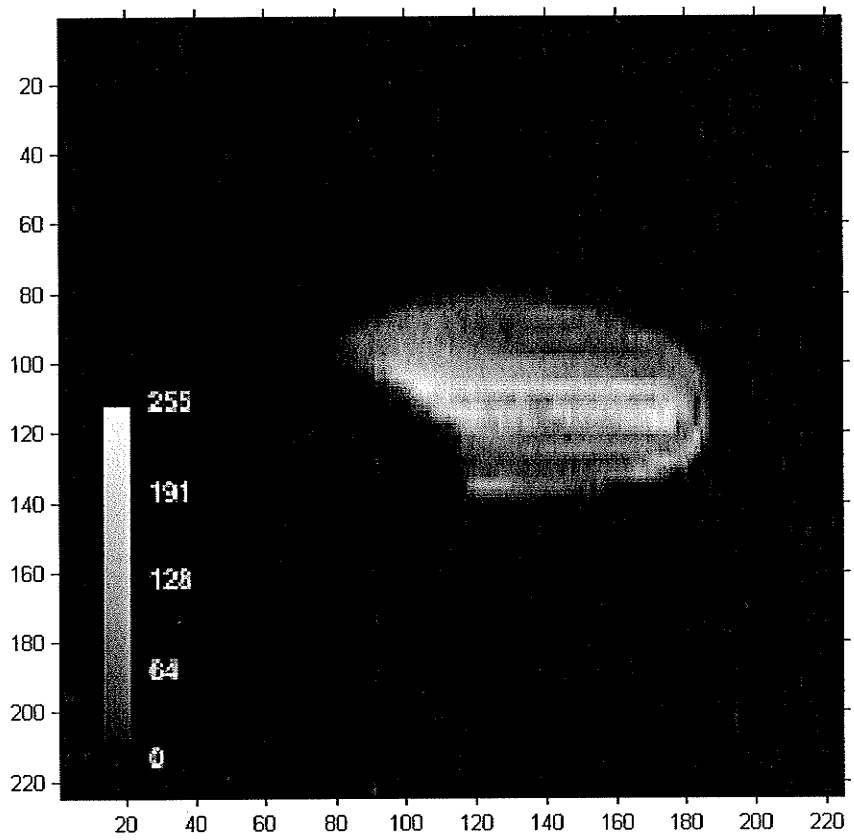

Figure 4.7 Subtracted image of an embryo-removed kernel (after 1 h of drying) obtained from Fig. 4.4b. The scales show the pixels and the sidebar in the image represents the moisture movements in terms of the grayscale intensity; high gray values represent moisture increase and low gray values represent moisture decrease.

amplitude of the vectors is long. Long arrows are also detected at the incision-part of the pericarp region that tend towards outward direction of the kernel. It is assumed that when incision in the pericarp was done, the outer pericarp layers of wheat (epidermis and hypodermis) as well as the inner layers of the pericarp were broken. Moreover, the inner layers of the pericarp consist of thinner walled cross-cells and tube-cells containing intercellular spaces through which water could move rapidly. Therefore, water was released relatively faster from the scarified regions of the pericarp. This means the pericarp plays an important role in moisture movement inside the grain during drying. Intact pericarp behaves as a moisture barrier after the initial stages of drying and resists the movement of water from the kernel. However, a damaged pericarp allows moisture to move from the kernel. In the case of embryo-removed kernels, moisture moved out in a uniform manner from the wheat kernel as the outermost vectors tend towards the environment but one layer deeper the arrows show inward movement (Fig. 4.8). When the germ was removed from the wheat kernel, the water moved uniformly through the capillaries of the endosperm towards the large rectangular aleurone layer of the endosperm. The aleurone layer is the outermost layer of the endosperm, which is attached to the innermost paricarp layer of the wheat kernel. Once the water comes to the aleurone layer of the endosperm, it then moved out from the wheat kernel through the intercellular spaces of the pericarp. Arrows showing inward movement would be arising due to the inner bran layers (the aleurone) high in protein and the outer bran layer (pericarp, seed coats, and nucellus) high in cellulose, hemicellulose and minerals, which had started functioning as a protective coating with the closely adhered thick-walled cells and started to offer more water resistance. Thus, the MRI images and the gradient vector analyses

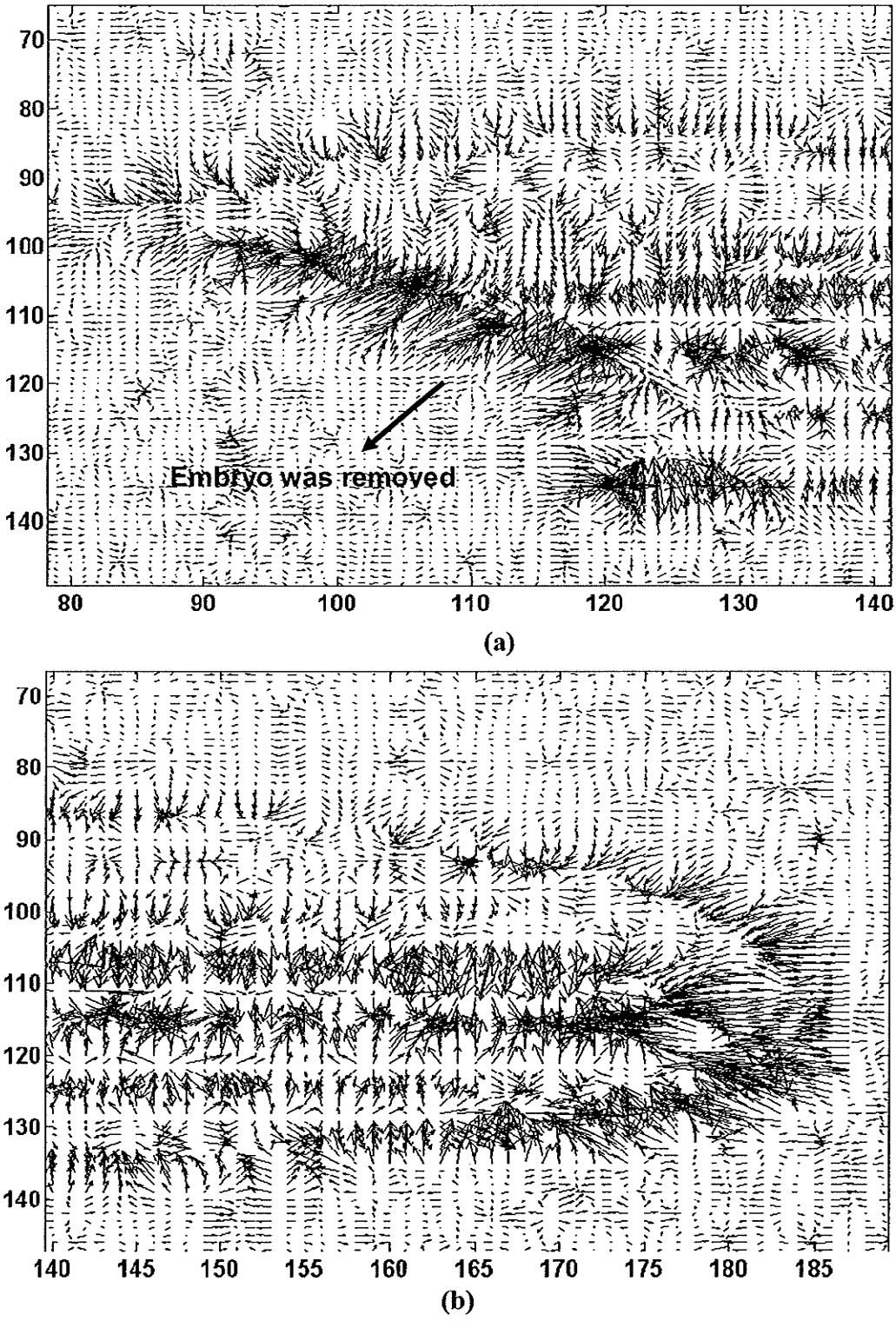

Figure 4.8 Gradient vectors of the subtracted image matrix of Fig. 4.7: (a) the left portion, and (b) the right portion.

give a clear indication of the moisture removal pattern that was highly influenced by the grain structural components.

4.4 Conclusions

The MRI technique was found to be a powerful tool to study moisture movement inside a grain kernel during drying. The MR images showed that the moisture removal pattern during drying of a wheat kernel was non-uniform. Moisture removal was also dependent on the grain structural inhomogeneties. Mechanical scarification of the wheat kernel and embryo-removal from the kernel made it easy to visualize the underlying drying phenomena. Moisture appeared to move through the germ end of the wheat kernel from the endosperm after initial stages of drying whereas the pericarp dried faster and presumably acted as a moisture barrier. The germ portion plays an important role in moisture migration during drying. A gradient vector analysis of the MRI intensities provided a mathematical description of the real moisture loss from the kernel during drying. Results of this study will help in mathematical modeling of drying processes and in practical application of the drying theory.

Acknowledgements

The authors thank the Canada Research Chairs program, University of Manitoba Graduate Fellowship Committee, and the Natural Sciences and Engineering Research Council of Canada for the funding of this study.

References

ASAE. 2003. ASAE Standards S352.2. Moisture measurement – unground grain and seeds. St. Joseph, MI: ASAE.

Czaba, I. and M. Neményi. 1997. Investigation of simultaneous heat and mass transfer within the individual maize kernels during drying time. *Hungarian Agricultural Engineering* 10:58-60.

Ghosh, P.K. and D.S. Jayas. 2004. Magnetic resonance imaging: potential use for grain research. In *Proceedings of International Conference on Emerging Technologies in Agricultural Engineering,* 130-136. Indian Institute of Technology, Kharagpur, India. December 14-17.

Ghosh, P.K., D.S. Jayas, M.L.H. Gruwel and N.D.G. White. 2004. Magnetic resonance image analysis to explain moisture movement in wheat drying. ASAE Paper No. 043118. St. Joseph, MI: ASAE.

Haghighi, K. and L.J. Segerlind. 1988. Modeling simultaneous heat and mass transfer in an isotropic sphere – A finite element approach. *Transactions of the ASAE* 31(2):629-637.

Haghighi, K., J. Irudayaraj, R.L. Stroshine and S. Sokhansanj. 1990. Grain kernel drying simulation using the finite element method. *Transactions of the ASAE* 33(6):1957-1965.

Hahn, E.L. 1950. Spin echoes. *Physical Review* 80(4):580-594.

Husain, A., C.S. Chen and J.T. Clayton. 1973. Simultaneous heat and mass diffusion in biological materials. *Journal of Agricultural Engineering Research* 18(4):343-354.

Kovács, A.J. and M. Neményi. 1999. Moisture gradient vector calculation as a new method for evaluating NMR images of corn (*Zea mays* L.) kernels during drying. *Magnetic Resonance Imaging* 17(7):1077-1082.

Luikov, A.V. 1966. *Heat and mass transfer in capillary-porous bodies.* Oxford, U.K.: Pergammon Press.

Sokhansanj, S. and D.M. Bruce. 1987. A conduction model to predict grain temperature in grain drying simulation. *Transactions of the ASAE* 30(4):1181-1184.

Sokhansanj, S. and R.J. Gustafson. 1980. Prediction of heat and mass transfer within a grain kernel – a finite element application. In: *Drying 80 vol. 2*, 229-232. A.S. Majumdar, ed. New York, NY: McGraw-Hill International Book Company.

Solomon, M.E. 1951. Control of humidity with potassium hydroxide, sulphuric acid or other solutions. *Bulletin of Entomological Research* 42:543-554.

Song, H. and J.B. Litchfield. 1990. Nondestructive measurement of transient moisture profiles in ear corn during drying using NMR imaging. *Transactions of the ASAE* 33(4):1286-1290.

Song, H.P., J.B. Litchfield and H.D. Morris. 1992. Three dimensional microscopic MRI of maize kernels during drying. *Journal of Agricultural Engineering Research* 53(1):51-69.

A MAGNETIC RESONANCE IMAGING STUDY OF WHEAT DRYING KINETICS[3]

Prabal K. Ghosh[1], Digvir S. Jayas[1], Marco L.H. Gruwel[2, 3], Noel D.G. White[1, 4, 5]

[1]Department of Biosystems Engineering, University of Manitoba, Winnipeg, Manitoba, Canada, R3T 5V6

[2]NRC Institute for Biodiagnostics, 435 Ellice Avenue, Winnipeg, Manitoba, Canada, R3B 1Y6

[3]Department of Chemistry, University of Manitoba, Winnipeg, Manitoba, Canada, R3T 2N2

[4]Cereal Research Centre, Agriculture and Agri-Food Canada, 195 Dafoe Road, Winnipeg, Manitoba, Canada, R3T 2M9

[5]Department of Entomology, University of Manitoba, Winnipeg, Manitoba, Canada, R3T 2N2

Abstract

A spin-echo (SE) magnetic resonance imaging (MRI) technique was used to study non-invasively moisture levels as a function of time in single wheat kernels. Internal moisture distribution during drying of wheat at temperatures of 30, 40, and 50°C for 4 h was analyzed from the MR images. The influence of the individual wheat components on the drying process was observed using physically different wheat kernels: intact kernels, mechanically scarified kernels with incisions in the pericarp, and kernels with the embryo removed. Drying rate curves for these different kernels were obtained at three different temperatures and the effects of temperature on the drying curves were discussed. A calibration curve of MR image intensity versus the actual moisture content of the grain

[3] This paper is accepted in March 2007 for publication in ***Biosystems Engineering***. Manuscript No. be 06 167.

was obtained using nuclear magnetic resonance (NMR) spectra of wheat at different, known, moisture contents. Results obtained from this study provided details of the drying kinetics in wheat kernels.

Keywords: *Drying, Magnetic resonance imaging, Moisture, Wheat.*

5.1 Introduction

Wheat is a world leading cereal grain in terms of production and consumption. Global wheat production for 2004-05 was 624 million tonnes (Mt) and has increased about 13% from 553 Mt in 2003-04 (USDA 2005). In general, high moisture levels can spoil grains during storage. Therefore, there is a need to preserve wheat by drying, which is a commonly used practice around the world. Knowledge of kernel moisture, and most importantly, knowledge of the moisture distribution within the kernel, is essential to understand the drying phenomena.

The structure of a wheat kernel consists of an embryo and an endosperm surrounded by the pericarp. However, the internal structure and composition of a wheat kernel is very complicated and therefore the anatomy of the entire kernel is of importance in determining the movement of moisture during drying. Details of the wheat structure are published elsewhere (MacMasters et al. 1964; Brooker et al. 1992; Pomeranz and Bechtel 1978; Evers and Bechtel 1988).

Since the structure of wheat is heterogeneous, the prediction of kernel drying becomes very complicated as it involves both heat and mass transfer. Several studies have been

reported which incorporate one or more of diffusion, capillary flow, or evaporation-condensation mechanisms to develop single kernel drying models (rice: Husain et al. 1973; corn and rice: Sokhansanj and Gustafson 1980; wheat: Fortes et al. 1981; barley: Haghighi et al. 1990; corn: Czaba and Neményi 1997; wheat: Jia et al. 2000; grain: Ranjan et al. 2001; rice: Yang et al. 2002). All of these studies used an invasive method to measure the kernel moisture level, destroying the sample.

Magnetic resonance imaging offers the possibility to study the water distribution in grains non-invasively and non-destructively. Magnetic resonance imaging technology uses radio waves and powerful magnets to generate images of water-containing materials. Grain moisture content determination using MRI has been reported by few researchers (wheat: Miller et al. 1980, Brusewitz and Stone 1987, Chambers et al. 1989, Tollner and Hung 1992; barley: Miller et al. 1980; corn: Miller et al. 1980, Tollner and Hung 1992). Moisture distribution inside the grain kernels during drying has been studied by several researchers (corn: Song and Litchfield 1990; Song et al. 1992; Kovács and Neményi 1999; rice: Ishida et al. 2004). A detailed study on the moisture migration paths in a wheat kernel during drying was recently published by Ghosh et al. (2006a) using a gradient vector analysis of the MR image intensities. Further, the influence of the wheat structural components (pericarp, endosperm, and embryo) on the internal moisture removal and distribution pattern was studied by Ghosh et al. (2006b) with the help of MR images. These two studies revealed that (a) non-uniform moisture distribution exists inside intact wheat kernels before and during drying, and (b) moisture loss from the three different seed parts occurs at different rates and is dependent on grain components.

This information led to the objective of the present research which was to be able to identify the actual physical phenomena, which occur during drying of a wheat kernel. Real time conditions from the present research will be the basis of developing accurate grain drying models describing mass- and heat-transport in individual kernels. Further, this research will allow selecting proper boundary conditions and treating the kernels as a composition of three components: a pericarp, an endosperm and an embryo for a microscopic analysis of the drying process.

5.2 Materials and methods

5.2.1 Materials and Sample Preparation

Canada Western Red Spring (CWRS) wheat (*Triticum aestivum* L.), cultivar A.C. Barrie, used as the test sample, was obtained from the Cereal Research Centre, Agriculture and Agri-Food Canada, Winnipeg, MB. The wheat kernels containing approximately 15.7±0.03% d.b. (dry basis) moisture content were stored at 4°C prior to the experiments. All the moisture contents in this article are presented on dry mass basis except for cases noted otherwise.

Fresh kernels at typical harvest moisture contents are difficult to visualize with MRI in a short time span due to the low moisture level. Also during drying, moisture will go below 16%, therefore it would be more time-consuming and difficult to study the drying process. Therefore, we conducted this study with reconditioned high moisture kernels. We realize that rehydrated wheat kernels will dry to a different final moisture content than the fresh kernels due to hysteresis effect but are an acceptable substitute for studying

drying phenomena. Small batches of approximately 15 kernels were imbibed overnight at room temperature in distilled water using a 50 mL beaker while shielded from air and light. Before starting the drying experiments, imbibed kernels were blotted with a paper towel to remove excess water attached to the surface. Wheat kernels with no trace of germination were selected for this study. Wheat kernels with a high moisture level (greater than 25%) were used in this study to acquire bright MR images which helped in studying the intrinsic details. For every MRI experiment, a new wheat kernel was glued inside a small standard glass tube (12 mm long and 7 mm outer diameter) which was inserted in the centre of the MR imaging probe which was then placed into the bore of the magnet. Prior to the MRI experiments the initial moisture content of the wheat kernels was determined by drying 10 g samples at 130°C for 19 h using the standard air-oven method (ASAE 2003).

To observe the influence of the kernel components on the drying process, we used three different types of wheat kernels: intact kernels (with all three components: pericarp, embryo, and endosperm); mechanically scarified kernels, which were achieved by making incisions in the pericarp; and kernels with the embryo removed. The intact kernels were imbibed for moisture equilibration before starting each experiment. The incisions on the intact kernels were made after the moisture equilibration to prepare the scarified kernels. However, the embryo was removed from the intact kernels prior-to the moisture equilibration. This was done to reduce possible loss or redistribution of soluble materials of the imbibed kernels and thus to achieve more accurate results (MacMasters

et al. 1964). The embryo-removed kernels were at lower moisture content (about 50%) than the intact or the scarified kernels (about 60%).

5.2.2 Magnetic Resonance Imaging System

All MRI experiments were performed on an 11.7 T (500 MHz) Magnex (Magnex Scientific Ltd., Yarnton, UK) super-conducting vertical-bore magnet equipped with a Magnex SGRAD 123/72/S 72 mm self-shielded, water-cooled, gradient set capable of producing a maximum gradient strength of 550 mT m^{-1}, located at the Institute for Biodiagnostics, National Research Council of Canada, Winnipeg, MB. A Bruker (Milton, ON) Avance DRX console was interfaced to the magnet to record the MR images using ParaVision software. The MR imaging probe and coil (Helmholtz configuration: 7 mm inner diameter) were home-built.

5.2.3 Drying Apparatus

Nitrogen gas was used as the drying medium, instead of ambient air, because it is dry (no humidity) and is also non-corrosive to most of the instrument materials. Dry nitrogen gas was supplied using an in-line variable temperature and flow controller unit (Bruker BVT-1000, Milton, ON). This ensured a regulated low flow of N_2 gas with controlled temperature. The heater assembly to condition N_2 was attached beneath the MRI probe and the magnet. The gas exits through the top of the probe. A long flexible tube (5 mm internal diameter) for conducting the heated N_2 was covered by heat-insulating material (Fibre Glass R21) to prevent any heat-loss from the tube. The temperature of the gas supply was measured at a close proximity to the sample using a copper-constantan

thermocouple connected to the Bruker BVT-1000. A schematic diagram of the experimental set-up is shown in Fig. 5.1.

5.2.4 Drying of Wheat Kernels

Moisture movement within and out of a wheat kernel during drying was observed under the following conditions: initial average moisture contents: 60.3±0.8% (intact or scarified kernels) and 49.7±3.2% (embryo-removed kernels); three types of wheat kernels: intact, mechanically scarified, and embryo-removed; and drying temperatures: 30, 40 and 50°C with an accuracy of ±1°C. This range of drying temperatures was chosen because the results obtained from this study would help to develop a drying model of practical importance. Although drying of wheat grains at temperature more than 43°C is not recommended for use of wheat as seed, but drying at 50°C is safe for bread baking and other commercial uses (Brooker et al. 1992). The preheated N_2 gas flow rate around the wheat kernel was 0.23 m s^{-1}. The selected flow rate of nitrogen was high enough to ensure internally controlled drying. The N_2 flow was parallel to the long axis of the wheat kernel. The drying experiments were started after a very rapid warm up time of the drying set up which took approximately 3-5 min to reach a steady-state temperature (30-50°C). During the 20 min MRI setup procedure, the kernel was not exposed to flowing gas and kept at room temperature. Each drying experiment continued for 4 h. After this time, the signal intensity is of the same order of magnitude as the noise level in the image. We were interested in comparing relative drying rates for individual kernel components, therefore drying experiments were replicated three times at each

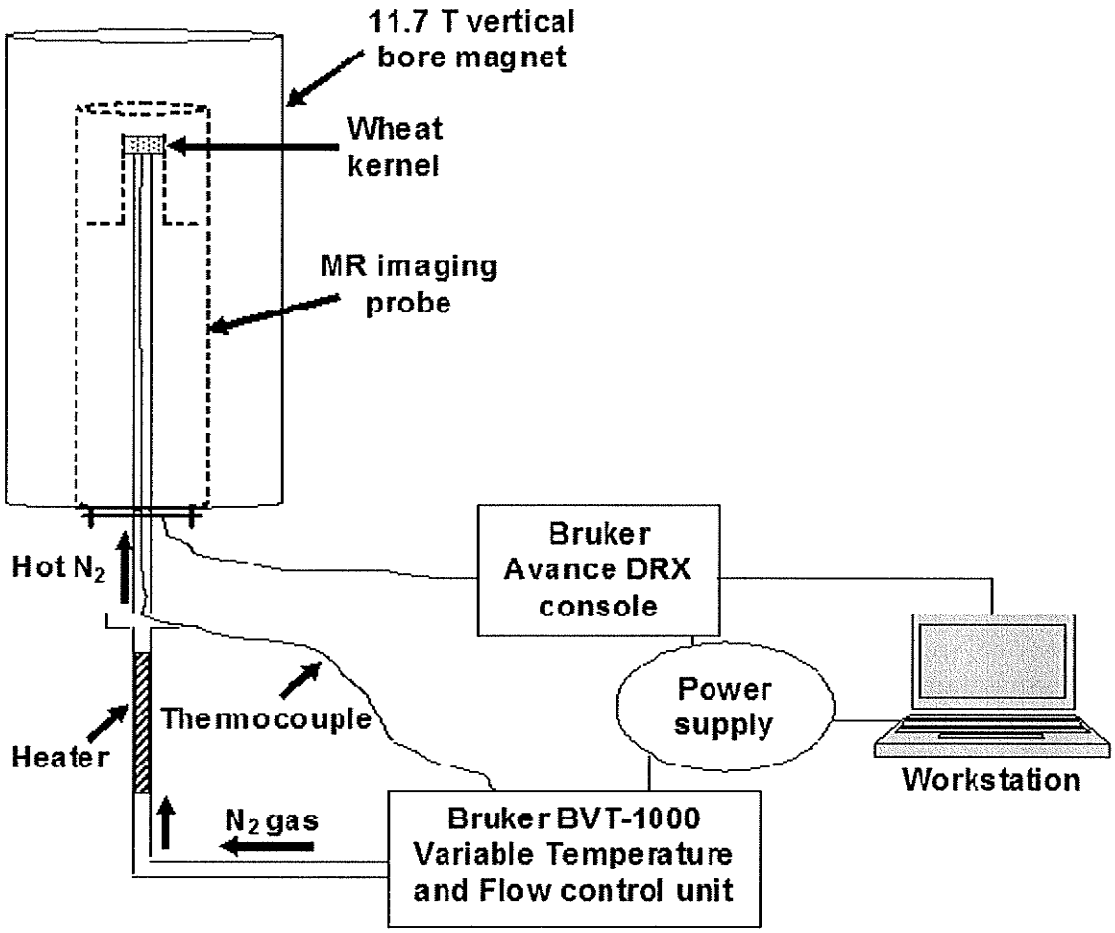

Figure 5.1 Schematic diagram of the magnetic resonance imaging experimental set up with the dryer assembly.

temperature with similar sized wheat kernels selected by visual inspection. Results analyzed in this article are the average normalized image intensities of three replicates.

5.2.5 Magnetic Resonance Image Data Acquisition

For the acquisition of micro images a two-dimensional, multi-slice Hahn spin-echo pulse sequence was used (Hahn 1950). Gradient-echo experiments were used for scout images to determine the position and orientation of the kernel. The spin-spin or transverse relaxation time T_2 for the individual components of a wheat kernel (embryo: 9.99 ms, pericarp: 7.16 ms, and endosperm: 3.08 ms) was measured by recording the signal intensities as a function of the echo time (TE) using the spin-echo sequence (Ghosh et al. 2006b). Data were fitted assuming a mono-exponential decay. The spin-lattice relaxation time T_1 of protons in wheat samples is generally of the order of 400 ms as reported by Stapley et al. (1997). Based on a compromise between image contrast and imaging time, the repetition time, TR, and the echo time were set to 200 ms and 3.375 ms, respectively. A total of eight slices, each of 0.5 mm thickness, were obtained from each wheat kernel. The total image acquisition time was 10 min 18 s for six scans, acquired for signal averaging. Images were processed as 8-bit, in a 128 × 64 × 8 pixel matrix with a field-of-view of 1.28 × 1.28 × 0.4 cm, resulting in a pixel resolution of 100 μm × 200 μm × 500 μm. The MR image size was increased by zero-filling. Figure 5.2 shows a representation of the eight slices obtained from an intact wheat kernel (approximately 60% moisture content). A particular transverse slice out of 8 slices was selected (Fig. 5.2 slice 4) to best illustrate the moisture distribution in the kernel with the greatest anatomical detail for the analysis of drying as a function of time.

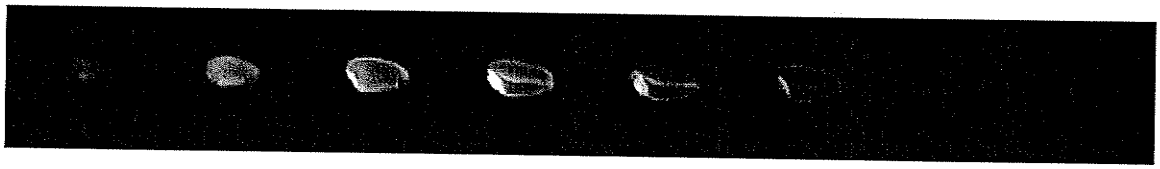

Figure 5.2 Representative set of 8 transverse slices of an intact wheat kernel obtained from magnetic resonance imaging.

One dimensional nuclear magnetic resonance (NMR) spectral data were obtained with a spectral width 50 kHz, an acquisition time of 0.0102 s and 60 acquisitions. Signal calibration was performed with a small water phantom.

5.2.6 Magnetic Resonance Image Data Analysis

Multi-slice MR image data were scaled with respect to the first image of the time series. Marevisi v. 7.1 (Institute for Biodiagnostics, National Research Council Canada, Winnipeg, MB) and NIH's public domain Java image processing program ImageJ (http://rsb.info.nih.gov/ij/) were used to process the data sets. All the reported image intensities were derived by the following equation to eliminate the effect of the noise on the analysis of drying curves (Bernada et al. 1998a):

$$I_{avg} = \frac{I_{kernel} - I_{noise}}{I_{noise}} \tag{5.1}$$

Where I_{avg} is the average pixel intensity (arbitrary units); I_{kenel} is the overall pixel intensity of the selected kernel component (arbitrary units); I_{noise} is the overall pixel intensity of the same size area in a region of noise only (arbitrary units); and

where by definition:

$$I_i = \frac{1}{A_{I_i}} \iint_{A_{I_i}} I(x,y)\, dx\, dy \tag{5.2}$$

where I_i is the pixel intensity at coordinate (x,y) in the kernel or noise area (arbitrary units); A_{I_i} is the average area (arbitrary units); and x, y are the pixel coordinates in the kernel or noise area.

Image analysis (image reconstruction and visualization, normalization, pixel selection, and thresholding) was performed with ImageJ and Matlab v. 7, R14 (The Mathworks, Natick, MA). Data were analyzed using the statistical procedures in Microsoft® Excel (v. SP-2, 2002) and SigmaPlot v. 6.0 (SPSS Inc., Chicago, IL). The normalized MR image intensities for the drying temperature and the three types of wheat kernels are tabulated in Table 5.1.

One-dimensional NMR spectra were processed using XWIN-NMR v. 3.2 and MestRe-C v. 2.3a (Mestrelab Research, A Coruña, Spain) NMR data processing software. The two-dimensional (2D) geometry objects from the MR images of three different kinds of wheat kernels were generated using Comsol Multiphysics 3.2 (COMSOL Inc., Burlington, MA) along with Matlab to show the physical conditions schematically (Fig. 5.3).

5.3 Results and Discussion

Examples of the two dimensional (2D) geometry objects of an intact, a mechanically-scarified, and an embryo-removed wheat kernel are shown in Fig. 5.3(a) through 5.3(c) in which the general shape of the seeds, approximately ellipsoidal, are easily distinguishable with approximately 6 mm length and 3 mm diameter. Figure 5.3(b) shows the incisions in the pericarp region. In harvested wheat kernels (generally 15 to 19% moisture content), the oil content is generally very low, not exceeding 2.3% on a dry mass basis (Pomeranz 1988), therefore the proton NMR signal generally originates primarily from water. In dried wheat kernels, water constitutes up to 13% of the dry weight of the seed (Pomeranz 1988). A static proton NMR spectrum of a single seed of 18.8% moisture content is shown in Fig. 5.4. The NMR spectrum shows the water peak centered at 0 Hz and a

Table 5.1 Image intensities* with varying drying time and grain conditions

Temp. (°C)	Drying time (min)	Intact kernel		Mechanically scarified kernel		Embryo-removed
		Embryo	Endosperm	Embryo	Endosperm	Endosperm
30	0	52.3±29.6	14.2±8.5	57.4±36.5	11.3±7.9	8.7±2.9
	30	50.6±26.7	13.8±8.0	49.2±34.8	10.2±8.2	7.8±2.8
	60	41.9±19.1	12.5±7.7	48.5±38.4	9.5±7.8	7.0±2.3
	90	36.1±19.2	11.0±6.2	34.2±25.4	8.1±7.3	5.6±1.6
	120	32.1±16.7	9.0±5.3	26.5±17.9	6.8±6.1	4.8±1.1
	150	28.5±12.8	7.2±4.1	21.5±14.7	5.7±5.6	3.9±0.8
	180	26.2±10.7	5.8±3.4	21.3±12.7	4.8±4.9	3.3±0.7
	210	23.9±7.9	4.7±2.9	19.0±12.1	3.9±4.1	2.8±0.5
	240	22.0±7.1	3.9±2.4	18.8±11.7	3.2±3.4	2.5±0.5
40	0	41.2±23.4	11.5±8.5	68.9±74.6	13.7±15.1	22.0±16.5
	30	29.3±17.0	9.8±7.4	43.2±43.5	12.1±12.8	19.4±15.8
	60	19.4±8.1	7.8±5.0	24.4±15.1	8.5±9.1	13.9±10.6
	90	17.6±5.7	5.4±3.1	15.5±1.7	4.8±5.2	8.6±6.4
	120	14.2±2.5	3.8±2.5	11.6±1.2	2.4±2.3	6.0±4.3
	150	14.5±2.3	2.6±1.7	11.8±2.4	1.6±1.2	3.7±2.8
	180	13.4±3.1	1.8±1.2	10.5±2.7	1.1±0.8	2.6±1.7
	210	13.5±3.8	1.4±0.8	9.0±1.3	0.8±0.5	1.7±1.1
	240	14.2±3.1	1.2±0.6	10.6±2.4	0.7±0.3	1.4±0.8
50	0	37.7±26.3	9.5±9.4	52.7±16.8	15.1±9.7	16.2±8.6
	30	22.1±12.0	6.4±6.6	30.1±5.3	9.6±6.0	9.6±5.2
	60	15.0±4.8	4.5±5.2	15.2±3.4	6.1±3.4	4.7±2.9
	90	12.6±3.8	2.6±2.9	11.0±4.6	3.3±1.4	2.4±1.5
	120	10.9±1.9	1.6±1.7	10.8±4.7	2.1±1.0	1.5±1.0
	150	11.7±2.4	1.1±1.1	9.9±5.4	1.2±0.4	0.9±0.5
	180	12.2±2.8	0.8±0.7	10.7±5.9	0.9±0.3	0.6±0.5
	210	11.4±2.7	0.6±0.4	10.4±6.4	0.6±0.3	0.6±0.5
	240	11.7±2.3	0.6±0.4	10.0±5.2	0.5±0.2	0.5±0.5

* Mean ± Standard Deviation (3 replications)

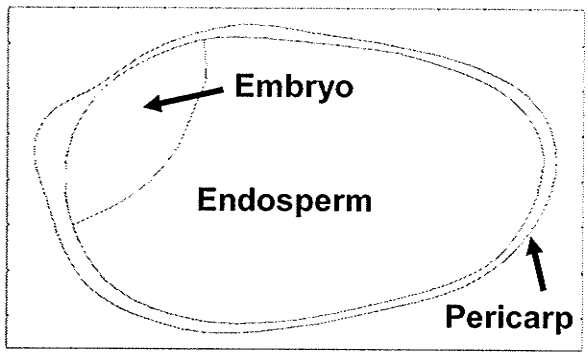

(a)

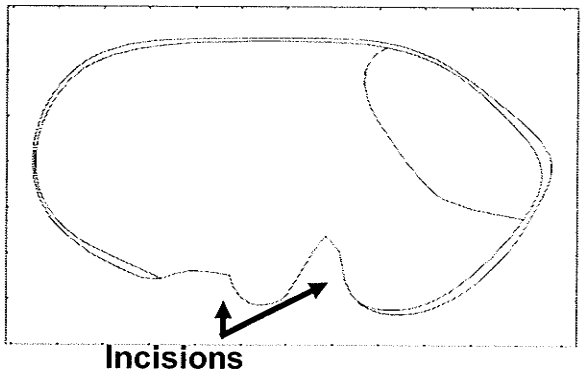

(b)

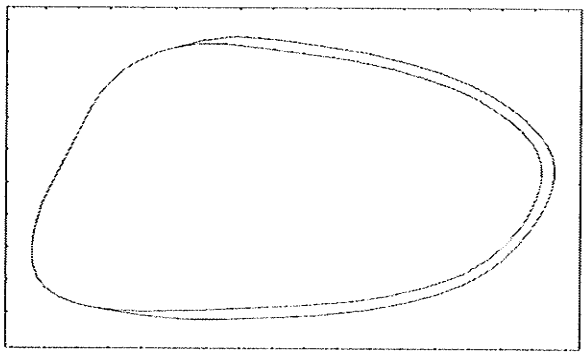

(c)

Figure 5.3 Two-dimensional geometry object representation of a wheat kernel as obtained from the magnetic resonance images: (a) intact, (b) mechanically scarified, and (c) embryo-removed.

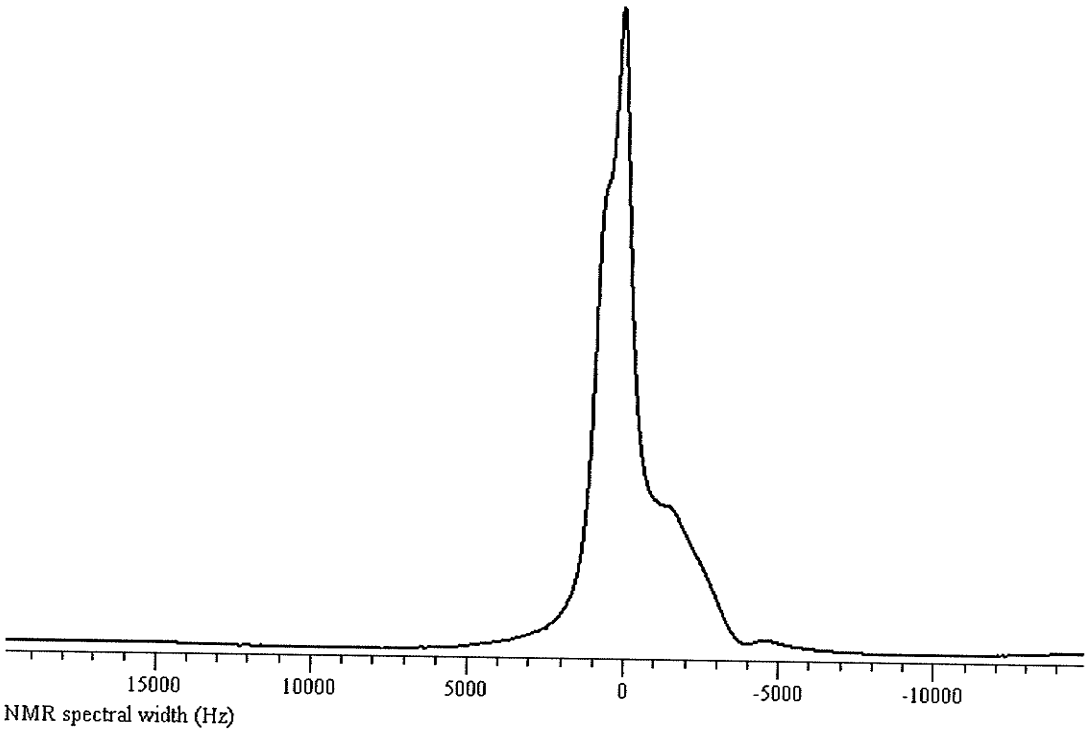

Figure 5.4 Proton nuclear magnetic resonance spectrum of an 18.8% moisture content (d.b.) wheat kernel.

shoulder due to lipid resonances at approximately -1700Hz. It should be noted that no effort was made to shim the magnetic field for each kernel. Figures 5.5, 5.6 and 5.7 show MR images for an intact kernel, a mechanically scarified kernel, and an embryo-removed kernel, respectively, as a function of drying time. Images in each row in Figs. 5.5 through 5.7 were scaled primarily based on the minimum and maximum pixel values in the first image at the beginning of drying. The MR images show the variation in the internal distribution of water prior-to and during drying. Water was concentrated mainly in the embryo region and the embryo signal intensity remained high, even after 4 h of drying at all three temperatures. Previously measured (Ghosh et al. 2006b) higher T_2 values of the embryo region, in combination with the relatively high signal amplitude indicate the presence of mobile ("free") water in the embryo.

The lowest T_2 values were observed in the endosperm region and, in combination with the low signal amplitude, indicated that water interacts more strongly with the starch matrix. Semi-logarithmic plots of the ratio of the averaged local normalized image intensity (I) to the initial normalized image intensity (I_o) of the three different kinds of kernels with their major components at various temperatures versus drying time are shown in Figs. 5.8 through 5.10. These graphs were made to estimate the difference in moisture content of different wheat components during drying. With the exception of Fig. 5.10, these drying curves did not indicate a single exponential relationship between the image intensity ratio and the drying time. This indicated that water reduction is dependent not only on the water content of the kernels but also on the grain composition. For the three different kinds of wheat samples, the drying rate increased in general from 30°C to

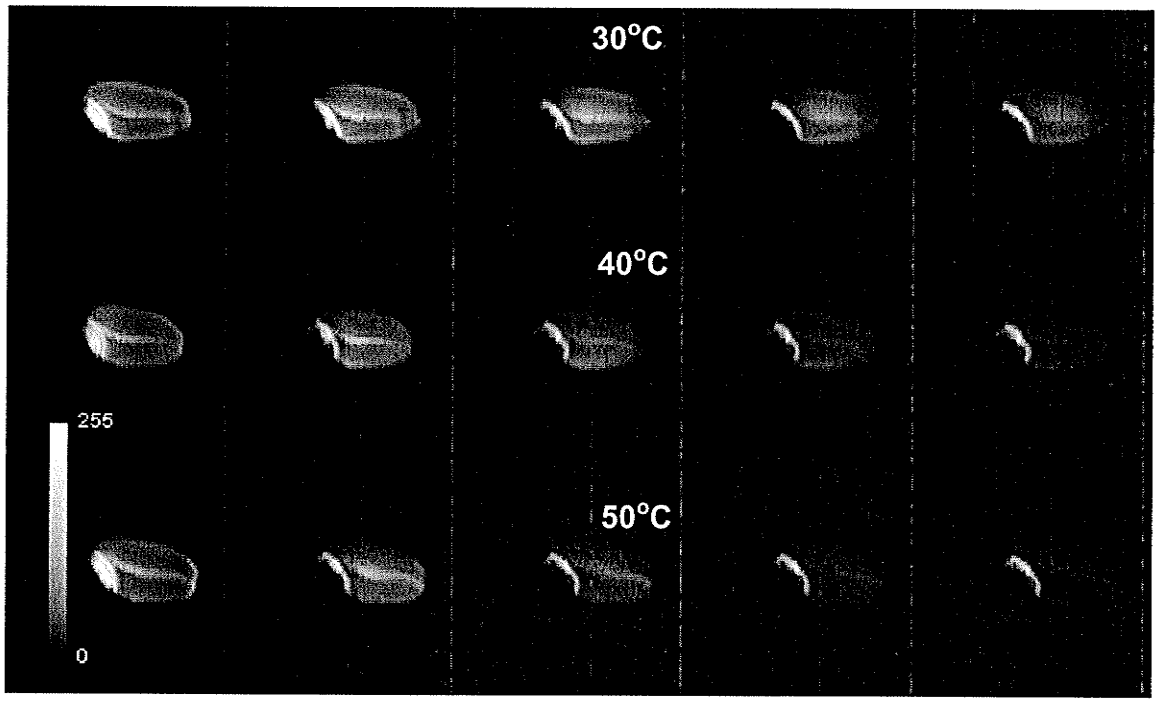

Figure 5.5 Two-dimensional magnetic resonance (MR) images of intact wheat kernels dried at three different temperatures; images in series are shown after every 1 h from the beginning of drying; the signal-to-noise ratio (SNR) of the first image (prior-to drying) in serial MR images were: 30°C: 31.6, 40°C: 28.6, and 50°C: 28.9; the SNR was calculated as the ratio of average pixel intensity of a region of interest (ROI) in the whole grain to the average pixel intensity of the same size area in a region of noise only.

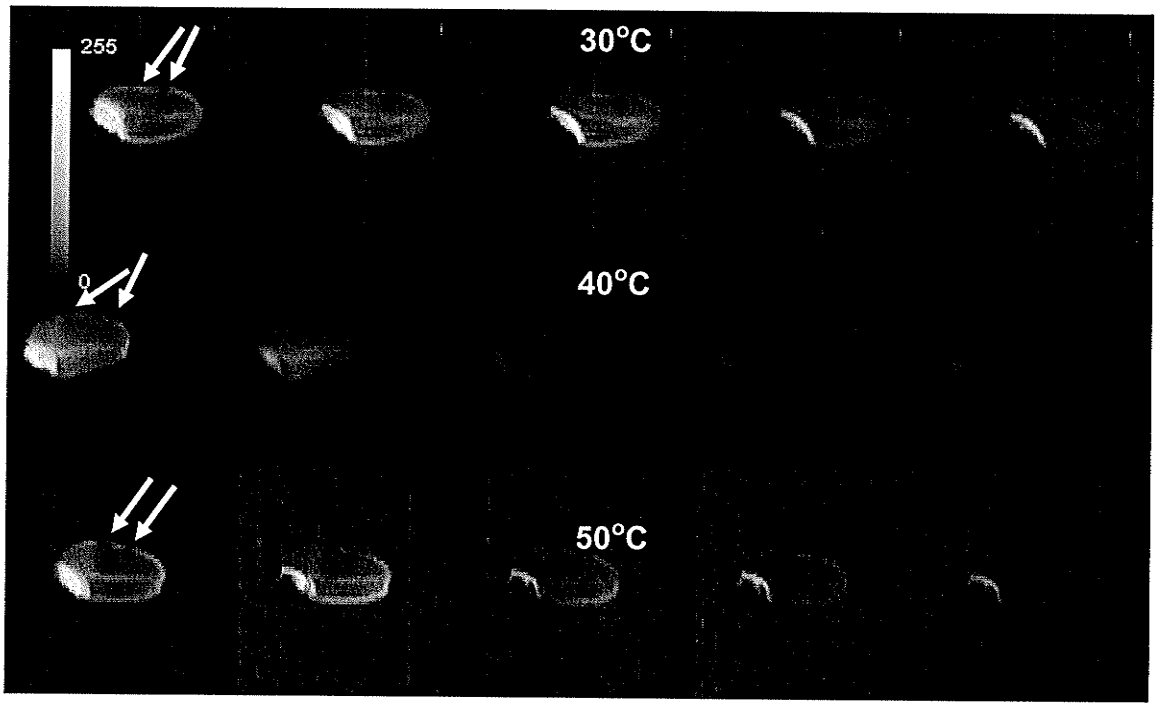

Figure 5.6 Two-dimensional magnetic resonance (MR) images of mechanically scarified wheat kernels dried at three different temperatures; images in series are shown after every 1 h from the beginning of drying; arrows indicate the incision parts in the pericarp; the signal-to-noise ratio (SNR) of the first image (prior-to drying) in serial MR images were: 30°C: 21.7, 40°C: 48.7, and 50°C: 17.4; the method of SNR calculation is given in Fig. 5.5.

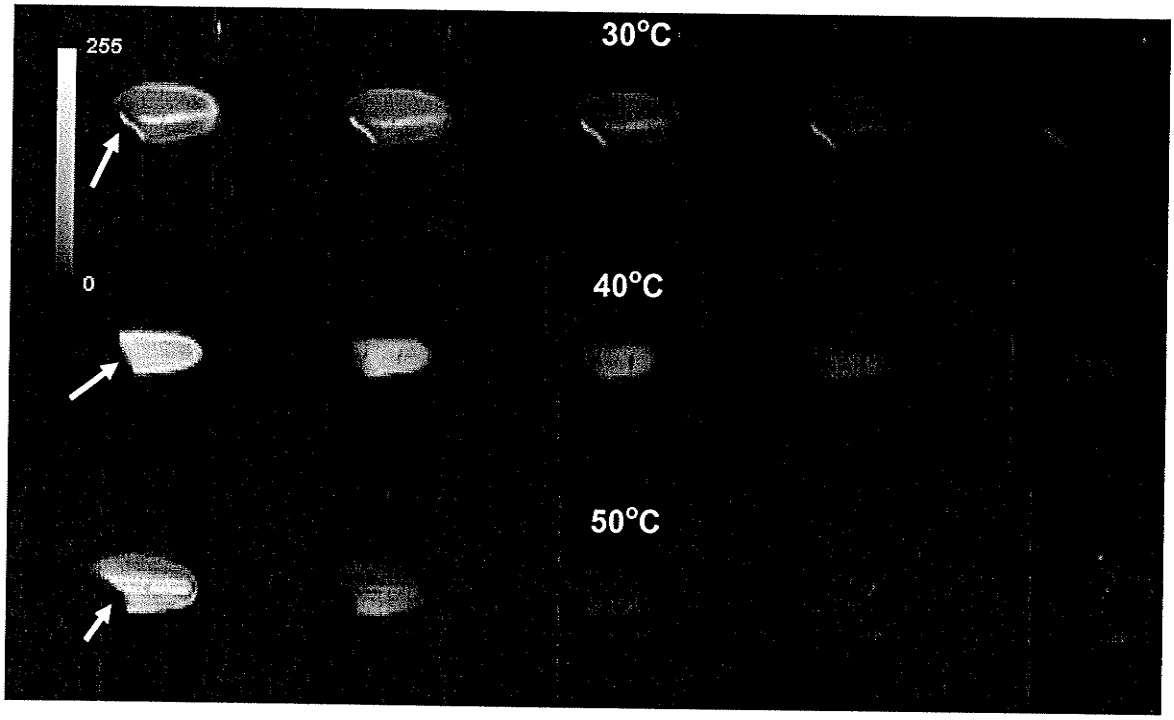

Figure 5.7 Two-dimensional magnetic resonance (MR) images of embryo-removed wheat kernels dried at three different temperatures; images in series are shown after every 1 h from the beginning of drying; arrows indicate the location of embryo removal; the signal-to-noise ratio (SNR) of the first image (prior-to drying) in serial MR images were: 30°C: 13.0, 40°C: 36.9, and 50°C: 17.7; the method of SNR calculation is given in Fig. 5.5.

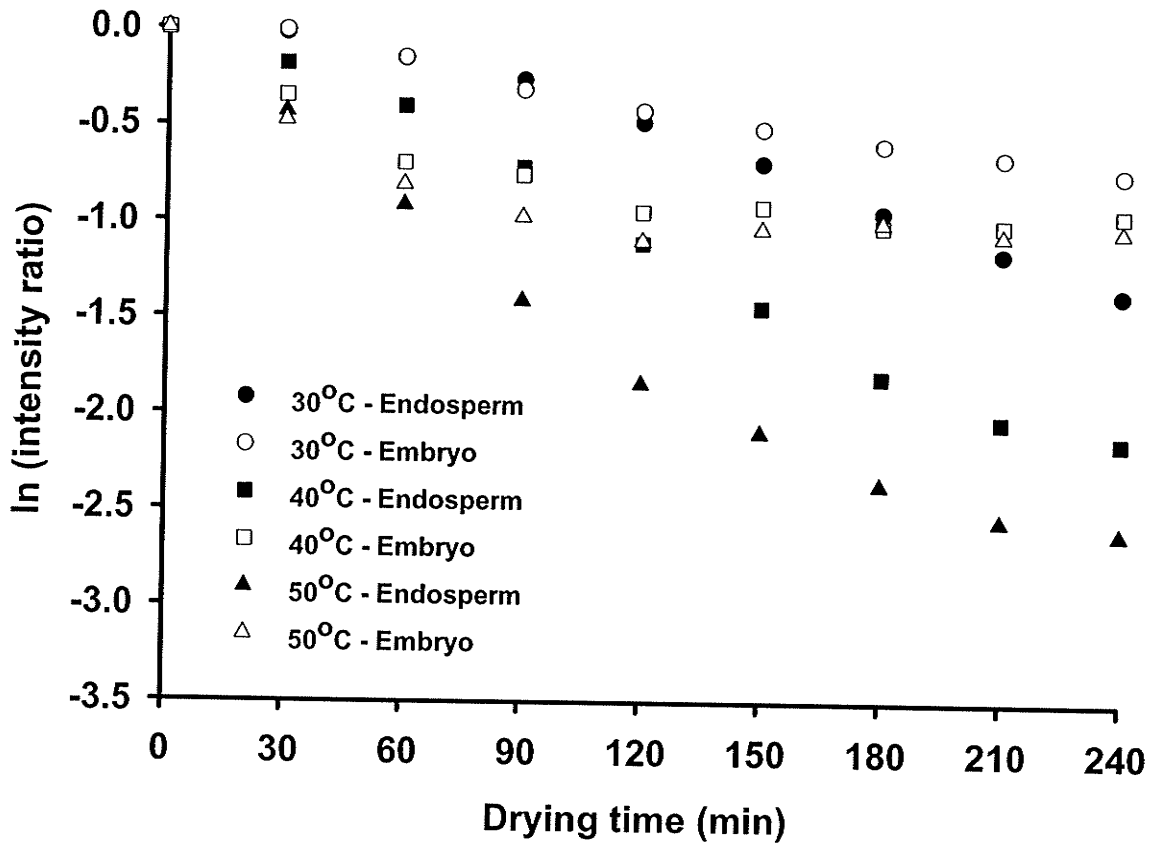

Figure 5.8 Drying curves of intact kernels obtained from the magnetic resonance images.

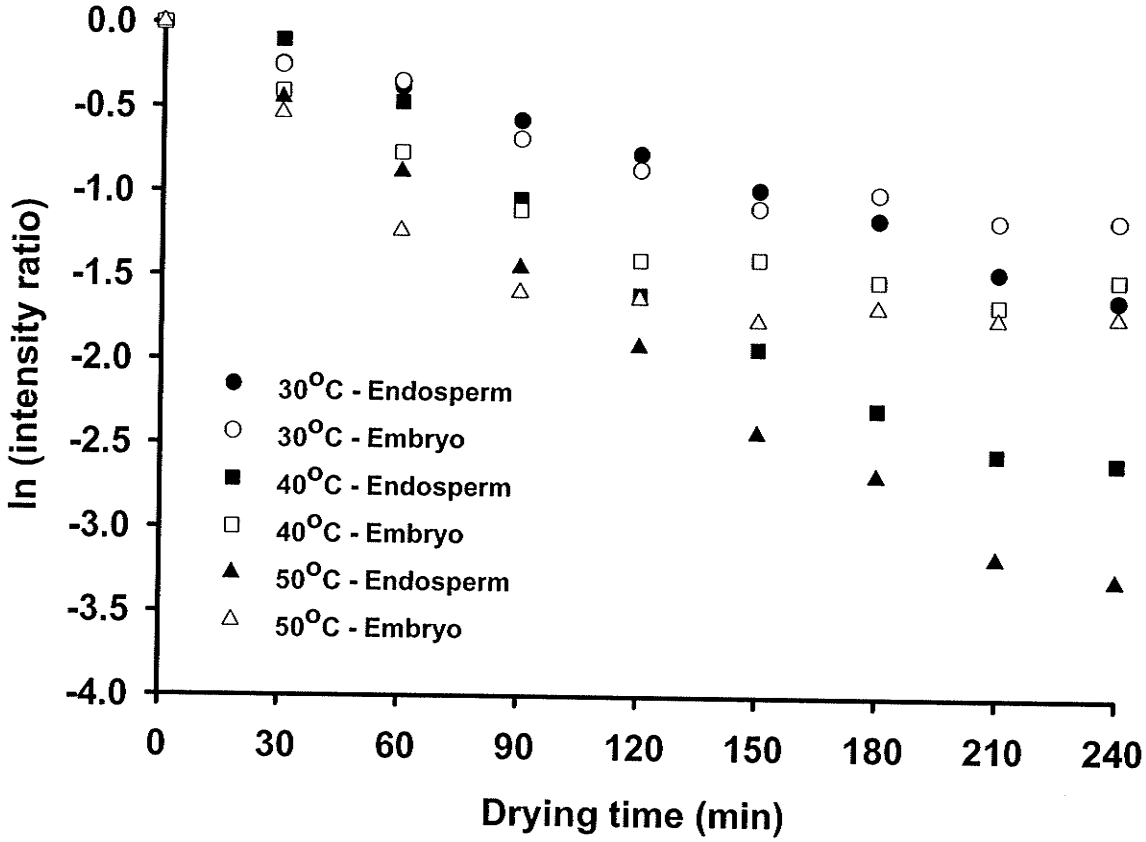

Figure 5.9 Drying curves of mechanically scarified kernels obtained from the magnetic resonance images.

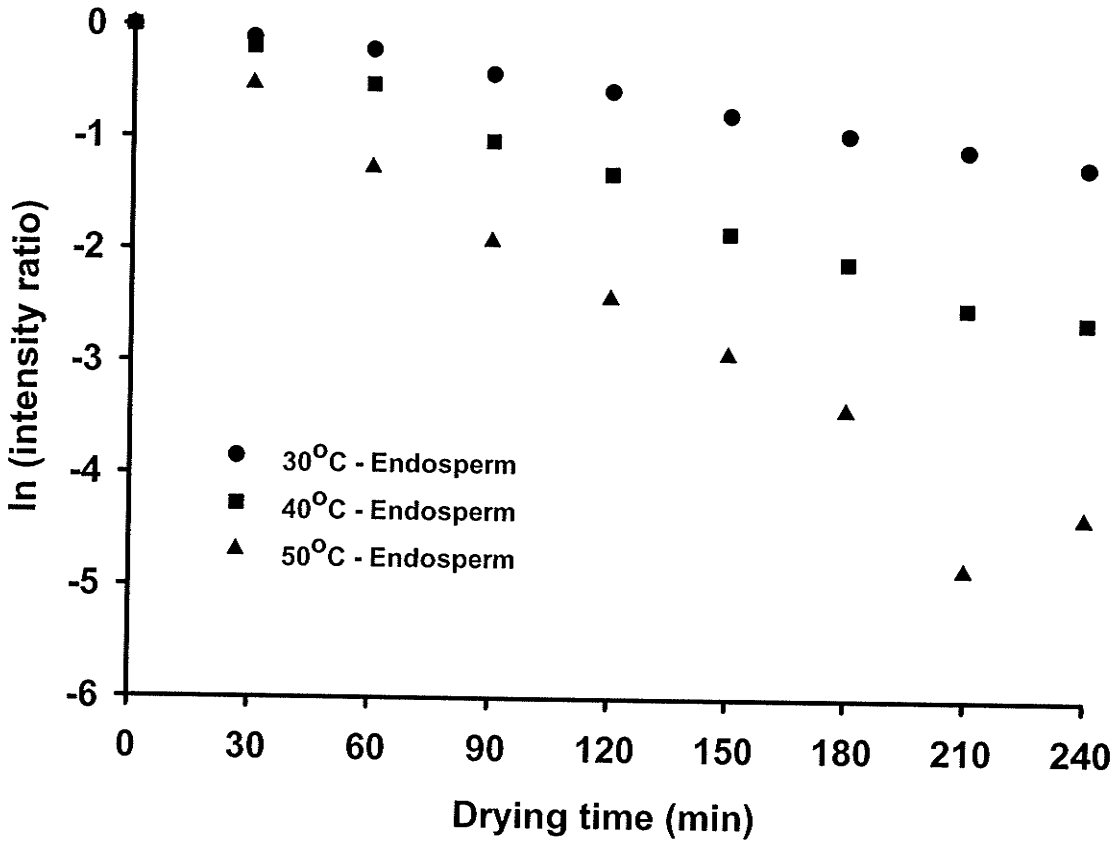

Figure 5.10 Drying curves of embryo-removed kernels obtained from the magnetic resonance images.

50°C, certainly during the first two hours of drying. However, Figs. 5.8 and 5.9 show that the drying rate of the embryo region was much lower than that of the endosperm region for an intact as well as a mechanically-scarified wheat kernel since the embryo has high moisture content compared to the endosperm.

5.3.1 Moisture Calibration

Since the MR signal intensity is not always linearly proportional to the actual moisture content at different locations in an MR image of a wheat kernel, a calibration curve was constructed. A moisture calibration curve was determined using the NMR spectra of an individual wheat kernel with a known moisture content obtained by the gravimetric method (ASAE 2003). The NMR signal integral is directly related to the total proton content (water, oil, protein) of the wheat kernel. However, at the moisture contents considered here, contributions from oil and proteins were neglected. The calibration curve was constructed using eleven replicates at each of the five moisture levels used, ranging from 18.8 to 39.5% (Fig. 5.11). Similar sized wheat kernels were selected by visual inspection for developing the calibration curve. The integrated NMR spectra were found to be linearly related to the wheat moisture content (M) over the range of 18.8 to 39.5% dry basis with a 0.996 correlation coefficient. The calibration equation was of the following form:

$$I_s = 54.7\,M + 90.7 \tag{5.3}$$

where I_s is the NMR signal intensity (arbitrary units).

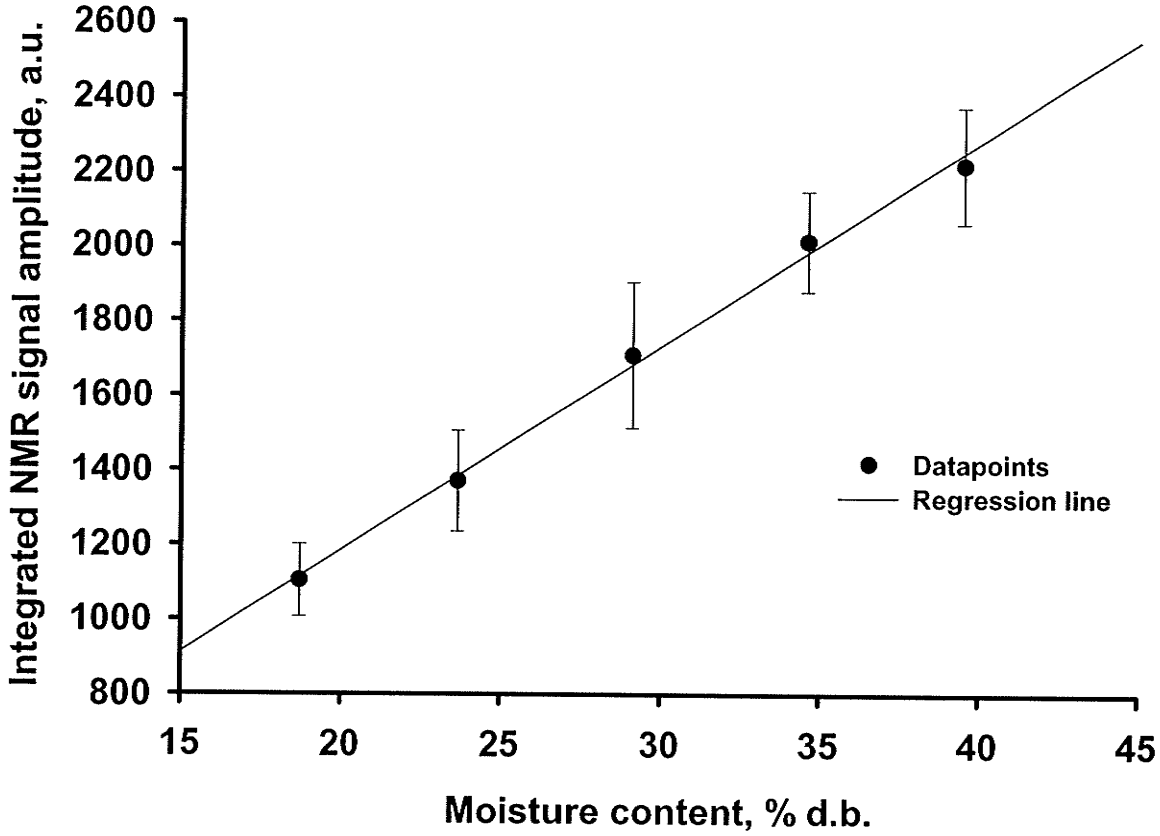

Figure 5.11 Wheat nuclear magnetic resonance (NMR) integrated spectral intensity vs. gravimetric moisture calibration curve.

The calibration curve has a small positive intercept associated with it. This value is directly related to signals from oil and proteins. The moisture contents of the different wheat kernels obtained by using Eq. (5.3) for varying temperature are given in Table 5.2. However, the limitation of adopting this calibration technique is largely dependent upon the homogeneity of the grains (Stapley et al. 1997). It was reported by a few researchers that the linearity of the moisture calibration curve cannot be confirmed since practically no water signal can be detected from the wheat kernels below 10% moisture content (Miller 1980; Brusewitz and Stone 1987).

5.3.2 Drying Rate Curves

The moisture calibration equation (Eq. 5.3) was used to determine the moisture content of the individual grain components used in the MRI experiments (Table 5.2). This calibrated moisture content was then used to obtain the drying rate curves for the individual grain components (embryo and endosperm) of the intact, mechanically-scarified, and embryo-removed wheat kernels at the average drying times (Figs. 5.12 through 5.14). The drying rate curves summarize the basic mechanisms of the entire drying process of a selected kernel. In all cases, the drying rate decreased continuously during drying. The drying rate vs. moisture content plots (not shown) indicated that the drying of the intact, scarified and embryo-removed wheat kernels was in the falling rate period. At this stage, the rate of evaporation of water from the surfaces of the wheat was not equivalent to the rate of supply of water from the interior of the kernel. Brooker et al. (1992) also indicated that individual cereal grains usually dry only within the falling-rate period. Figure 5.12 shows that the embryo region in an intact kernel dried at a relatively faster falling rate during the

Table 5.2 Moisture contents as obtained from the calibration curve with varying drying time and grain conditions.

Temp (°C)	Drying time (min)	Intact kernel				Mechanically scarified kernel				Embryo-removed kernel	
		Embryo		Endosperm		Embryo		Endosperm		Endosperm	
		d.b.[a]	w.b.[b]	d.b.	w.b.	d.b.	w.b.	d.b.	w.b.	d.b.	w.b.
30	0	156.6	61.0	41.3	29.2	168.7	62.8	31.9	24.2	50.3	33.5
	30	151.5	60.2	40.1	28.6	144.4	59.1	28.6	22.3	44.9	31.0
	60	125.1	55.6	36.2	26.6	142.3	58.7	26.5	21.0	40.1	28.6
	90	107.6	51.8	31.6	24.0	99.9	50.0	22.4	18.3	31.8	24.1
	120	95.5	48.8	25.6	20.4	77.0	43.5	18.5	15.6	27.0	21.3
	150	84.6	45.8	20.1	16.8	62.2	38.3	15.3	13.2	21.6	17.8
	180	77.6	43.7	15.9	13.7	61.6	38.1	12.6	11.2	18.0	15.3
	210	70.7	41.4	12.6	11.2	54.7	35.4	9.9	9.0	15.1	13.1
	240	64.9	39.4	10.1	9.2	54.1	35.1	7.8	7.3	13.3	11.7
40	0	152.3	60.4	41.3	29.2	208.9	67.6	40.2	28.7	51.4	33.9
	30	107.8	51.9	35.0	25.9	130.4	56.6	35.3	26.1	45.1	31.1
	60	70.8	41.5	27.5	21.6	72.9	42.2	24.3	19.6	31.8	24.2
	90	64.1	39.1	18.5	15.6	45.7	31.4	13.0	11.5	19.1	16.0
	120	51.4	34.0	12.5	11.1	33.8	25.3	5.7	5.4	12.8	11.4
	150	52.5	34.4	8.1	7.5	34.4	25.6	3.2	3.1	7.3	6.8
	180	48.4	32.6	5.1	4.8	30.4	23.3	1.7	1.7	4.6	4.4
	210	48.8	32.8	3.6	3.5	25.8	20.5	0.8	0.8	2.4	2.4
	240	51.4	34.0	2.8	2.7	30.7	23.5	0.5	0.5	1.7	1.7
50	0	171.6	63.2	42.0	29.6	188.4	65.3	52.8	34.6	50.6	33.6
	30	99.9	50.0	27.8	21.7	106.9	51.7	33.0	24.8	29.3	22.7
	60	67.3	40.2	19.0	16.0	53.2	34.7	20.3	16.9	13.5	11.9
	90	56.2	36.0	10.3	9.3	38.0	27.5	10.2	9.3	6.1	5.7
	120	48.4	32.6	5.7	5.4	37.3	27.2	5.9	5.6	3.2	3.1
	150	52.1	34.3	3.4	3.3	34.1	25.4	2.7	2.6	1.2	1.2
	180	54.4	35.2	2.0	2.0	36.9	27.0	1.6	1.6	0.3	0.3
	210	50.7	33.7	1.1	1.1	35.9	26.4	0.5	0.5	0.3	0.3
	240	52.1	34.3	1.1	1.1	34.4	25.6	0.1	0.1	0.0	0.0

[a]% dry basis, [b]% wet basis

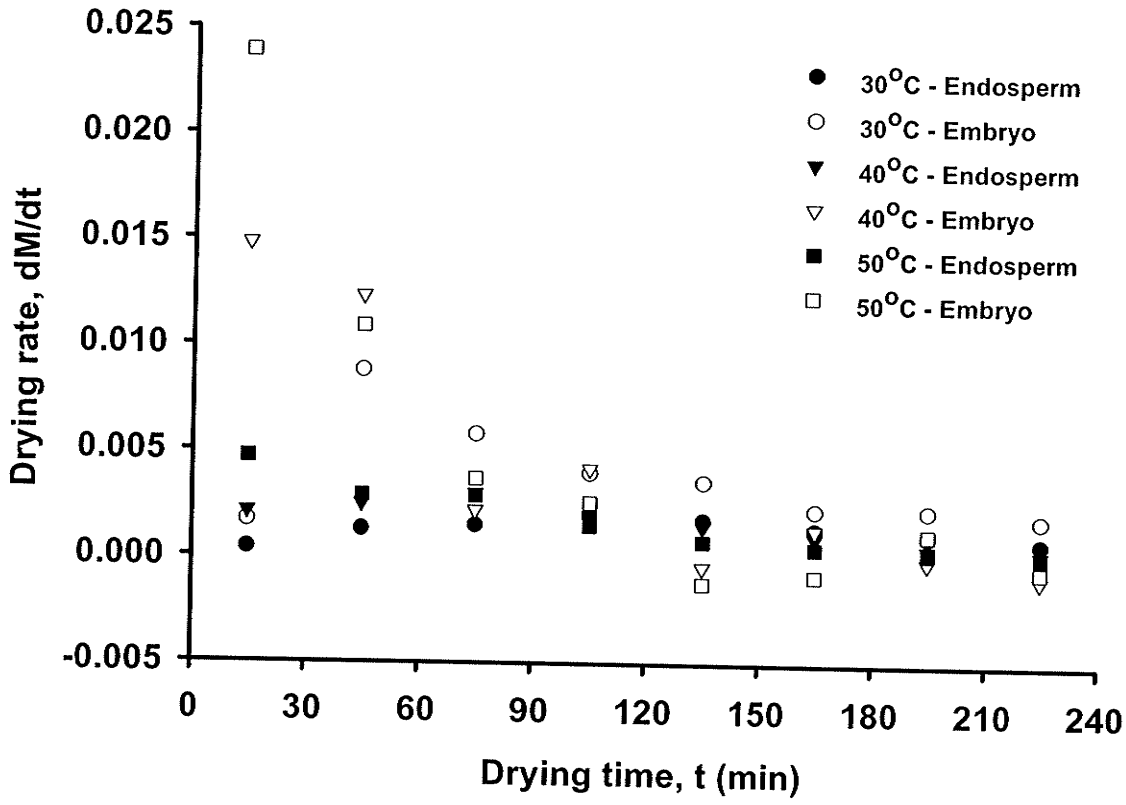

Figure 5.12 Drying rate curves of intact kernels obtained from the magnetic resonance images.

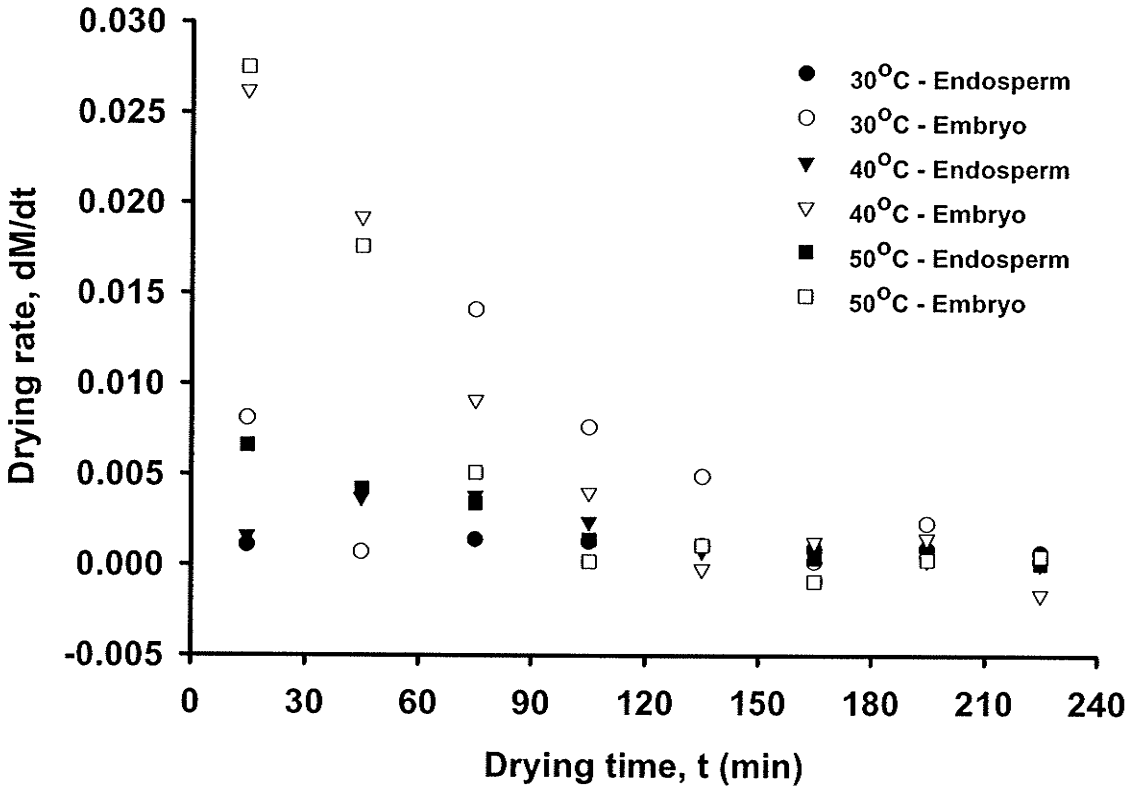

Figure 5.13 Drying rate curves of mechanically scarified kernels obtained from the magnetic resonance images.

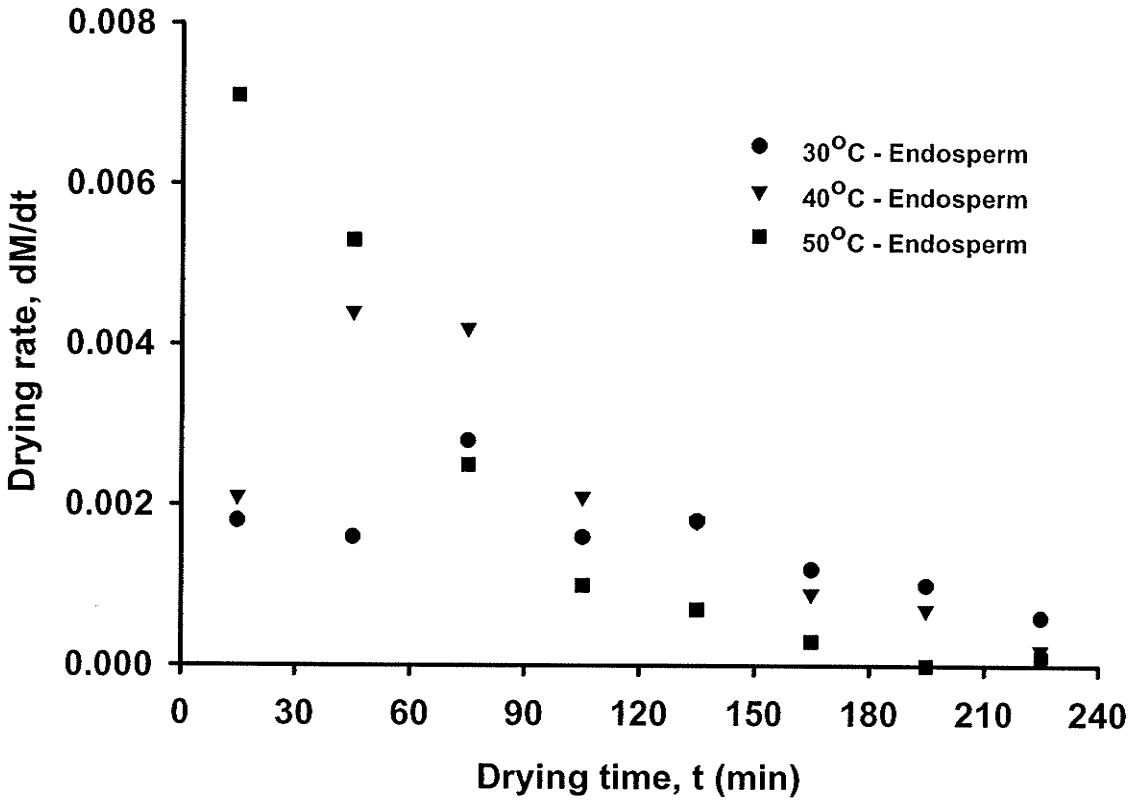

Figure 5.14 Drying rate curves of embryo-removed kernels obtained from the magnetic resonance images.

first 90 min of drying and the rate was gradually lowered as drying progressed for all three drying temperatures. This lower falling rate of drying was found after about 2 h since the onset of drying of the embryo in the mechanically scarified kernel (Fig. 5.13). Thus two distinct falling rate periods were easily evident particularly in the embryo of the wheat kernel. The absence of the lower falling rate in the embryo region at the initial period of drying (first falling rate period) suggests that the drying was mainly governed by the liquid diffusion for that specific period. It can also be assumed that during this period, the capillary forces maintained a continuous liquid phase from one pore to another to move the water towards the surface for evaporation. But lower rate of drying at the later periods (second falling rate period) can be assumed to fall under an "internal evaporation zone" (Toei and Okazaki 1970), where moisture transfer is solely governed by the vapor pressure gradient from the capillaries. At this point, the surface liquid saturation would have reached the irreducible water content as the liquid phase becomes discontinuous (Bernada et al. 1998b). At this stage, moisture was almost trapped in the capillaries and thereby the moisture transfer almost became nonexistent. The kernel would have only the absorbed water, which was not free to move and a receding evaporation front inside the kernel became predominant which increased the length of the path of the vapor molecular diffusion. Both the penetrating evaporation front and the tortuosity of the pore network keep the drying rate low (Bernada et al. 1998b). However, comparison of Figs. 5.12 through 5.14 indicate that the falling rate of drying began from about 0.007 min^{-1} for the endosperm of all the three different kinds of wheat and gradually lowered in an exponential pattern until the endosperm became completely dry at all the three drying temperatures. The endosperm did not show a variable falling rate of

drying like the embryo. Therefore liquid diffusion was assumed to be predominant for the moisture transfer from the endosperm. Thus it can be postulated that the embryo plays a significant role in the overall moisture transfer mechanism from a wheat kernel when it is attached to the endosperm.

In addition, in the intact kernel, the drying rate initially increased with the drying time for the endosperm dried at 30 and 40°C and for the embryo dried at 30°C, reached a peak and then decreased during drying under the constant temperature. This might be due to the initial heating of the wheat kernel to the drying "N_2" temperature and the consequent variation in the moisture content in the interior grain components. A similar observation was made for the endosperm of the mechanically scarified and embryo-removed kernels at 40°C. However, the drying rate in the embryo region of the mechanically scarified kernels decreased quickly at the very beginning at 30°C and then reached to the peak before it started decreasing. Possibly water transport through the incision-parts of the endosperm was more significant than from the embryo during the initial stage of drying. For high temperature drying (50°C), these initial trends of the drying rate for all the three different kernels have shown a decreasing pattern. In these cases, the kernel temperature rapidly equilibrated to the drying air temperature. This initial short period of unsteady state adjustment which is usually ignored in the drying analysis (Geankoplis 1999) was clearly visible in these drying curves because they were developed based on the MR images that map the actual water distribution within the wheat kernels.

However, it was noticed in all cases that raising the temperature from 30 to 50°C increased the specific drying rate at the beginning of drying because of the faster removal of the capillary water as the water viscosity reduced with higher temperatures so that the liquid water moved easily by the capillary forces. Even so, as drying progressed, the drying rates approached closer to each other towards attaining the equilibrium moisture content irrespective of the drying temperatures. In general, initial higher drying rate from the embryo than from the endosperm was observed in the case of intact and the scarified kernels because the embryo has a high moisture content. The endosperm has a lower moisture content which requires more time to be transferred from the interior of the grain.

5.4 Conclusions

The magnetic resonance imaging (MRI) technique was successfully used to determine the actual physical phenomena which affect the subsequent movement of moisture in a wheat kernel during drying. Physical manipulation of the kernel composition helped to properly investigate the drying phenomena. Results obtained from this study were unique and indicated that in general, structural components of a grain kernel play a significant role in grain drying characteristics. A proper synthesis of the results from these analyses will lead to the development of mathematical models to follow the moisture distribution inside a grain kernel as a function of drying time.

Acknowledgements

The authors thank the Natural Sciences and Engineering Research Council of Canada, University of Manitoba Graduate Fellowship Committee, and Canada Research Chairs program for funding this study.

References

ASAE. 2003. *ASAE Standards* S352.2: Moisture measurement – Unground grain and seeds. St. Joseph, MI: ASAE.

Bernada, P., S. Stenström, and S. Månsson. 1998a. Experimental study of the moisture distribution inside a pulp sheet using MRI-Part I: Principles of the MRI technique. *Journal of Pulp and Paper Science* 24(12): 373-379.

Bernada, P., S. Stenström, and S. Månsson. 1998b. Experimental study of the moisture distribution inside a pulp sheet using MRI-Part II: Drying experiments. *Journal of Pulp and Paper Science* 24(12): 380-387.

Brooker, D.B., F.W. Bakker-Arkema, and C.W. Hall. 1992. *Drying and storage of grains and oilseeds*. New York, NY: Van Nostrand Reinhold.

Brusewitz, G. H., and M. L. Stone. 1987. Wheat moisture and NMR. *Transactions of the ASAE* 30(3): 858-862.

Chambers, J., N. J. McKevitt, K. A. Scudamore, and C. E. Bowman. 1989. Nondestructive determination of the moisture content of individual wheat grains by nuclear magnetic resonance. *Journal of Food Science and Agriculture* 49(2): 211-224.

Czaba, I., and M. Neményi. 1997. Investigation of simultaneous heat and mass transfer within the individual maize kernels during drying time. *Hungarian Agricultural Engineering* 10: 58-60.

Evers, A.D., and D.B. Bechtel. 1988. Vol. I. Microscopic structure of the wheat grain. In *Wheat – Chemistry and Technology*, 47-96. Y. Pomeranz, ed. St. Paul, MN: Amercian Association of Cereal Chemists, Inc.

Fortes, M., M.R. Okos, and J.R. Barrett. 1981. Heat and mass transfer analysis of intra-kernel wheat drying and rewetting. *Journal of Agricultural Engineering Research* 26(2): 109-125.

Geankoplis, C.J. 1999. *Transport processes and unit operations.* New Delhi, India: Prentice-Hall of India Private Limited.

Ghosh, P.K., D.S. Jayas, M.L.H. Gruwel, and N.D.G. White. 2006a. Magnetic resonance imaging studies to determine the moisture removal patterns in wheat during drying. *Canadian Biosystems Engineering* 48: 7.13-7.18.

Ghosh, P.K., D.S. Jayas, M.L.H. Gruwel and N.D.G. White. 2006b. Magnetic resonance image analysis to explain moisture movement during wheat drying. *Transactions of the ASABE* 49(4): 1181-1191.

Haghighi, K., J. Irudayaraj, R.L. Stroshine, and S. Sokhansanj. 1990. Grain kernel drying simulation using the finite element method. *Transactions of the ASAE* 33(6):1957-1965.

Hahn, E. L. 1950. Spin echoes. *Physical Review* 80(4): 580-594.

Husain, A., C.S. Chen, and J.T. Clayton. 1973. Simultaneous heat and mass diffusion in biological materials. *Journal of Agricultural Engineering Research* 18(4): 343-354.

Ishida, N., S. Naito, and H. Kano. 2004. Loss of moisture from harvested rice seeds on MRI. *Magnetic Resonance Imaging* 22(6): 871-875.

Jia, C.C., D.A. Sun, and C.W. Cao. 2000. Mathematical simulation of temperature and moisture fields within a grain kernel during drying. *Drying Technology* 18(6): 1305-1325.

Kovács, A.J., and M. Neményi. 1999. Moisture gradient vector calculation as a new method for evaluating NMR images of corn (*Zea mays* L.) kernels during drying. *Magnetic Resonance Imaging* 17(7):1077-1082.

MacMasters, M.M., D. Bradbury, and J.J.C. Hinton. 1964. Microscopic structure and composition of the wheat kernel. In *Wheat – Chemistry and Technology*, 55-110. I. Hlynka, ed. St. Paul, MN: Amercian Association of Cereal Chemists, Inc.

Miller, B. S., M. S. Lee, J. W. Hughes, and Y. Pomeranz. 1980. Measuring high moisture content of cereal grains by pulsed nuclear magnetic resonance. *Cereal Chemistry* 57(2): 126-129.

Pomeranz, Y. 1988. Chemical composition of kernel structures. In *Wheat – chemistry and technology*, Vol. I, 97-158. Y. Pomeranz, ed. St. Paul, MN: American Association of Cereal Chemists, Inc.

Pomeranz, Y., and D.B. Bechtel. 1978. Structure of cereal grains as related to end-use properties. In *Cereals'78: Better nutrition for the world's millions*: Proc. Sixth

International Cereal and Bread Congress, 85-104. Y. Pomeranz, ed. St. Paul, MN: American Association of Cereal Chemists, Inc.

Ranjan, R., J. Irudayaraj, and S. Jun. 2001. A three-dimensional control volume approach to modeling heat and mass transfer in food materials. *Transactions of the ASAE* 44(6): 1975-1982.

Sokhansanj, S, and R.J. Gustafson. 1980. Prediction of heat and mass transfer within a grain kernel – a finite element application. In: *Drying '80*, Vol. 2, 229-232. A.S. Majumdar ed. New York, NY: McGraw-Hill International Book Company.

Song, H., and J. B. Litchfield. 1990. Nondestructive measurement of transient moisture profiles in ear corn during drying using NMR imaging. *Transactions of the ASAE* 33(4): 1286-1290.

Song, H. P., J. B. Litchfield, and H. D. Morris. 1992. Three-dimensional microscopic MRI of maize kernels during drying. *Journal of Agricultural Engineering Research* 53(1): 51-69.

Stapley, A.G.F., M.H. Thomas, L.F. Gladden, and P.J. Fryer. 1997. NMR imaging of the wheat grain cooking process. *International Journal of Food Science and Technology* 32(5):355-375.

Toei, R., and M. Okazaki. 1970. Drying mechanism of capillary-porous bodies. *Inzhenerno-Fizicheskii Zhurnal* 19(3): 464-475.

Tollner, E. W., and Y. C. Hung. 1992. Low-resolution pulse magnetic resonance for measuring moisture in selected grains and kernels. *Journal of Agricultural Engineering Research* 53(3): 195-208.

USDA. 2005. *Wheat Yearbook.* Stock # 88008B. Economic Research Service. Washington, DC: United States, Department of Agriculture.

Yang, W. C.C. Jia, T.J. Siebenmorgen, T.A. Howell, and A.G. Cnossen. 2002. Intra-kernel moisture responses of rice to drying and tempering treatments by finite element simulation. *Transactions of the ASAE* 45(4): 1037-1044.

MATHEMATICAL MODELING OF WHEAT KERNEL DRYING WITH INPUT FROM MOISTURE MOVEMENT STUDIES USING MAGNETIC RESONANCE IMAGING[4]

P.K. Ghosh[1], D.S. Jayas[1], E.A. Smith[2], M.L.H. Gruwel[3,4], N.D.G. White[1,5,6], P.A. Zhilkin[3]

[1]Department of Biosystems Engineering, University of Manitoba, Winnipeg, Manitoba, Canada, R3T 5V6

[2]Department of Mathematics and Statistics, University of Paisley, Paisley, Scotland, UK, PA1 2BE

[3]National Research Council, Institute for Biodiagnostics, 435 Ellice Avenue, Winnipeg, Manitoba, Canada, R3B 1Y6

[4]Department of Chemistry, University of Manitoba, Winnipeg, Manitoba, Canada, R3T 2N2

[5]Agriculture and Agri-Food Canada, Cereal Research Centre, 195 Dafoe Road, Winnipeg, Manitoba, Canada, R3T 2M9

[6]Department of Entomology, University of Manitoba, Winnipeg, Manitoba, Canada, R3T 2N2.

Abstract

A two-dimensional (2D) simultaneous heat and moisture transfer drying model for a single wheat kernel was developed. The model assumed a non-uniform initial moisture distribution in the germ and endosperm of a wheat kernel. The model was theoretically developed using a 2D finite element method and then solved using COMSOL® Multiphysics™, a commercial finite element software package. Model-simulated moisture prediction data were validated against two published semi-empirical thin layer wheat

[4] This paper is under review for publication in the ***Transactions of the ASABE.*** Submitted in November (2006), Manuscript No. FPE-06755-2006.

drying models and a published 2D heat and mass transfer model for a single wheat kernel which assumed uniform initial moisture distribution within the whole kernel. The model predictions agreed well with observations obtained from the Magnetic Resonance Imaging (MRI) and from the published models. A sensitivity analysis was performed for selecting proper model parameters which indicated that water diffusivities in the germ and endosperm are the main parameters in the grain drying process. Moisture and temperature distributions inside the wheat kernel and the effect of drying temperature on the wheat quality were explained by calculating the Biot and Lewis numbers, and the activation energy of the water removal process. This model has the potential to predict the actual moisture and temperature distributions inside any type or size of grain kernel during drying considering non-uniform initial moisture distributions was shown by the MRI experiments.

Keywords: *Mathematical modeling, Heat and mass transfer, Finite element method, Wheat, Drying, Moisture movement, MRI.*

6.1 Introduction

Grains are usually harvested at a moisture content higher than is safe for storage to reduce field losses resulting from weather conditions, wildlife damage, or shattering loss due to overdrying. Cereal grains are usually harvested at more than 17% w.b. (wet mass basis) moisture content (m.c.) (Friesen 1980). Grain drying is a common method to artificially remove the moisture from the harvested grain to attain a safe storage moisture content. Drying of grains prevents damage caused by occurrence of hot spots due to mould growth. For example, wheat is usually harvested at 18-20% w.b. and dried to 14% w.b. for short-term storage (6-12 mo) and 13% w.b. for long-term storage (over 1 y)

(Brooker et al. 1992). Drying of grains is commonly performed by forcing air through the bulk grain at different temperatures: natural (ambient) temperature, near-ambient temperature, low temperature, or high temperature. Grain dryers are usually interfaced with a computer control system which maintains the residence time of the grain in the dryer to give improved grain quality with target moisture content without over-drying (wasted energy and reduced dried grain mass) or under-drying (unmarketable grain). Mathematical models that can accurately predict the variations of moisture contents in grains during drying, to achieve the target moisture content, can regulate the proper functioning of the computer controlled system.

Simulation studies of grain drying rely on the solution of equations for simultaneous heat and moisture distribution inside the grain mass. Several semi-theoretical and empirical models describing the thin-layer (a single grain kernel or one layer of grain kernels or a polylayer of many kernels thick) as well as the deep-bed drying (more than 20 cm deep) process for specific grains have already been reviewed and compared (Jayas et al. 1991; Cenkowski et al. 1993; Pabis et al. 1998; Parde et al. 2003; Ghosh et al. 2004). These models can predict the moisture loss from the grain bulk during drying but cannot predict the internal moisture and temperature distributions within individual grain kernels with drying time. Since cereal grains are hygroscopic capillary porous materials and drying can generate considerable temperature and moisture gradients in the grains, hydro-thermal stress can develop which deteriorates the grain quality in many ways. Improper drying due to lack of knowledge about internal moisture and temperature distributions can adversely affect the test weight, milling and baking characteristics, and head-rice

yield and cause physical damage and increase stress-crack susceptibility. For example, wheat drying is usually accomplished with near-ambient air or hot air with a recommended drying temperature preferably below 60°C to maintain its milling and baking characteristics (e.g., loaf volume). However, stress-cracking is not prevalent in wheat (Nellist and Bruce 1995).

Internal mass (moisture) transfer in wheat or other cereal grains during drying is caused by a concentration gradient resulting from liquid or vapour diffusion or their combination (corn: Hall and Rodrigues-Arias 1958, Hustrulid and Flikke 1959, Allen 1960, Pabis and Henderson 1961, Chittenden and Hustrulid 1966, Chu and Hustrulid 1968a,b, Fortes and Okos 1978, Sokhansanj and Gustafson 1980, Walton et al. 1988, Czaba and Neményi 1997, Neményi et al. 2000; rice: Allen 1960, Husain et al. 1973, Sokhansanj and Gustafson 1980, Steffe and Singh 1982, Yang et al. 2002; and wheat: Babbitt 1949, Simmonds et al. 1953, Becker and Sallans 1955, Becker 1959, Watson and Bhargava 1974, Fortes et al. 1981, Jia et al. 2000). Simmonds et al. (1953) indicated that capillary forces play a minor role in the mass transfer during wheat drying. Further, Brooker et al. (1992) experimentally determined that the initial moisture content distribution in a freshly harvested corn kernel is non-uniform (whole kernel 36% m.c., w.b.; germ 48% m.c., w.b.; endosperm 31% m.c., w.b.; and pericarp 53% m.c., w.b.). This feature was further evidenced in most of the cereal grains, including corn, by adopting non-invasive and non-destructive magnetic resonance imaging (MRI) technique by several researchers (barley: McEntyre et al. 1998, Gruwel et al. 2001, Gruwel et al. 2002, Glidewell 2006; corn: Ratković 1987, Song and Litchfield 1990, Bačić et al. 1992, Song et al. 1992, Ruan

et al. 1992, Ruan and Litchfield 1992, Song et al. 1998, Kovács and Neményi 1999; rice: Takeuchi et al. 1997, Horigane 2001, Frìas et al. 2002, Ishida et al. 2004, Mohorič et al. 2004, Kasai et al. 2005; and wheat: Jenner et al. 1988, Stapley et al. 1997, Song et al. 1998, Fukuoka et al. 2000, Turhan et al. 2001, Gruwel et al. 2004, Ghosh et al. 2006a,b,c). Application of MRI in drying studies indicated a non-uniform moisture transfer during drying and that moisture transfer depends on the grain's structural components (Ghosh et al. 2006a,b).

In recent years, with the advent of powerful computers, single grain kernel drying has been simulated by simultaneous heat and mass transfer models considering various moisture transfer phenomena and geometrical shapes (barley: Haghighi et al. 1990, Irudayaraj et al. 1992, Miketinac et al. 1992; corn: Sokhansanj and Gustafson 1980, Irudayaraj et al. 1992, Czaba and Neményi 1997, Neményi et al. 2000; rice: Husain et al. 1973, Sokhansanj and Gustafson 1980, Yang et al. 2002, Wu et al. 2004; and wheat: Jia et al. 2000). All of these models were solved numerically mostly using a finite element method, in which the moisture distribution was approximated by a discrete model composed of a set of piecewise continuous functions defined over a finite number of sub-domains or elements (Segerlind 1984). A summary of these models is discussed in Miketinac et al. (1992). These models assumed that the moisture transfer towards the surface of the kernel is either due to liquid diffusion or due to a cumulative effect of liquid and vapor diffusion before the convective mass transfer takes place at the kernel surface. All of the published grain-drying models were derived assuming that moisture distribution is uniform in a grain at the beginning of drying and during drying to simplify

these models for computation. However, these simplifications do not represent reality as has been demonstrated by published studies of moisture distribution using MRI and therefore, may reduce the accuracy of the model predictions. There is a need to develop and solve mathematical models of coupled heat and moisture transfer in grain that take into consideration the non-uniform distribution of moisture before the start of drying and the non-uniform movement of moisture from grain during drying.

Therefore, the objective of this study was to develop and validate mathematical model of two-dimensional (2D) simultaneous heat and moisture transfer during drying of wheat using information obtained from MRI experiments. Wheat was selected in this study as it is a major cereal crop being consumed as a staple food by most of the world's population.

6.2 Materials and Methods

6.2.1 Development of Mathematical Model

During grain drying, heat is transferred by convection from hot air to the grain surface and then by conduction inside the grain. Due to heat transfer, grain loses moisture. Moisture is transferred by diffusion phenomena from the grain towards its surface and then evaporates from the surface to the ambient air. Therefore, grain drying is a simultaneous heat and mass transfer process. Further, the complex anatomy of the wheat kernel makes the entire drying process complicated. Wheat is categorized as a hygroscopic capillary-porous material in which the pores are partially filled with liquid water and partially with an air/water-vapour mixture (Brooker et al. 1992). Since wheat is normally dried to remove 4 to 5 percentage points of moisture content in practice,

shrinkage can be negligible. However, to estimate the extent of shrinkage, a series of MR images acquired during 4 h of drying at 50°C were registered against one of the images. The 2-dimensional registration was performed on single slices extracted from the 3-dimensional MR images. First the images were corrected for possible global motion using an affine model for displacement field (Zhilkin and Alexander 2000). Then a unimodal version of a nonlinear registration algorithm (Zhilkin and Alexander 2005) was employed to correct for distortions. In both cases the mean square error between image pair computed over the central part of the images (to avoid boundary artifacts) was an objective function minimized during registration. It was found that most of the wheat kernel motion was corrected by affine registration. Distortion registration insignificantly reduced the value of objective function, and may be neglected. Linear regression was performed on the ratio of the averaged local normalized MR image intensity obtained from the unregistered and the registered images and the correlation coefficient was about 0.98 (Fig. 6.1). Hence, image registration plays a minor role, and may be unnecessary and therefore, shrinkage was neglected in the development of the present model and unregistered MR images were used for model validation.

The entire domain of a wheat kernel (Ω) is composed of pericarp (Ω_P), endosperm (Ω_E) and germ (Ω_G) (Fig. 6.2), and can be expressed as:

$$\Omega = \Omega_P \cup \Omega_E \cup \Omega_G \tag{6.1}$$

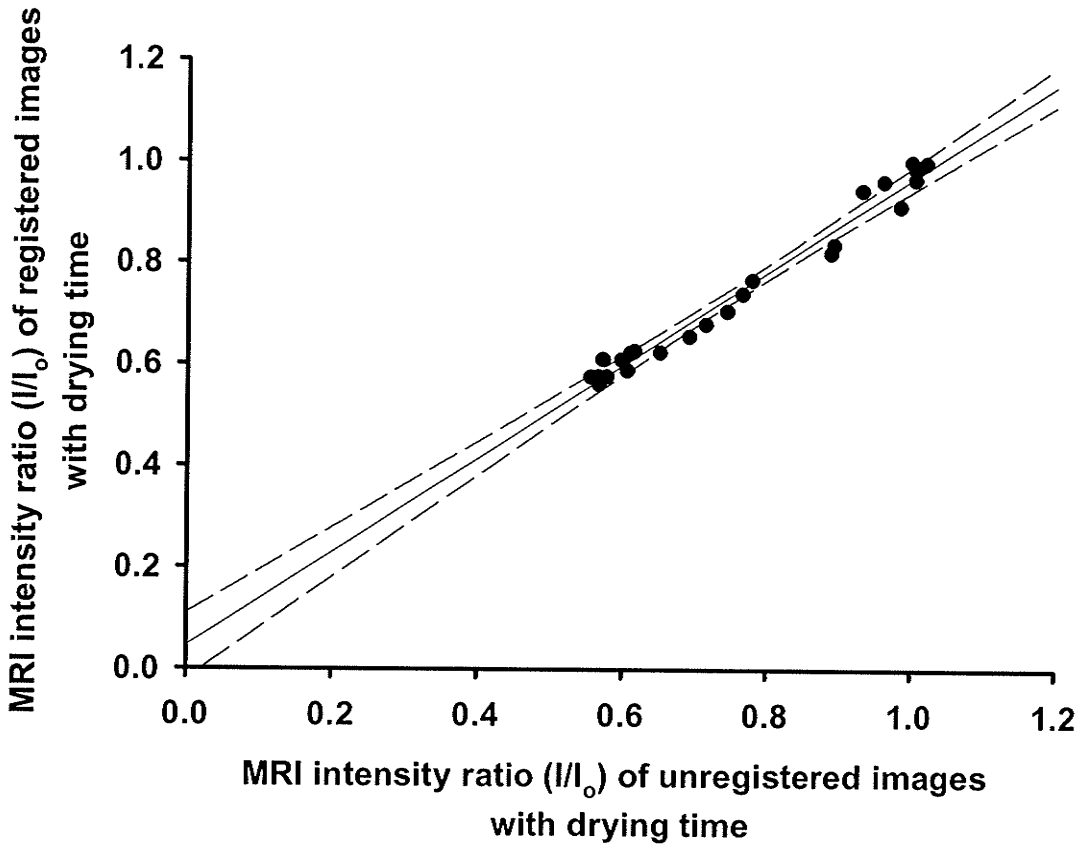

Figure 6.1 Study of the shrinkage effect from both unregistered and registered magnetic resonance images of a wheat kernel during drying at 50°C for 4 h. Dashed lines show the 99% confidence limits for the data points. Intensity ratio was calculated by dividing the average image intensity computed for a specific oval shaped region of interest (ROI) inside the wheat kernel consisting of some portion of germ and endosperm in all images of both unregistered and registered series (with drying time) by the average image intensity for the first image of the respective series (before drying). The selected ROI did not contain the boundary of the kernel.

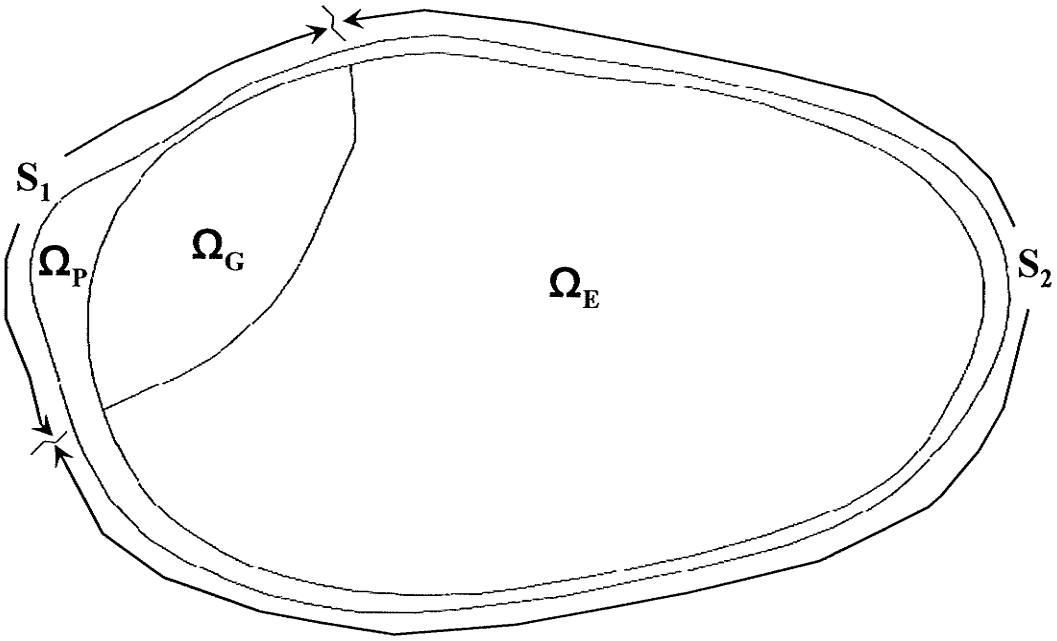

Figure 6.2 Schematic diagram for boundary conditions definitions.

The external boundary of the entire domain (Ω) can be defined as S, which is composed of one or more well-defined segments. Since the heat and moisture transfer equations for Ω_P, Ω_E and Ω_G are the same, no specific designation for an interface between these regions is required.

The moisture transfer was modelled following Fick's law of mass diffusion as:

$$\frac{\partial M}{\partial t} = D\left(\frac{\partial^2 M}{\partial x^2} + \frac{\partial^2 M}{\partial y^2}\right) \tag{6.2}$$

where M is the moisture content (dry basis, decimal); and D is the effective diffusivity (considering both liquid and vapour diffusion) ($m^2\ s^{-1}$). In this work, we used a Cartesian coordinate system to represent a wheat kernel as a 2-dimensional (x, y) body.

The boundary conditions for the moisture transfer model are:

$$M(x, y, t) = M_i \quad \text{at } S_1 \tag{6.3}$$

$$\text{and } D\left(\frac{\partial M}{\partial x} l_x + \frac{\partial M}{\partial y} l_y\right) + h_m (M - M_e) = 0 \quad \text{at } S_2 \tag{6.4}$$

where l_x and l_y are the direction cosines of the outward drawn normal to the boundary; h_m is the moisture transfer coefficient ($m\ s^{-1}$); M_e is the equilibrium moisture content (d.b., decimal); and $S = S_1 \cup S_2$.

The initial conditions are:

$$M(x, y, t = 0) = M_{oP} \quad \text{for } \Omega_P \tag{6.5a}$$

$$M(x, y, t = 0) = M_{oE} \quad \text{for } \Omega_E \tag{6.5b}$$

$$M(x, y, t = 0) = M_{oG} \quad \text{for } \Omega_G \tag{6.5c}$$

The initial condition was based on different initial moisture content values in different grain components. This concept is the major contribution to the present model development obtained from the MRI experiments (Ghosh et al. 2006 a,b).

Heat transfer inside the grain kernel was modeled following Fourier's law of heat conduction. The heat transfer model is:

$$\rho_g C_g \frac{\partial T}{\partial t} = K\left(\frac{\partial^2 T}{\partial x^2} + \frac{\partial^2 T}{\partial y^2}\right) + L \rho_g \frac{\partial M}{\partial t} \tag{6.6}$$

where ρ_g is the density of wheat (kg m^{-3}); C_g is the specific heat of wheat (J kg^{-1} K^{-1}); K is the thermal conductivity of wheat (W m^{-1} K^{-1}); L is the latent heat of evaporation of water in wheat (J kg^{-1}), all of these parameters or properties depend on transient moisture content; and T is the temperature of wheat (K). This equation takes into consideration the evaporation of water inside the grain kernel. The heat transfer model was subjected to the following boundary conditions:

$$T(x, y, t) = T_i \quad \text{at } S_1 \tag{6.7}$$

and

$$K\left(\frac{\partial T}{\partial x} l_x + \frac{\partial T}{\partial y} l_y\right) + h_t (T - T_a) = 0 \quad \text{at } S_2 \tag{6.8}$$

where h_t is the convective heat transfer coefficient (W m^{-2} K^{-1}) and T_a is the drying air temperature (K).

The initial condition is:

$$T(x, y, t = 0) = T_o \tag{6.9}$$

6.2.2 Theoretical Analysis

The system of 2D heat and mass transfer equations (Eqs. 6.2 through 6.9) were solved using finite element analysis in a Cartesian coordinate system (Segerlind 1984; Hutton 2004). These equations were finally expressed in the following general matrix form for each element:

For moisture transfer:

$$\left[C_{M1}^{(e)}\right] \bullet \frac{\partial\{M\}}{\partial t} + \left[K_{M1}^{(e)}\right] \bullet \{M\} = \left\{F_{M1}^{(e)}\right\} \tag{6.10}$$

and for heat transfer:

$$\left[C_{T2}^{(e)}\right] \bullet \frac{\partial\{T\}}{\partial t} + \left[K_{T2}^{(e)}\right] \bullet \{T\} + \left[C_{M2}^{(e)}\right] \bullet \frac{\partial\{M\}}{\partial t} = \left\{F_{T2}^{(e)}\right\} \tag{6.11}$$

where [C] is the element capacitance matrix; [K] the element conductance matrix; and $\{F\}$ the element force vector. Equations 6.10 and 6.11 were further contracted with a general matrix form for each element:

$$[C] \bullet \begin{Bmatrix} \dot{M} \\ \dot{T} \end{Bmatrix} + [K] \bullet \begin{Bmatrix} M \\ T \end{Bmatrix} = \{F\} \tag{6.12}$$

Equation 6.12 can be evaluated at a general location in the time step denoted by the dimensionless parameter θ:

$$[C] \bullet \left\{ \begin{Bmatrix} \dot{M} \\ \dot{T} \end{Bmatrix}_{\theta} + [K] \bullet \begin{Bmatrix} M \\ T \end{Bmatrix}_{\theta} = \{F\}_{\theta} \right. \tag{6.13}$$

where

$$\theta = \frac{t - t_{n-1}}{\Delta t_n},\ 0 < \theta < 1 \text{ over the time step and } \Delta t_n = t_n - t_{n-1}. \tag{6.14}$$

$\left\{\frac{\partial\{M\}}{\partial t}\right\}_\theta, \left\{\frac{\partial\{T\}}{\partial t}\right\}_\theta, \{M\}_\theta, \{T\}_\theta, \{F\}_\theta$ were obtained by approximating $\{M\}_\theta, \{T\}_\theta, \{F\}_\theta$ by linear polynomials over the time step (Burnett 1987). Thus,

$$\{M\}_\theta \approx (1-\theta) \bullet \{M\}_{n-1} + \theta \bullet \{M\}_n \tag{6.15}$$

$$\{T\}_\theta \approx (1-\theta) \bullet \{T\}_{n-1} + \theta \bullet \{T\}_n \tag{6.16}$$

$$\{F\}_\theta \approx (1-\theta) \bullet \{F\}_{n-1} + \theta \bullet \{F\}_n \tag{6.17}$$

Differentiating equations 6.15 and 6.16 gives:

$$\left\{\frac{dM}{dt}\right\}_\theta = \frac{\{M\}_n - \{M\}_{n-1}}{\Delta t_n} \tag{6.18}$$

and

$$\left\{\frac{dT}{dt}\right\}_\theta = \frac{\{T\}_n - \{T\}_{n-1}}{\Delta t_n} \tag{6.19}$$

Substituting equations 6.15 to 6.19 in equations 6.10 and 6.11 yields:

$$\begin{aligned} &[C] \bullet \frac{\{M\}_n - \{M\}_{n-1}}{\Delta t_n} + [K] \bullet \{(1-\theta)\{M\}_{n-1} + \theta\{M\}_n\} = (1-\theta) \bullet \{F\}_{n-1} + \theta \bullet \{F\}_n \\ &\Rightarrow \left\{\frac{[C]}{\Delta t_n} + \theta \bullet [K]\right\} \bullet \{M\}_n - \left\{\frac{[C]}{\Delta t_n} - (1-\theta) \bullet [K]\right\} \bullet \{M\}_{n-1} = (1-\theta) \bullet \{F\}_{n-1} + \theta \bullet \{F\}_n \end{aligned} \tag{6.20}$$

and

$$\begin{aligned} &[C] \bullet \frac{\{T\}_n - \{T\}_{n-1}}{\Delta t_n} + [K] \bullet \{(1-\theta) \bullet \{T\}_{n-1} + \theta \bullet \{T\}_n\} + [C] \bullet \frac{\{M\}_n - \{M\}_{n-1}}{\Delta t_n} \\ &= (1-\theta) \bullet \{F\}_{n-1} + \theta \bullet \{F\}_n \\ &\Rightarrow \left\{\frac{[C]}{\Delta t_n} + \theta \bullet [K]\right\} \bullet \{T\}_n - \left\{\frac{[C]}{\Delta t_n} - (1-\theta) \bullet [K]\right\} \bullet \{T\}_{n-1} + \frac{[C]}{\Delta t_n} \bullet \{M\}_n - \frac{[C]}{\Delta t_n} \bullet \{M\}_{n-1} \\ &= (1-\theta) \bullet \{F\}_{n-1} + \theta \bullet \{F\}_n \end{aligned} \tag{6.21}$$

These equations, defining the process of coupled heat and mass transfer inside the wheat kernel, were solved to obtain the moisture and temperature for a time step of Δt_n. The value of θ can be chosen following different schemes (θ is 0 for the forward difference scheme, 0.5 for the Crank-Nicholson scheme, 0.667 for the Galerkin method or 1 for the backward difference scheme). The overall grain moisture and temperature distribution was determined by following the area-average concept for every time step instead of nodal values:

$$\overline{M} = \frac{\iint M(x,y)\,dx\,dy}{\iint dx\,dy} \tag{6.22}$$

and

$$\overline{T} = \frac{\iint T(x,y)\,dx\,dy}{\iint dx\,dy} \tag{6.23}$$

6.2.3 Simulation of a Wheat Drying Model

The equations of state in the previous section were solved using COMSOL® Multiphysics™ version 3.2b (COMSOL, Inc., Burlington, MA) running on a Windows XP OS with Intel® Pentium 4 2.4 GHz processor with 512 MB RAM. COMSOL® is a generic finite element solver package that deals with 3D heat and mass transfer problems so it could be used to investigate most grain drying and storage problems in realistic bins. To import the model geometry into COMSOL®, image processing algorithms were written in Matlab v. 7, R14 (The Mathworks, Natick, MA) for selected MR images of the coronal slices (xy) of: (i) an intact wheat kernel (with three components: pericarp, endosperm and germ), (ii) a scarified kernel (incisions in the pericarp), and (iii) a germ-

removed kernel to generate 2D curved geometry objects (Figs. 6.3-6.5). The model equations were formed and the corresponding physical and material properties (*vide infra*) together with the initial and boundary conditions were entered simultaneously into the 'Transient Conduction Heat Transfer' and 'Transient Diffusion' application modes in COMSOL®. Numerical simulations were carried out using Lagrange-quadratic elements over a triangular mesh on each object. The number of elements, degrees of freedom (DOF) and the maximum element quality are given in Table 6.1.

The time dependent solver was used starting at 0 with a time step of 10 min up to 4 h to compare with the results obtained from the MRI study (*vide infra*). The COMSOL® solver uses backward differentiation formula (thus $\theta = 1$ in Eqs. 6.20 and 6.21) for the time stepping algorithm. In our case, the system was non-symmetric and had a high degree of stiffness (low time step size of 10 min to maintain stability of the system). Since the set of equations are of the Laplace-type we used the default direct linear system solver (UMFPACK). The relative and absolute tolerances were kept as default values to control the error in each integration step.

6.2.4 Selection of Physical and Material Properties

The accuracy of the model prediction depends on supplying accurate physical and material properties needed in the model. Of them, initial moisture contents and water diffusivity in the individual grain components play the major role in wheat drying kinetics as is evident from the reported MRI experiments (Ghosh et al. 2006 a,b). Both the initial moisture content in the individual grain components and moisture changes during drying were measured by developing a calibration equation (Eq. 6.24) using the

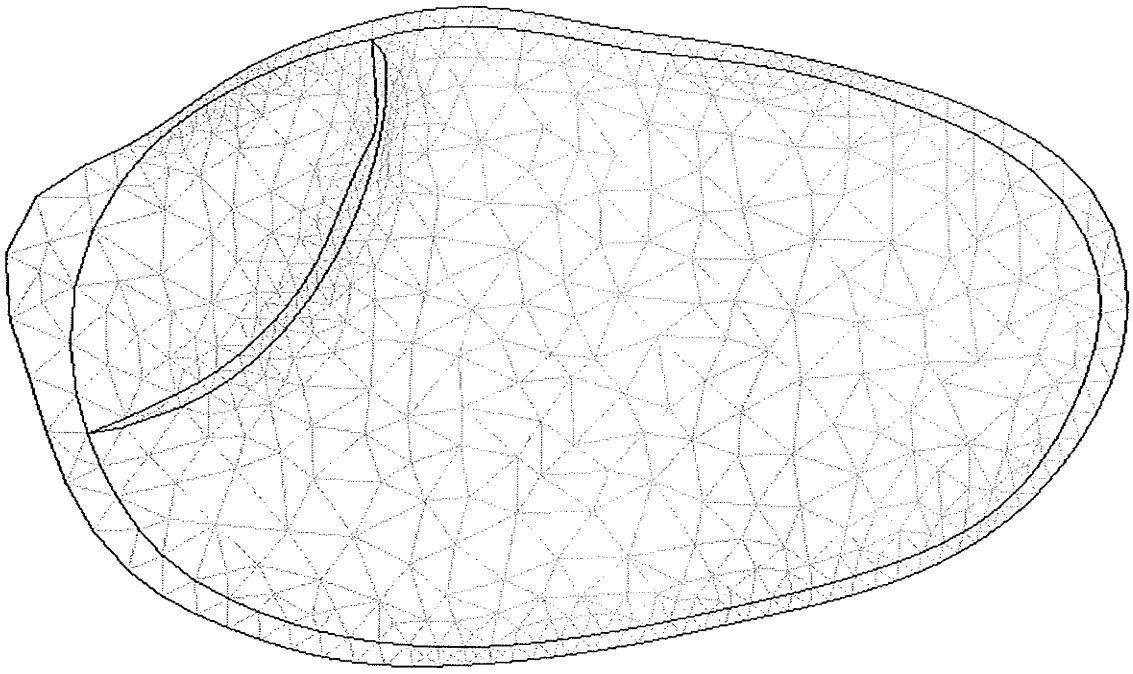

Figure 6.3 Two-dimensional geometry object of an intact wheat kernel used for model simulation.

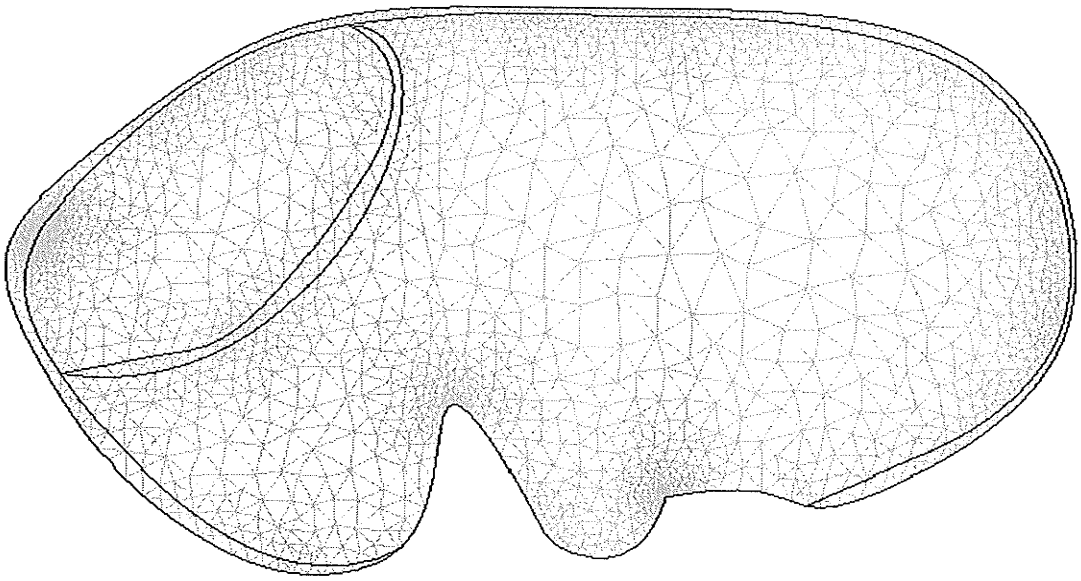

Figure 6.4 Two-dimensional geometry object of a scarified wheat kernel used for model simulation.

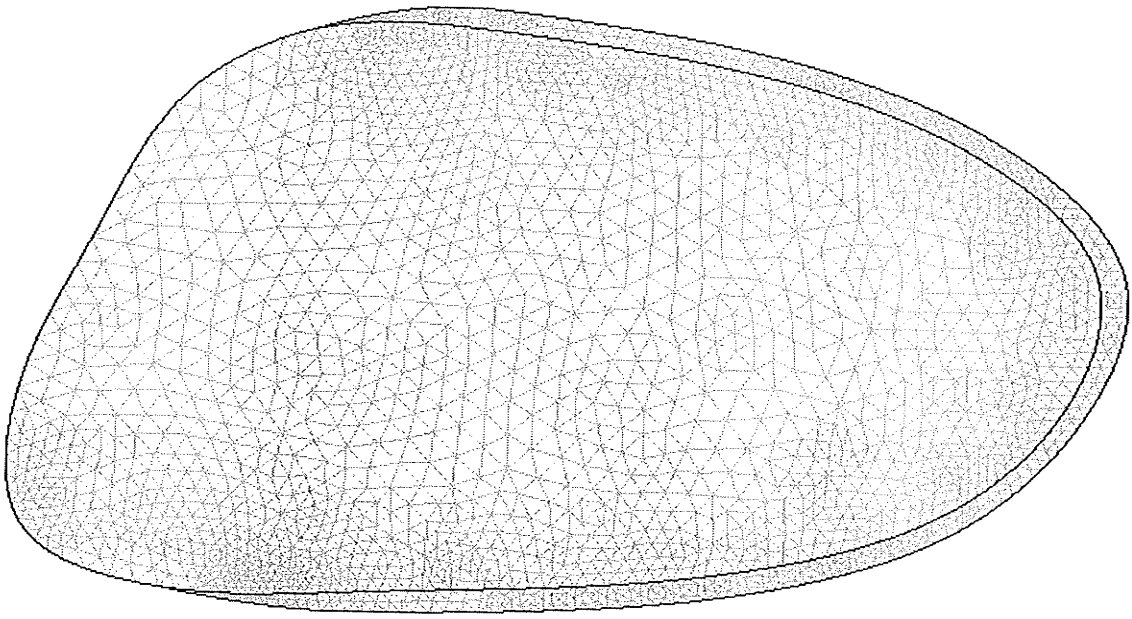

Figure 6.5 Two-dimensional geometry object of a germ-removed wheat kernel used for model simulation.

Table 6.1 Summary of elements information.

Grain	Number of elements	DOF	Maximum element quality
Intact	1179	3894	0.1957
Scarified	7817	21560	0.2670
Germ-removed	1005	3338	0.1441

NMR spectra of an individual wheat kernel with a known moisture content, obtained by the gravimetric method (ASAE, 2003):

$$\text{NMR signal intensity} = 54.7 \times M + 90.7 \tag{6.24}$$

Further, MRI experiments indicated that the pericarp dries fastest of all grain components (Ghosh et al. 2006 a,b). It was hard to obtain any signal from the pericarp region, therefore, in this study, we neglected the existence of the pericarp in the model simulation. The initial moisture content in the endosperm (M_{oE}) varied from 31.9-52.8% d.b. (24-35% w.b.) and in germ (M_{oG}) it varied from 152.3-208.9% d.b. (60-68% w.b.). From this point forward, moisture contents are given in dry basis unless mentioned otherwise. Since dry nitrogen gas (N_2) was used as a drying medium in this study (see experimental section), an equilibrium moisture content (M_e) of 2% was used in all model simulations to match the drying conditions in our MRI study. The initial temperature of the wheat kernel and its parts was considered to be room temperature (T_o = 25°C). The other physical and material properties used in this model are given in Table 6.2. The convective heat and moisture transfer coefficients (h_t and h_m) were calculated assuming external flow past a cylinder analogy (Incorpera and Dewitt 1996). The values of h_t and h_m were calculated for both air and N_2 gas.

6.2.5 Calculation of Convective Heat Transfer Coefficient

The following formula was used for the calculation of the convective heat transfer coefficient:

Table 6.2 Physical and material properties of wheat used in this study.

Property	Symbol	Value	Reference
Thermal conductivity	K	$(0.14+0.68\,M)$ W m^{-1} K^{-1}	Sokhansanj and Bruce (1987)
Specific heat	C_g	$(1300+4187\,M)$ J kg^{-1} K^{-1}	Giner and Mascheroni (2001)
Density	ρ_g	$774.4-7.03\,m+1.85\,m^2$ $-0.149\,m^3+0.003116\,m^4$ kg m^{-3}	Pabis et al. (1998)
Latent heat of vaporization of water in wheat	L	$2500.8\times10^3\{1+1.7\exp(-17.6\,m)\}$ J kg^{-1}	Pabis et al. (1998)
Water diffusivity in endosperm	D_E	$0.0105\exp(-6155/T_{med})$ m^2 s^{-1}	Devahastin and Majumdar (1999)
Water diffusivity in germ	D_G	$7.507\times10^{-8}\exp(-2806.5/T_{med})$ m^2 s^{-1}	Giner and Mascheroni (2001)

M is the dry basis moisture content (decimal); m is the wet mass basis moisture content (%); T_{med} is the hot drying medium temperature (K).

$$Nu = \frac{h_t\, d_p}{K} = 0.51\, Re^{0.5}\, Pr^{0.37} \left(\frac{Pr}{Pr_s}\right)^{0.25} \qquad (6.25)$$

where Nu is the Nusselt number; Re is the Reynold's number $\left(\frac{V\, d_p}{\gamma}\right)$; Pr is the Prandtl number $\left(\frac{C\ \mu}{K}\right)$; d_p is the equivalent diameter of a wheat kernel (3 mm in this study); K is the thermal conductivity of drying medium at a given temperature (air or 100% N_2 gas) (W m^{-1} K^{-1}); V is the velocity of gas flow (0.23 m s^{-1} in this study); γ is the kinematic viscosity of the drying medium (m^2 s^{-1}); C is the specific heat of drying medium (kJ kg^{-1} K^{-1}); μ is the dynamic viscosity of the drying medium (N s m^{-2}); and suffix s is for the values at the room temperature. The calculated heat transfer coefficients for both air and N_2 gas are given in Table 6.3.

6.2.6 Calculation of Moisture Transfer Coefficient

The moisture transfer coefficient was calculated by:

$$Sh = \frac{h_m\, d_p}{D_{AB}} = 0.51\ Re^{0.5}\, Sc^{0.37} \qquad (6.26)$$

where Sh is the Sherwood number; Sc is the Schimdt number $\left(\frac{\gamma}{D_{AB}}\right)$; D_{AB} is the diffusion coefficient of water in air (0.26×10^{-4} m^2 s^{-1} at 1 atm and 25°C). The calculated moisture transfer coefficient values are given in Table 6.4.

Table 6.3 Calculation of heat transfer coefficients used in this study.

Temp. (°C)	γ ($m^2 s^{-1}$) × 10^6		C ($kJ kg^{-1} K^{-1}$)		μ ($N s m^{-2}$) × 10^7		K ($W m^{-1} K^{-1}$) × 10^3		Pr		Re		h_t ($W m^{-2} K^{-1}$)	
	Air	N_2	Air	N_2	Air	N_2	Air	N_2	Air	N_2	Air	N_2	Air	N_2
25*	15.71	15.68	1.007	1.041	183.6	177.3	26.14	25.8	0.707 (Pr_s)	0.715	43.92	44.01	--	--
30	16.20	16.15	1.007	1.041	186.02	179.5	26.52	26.7	0.706	0.716	42.59	42.72	25.86	25.53
40	17.20	17.14	1.007	1.041	190.74	183.9	27.26	26.8	0.705	0.714	40.12	40.26	25.77	25.42
50	18.20	18.12	1.008	1.041	195.45	188.2	28.00	27.5	0.704	0.712	37.91	38.08	25.71	25.8

*Room temperature

Table 6.4 Calculation of moisture transfer coefficients used in this study.

Drying Temperature (^{o}C)	D_{AB}*	Sc	h_m (m s^{-1})
30	0.000026	0.621	0.024
40	0.000028	0.612	0.025
50	0.000029	0.625	0.025

*$D_{AB} = D_{AB_{T_a}} \times \left(\frac{T_{med}}{T_a}\right)^{1.5}$, where T_a is the absolute value of the ambient air temperature (298 K) and T_{med} the absolute value of the drying medium temperature. The values of the moisture transfer coefficients were identical for both nitrogen gas and air.

6.2.7 Drying Experiment

Canada Western Red Spring (CWRS) wheat (*Triticum aestivum* L., cv. A.C. Barrie) containing approximately 15.7±0.03% m.c. was used in this study. A kernel of wheat consists of three major components, the endosperm (85-90% by mass), the germ or embryo (2-3% by mass), and the pericarp (7-8% by mass) (Simmonds et al. 1953). Detailed information on a wheat kernel structure can be obtained from several excellent sources (MacMasters et al. 1964; Brooker et al. 1992; Pomeranz and Bechtel 1978; Evers and Bechtel 1988). Magnetic resonance imaging experiments were carried out on an 11.7 T (500 MHz) vertical bore magnet (Magnex Scientific Ltd., Yarnton, UK) and an in-line variable temperature and flow controller unit (Bruker BVT-1000, Milton, ON) attached to a custom built imaging probe (Helmholtz configuration, 7 mm inner diameter). Prior to MRI, wheat kernels were preconditioned to a known moisture level (greater than 25%) to acquire bright MR images that helped in studying the intrinsic details. For every MRI experiment, individual kernels were placed into the imaging probe which was then placed into the bore of the vertical MRI magnet. Drying was started following a short setup period, and continued for 4 h at 30, 40, and 50°C at a constant nitrogen gas flow (~0.23 m/s). The wheat kernels were preconditioned to selected moisture content by soaking in distilled water for overnight at the beginning of every MR imaging experiment. Moisture movement within and out of wheat kernels during drying was observed under the following conditions: initial average moisture contents: 60.3±0.8% (intact or scarified kernels) [same level of moisture content was reported by Stapley et al. (1998)] and 49.7±3.2% (germ-removed kernels); three types of wheat kernels: intact, mechanically-

scarified, and germ-removed; and drying temperatures: 30, 40 and 50°C with an accuracy of ±1°C. The parameters used for MR imaging are given in Table 6.5.

Since we were interested in studying the moisture transfer pattern, we worked on the 2D MR images. We increased the obtained MR image matrix of 128 × 64 to 224 × 224 by zero-filling using Marevisi v.7.2 (Institute for Biodiagnostics, Winnipeg, MB). A particular coronal slice out of 8 slices was selected to best illustrate the moisture distribution in the kernel with the greatest anatomical detail. The acquired MR images were gray-scale representations of the number of protons in the water-containing parts of the wheat kernels, which in turn represents water distribution. The brighter the image, the greater the number of protons. The darker the image, the fewer the number of protons. We were interested to model the influence of the grain components on the drying process. Therefore, we used samples of 1) intact kernels (with all three components: pericarp, germ, and endosperm), 2) mechanically scarified kernels by making incisions in the pericarp, and 3) kernels with the germ removed. The incisions on the intact kernels were made after the moisture equilibration to prepare the scarified kernels. The germ was removed from the intact kernels prior-to the moisture equilibration. This was done to reduce possible loss or redistribution of soluble materials of the imbibed kernels and thus to achieve more accurate results (MacMasters et al. 1964). The germ-removed kernels were at lower moisture content (about 50%) than the intact or the scarified kernels (about 60%). All the drying experiments were replicated thrice at each temperature with similar sized wheat kernels selected by visual inspection. Thus a total of 27 MRI-drying experiments (3 different kernels × 3 drying temperatures × 3 replications) were

Table 6.5 Parameters used in all magnetic resonance imaging experiments.

Parameters	Description/values
Imaging sequence	3D multi-slice Hahn Spin-Echo sequence (Hahn 1950)
Repetition time (TR)	200 ms
Echo delay time (TE)	3.375 ms
Direction of slices	Coronal
Number of slices	8
Thickness of slices	0.5 mm
Field-of-view (FOV)	12.8 mm × 12.8 mm × 4 mm
Image resolution	100 μm × 200 μm × 500 μm
Image acquisition time	10 min 18 s
Number of scans	6

performed for the model validation. The MR image intensities were derived by the following equation to eliminate the effect of the noise on the analysis of drying curves (Bernada et al. 1998):

$$I_{avg} = \frac{I_{kernel} - I_{noise}}{I_{noise}} \tag{6.27}$$

where by definition:

$$I_i = \frac{1}{A_{I_i}} \iint_{A_{I_i}} I(x,y)\, dx\, dy \tag{6.28}$$

where i is the kernel or noise area; I is the pixel intensity at coordinate (x,y); and A_{I_i} is the average area.

6.3 Results and Discussion

6.3.1 Magnetic Resonance Images

The representative MR images of sequential slices (2D) from MRI data sets (3D) collected as a function of drying time of an intact kernel, a mechanically scarified kernel, and a germ-removed kernel during drying at 30°C are shown in Figure 6.6. Images in each row were scaled primarily based on the minimum and maximum pixel values in the first image at the beginning of drying. The signal-to-noise ratio (SNR) of the first image (just before drying) in serial MR images were: intact: 28.9, mechanically scarified: 17.4, and embryo-removed: 17.7. The SNR was calculated as the ratio of average image intensity of an irregular polygon shaped region of interest (ROI) in the whole grain including both endosperm and germ to the average image intensity of the same size area in a region of noise only. As drying proceeds, water moves out from the kernel, the moisture content drops, as does the signal intensity, and therefore the signal-to-noise ratio

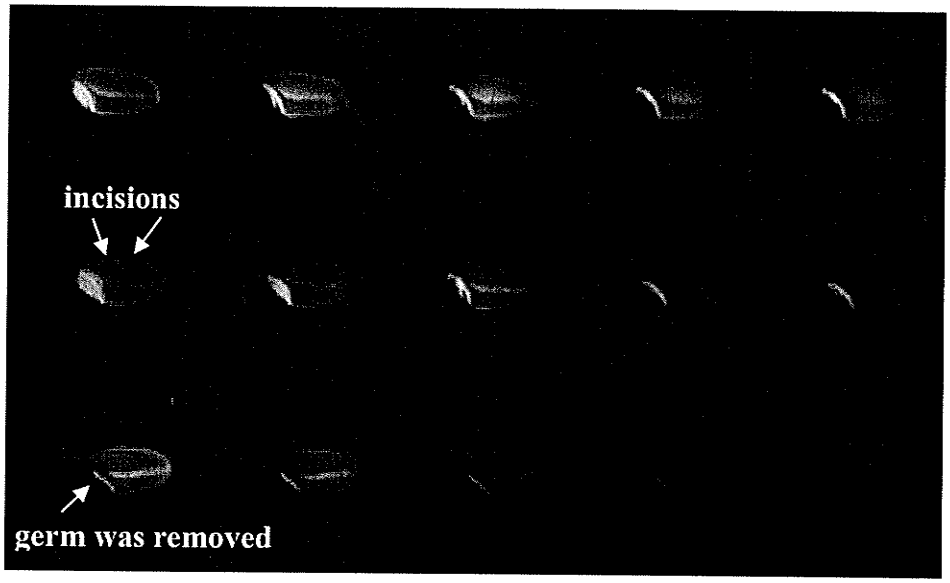

Figure 6.6 Two-dimensional magnetic resonance image series of intact, mechanically scarified and germ-removed wheat kernels dried at 30°C after every 1 h from the beginning of drying.

decreases. MR images showed the variation in the internal distribution of water prior-to and during drying. The pericarp hardly showed any signal intensity at the onset of the drying process since moisture moved out quickly from this region and the entire region started offering resistance to the water flow. Discontinuity in cellular structure between the inner hypodermis and the outer hypodermis helps in faster movement of water from the pericarp region at the initial stages of drying. Water moves through the intercellular spaces of cross and tube cells to reach the pericarp region. However, after the initial stages of drying, water movement through the pericarp of the endosperm region becomes restricted because the thick-walled nucellar epidermis, which lies between the seed coat and the aleurone layer, resists the movement of water through them. Therefore, this layer contains less water and thus no MRI signal can be detected from this region. Water was concentrated mainly in the germ region and the germ image intensity remained high, even after 4 h of drying at all three temperatures. Previously measured (Ghosh et al. 2006b) relatively high T_2 values (about 10 ms) of the germ region, in combination with relatively high signal amplitude indicate the presence of mobile ("free") water in the germ. The lowest T_2 values (about 3 ms) were observed in the endosperm region indicating that water interacts more strongly with the starch matrix. Further, image profile analysis for a hypothetical line on an intact kernel indicated a very small attachment region between the germ and the endosperm with considerably low intensity. This small attachment region is a depleted layer of collapsed, digested and hydrolyzed modified endosperm cells containing a negligible amount of protein and starch bodies, which originates during the development of the germ (Smart and O'Brien 1983). As a result, this region creates a high moisture gradient between the germ and the endosperm for which moisture moves

towards the germ area from the endosperm (Jenner and Jones 1990). Therefore, a thin section was drawn in the model geometry objects for intact and mechanically-scarified kernels before the model simulation (Figs. 6.3-6.5). The moisture content in this region was assumed to be half of the endosperm region but the diffusivity was assumed to be the same as of endosperm for the model simulation.

6.3.2 Predictions by the Proposed Model

The predictions of moisture content by our model were compared with two thin-layer drying models for wheat published by Jayas and Sokhansanj (1986) and Sinico et al. (1995). Thin-layer drying models can better predict the deep bed drying simulations where the deep bed is divided into a finite number of thin layers. The amount of moisture removed from the grain can be determined by a thin-layer drying equation. Therefore, it is more realistic to validate our model with the published thin-layer drying models. In addition, the developed model was compared with a two-dimensional heat and mass transfer drying model for a single wheat kernel developed by Jia et al. (2000). Jia et al. (2000) considered the moisture movement by liquid diffusion from the inside to the surface and by evaporation within and at the surface of the kernel. Further, they assumed a uniform initial moisture content distribution throughout the wheat kernel at the beginning of drying and a single value of water diffusivity for the entire kernel of wheat. Table 6.6 gives the detail of these models with their corresponding parameters.

Our model was solved for drying air temperature of 35°C with relative humidity of 0.35, initial overall grain moisture content of 21%, equilibrium moisture content of

Table 6.6 Models compared in this study.

Models	Parameters	Reference
$MR = \frac{M - M_e}{M_o - M_e} = \exp(-k\,t)$	M_e (% d.b.) was calculated as the average of values obtained from the following equations: (a) Modified Henderson Eqn.: $RH = 1 - \exp[-0.000043295\,(T'_{med} + 41.585)\,(M_e)^{2.1119}]$ where RH is the relative humidity, decimal and (b) Modified Chung-Pfost Eqn.: $RH = \exp\left[-\frac{377.52}{T'_{med} + 35.59}\exp(-0.16456.\,M_e)\right]$ T'_{med} is the drying medium temperature (°C) $k = 0.001791 + 6.06\times10^{-6}\times T'^{2}_{med}$	Jayas and Sokhansanj (1986)
$MR = \frac{M - M_e}{M_o - M_e} = \exp(-k\,t^n)$	$M_e = \left\{\frac{-1}{20.25}\ln\left[\frac{(T_{med} - 239.9)\ln(RH)}{-\{1134 + 307.6\ln(M_o)\}}\right]\right\}$ $k = 0.6348\times10^{-6}\exp(0.03733\,T_{med})$ $(M_o - M_e)^{(0.1824\,RH^{-0.6724})}$ $n = 1.13\,M_o^{0.3225}$	Sinico et al. (1995)
$\frac{\partial M}{\partial t} = D\left(\frac{\partial^2 M}{\partial x^2} + \frac{\partial^2 M}{\partial y^2}\right)$ $\rho_g\,C_g\frac{\partial T}{\partial t} = K\left(\frac{\partial^2 T}{\partial x^2} + \frac{\partial^2 T}{\partial y^2}\right) + L\,\rho_g\frac{\partial M}{\partial t}$ Initial conditions: at $t = 0$, $M_o = T_o = 0$ Boundary conditions:	D^* is the diffusivity of whole wheat as follows: $D^* = (461.5\times2.01\times10^{-12})\,RH^3\exp\left(\frac{-1331}{T_{med}}\right)$ $\rho_g = 1265$ kg m^{-3} $C_g = (1396 + 2688\,M)/(1 - M)$ J kg^{-1} $K = (0.1170 - 0.003808\,M)/(1 - M)$ W m^{-1} K^{-1} $L = \{(3.11\times10^6) - (2.11\times10^3)T_{med}\} + \frac{461.5\,T^3_{med}}{RH^2}$ J kg^{-1} $RH = 1 - \exp[-5869\,T_{med}^{-0.775}\,M^{5203\,T_{med}^{-1.363}}]$ $h_m = \frac{1.47}{T_{med}}$ m s^{-1} $h_t = 1.147$ W m^{-2} K^{-1}	Jia et al. (2000)

$D_x^* \frac{\partial M}{\partial x} l_x + D_y^* \frac{\partial M}{\partial y} l_y + h_m (M - M_e) = 0$	C_v is the specific heat of water vapor in wheat = 1880 J kg^{-1} K^{-1} V is the volume of wheat kernel = 5.65e-08 m^3
$K_x \frac{\partial T}{\partial x} l_x + K_y \frac{\partial T}{\partial y} l_y + h_t (T - T_a) + \rho_g [L + C_v (T_a - T)] \frac{\partial M}{\partial t} \frac{V}{A} = 0$	A is the area of wheat kernel = 1.41e-05 m^2

10% and an ambient temperature of 25°C. The time step used was 10 min and the solution time was 30.6 s. The model predictions were graphically compared with three above mentioned models with the same conditions. It is noteworthy that in case of a wheat kernel of about 60% m.c., the germ contains an average of 174% moisture and the endosperm contains approximately 41% moisture as computed from the MR calibration equation (Eq. 6.24). With a linear analogy, we used germ moisture content of 58% and endosperm moisture content of 14% for an overall wheat moisture content of 21% in our model. The simulated mass average moisture content values from our model were between the results obtained by Jayas and Sokhansanj (1986) and Sinico et al. (1995). Our model prediction indicated a close agreement to the prediction of Sinico et al. (1995) while the model of Jia et al. (2000) deviated greatly from the other models (Fig. 6.7). The model of Sinico et al. (1995) was based on a wide initial moisture content range of 10 to 20.5%, therefore, it provided the closest agreement with our model results. The computed moisture content values from our model were slightly lower than that predicted by Sinico et al. (1995) presumably due to the exclusion of moisture condensation from the inner parts of the kernel to the surface in our model. Similar results were observed by Ranjan et al. (2001) for barley drying. Although Jia et al. (2000) included the evaporation phenomena in their model, only liquid diffusion was considered instead of incorporating both liquid and vapor diffusion in the model simulation. Solution time for the model of Jia et al. (2000) was 44.1 s in COMSOL®. Their model highly under-predicted the results obtained by Sinico et al. (1995). The difference between our model and the model of Jayas and Sokhansanj (1986) increased after the first 90 min of drying. This deviation is

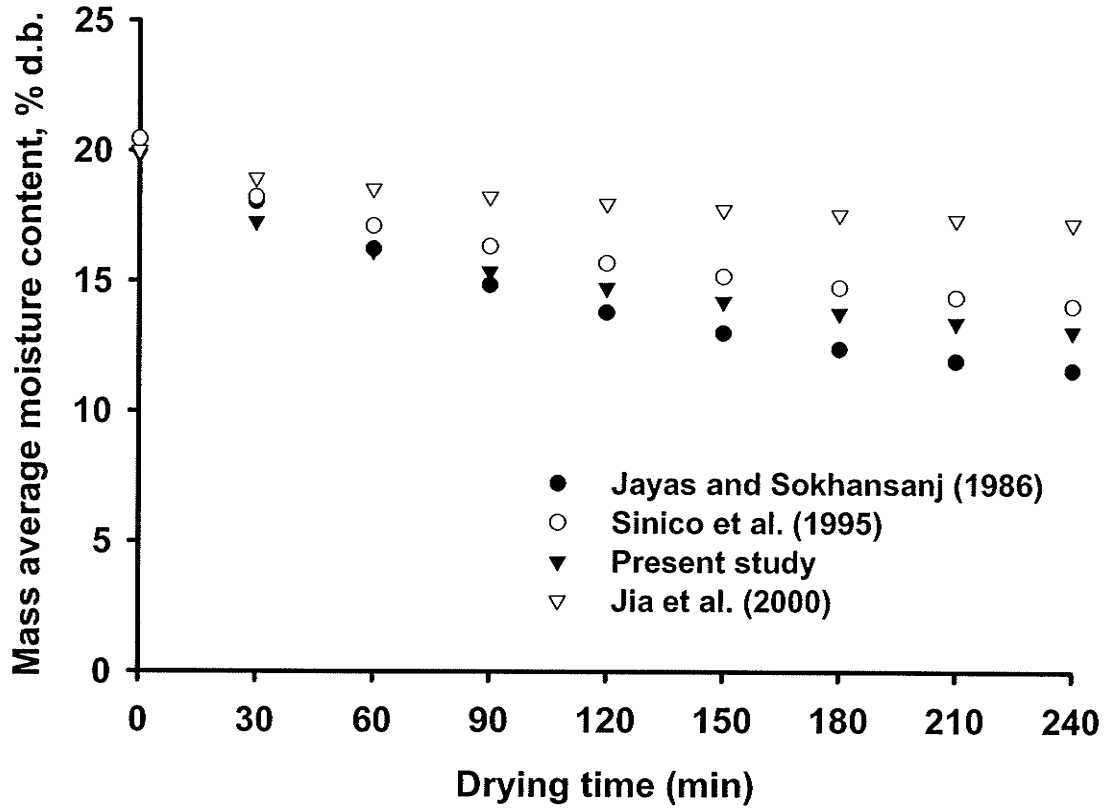

Figure 6.7 Comparison of drying equations for drying of wheat (20.5% d.b.) at 35°C.

expected because the model of Jayas and Sokhansanj was based on a single initial moisture content value (22.7%) instead of a range of values. The moisture content values of germ and endosperm were also obtained from our model (Fig. 6.8). This is the unique feature of this study. Knowledge of water distribution in individual grain components is beneficial to maintain an overall grain quality. For example, in wheat milling, it is essential to maintain about 16% m.c. in the wheat endosperm for superior bread making (Bechtel and Wilson 2005). Figure 6.8 indicated that the endosperm reached equilibrium very quickly whereas the germ took a long time to reach the equilibrium. A sharp moisture decrease at the initial stages of drying in both the germ and in the endosperm was also evident from Fig. 6.8. This indicated that a large moisture gradient was produced in the grain kernel at the beginning of drying, which can lead to stress crack development. Since the wheat endosperm comprises 85-90% of the total kernel weight and the magnitude of the moisture gradient is less as depicted by our model (Fig. 6.8), and the germ contains more water. Despite the high moisture gradient, stress-cracking is not prevalent in wheat during drying compared to a corn kernel (Nellist and Bruce 1995). Ghosh et al. (2006a) indicated that the moisture moved from the endosperm to the germ through the fingerlike cells of the scutellum epithelium to finally move out from the kernel. Absence of the aleurone layer in the germ region reduces the resistance to water removal (McEwen et al. 1954). Ghosh et al. (2006b) reported that the moisture-loss rate during drying was lower in the germ than in the endosperm. In other words, water diffusivity in the endosperm could be higher than in the germ. Water diffusion coefficients for wheat endosperm and/or the whole grain have been reported by several researchers (Callaghan et al. 1979; Eccles et al. 1988; Jenner and Jones 1990; Stapley et

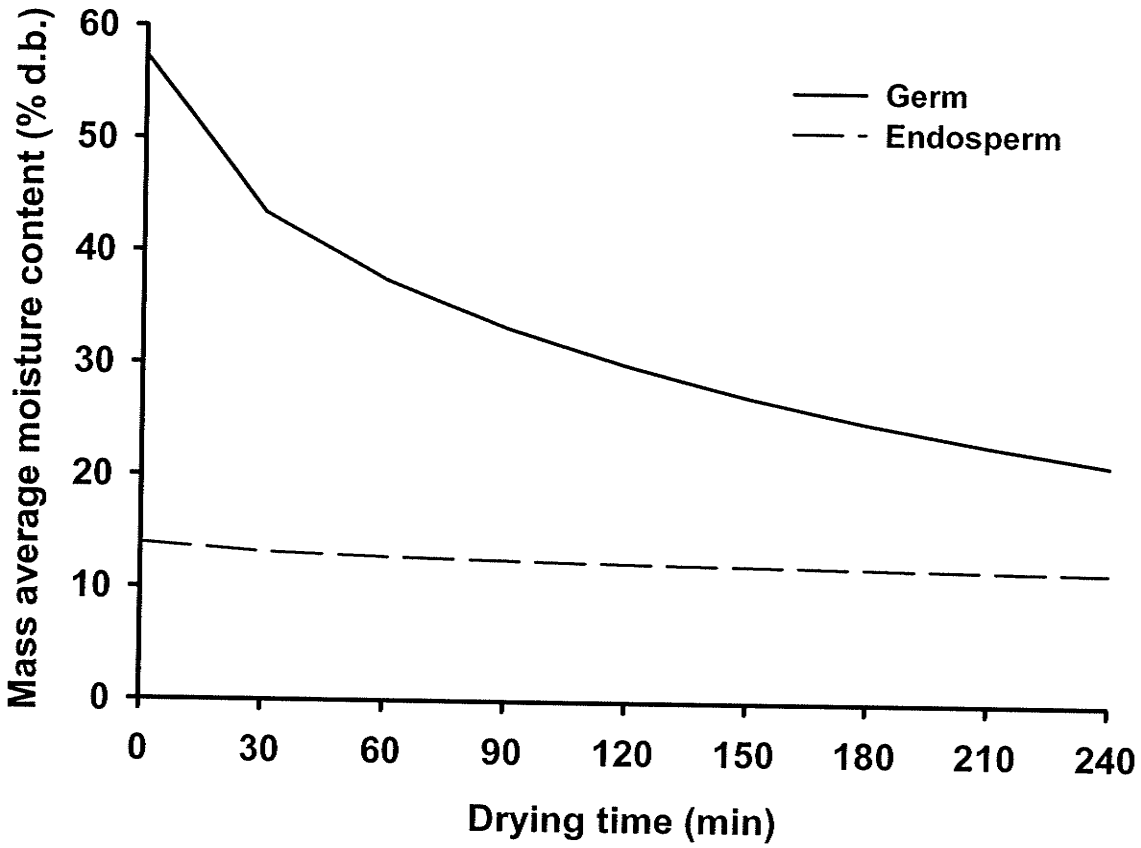

Figure 6.8 Drying curves of wheat components (overall initial grain moisture content 20.5% d.b.) computed from the present study during drying at 35°C.

al. 1998; Kang and Delwiche 1999). However, at the moment, no information is available about the water diffusion coefficient in the wheat germ. Further, no particular water diffusion coefficient for the wheat components has been suggested. Although Callaghan et al. (1979) and Sokhansanj and Gustafson (1980) indicated that water diffusion coefficient in grain is a function of moisture content, no experimental wheat drying data have been reported to show the dependency of water diffusivity on the moisture content. Therefore, in our model, we used Arrhenius-type temperature-dependent water diffusivity and used the equations of Devahastin and Majumdar (1999) and Giner and Mascheroni (2001) to provide the values of water diffusion coefficients of wheat endosperm and germ. Calculated diffusivity values explained that water diffusivity in the germ is lower than that in the endosperm for any specific drying temperature. Sokhansanj and Gustafson (1980) also indicated a lower water diffusivity value for the germ compared to the endosperm of a corn kernel.

Figure 6.9 compares the corresponding mass average moisture content data predicted by our model to the data predicted by Jia et al. (2000) for wheat drying at a temperature of 47°C, with an initial moisture content of 21.1%, an equilibrium moisture content of 15%, and an initial temperature of 26.7°C. A time step of 1 min was chosen for this analysis. Solution time for our model was 28.8 s in COMSOL® whereas it was 45.2 s to solve the model of Jia et al. (2000) for this analysis. Although our model slightly over-predicted the drying process, the correlation coefficient between the two model predictions was over 0.99 indicating a good overall agreement of the drying data. Since the average mass

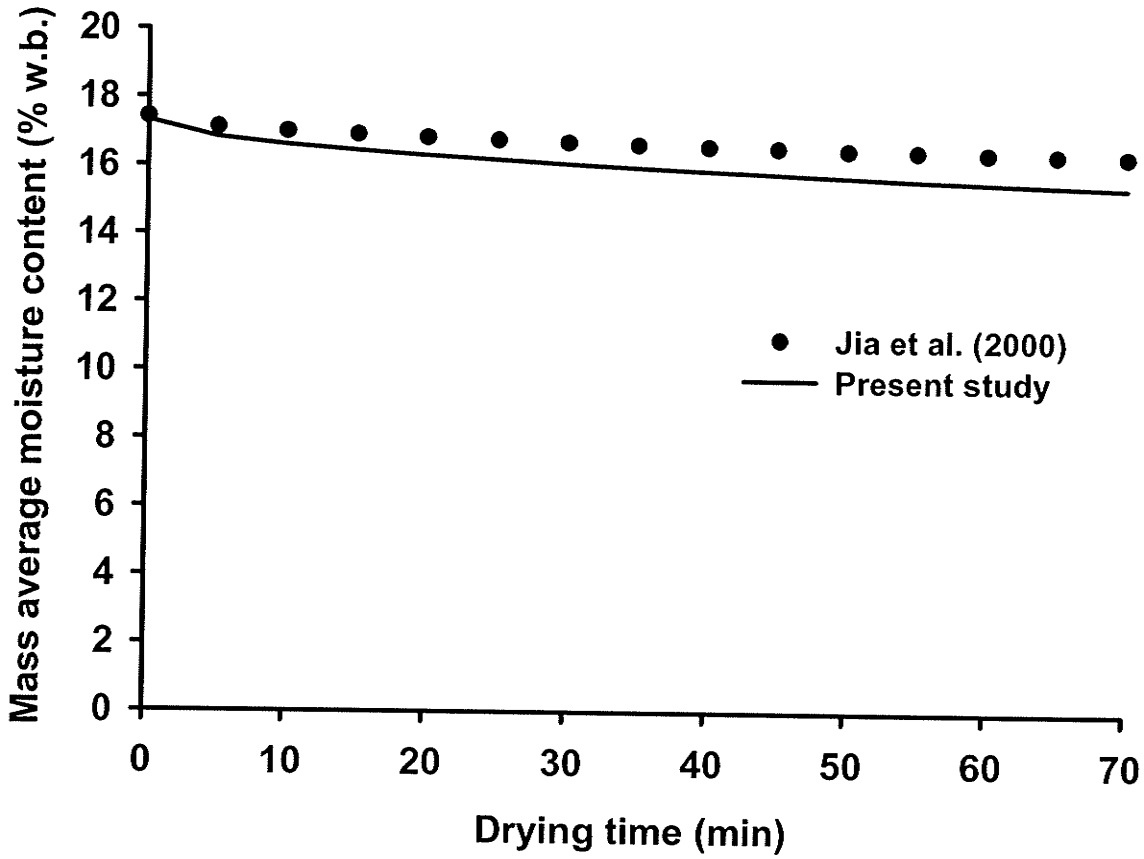

Figure 6.9 Comparison of model predictions on the mass average moisture during drying of wheat at 47°C.

moisture content prediction by Jia et al. (2000) had under-estimated the experimental data provided by Fortes et al. (1981) by about 2-3%, our model prediction is more realistic.

6.3.3 Comparison with the Magnetic Resonance Imaging Studies

Since we were interested in finding the similarities between our model prediction on the moisture movement pattern and the MR images obtained from three different wheat kernels, simulations were performed using the same conditions for the MRI-wheat drying study. The initial moisture contents were varied according to the measured data obtained from the MR images (Table 6.7). Drying data (i.e. moisture loss as a function of drying time) were collected periodically by converting the MR proton density image intensities into the actual moisture contents (% d.b.) using the calibration equation (Eq. 6.24) at particular drying temperatures. Drying curves generated from these drying data were used to validate the model simulations.

Figures 6.10-6.12 show the trend of model predicted moisture ratio and the ratio of the averaged local normalized MR image intensity of the three different kinds of kernels with their major components (germ and endosperm) dried at 30, 40, and 50°C. The moisture ratio ranges obtained from the model simulation were 0.35-0.62 in the endosperm and 0.40-0.60 in the germ of a mechanically-scarified kernel compared to 0.45-0.80 in the endosperm and 0.38-0.55 in the germ of an intact kernel during initial 1.5 h of drying at three temperatures. These results indicated faster moisture removal from the incised parts of the grain (Ghosh et al. 2006a). Incisions in the pericarp locally destroy the epidermis, hypodermis, cross and tube cells. Therefore, the portions of endosperm cells directly

Table 6.7 Initial mass average moisture content (%, d.b.) values as obtained from the magnetic resonance images to be used for the model simulations.

Temp (°C)	Intact kernel		Mechanically-scarified kernel		Germ-removed kernel
	Germ	Endosperm	Germ	Endosperm	Endosperm
30	156.6	41.3	168.7	31.9	50.3
40	152.3	41.3	208.9	40.2	51.4
50	171.6	42.0	188.4	52.8	50.6

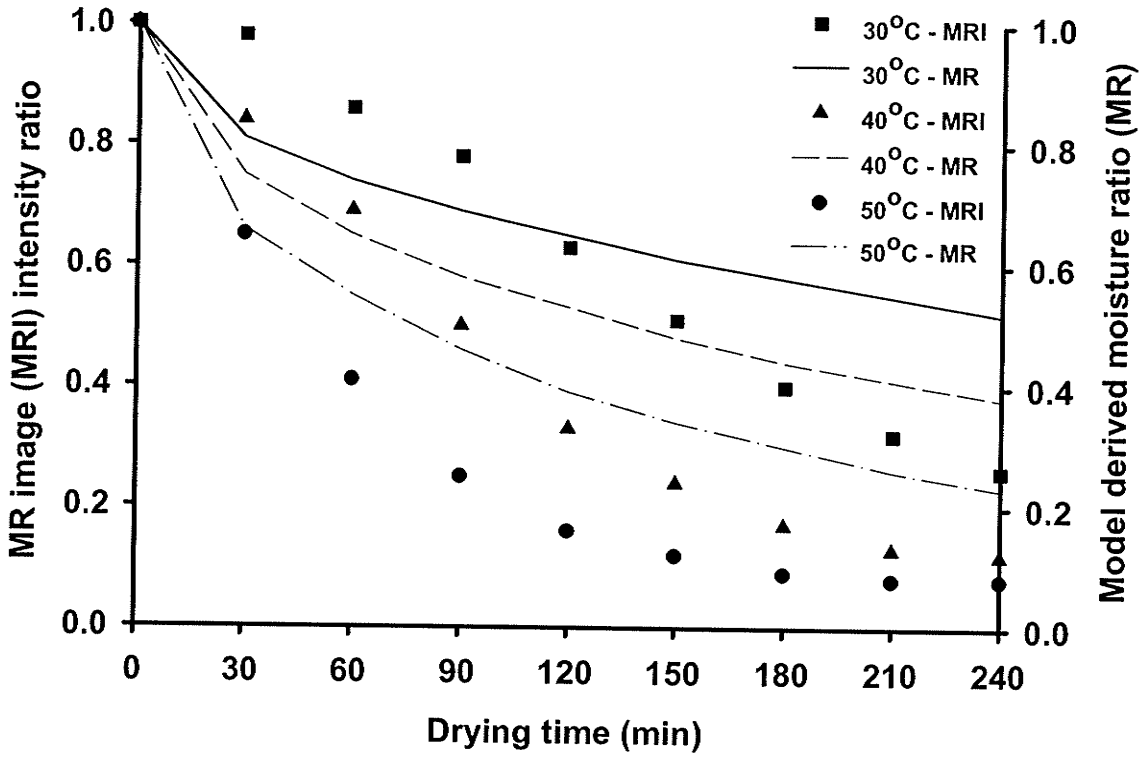

Figure 6.10(a) Trends of magnetic resonance imaging data and predicted drying curves for endosperm of an intact wheat kernel dried at 30, 40, and 50°C temperatures.

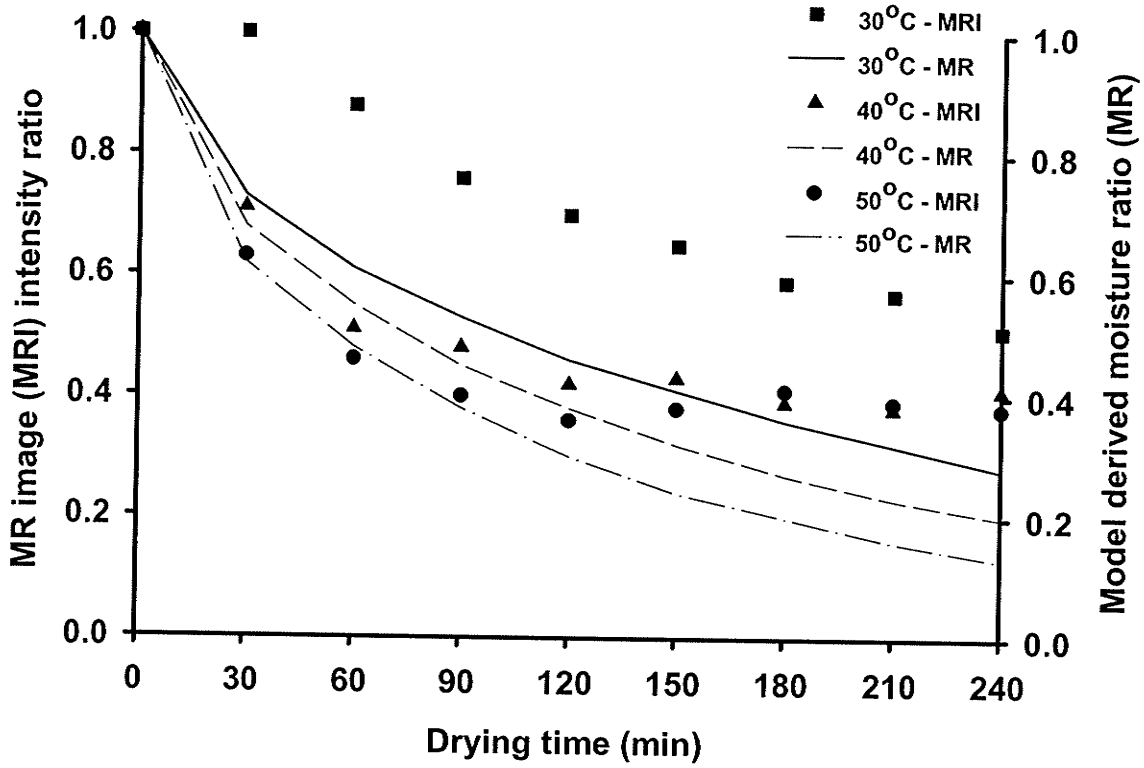

Figure 6.10(b) Trends of magnetic resonance imaging data and predicted drying curves for germ of an intact wheat kernel dried at 30, 40, and 50°C temperatures.

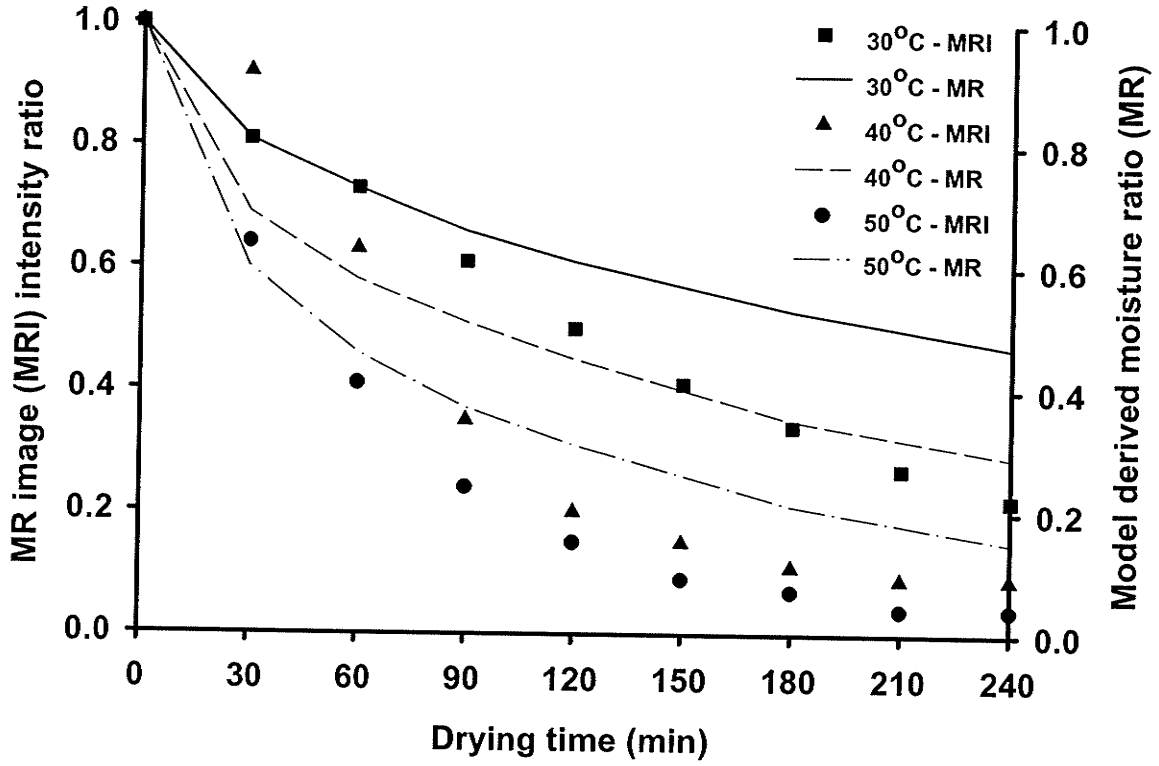

Figure 6.11(a) Trends of magnetic resonance imaging data and predicted drying curves for endosperm of a mechanically-scarified wheat kernel dried at 30, 40, and 50°C temperatures.

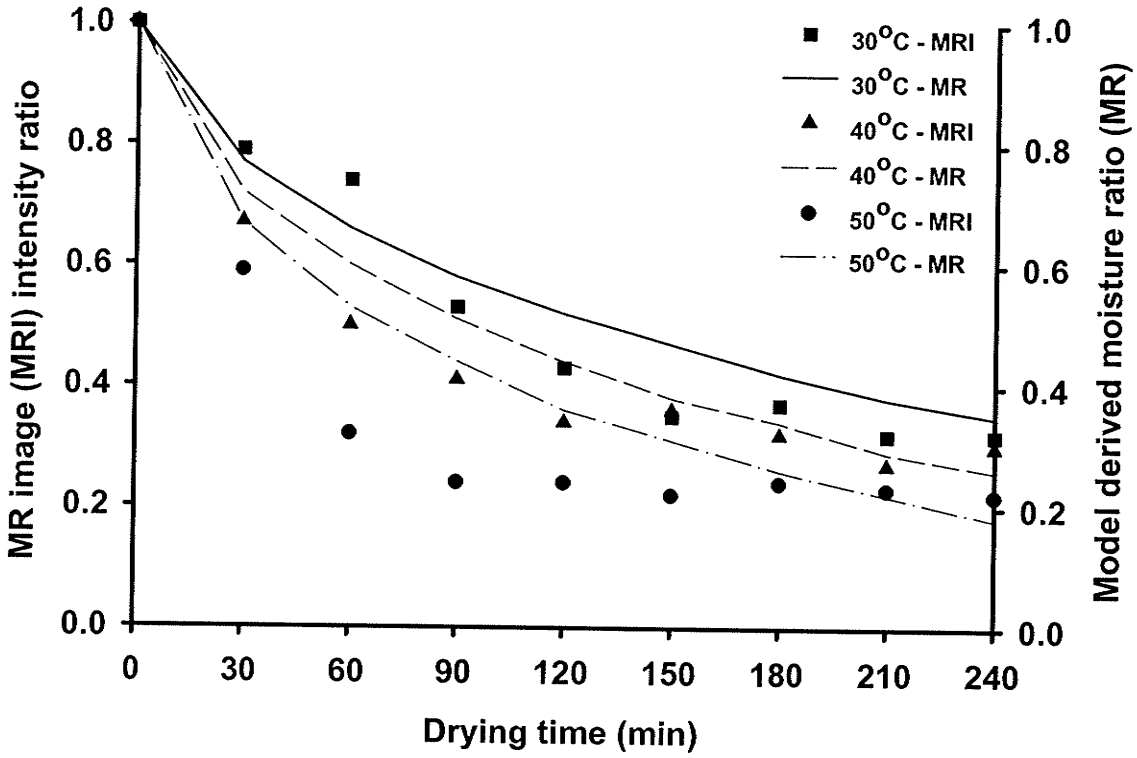

Figure 6.11(b) Trends of magnetic resonance imaging data and predicted drying curves for germ of a mechanically-scarified wheat kernel dried at 30, 40, and 50°C temperatures.

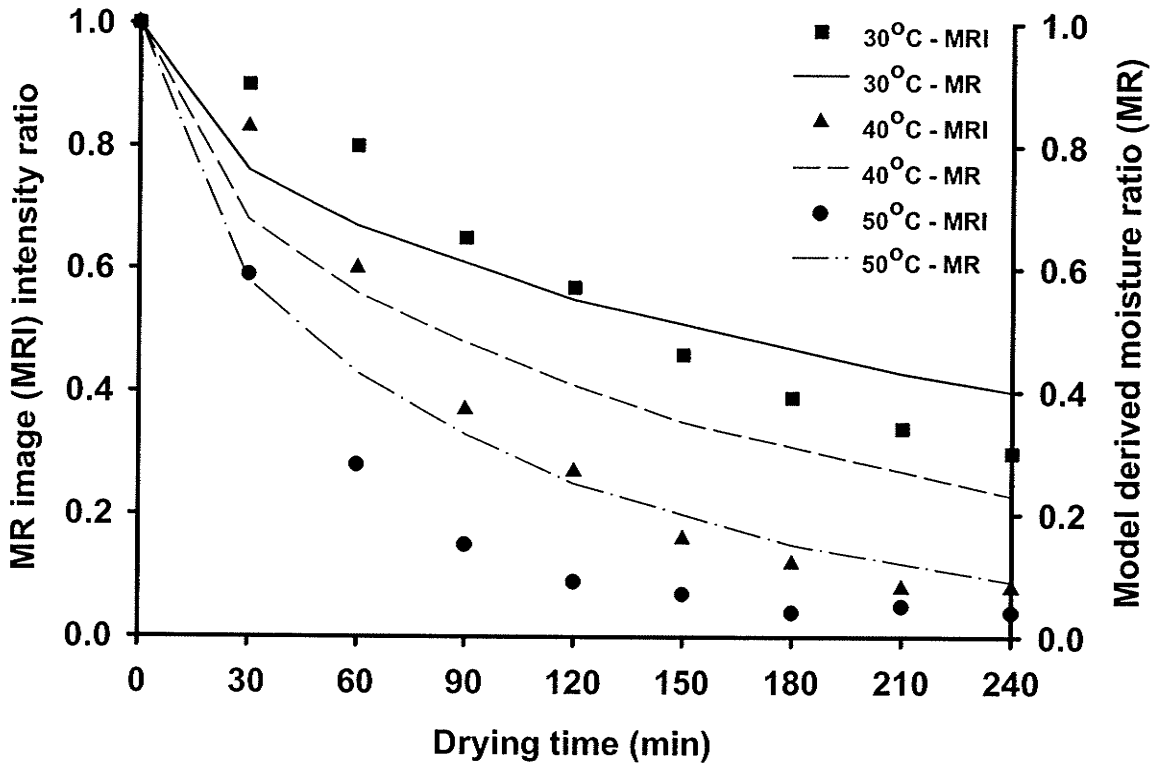

Figure 6.12 Trends of magnetic resonance imaging data and predicted drying curves for endosperm of a germ-removed wheat kernel dried at 30, 40, and 50°C temperatures.

exposed to the ambient air and water comes out through the capillaries through these incised regions. Additionally, cuts increase the surface area through which diffusion occurs; therefore the rate of diffusion (i.e., the amount of moisture crossing a boundary, per unit time) might increase since the surface area is directly proportional to it according to the Fick's law of diffusion. However, differences between the model predicted moisture ratio and the MRI-derived intensity ratio were observed which occurred possibly due to an imperfect value of the physical or material properties used in the model. Ishida et al. (2004) explained that this discrepancy was obtained from the variation in the detectable water in kernels where MRI detects only adsorbed water, whereas the gravimetric method detects the total water. Therefore, sensitivity analysis was performed on each of the physical and material properties (*vide infra*) to determine actual values of these parameters which reduced the differences between the model predicted moisture ratio and the MRI-derived intensity ratio. Comparative model derived images of three kernels are shown in Figs. 6.13-6.15. The model-derived images showed the variation in the internal distribution of water prior-to and during drying. Water was concentrated mainly in the germ region and it remained high, even after 4 h of drying at all three temperatures. Further it can be seen that the moisture content towards the periphery of the wheat kernel decreased more rapidly. Representative images in Figs. 6.16(a-c) show the directions of the moisture movement during drying in three physically different wheat kernels after 1.5 h drying at 40°C. It was clearly visible from these images that in intact and mechanically-scarified kernels, moisture from the endosperm

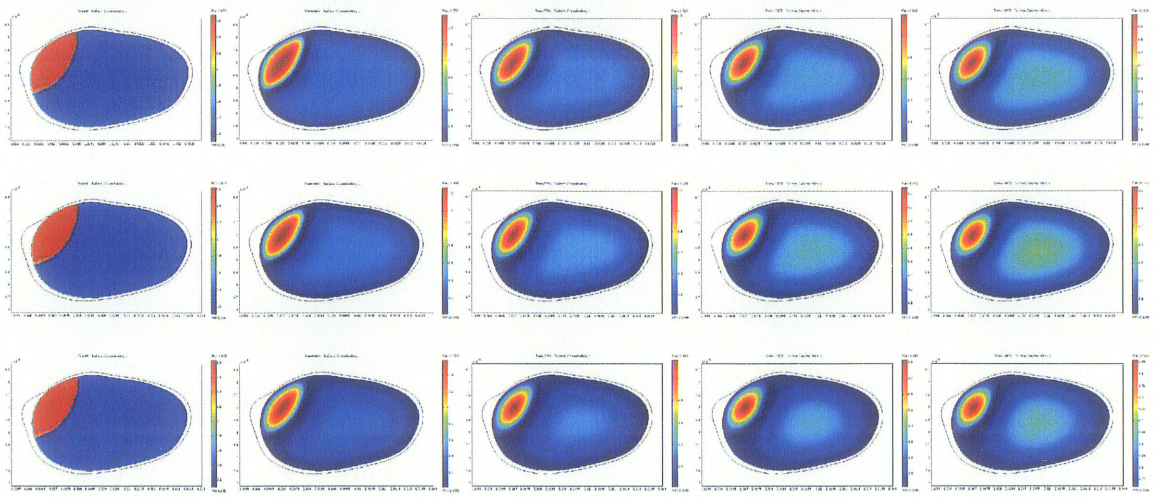

Figure 6.13 Model-derived images of intact wheat kernels dried at three different temperatures. Top row corresponds to 30°C, middle to 40°C, and bottom to 50°C temperature and images in each row are shown at every 1 h from the beginning of drying up to 4 h drying. Solution time: 30°C – 33.53 s; 40°C – 34.14 s; and 50°C – 34.78 s. The colorbar represents the moisture concentration; higher values (more brown color intensity) represent high moisture content and lower values (more blue color) represent low moisture content.

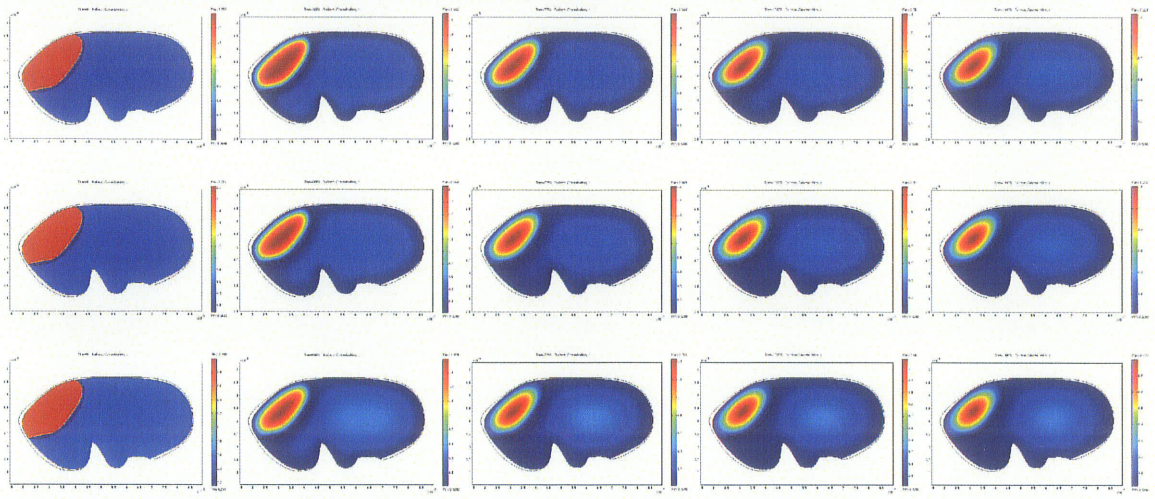

Figure 6.14 Model-derived images of mechanically-scarified wheat kernels dried at three different temperatures. Top row corresponds to 30°C, middle to 40°C, and bottom to 50°C temperature and images in each row are shown at every 1 h from the beginning of drying up to 4 h drying. Solution time: 30°C – 186.34 s; 40°C – 183.58 s; and 50°C – 184.64 s. The colorbar represents the moisture concentration; higher values (more brown color intensity) represent high moisture content and lower values (more blue color) represent low moisture content.

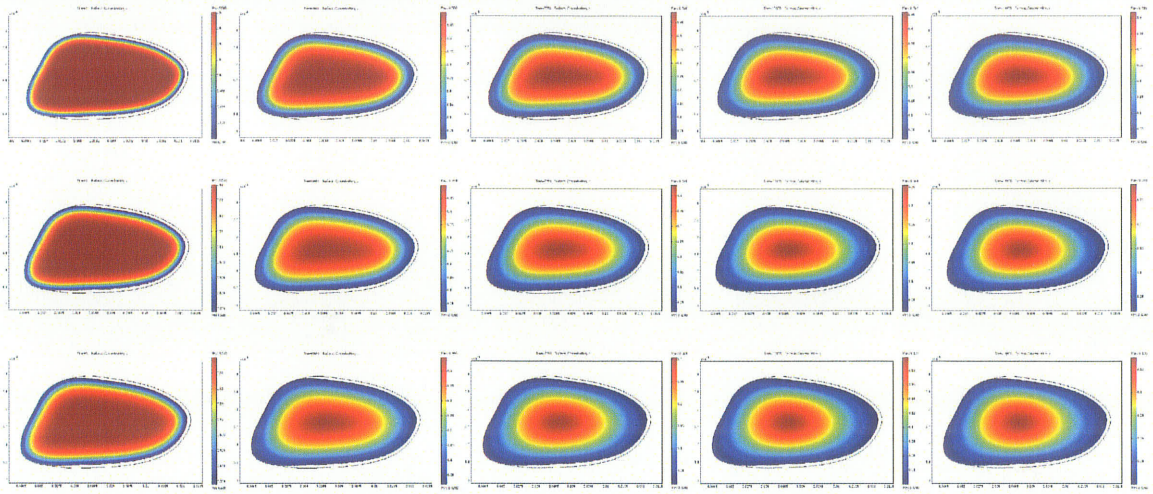

Figure 6.15 Model-derived images of germ-removed wheat kernels dried at three different temperatures. Top row corresponds to 30°C, middle to 40°C, and bottom to 50°C temperature and images in each row are shown at every 1 h from the beginning of drying up to 4 h drying. Solution time: 30°C – 19.14 s; 40°C – 19.38 s; and 50°C – 19.22 s. The colorbar represents the moisture concentration; higher values (more brown color intensity) represent high moisture content and lower values (more blue color) represent low moisture content.

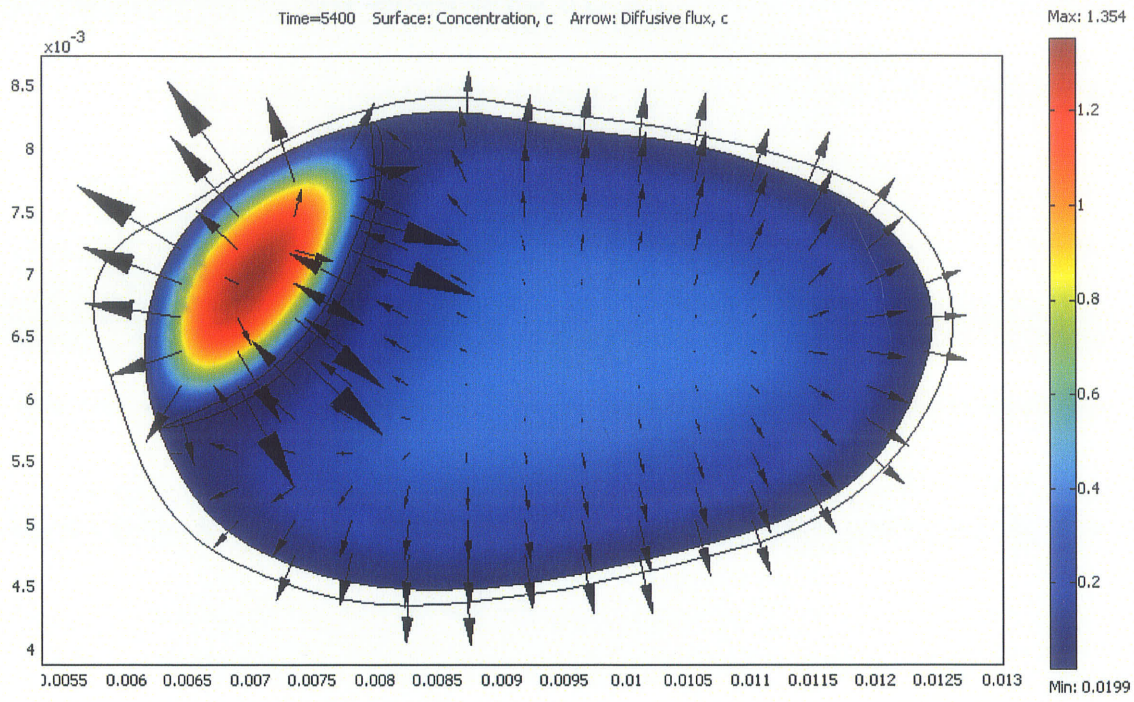

Figure 6.16(a) Direction of moisture movement in an intact wheat kernel during drying at 40°C after 1.5 h drying.

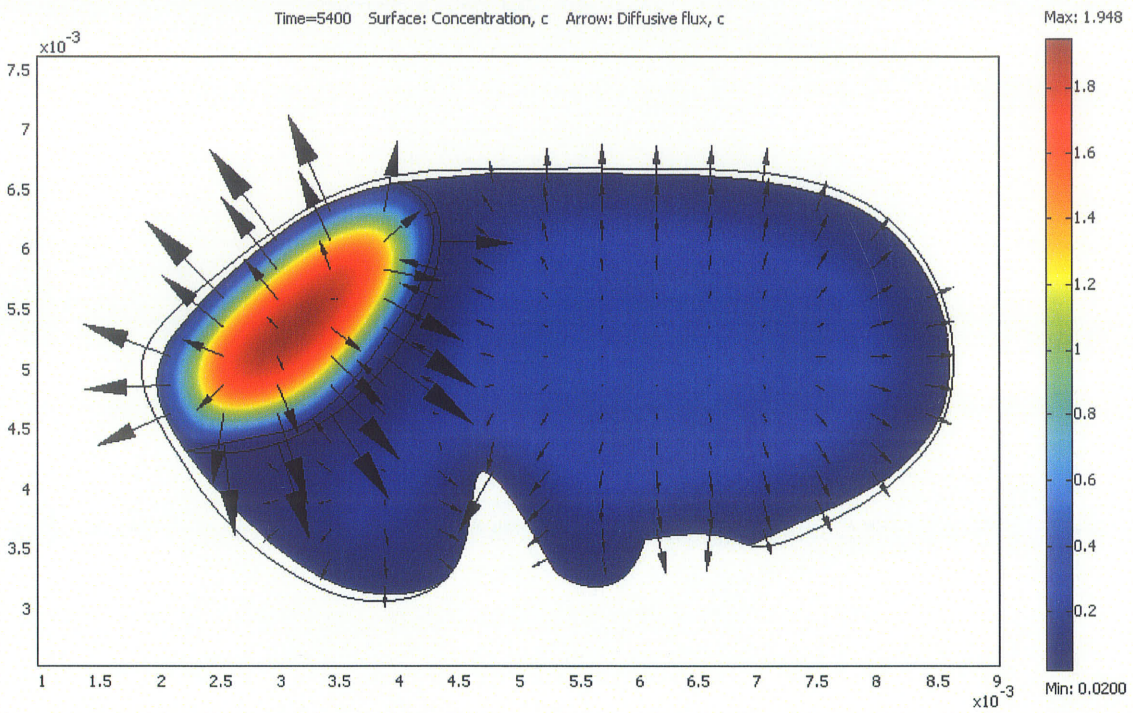

Figure 6.16(b) Direction of moisture movement in a scarified wheat kernel during drying at 40°C after 1.5 h drying.

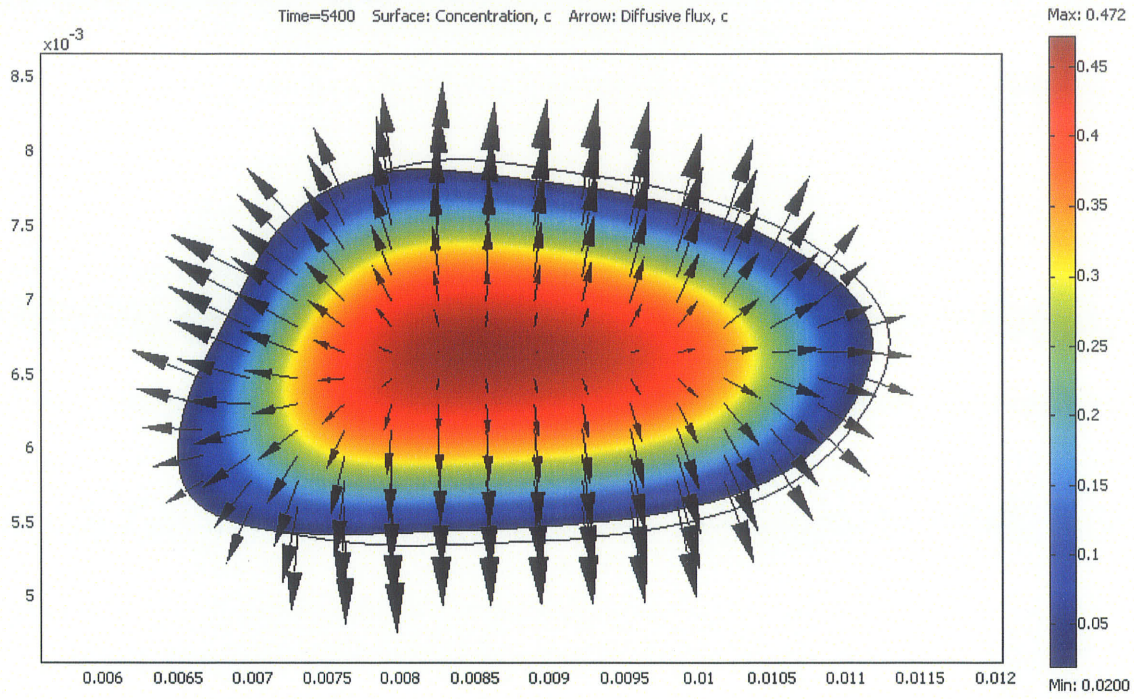

Figure 6.16(c) Direction of moisture movement in a germ-removed wheat kernel during drying at 40°C after 1.5 h drying.

moved less towards the surface and more towards the germ to finally move out from the kernel. Various reasons are associated with the occurrence of water mobility towards the germ and from the endosperm. These include the attachment region of the endosperm and germ, which creates a high moisture gradient for the water to move from the endosperm to the germ. Again, the scutellum portion of the germ acts as an absorption organ, which absorbs water from the endosperm through its highly conductive provascular bundles. Further the seed coat surrounding the germ region is very thin which enhances water movement from the germ to the surroundings. The model also indicated the direction of diffusive flux through the incised parts of the kernel. However, in the case of the germ-removed kernel, moisture moved out uniformly throughout the kernel. These results were directly comparable to the results as have been demonstrated by the MR image predictions (Ghosh et al. 2006a,b). Thus the proposed model considering non-uniform initial moisture distribution has a significant importance for accurate prediction of the internal moisture distribution during wheat drying. The developed mathematical model quantified the MR images, using the actual initial moisture as obtained from the MR images.

Biot numbers for moisture transfer were calculated for the wheat components corresponding to the drying temperatures from the following equation:

$$Bi_{mt} = \frac{h_m L_c}{D} \tag{6.29}$$

where L_c is the characteristic length (i.e., the ratio of volume to surface area which is equal to 4 mm for a prolate ellipsoidal shaped wheat kernel of approximately 6 mm

length and 3 mm diameter); and D is the diffusivity of either endosperm (D_E) or germ (D_G).

The values of Biot numbers for moisture transfer are given in Table 6.8 at different drying temperatures. High Biot number indicates very high internal resistance that controls the moisture transfer inside the wheat structural components. A similar observation of internal control for moisture flux in a wheat kernel was reported by Giner and Mascheroni (2001) in which Bi_{mt} ranged from 50-3000. However, Giner and Mascheroni (2001) modified the definition of Bi_{mt} by considering a constant grain density and adding a conversion factor for a uniform vapor pressure gradient across the grain-air interface. Therefore, they mentioned that their calculation of Bi_{mt} can vary from other definitions of Bi_{mt}, which can be seen from our calculation of Bi_{mt}. Biot numbers displayed an increasing trend with an increase in temperature. Further, Biot numbers for germ were comparatively higher than that for the endosperm which indicated higher moisture gradient development inside the germ than in the endosperm. The model predicted moisture profiles along a hypothetical line chosen in the middle of the three different kinds of wheat kernels during drying at 30°C after 2 h drying are shown in Figs. 6.17 (a-c). The regions of the germ and endosperm of the wheat kernel were clearly visible. The moisture profile in the germ region showed a higher moisture level compared to a plateau-like profile in the endosperm region showing a uniform moisture level. A sudden drop in moisture profile in the attachment region of germ and endosperm showed the lowest moisture region which agreed with the structural observation of Smart and O'Brien (1983) and Jenner and Jones (1990). Therefore, the model could appropriately

Table 6.8 Biot numbers for moisture transfer in wheat components at different drying temperatures.

Drying temperature(°C)	Biot number for moisture transfer	
	Endosperm	Germ
30	6075949.37	13464235.62
40	3300330.03	10438413.36
50	1798561.15	7936507.94

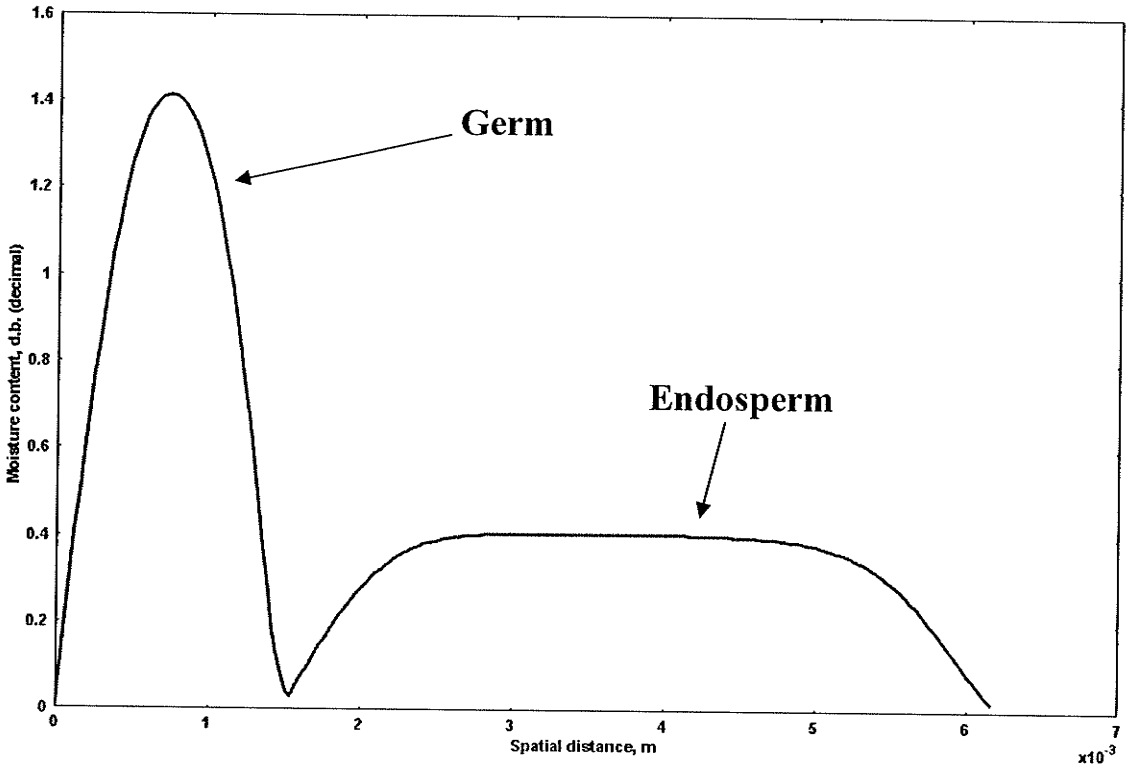

Figure 6.17(a) Model simulated moisture profile of an intact kernel during drying at 30°C after 2 h drying.

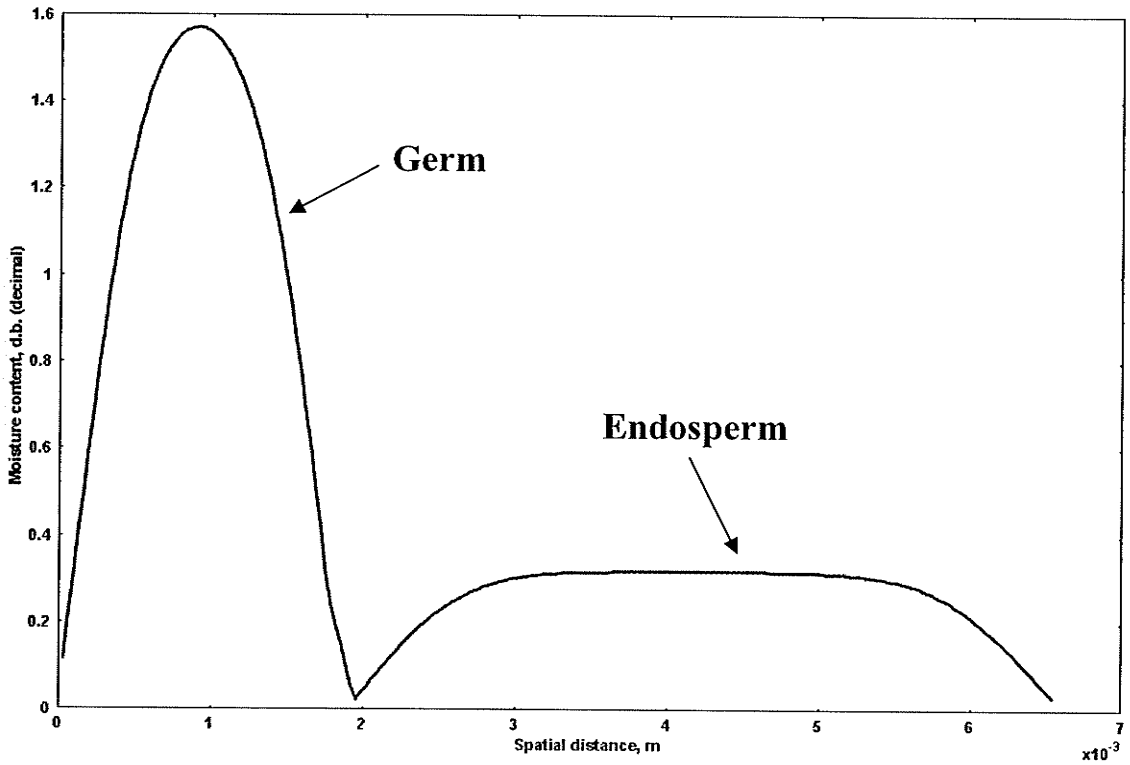

Figure 6.17(b) Model simulated moisture profile of a scarified kernel during drying at 30°C after 2 h drying.

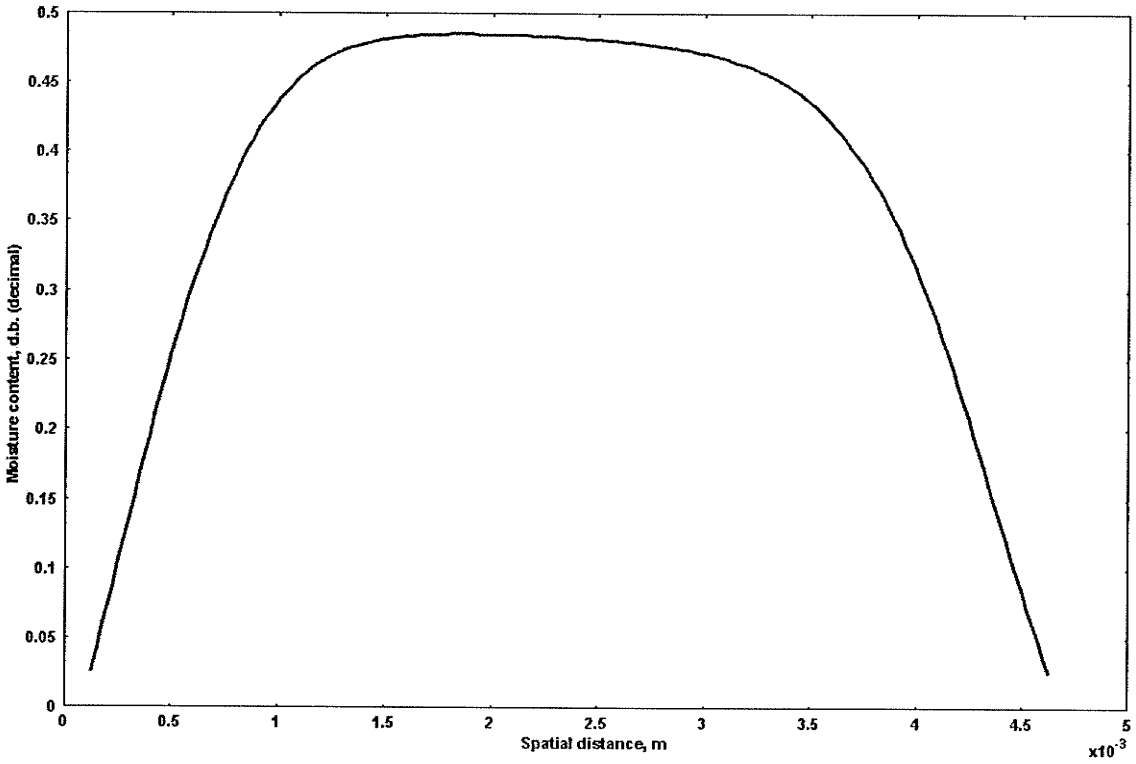

Figure 6.17(c) Model simulated moisture profile of a germ-removed kernel during drying at 30°C after 2 h drying.

predict the anisotropic and non-uniform nature of water migration during the drying of wheat kernels and its dependency on the structural heterogeneities of the kernel as observed in the MRI studies (Ghosh et al. 2006a,b). Giner and Mascheroni (2001) also indicated that the Biot number for mass transfer inside a wheat kernel increased with drying time.

6.3.4 Temperature Distribution

Biot numbers for heat transfer through the wheat components at different drying temperatures were calculated by the following equation:

$$Bi_{ht} = \frac{h_t L_c}{K} \tag{6.30}$$

Values of Biot numbers for heat transfer are plotted in Fig. 6.18 as a function of moisture content in the grain components obtained from our model simulated data for 4 h drying. Since moisture content of the endosperm region is less than that in the germ region, Biot numbers were higher for endosperm region than the germ region. The Biot number is a ratio of internal conduction resistance to the convective resistance to heat transfer at the surface. Wheat is a small kernel for which internal resistance is less than the external resistance and for which heat transfer is controlled by an external resistance without internal temperature gradients (Giner and Mascheroni 2001). The measured Biot numbers for the endosperm region are in the range of 0.24-0.47 which comply with the observation of Giner and Mascheroni (2001) who indicated that external control is valid for $Bi_{ht} \leq 1.5$. Further, the measured Biot numbers for the germ region are in the range of 0.08-0.33 which is of the same order (0.5) as indicated by Giner and Mascheroni (2001) in the absence of gradients. Since the internal resistance was found very small, the

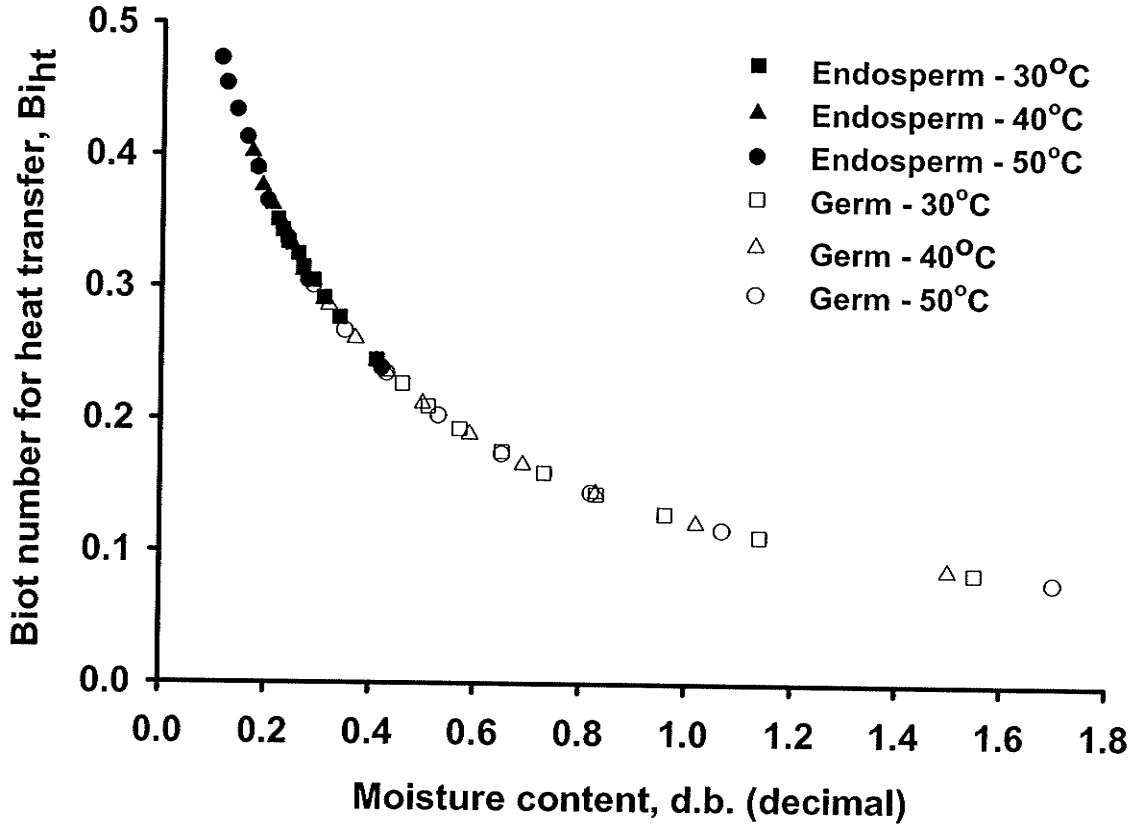

Figure 6.18 Biot number for heat transfer as a function of moisture content of intact wheat kernel components for three drying temperatures for 4 h drying.

temperature within the wheat kernels was essentially uniform at any given time during drying. This phenomenon was further visualized from the temperature distribution pattern in the wheat kernels from the model simulation. Figure 6.19 illustrates the model predicted temperature distributions at the center and on the surface of an intact wheat kernel during drying at 50°C. The wheat temperature increased rapidly during early stages of drying. Further, the surface of the kernel reaches the maximum temperature at about 12 min before the center reaches the maximum at 15 min. However the largest temperature gradient was observed at the first 5 min of drying. The effect of temperature gradient is significant at the early stages of drying because it creates thermal stress causing stress-cracks. The temperature distribution profile obtained from our model was in close agreement with the model of Jia et al. (2000) for the same drying conditions. Similar results were reported by Haghighi et al. (1990) and Ranjan et al. (2001) for barley drying (initial moisture content of 27% d.b., drying temperature of 50°C and an initial grain temperature of 27°C). However, Sokhansanj and Gustafson (1980) indicated a rapid onset of a strong temperature gradient with grain temperatures larger than 60°C during the first 2 min of drying at 50°C in a corn kernel. These results clearly indicate comparatively high stress-crack susceptibility of corn kernels with respect to wheat kernels. Our model simulated temperatures slightly deviated from the predictions by Jia et al. (2000) because temperature prediction in their model is strongly dependent on the values of h_t and h_m (Miketinac et al. 1992). The occurrence of faster heat transfer was further examined by calculating the Lewis number which gives the ratio of thermal to moisture diffusivity by the following relationship:

$$Le = \frac{K}{\rho_g C_p D} \tag{6.31}$$

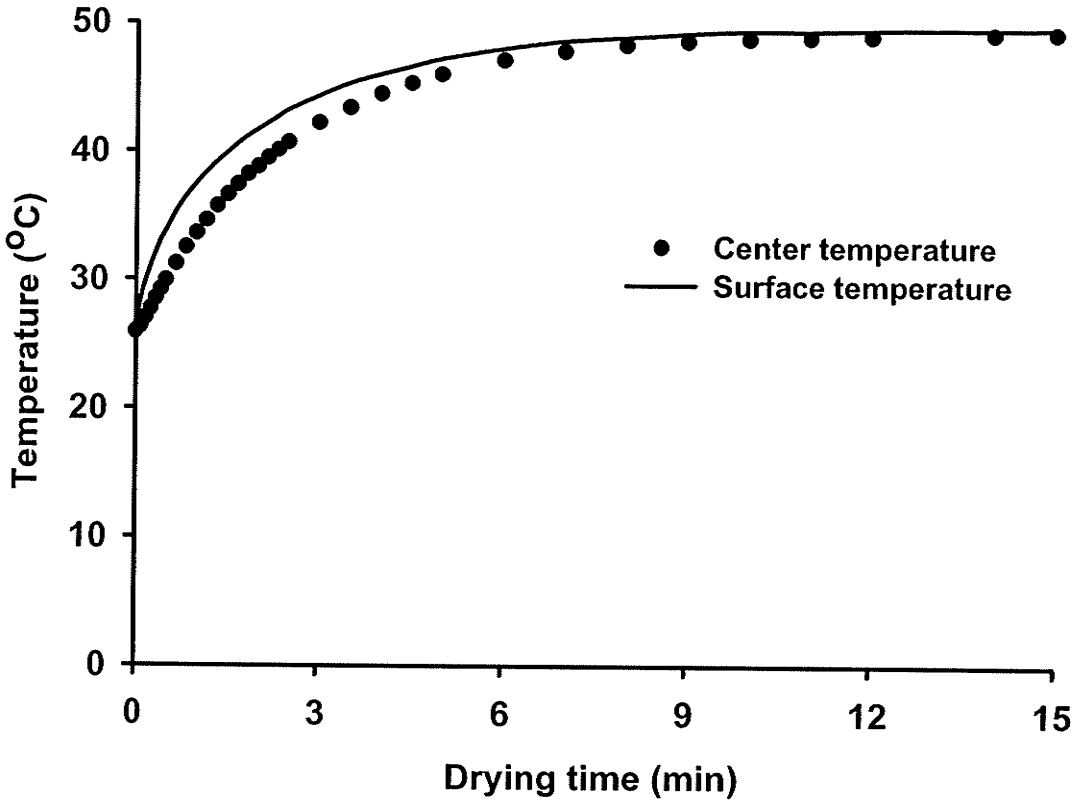

Figure 6.19 Prediction of temperature distribution in wheat at the center and on the surface during drying at 50°C for an ambient temperature of 25°C, initial moisture content of 37% w.b.

where D is the diffusivity of either endosperm (D_E) or germ (D_G). Calculated values of Lewis numbers are plotted in Fig. 6.20 as a function of simulated moisture content for endosperm and germ of intact wheat kernels at three drying temperatures for 4 h drying. It was observed that the rate of heat transfer was very high compared to that of mass transfer in both endosperm and germ. Although high, the decreasing trend of Lewis number in the endosperm region was evidenced by Giner and Mascheroni (2001) in the case of a whole wheat kernel. However, the trend has an opposite pattern particularly in the germ region which indicated that higher moisture concentration plays a significant role in transferring the heat. This result matched the actual slow moisture transfer phenomena from the germ as evident from the MR images. Overall the high values of Lewis number indicated that heat transfer was immediate whereas moisture transfer was slow. In our case, thermal diffusivity values varied between 10^{-7} and 10^{-9} m^2 s^{-1} and the moisture diffusivity values varied between 10^{-11} and 10^{-12} m^2 s^{-1} for both endosperm and germ. A similar range was mentioned by Giner and Mascheroni (2001). These observations indicated an isothermal drying phenomenon in the wheat kernels.

6.3.5 Activation Energy – Effect of Temperature

The effect of temperature on the moisture transfer during drying of individual grain components was further investigated by measuring the activation energy required in the moisture removal process for the three physically altered wheat kernels. The analysis was performed following the procedures given by Ishida et al. (2004). Semi-logarithmic plots of the model predicted moisture ratio of wheat kernels with their major components

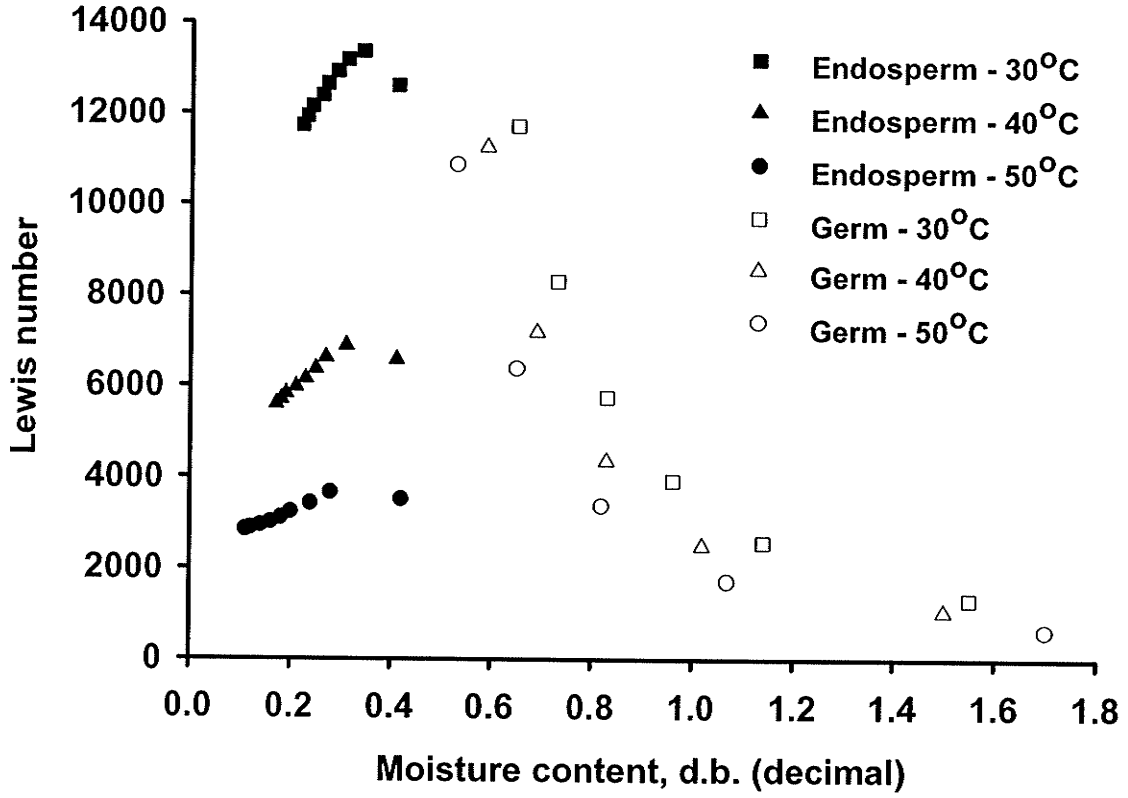

Figure 6.20 Lewis number as a function of moisture content of intact wheat kernel components for three drying temperatures for 4 h drying.

(germ and endosperm) at various temperatures versus drying time are shown in Figs. 6.21 (a-c). The plots do not show a general mono-exponential decay. This indicates that a single process cannot completely describe grain moisture removal. Similar results have been reported for rice (Ishida et al. 2004). It should be noted that in the experiments of Ishida et al. (2004) the kernels were not exposed to flowing hot air. The rate of moisture loss increased in grain components with increasing drying temperature (from 30°C to 50°C).

The effect of temperature on the drying curves of individual grain components was analyzed by normalizing the semi-logarithmic plots of intact, mechanically scarified and the germ-removed wheat kernels. These curves were normalized with respect to 30°C at each drying time after multiplying with a scale factor (k). A least square method of third-order polynomial regression was used for analysis (Table 6.9). Representative normalized drying curves for an intact kernel are shown in Fig. 6.22 in which the resulting curves coincided fairly well indicating no drastic change in the drying mechanism for the range of temperature being studied. Semi-logarithmic plots of the changing scale factors with the inverse temperature (K^{-1}) produced an Arrhenius type relationship of the following linearized form to determine the activation energy of the water removal process inside the grain components during drying:

$$\ln k = -\frac{E_a}{R}\left[\frac{1}{T}\right] + \ln k_o \qquad (6.32)$$

where, a plot of ln k (k being the scale factor) versus 1/T (K^{-1}) produces a straight line with a slope of $-E_a/R$ in which E_a is the activation energy (kJ mol^{-1}); R is the Universal gas constant (8.314×10^{-3} kJ mol^{-1} K^{-1}); and k_o is a constant. Figure 6.23 shows a plot of

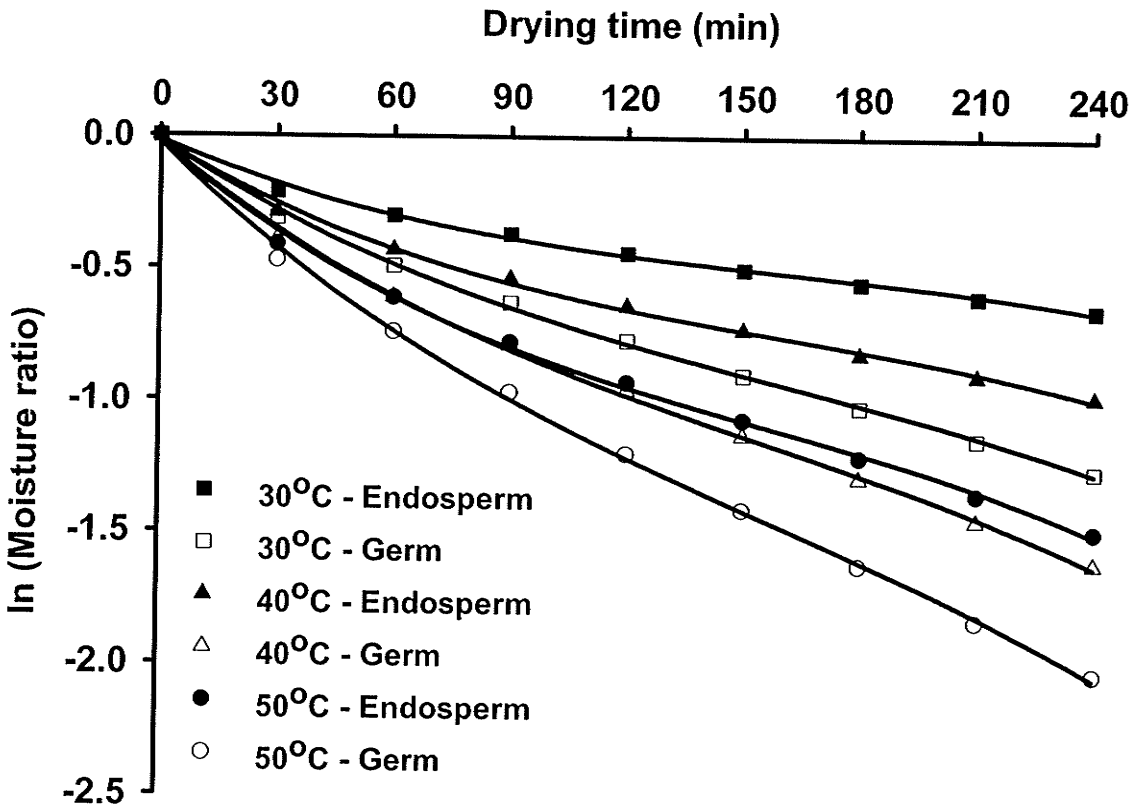

Figure 6.21(a) Drying curves of the intact kernel components at different temperatures.

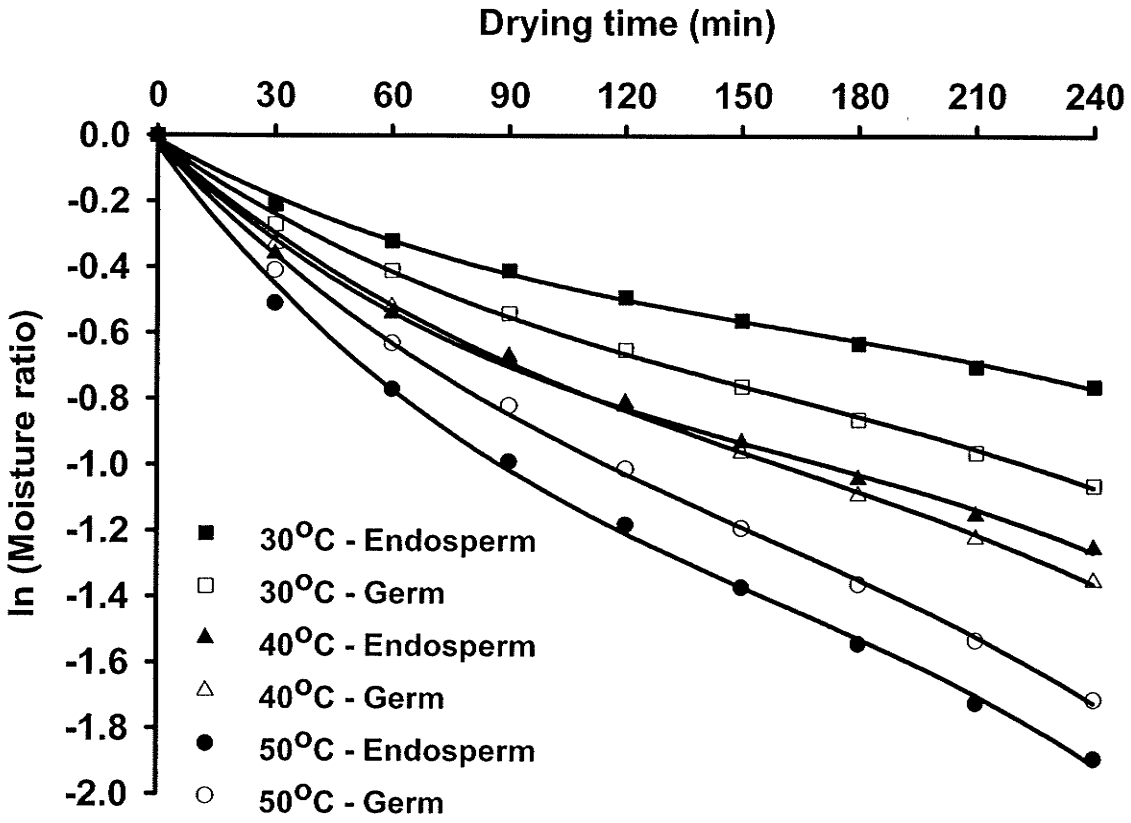

Figure 6.21(b) Drying curves of the mechanically scarified kernel components at different temperatures.

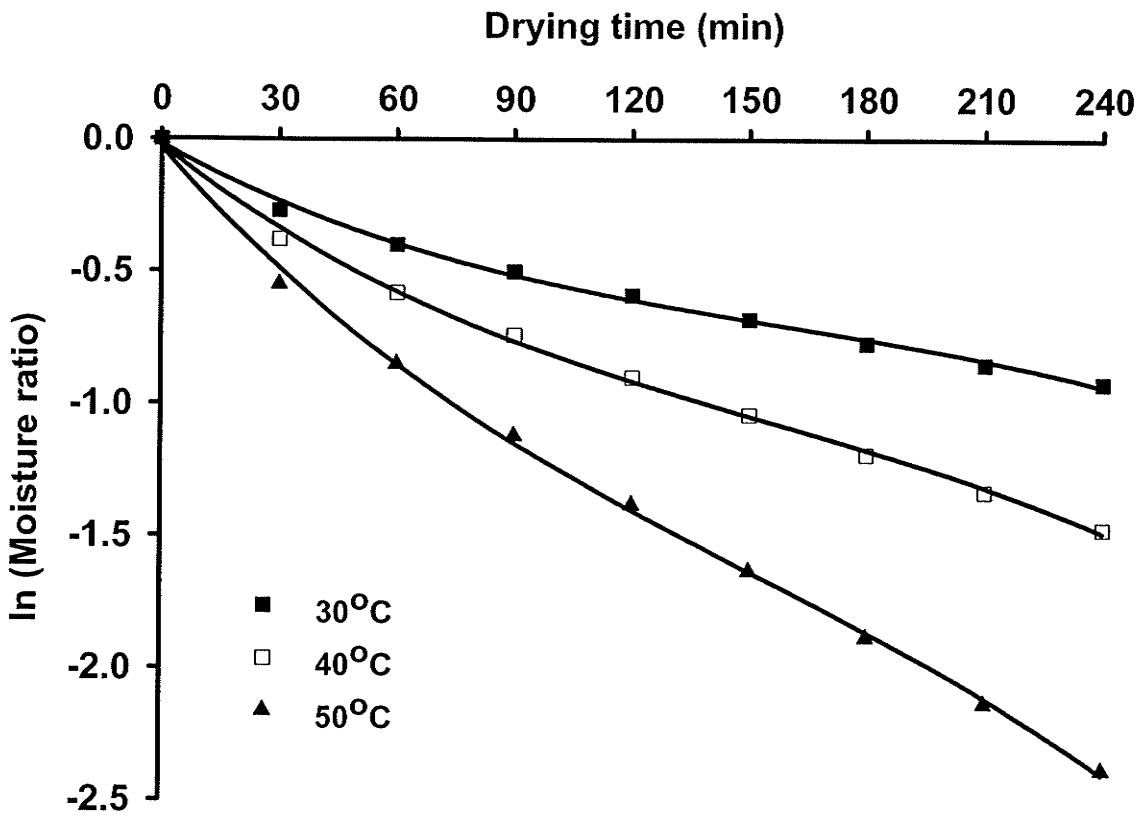

Figure 6.21(c) Drying curves of the germ-removed kernel components at different temperatures.

Table 6.9 Scale factors (k) used to normalize all the drying curves with respect to 30°C.

Temperature (°C)	Intact wheat				Mechanically-scarified wheat				Germ-removed wheat	
	Endosperm		Germ		Endosperm		Germ			
	Model derived	MR imaging	Model derived	MR imaging	Model derived	MR imaging	Model derived	MR imaging	Model derived	MR imaging
30	1	1	1	1	1	1	1	1	1	1
40	0.695	0.235	0.828	0.138	0.742	1.286	0.838	0.486	0.629	0.570
50	0.468	0.072	0.626	0.098	0.543	0.388	0.700	0.309	0.425	0.170

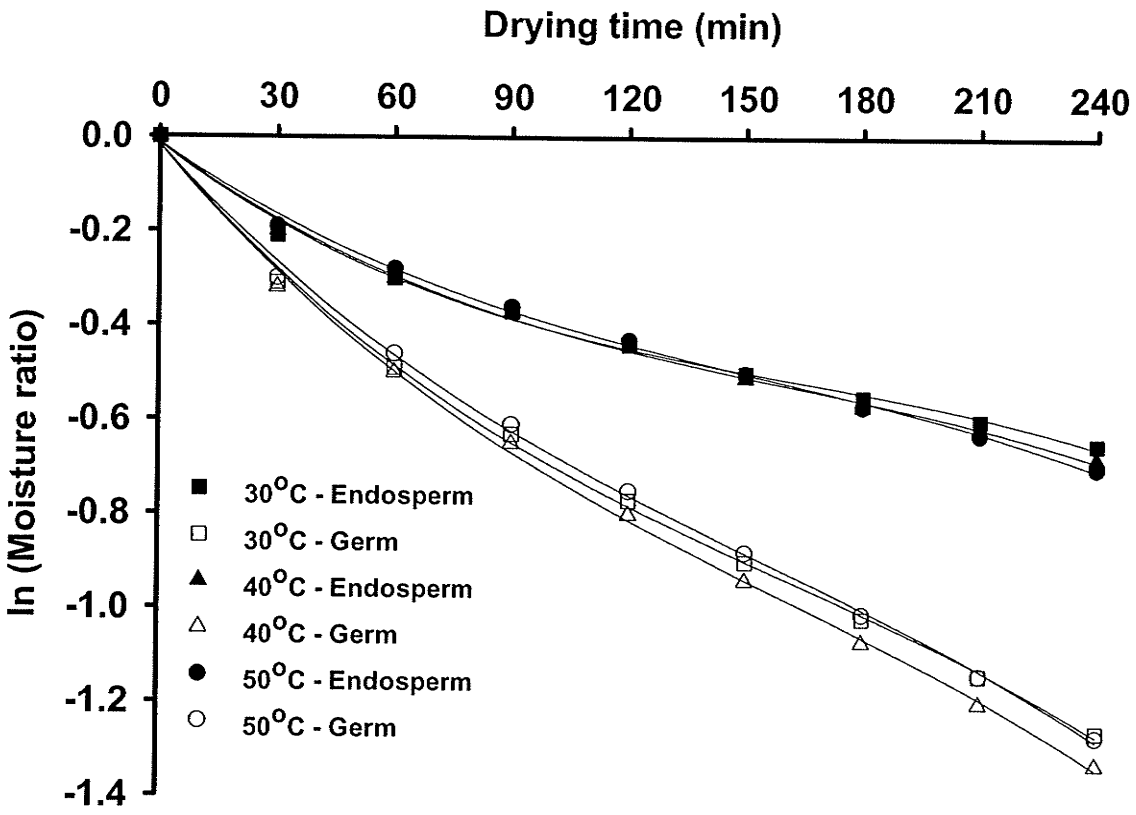

Figure 6.22 Normalized drying curves of intact kernel at different temperatures; normalization was done with respect to 30°C.

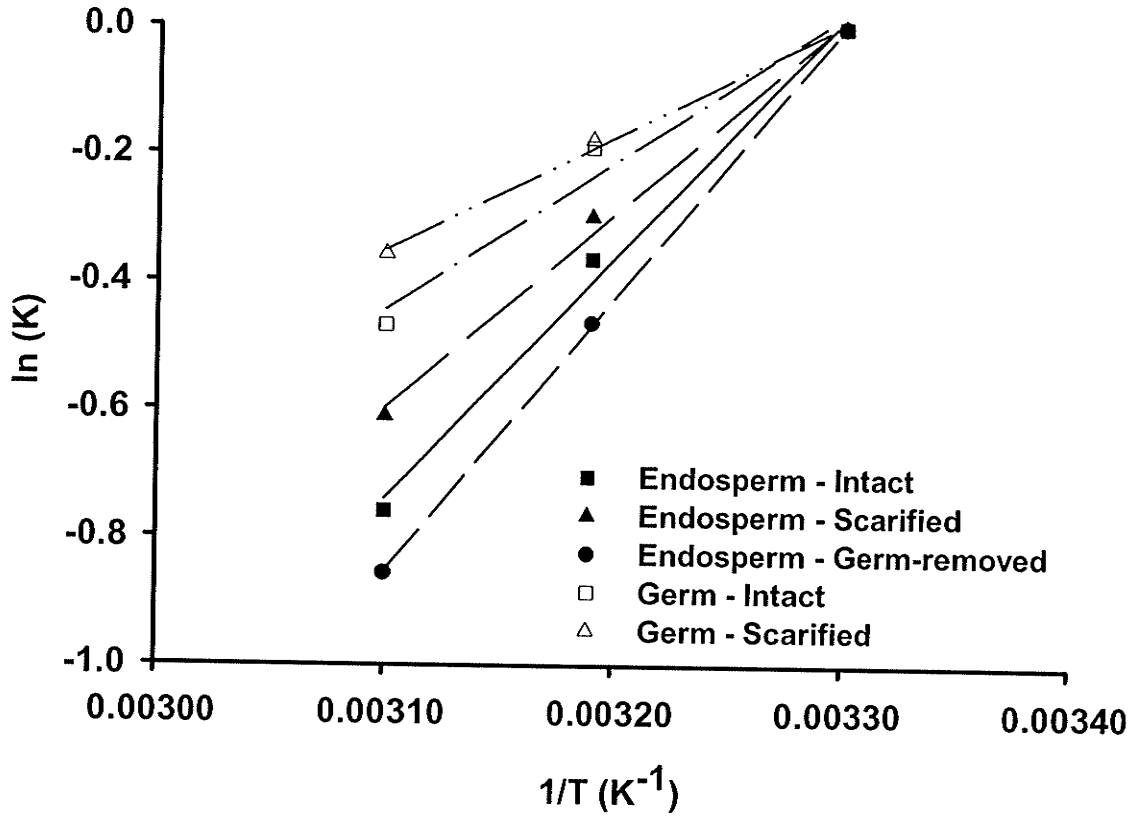

Figure 6.23 Temperature dependency of the scale factor (k) in case of model predicted data; k was used to normalize the curves with respect to 30°C.

the natural log of the scale factors of different kinds of wheat kernels along with their structural components for drying at different temperatures versus the inverse of the temperature in K^{-1}. A strong correlation of the water removal process to the drying temperature was observed in the case of the endosperm of an intact kernel, a mechanically scarified kernel and a germ-removed kernel. For the endosperm the activation energy of the water removal process was the lowest in a mechanically scarified kernel (E_a = 24.8 kJ mol^{-1}) compared to an intact kernel (E_a = 30.9 kJ mol^{-1}) and a germ-removed kernel (E_a = 34.8 kJ mol^{-1}), respectively. In case of the scarified kernel, the pericarp started offering a water resistance due to closely adhered thick-walled cells after initial stages of drying. Therefore, the moisture removal from this part became slower. Activation energy of the water removal process in the germ was higher in an intact kernel (E_a = 19.0 kJ mol^{-1}) than that in a scarified kernel (E_a = 14.5 kJ mol^{-1}). Since water was released relatively faster from the scarified regions of the endosperm-pericarp boundary at the initial stages of drying, less "free" water was available in the germ in the case of the scarified kernels. However, this was not the case in an intact kernel since more water was available in the germ. This might be the reason why the values of activation energy of water removal process for each components of a scarified kernel were less than that of an intact kernel. Becker and Sallans (1955) also indicated that physical changes of a wheat kernel can result in decrease in energy of activation for the water removal process. Watson and Bhargava (1974) reported an overall activation energy change for the water removal process of 18 kJ·mol^{-1} during the drying of an intact wheat kernel (37-80% relative humidity) at a temperature range of 27 to 49°C. Prediction of activation energy of the water removal process during drying based on the simulated moisture loss data was

compared to that based on MR image analysis. Figure 6.24 shows a plot of the natural log of the scale factors from the MR image analysis of different kinds of wheat kernels along with their structural components for drying at different temperatures versus the inverse of the temperature in K^{-1}. The values of activation energy for water removal process from these plots were somewhat higher as calculated by Ghosh et al. (2006c) than the values obtained from the model calculated values but almost a similar pattern of change in the activation energy for moisture removal is evident from Fig. 6.24. Variability in MRI-predicted data compared to the model prediction occurred apparently because of biological variability and selection of accurate model parameters. Moreover, osmotic processes were ignored in the model development.

6.3.6 Sensitivity Analysis

The relative importance of each model parameter for simulating moisture movement during wheat drying was determined by changing the parametric values by ±25% from its initial value. The effect of these changes were calculated on the basis of simulated moisture concentration values and compared with the data obtained from Jayas and Sokhansanj (1986) and Sinico et al. (1995) with some fixed parameters: drying air temperature 35°C with relative humidity of 35%, initial overall grain moisture content 21%, equilibrium moisture content 10%, and ambient temperature 25°C. Sensitivity of the parameters was also evaluated comparing the simulated moisture contents with moisture predictions from the MRI images. Five criteria were selected for comparison: mean relative percentage residual (MRPR), bias factor (BF), mean absolute relative

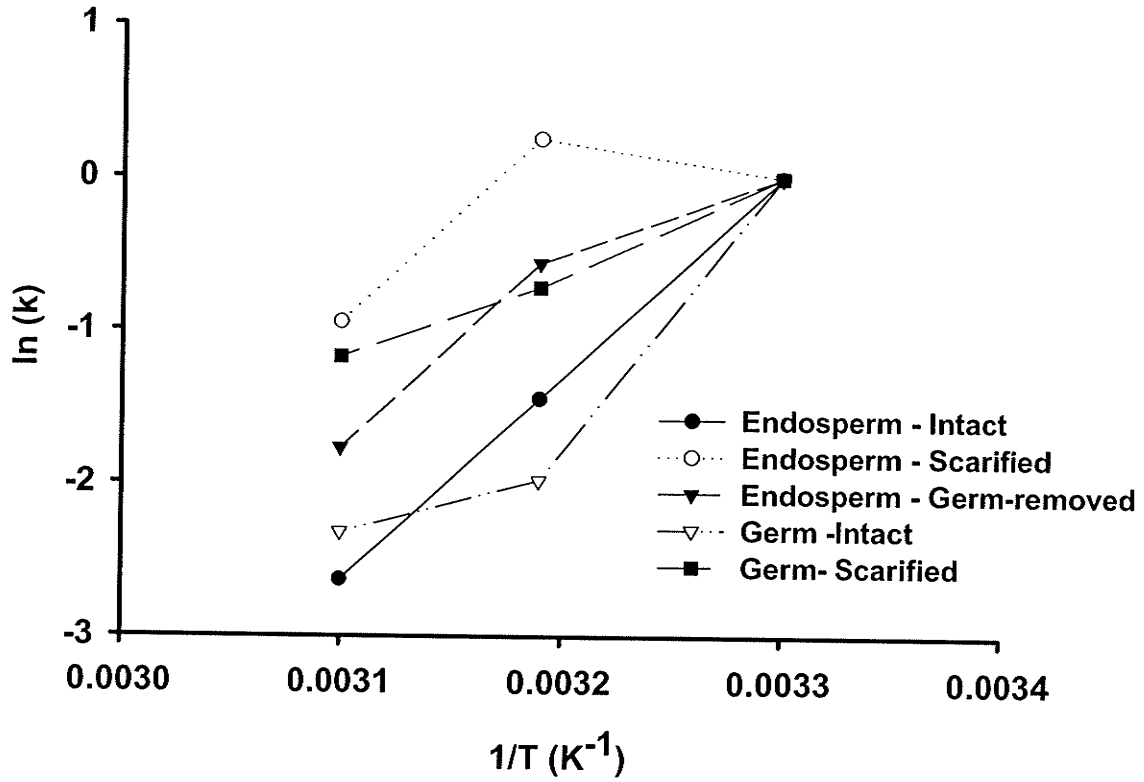

Figure 6.24 Temperature dependency of the scale factor (k) for magnetic resonance image data; k was used to normalize the curves with respect to 30°C.

residual (MARR), accuracy factor (AF), and root mean square residual (RMSR) (Jeyamkondan et al., 2001) (Eqs. 6.33-6.37).

$$\text{MRPR} = \frac{1}{N}\sum\frac{O-P}{O}\times 100 \tag{6.33}$$

$$\text{BF} = 10^{\sum \log(P/O)/N} \tag{6.34}$$

$$\text{MARR} = \frac{1}{N}\sum\left|\frac{O-P}{O}\right|\times 100 \tag{6.35}$$

$$\text{AF} = 10^{\sum |\log(P/O)|/N} \tag{6.36}$$

$$\text{RMSR} = \sqrt{\frac{\sum (O-P)^2}{N}} \tag{6.37}$$

where N is the number of observations; O is the observed value from either Jayas and Sokhansanj (1986) or Sinico et al. (1995); and P is the model predicted value after changing the parameters.

A positive MRPR value indicates under-prediction whereas negative value indicates over-prediction; BF over 1 indicates over-estimation whereas less than 1 indicates under-estimation; MARR indicates the deviation from the observed values; an AF of 1.5 indicates 50% deviation of the predicted value from the observed values. Table 6.10 shows the sensitivity of the model parameters on the grain moisture movement during drying. The mass average moisture content was insensitive to all other model parameters except the water diffusion coefficients of germ and endosperm. Insensitivity to the parameters associated with the heat transfer process is acceptable since the observation of Lewis number indicated strong internal control of moisture transfer and strong external

Table 6.10 Sensitivity of the model parameters to the closeness of moisture content values obtained from two thin-layer drying equations for wheat drying at 35°C, as determined by five criteria for sensitivity analysis.

Parameter	Change (%)	Jayas and Sokhansanj (1986)					Sinico et al. (1997)				
		MRPR	BF	MARR	AF	RMSR	MRPR	BF	MARR	AF	RMSR
Original	0	-5.41	1.05	7.15	1.07	1.06	5.79	0.94	5.79	1.06	0.93
M_{oLayer}	1/4 (M_{oE})	-5.42	1.05	7.24	1.07	1.07	5.78	0.94	5.78	1.06	0.92
M_{oLayer}	3/4 (M_{oE})	-5.44	1.05	7.12	1.07	1.06	5.75	0.94	5.75	1.06	0.92
h_l	+25	unchanged from the original					unchanged from the original				
h_l	-25										
h_m	+25	-5.42	1.05	7.17	1.07	1.06	5.78	0.94	5.78	1.06	0.92
h_m	-25	-5.44	1.05	7.16	1.07	1.06	5.76	0.94	5.76	1.06	0.92
K	+25	unchanged from the original					unchanged from the original				
K	-25										
C_g	+25										
C_g	-25										
ρ_g	+25										
ρ_g	-25										
D_G	+25	-3.35	1.03	5.72	1.06	0.85	7.58	0.92	7.58	1.08	1.21
D_G	-25	-8.01	1.08	9.38	1.09	1.38	3.54	0.96	3.54	1.04	0.58
D_E	+25	-4.26	1.04	6.35	1.06	0.94	6.79	0.93	6.79	1.07	1.09
D_E	-25	-6.86	1.07	8.33	1.08	1.23	4.53	0.95	4.53	1.05	0.73

control for heat transfer. Since our model prediction lies in between the predictions of Sinico et al. (1995) and Jayas and Sokhansanj (1986) 25% increase in the diffusivity values for both germ and endosperm produced our model prediction closer to Jayas and Sokhansanj (1986) whereas a 25% decrease in the diffusivity values for both germ and endosperm made the model prediction closer to Sinico et al (1995). This suggests that water diffusivity is an important factor for accurate prediction of moisture distribution during grain drying. Similar results have been reported by Sokhansanj and Gustafson (1980) for corn and rice drying. Further, it demonstrates that the finite element method is the best numerical solution tool which not only handles the complicated geometry and boundary conditions but also helps in obtaining accurate estimation of model parameters. The relative insensitivity to all model parameters except the water diffusion coefficients of germ and endosperm to the MR image calibrated mass average moisture content was also evident from the preliminary analysis. Further a general trend of reducing the diffusivity of germ and increasing the diffusivity of endosperm indicated a close match between the model prediction and MR image prediction. According to preliminary experiments, we examined the range of germ diffusivity by changing the original value from +25% to -50% and the range of endosperm diffusivity by changing the original to up to +200%. Tables 6.11 (a-c) shows the sensitivity of the model parameters for the MR image predicted moisture contents for three different conditions in wheat kernels (intact, mechanically-scarified and germ-removed) at three different drying temperatures. Based on the lowest values of all five criteria for sensitivity analysis, the most accurate diffusivity values for the endosperm and germ were detected which is given in Table 6.12. Thus moisture diffusivity of the endosperm was about 100% higher than the chosen

Table 6.11(a) Sensitivity of the model parameters to the closeness of moisture content values obtained from magnetic resonance imaging experiments for intact wheat kernel drying at different temperatures, as determined by five criteria for sensitivity analysis.

Drying Temperature (°C) ⟶			30					40					50				
Grain	Parameter	Change (%)	MRPR	BF	MARR	AF	RMSR	MRPR	BF	MARR	AF	RMSR	MRPR	BF	MARR	AF	RMSR
Endosperm	Original	0	-27.61	1.20	36.83	1.33	7.01	-157.50	2.03	160.53	2.10	10.01	-355.46	3.11	355.58	3.12	9.29
	D_E	+25	-20.35	1.14	31.67	1.29	6.32	-132.08	1.88	136.89	1.97	8.55	-284.57	2.76	285.27	2.78	7.49
		+100	-3.42	1.00	22.65	1.24	5.82	-76.43	1.52	85.65	1.68	5.86	-148.74	1.99	153.72	2.10	4.17
		+150	5.35	0.92	19.95	1.23	6.29	-50.26	1.33	63.51	1.55	5.17	-96.14	1.65	105.02	1.82	3.37
		+200	12.80	0.85	19.29	1.24	7.03	-29.40	1.18	46.69	1.44	5.11	-62.07	1.40	75.26	1.63	3.43
	D_G	+25	-27.64	1.20	36.86	1.33	7.01	-157.53	2.03	160.50	2.09	10.01	-355.60	3.11	355.72	3.12	9.30
		-25	-27.60	1.20	36.90	1.33	7.03	-157.48	2.03	160.55	2.10	10.02	-355.46	3.11	355.58	3.12	9.29
		-50	-27.56	1.20	36.89	1.33	7.03	-157.48	2.03	160.55	2.10	10.02	-355.43	3.11	355.55	3.12	9.29
Germ	Original	0	22.36	0.77	22.36	1.29	23.31	5.20	0.93	13.92	1.17	9.62	10.63	0.85	22.68	1.32	15.19
	D_E	+25	23.26	0.76	23.26	1.31	24.14	6.05	0.92	14.05	1.17	9.70	11.11	0.84	22.80	1.32	15.30
		+100	24.59	0.75	24.59	1.33	25.40	7.38	0.91	14.28	1.17	9.90	12.02	0.84	22.62	1.32	15.37
		+150	24.97	0.75	24.97	1.34	25.76	7.74	0.91	14.51	1.18	10.00	12.49	0.83	22.54	1.32	15.40
		+200	25.23	0.74	25.23	1.35	26.04	8.10	0.90	14.45	1.18	10.05	12.58	0.83	22.54	1.32	15.42
	D_G	+25	29.38	0.70	29.38	1.43	29.42	16.88	0.81	18.62	1.26	13.31	23.61	0.70	25.85	1.45	19.08
		-25	13.34	0.87	13.34	1.16	16.14	-9.56	1.08	14.48	1.14	10.87	-6.82	1.04	21.63	1.23	14.89
		-50	1.39	0.98	6.65	1.07	10.59	-30.20	1.29	30.47	1.29	20.05	-31.11	1.29	31.36	1.29	23.27

Table 6.11(b) Sensitivity of the model parameters to the closeness of moisture content values obtained from magnetic resonance imaging experiments for scarified wheat kernel drying at different temperatures, as determined by five criteria for sensitivity analysis.

Drying Temperature (°C) ⟶			30					40					50				
Grain	Parameter	Change (%)	MRPR	BF	MARR	AF	RMSR	MRPR	BF	MARR	AF	RMSR	MRPR	BF	MARR	AF	RMSR
Endosperm	Original	0	-19.20	1.20	36.83	1.33	7.01	-157.50	2.03	160.53	2.10	10.01	-355.46	3.11	355.58	3.12	9.29
	D_E	+25	-11.05	1.14	31.67	1.29	6.32	-132.08	1.88	136.89	1.97	8.55	-284.57	2.76	285.27	2.78	7.49
		+100	6.99	1.00	22.65	1.24	5.82	-76.43	1.52	85.65	1.68	5.86	-148.74	1.99	153.72	2.10	4.17
		+150	15.95	0.92	19.95	1.23	6.29	-50.26	1.33	63.51	1.55	5.17	-96.14	1.65	105.02	1.82	3.37
		+200	23.22	0.85	19.29	1.24	7.03	-29.40	1.18	46.69	1.44	5.11	-62.07	1.40	75.26	1.63	3.43
	D_G	+25	-19.27	1.20	36.86	1.33	7.01	-157.53	2.03	160.50	2.09	10.01	-355.60	3.11	355.72	3.12	9.30
		-25	-19.21	1.20	36.90	1.33	7.03	-157.48	2.03	160.55	2.10	10.02	-355.46	3.11	355.58	3.12	9.29
		-50	19.13	1.20	36.89	1.33	7.03	-157.48	2.03	160.55	2.10	10.02	-355.43	3.11	355.55	3.12	9.29
Germ	Original	0	-6.03	0.77	22.36	1.29	23.31	5.20	0.93	13.92	1.17	9.62	10.63	0.85	22.68	1.32	15.19
	D_E	+25	-4.91	0.76	23.26	1.31	24.14	6.05	0.92	14.05	1.17	9.70	11.11	0.84	22.80	1.32	15.30
		+100	-3.13	0.75	24.59	1.33	25.40	7.38	0.91	14.28	1.17	9.90	12.02	0.84	22.62	1.32	15.37
		+150	-2.55	0.75	24.97	1.34	25.76	7.74	0.91	14.51	1.18	10.00	12.49	0.83	22.54	1.32	15.40
		+200	-2.10	0.74	25.23	1.35	26.04	8.10	0.90	14.45	1.18	10.05	12.58	0.83	22.54	1.32	15.42
	D_G	+25	3.21	0.70	29.38	1.43	29.42	16.88	0.81	18.62	1.26	13.31	23.61	0.70	25.85	1.45	19.08
		-25	-17.30	0.87	13.34	1.16	16.14	-9.56	1.08	14.48	1.14	10.87	-6.82	1.04	21.63	1.23	14.89
		-50	-31.84	0.98	6.65	1.07	10.59	-30.20	1.29	30.47	1.29	20.05	-31.11	1.29	31.36	1.29	23.27

Table 6.11(c). Sensitivity of the model parameters to the closeness of moisture content values obtained from magnetic resonance imaging experiments for germ-removed wheat kernel drying at different temperatures, as determined by five criteria for sensitivity analysis.

Drying Temperature (°C) ⟶			30					40					50				
Grain	Parameter	Change (%)	MRPR	BF	MARR	AF	RMSR	MRPR	BF	MARR	AF	RMSR	MRPR	BF	MARR	AF	RMSR
Endosperm	Original	0	-15.46	1.13	22.32	1.21	5.29	-190.48	2.10	197.10	2.25	9.51	-1500.30	6.13	1500.30	6.13	8.48
	D_E	+25	-6.05	1.04	16.56	1.17	4.59	-142.87	1.84	151.90	2.04	7.82	-1097.37	5.05	1098.30	5.09	6.30
		+100	15.29	0.84	15.29	1.19	6.28	-54.54	1.31	71.94	1.61	6.79	-562.11	3.21	566.94	3.39	3.38
		+150	25.61	0.74	25.61	1.35	8.80	-20.72	1.07	48.30	1.49	7.66	-429.55	2.57	439.66	2.89	3.48
		+200	33.74	0.65	33.74	1.53	9.89	1.90	0.89	37.79	1.47	8.78	-373.13	2.20	390.89	2.73	4.22

Table 6.12. Selected diffusivity values to achieve the lowest values of the five criteria selected for the sensitivity analysis.

Grain	Drying Temperature (°C)		
	30	40	50
Intact	$D_E \times 2$; $D_G \times 0.5$	$D_E \times 3$; $D_G \times 1$	$D_E \times 3$; $D_G \times 0.75$
Mechanically-scarified	$D_E \times 2$; $D_G \times 1.25$	$D_E \times 3$; $D_G \times 1.25$	$D_E \times 3$; $D_G \times 1.25$
Germ-removed	$D_E \times 1.25$	$D_E \times 3$	$D_E \times 3$

original value for intact and mechanically-scarified kernels and 25% higher in the case of germ-removed kernels at 30°C whereas the value was 200% higher than the original for three different kernels at both 40°C and 50°C. Diffusivity of the germ was 25% higher in the case of mechanically-scarified kernels for 30 to 50°C whereas in the case of the intact kernels, it was 50% less at 30°C and 25% less at 50°C. Yet, these diffusivity values are very close, considering the rather simple model used in our calculations. However, model predictions could not exactly match the moisture loss predictions by the MR images. It was reported by a few researchers that the linearity of the moisture calibration curve cannot be confirmed at low moisture levels since practically no water signal can be detected from the wheat kernels in the moisture range of 0-11% (Miller 1980; Brusewitz and Stone 1987; Stapley et al. 1997). This could be due to significant shortening of T_2 as a result of strong association of water with the starch molecules. Further, MR images of the drying kernels (Fig. 6.6) indicated non-homogeneity in moisture content distribution for which perfect calibration between the moisture content and the image intensity is questionable. The average moisture content of the imaged plane is, in general, less than that in the overall grain measured gravimetrically (Stapley et al. 1997).

6.4 Conclusions

A two-dimensional simultaneous heat and mass transfer model based on non-uniform initial moisture distribution inside the grain kernels was developed and validated to predict moisture and temperature distribution during drying of wheat kernels. Drying of wheat was mainly governed by two major components, the germ and the endosperm. The model predicted a non-uniform moisture removal pattern from both components during

drying. The germ contained more moisture compared to the endosperm and the moisture release was faster from the endosperm than from the germ. Comparison of an intact kernel and a mechanically-scarified kernel with incisions in the pericarp showed that in scarified kernels, moisture removal was faster from the incised parts during the first 1.5 h of drying but in both cases moisture moved from the endosperm region to the germ during drying which was also observed in the MRI experiments. Calculation of activation energy also confirmed the similar pattern of moisture removal process. The germ-removed kernels almost showed a uniform pattern of moisture removal from the kernel. A very high internal resistance to moisture transfer was observed whereas the heat transfer was mainly controlled by external resistance without internal temperature gradients. Calculation of Lewis numbers for both endosperm and germ indicated an isothermal drying phenomenon in wheat kernels. The model could accurately predict the temperature and moisture distribution inside the wheat kernels during drying, which can help in maintaining the grain quality. Sensitivity analysis of the model parameters to the closeness of moisture content values obtained from the MR imaging showed that the model is most sensitive to changes in water diffusivity in the germ and endosperm.

Acknowledgments

Authors thank the financial assistance provided by the Natural Sciences and Engineering Research Council of Canada, the University of Manitoba Graduate Fellowship Committee and Canada Research Chairs program for conducting this study.

References

Allen, J.R. 1960. Application of grain drying theory to the drying of maize and rice. *Journal of Agricultural Engineering Research* 5(4): 363-385.

ASAE. 2003. *ASAE Standards* S352.2: Moisture measurement – Unground grain and seeds. St. Joseph, MI: ASAE.

Babbit, J.D. 1949. Observation on the adsorption of water vapor by wheat. *Canadian Journal of Research* 27(F): 55-72.

Bačić, G., R. Srejić, G. Lahajnar, I. Zupančić, and S. Ratković. 1992. Water and lipids in maize seed embryos: a proton NMR relaxation and diffusion study. *Seed Science and Technology* 20: 233-240.

Bechtel, D.B., and J.D. Wilson. 2005. Endosperm structural changes in wheat during drying of maturing caryopses. *Cereal Chemistry* 82(4): 385-389.

Becker, H.A. 1959. A study of diffusion in solids of arbitrary shape, with application to the drying of the wheat kernel. *Journal of Applied Polymer Science* 1(2): 212-226.

Becker, H.A. and H.R. Sallans. 1955. A study of internal moisture movement in the drying of the wheat kernel. *Cereal Chemistry* 32(3): 212-226.

Bernada, P., S. Stenström, and S. Månsson. 1998. Experimental study of the moisture distribution inside a pulp sheet using MRI-Part I: Principles of the MRI technique. *Journal of Pulp and Paper Science* 24(12): 373-379.

Brooker, D.B., F.W. Bakker-Arkema, and C.W. Hall. 1992. *Drying and storage of grains and oilseeds*. New York, NY: Van Nostrand Reinhold.

Brusewitz, G.H., and M.L. Stone. 1987. Wheat moisture and NMR. *Transactions of the ASAE* 30(3):858-862.

Burnett, D.S. 1987. *Finite Element Analysis – From Concepts to Applications*. Reading, MA: Addison-Wesley Publishing Company.

Callaghan, P.T., K.W. Jolley, and J. Lelievre. 1979. Diffusion of water in the endosperm tissue of wheat grains as studied by pulsed field gradient nuclear magnetic resonance. *Biophysics Journal* 28(1): 133-142.

Cenkowski, S., D.S. Jayas, and S. Pabis. 1993. Deep-bed grain drying – a review of particular theories. *Drying Technology* 11(7):1553-1581.

Chittenden, D.H., and A. Hustrulid. 1966. Determining drying constants for shelled corn. *Transactions of the ASAE* 9(1): 52-55.

Chu, S.T., and A. Hustrulid. 1968a. Numerical solution of diffusion equations. *Transactions of the ASAE* 11(5): 705-708.

Chu, S.T., and A. Hustrulid. 1968b. General characteristics of variable diffusivity process and the dynamic equilibrium moisture content. *Transactions of the ASAE* 11(5): 709-710,715.

Czaba, I., and M. Neményi. 1997. Investigation of simultaneous heat and mass transfer within the individual maize kernels during drying time. *Hungarian Agricultural Engineering* 10: 58-60.

Devahastin, S., and A.S. Majumdar. 1999. Batch drying of grains in a well-mixed dryer-effect of continuous and stepwise change in drying air temperature. *Transactions of the ASAE* 42(2): 421-425.

Eccles, C.D., P.T. Callaghan, and C.F. Jenner. 1988. Measurement of the self-diffusion coefficient of water as a function of position in wheat grain using nuclear magnetic resonance imaging. *Biophysics Journal* 53(1): 77-81.

Evers, A.D., and D.B. Bechtel. 1988. Vol. I. Microscopic structure of the wheat grain. In *Wheat – Chemistry and Technology*, 47-96. Y. Pomeranz, ed. St. Paul, Mich.: Amercian Association of Cereal Chemists, Inc.

Fortes, M., and M.R. Okos. 1978. A non-equilibrium thermodynamics approach to transport phenomena in capillary porous media. In *Proc. 1st International Symposium on Drying*, 100-109. A.S. Majumdar, ed. Princeton, NJ: Science Press.

Fortes, M. M.R. Okos, and J.R. Barrett. 1981. Heat and mass transfer analysis of intra-kernel wheat drying and rewetting. *Journal of Agricultural Engineering Research* 26(2): 109-125.

Frìas, J.M., L. Foucat, J.J. Bimbenet, and C. Bonazzi. 2002. Modelling of moisture profiles in paddy rice during drying mapped with magnetic resonance imaging. *Chemical Engineering Journal* 86(1-2): 173-178.

Friesen, O.H. 1980. *Heated-air grain dryers*. Manitoba Department of Agriculture Publication No. 1700. Ottawa, ON: Agriculture and Agri-Food Canada.

Fukuoka, M., T. Mihori, and H. Watanabe. 2000. MRI observation and mathematical model simulation of water migration in wheat flour during boiling. *Journal of Food Science* 65(8): 1343-1348.

Ghosh, P.K., D.S. Jayas, and Y.C. Agrawal. 2004. Drying of oilseeds – a review. In *Recent Research Developments in Crop Science*, 71-96. S.G. Pandalai, ed. Kerala, India: Research Signpost.

Ghosh, P.K., D.S. Jayas, M.L.H. Gruwel, and N.D.G. White. 2006a. Magnetic resonance imaging studies to determine the moisture removal patterns in wheat during drying. *Canadian Biosystems Engineering* 48: 7.13-7.18.

Ghosh, P.K., D.S. Jayas, M.L.H. Gruwel and N.D.G. White. 2006b. Magnetic resonance image analysis to explain moisture movement during wheat drying. *Transactions of the ASABE* 49(4): 1181-1191.

Ghosh, P.K., D.S. Jayas, M.L.H. Gruwel, and N.D.G. White. 2006c. Influence of grain structural components on the drying of wheat: a magnetic resonance imaging study. In *Magnetic Resonance in Food Science – From Molecules to Man*: Proc. 8th International Conference on the applications of Magnetic Resonance in Food Science. In Press. I.A. Farhat, P.S. Belton, G.A. Webb, eds. Cambridge, UK: Royal Society of Chemistry.

Giner, S.A., and R.H. Mascheroni. 2001. Diffusive drying kinetics in wheat, Part 1: Potential for a simplified analytical solution. *Journal of Agricultural Engineering Research* 80(4): 351-364.

Glidewell, S.M. 2006. NMR imaging of developing barley grains. *Journal of Cereal Science* 43(1): 70-78.

Gruwel, M.L.H., X.S. Yin, M.J. Edney, S.W. Schroeder, A.W. MacGregor, and S. Abrams. 2002. Barley viability during storage: use of magnetic resonance as a potential tool to study viability loss. *Journal of Agriculture and Food Chemistry* 50(4): 667-676.

Gruwel, M.L.H., B. Chatson, X.S. Yin, and S. Abrams. 2001. A magnetic resonance study of water uptake in whole barley kernels. *International Journal of Food Science and Technology* 36(2): 161-168.

Gruwel, M.L.H., P. Latta, V. Volotovskyy, M. Šramek, and B. Tomanek. 2004. Magnetic resonance imaging of seeds by use of single point acquisition. *Journal of Agriculture and Food Chemistry* 52(16): 4979-4983.

Haghighi, K, J. Irudayaraj, R.L. Stroshine, and S. Sokhansanj. 1990. Grain kernel drying simulation using the finite element method. *Transactions of the ASAE* 33(6): 1957-1965.

Hahn, E.L. 1950. Spin echoes. *Physical Review* 80(4): 580-594.

Hall, C.W., and J.H. Rodrigues-Aries. 1958. Applications of the Newton's equation to moisture removal from shelled corn at 40-140 F. *Journal of Agricultural Engineering Research* 3(4): 275-280.

Horigane, A.K., W.M.H.G. Engelaar, S. Maruyama, M. Yoshida, A. Okubo, and T. Nagata. 2001. Visualization of moisture distribution during development of rice caryopses (*Oryza sativa* L.) by nuclear magnetic resonance microimaging. *Journal of Cereal Science* 33(1): 105-114.

Husain, A., C.S. Chen, and J.T. Clayton. 1973. Simultaneous heat and mass diffusion in biological materials. *Journal of Agricultural Engineering Research* 18(4): 343-354.

Hustrulid, A., and A.M. Flikke. 1959. Theoretical drying curve for shelled corn. *Transactions of the ASAE* 2(1): 112-114.

Hutton, D.V. 2004. *Fundamentals of Finite Element Analysis*. 1st ed. New York, NY: McGraw Hill.

Incorpera, F.P., and D.P. DeWitt. 1996. *Fundamentals of Heat and Mass Transfer*. 4th ed. New York, NY: John Wiley & Sons.

Irudayaraj, J., K. Haghighi, and R.L. Sroshine. 1992. Finite element analysis of drying with application to cereal grains. *Journal of Agricultural Engineering Research* 53(3): 209-229.

Ishida, N., S. Naito, and H. Kano. 2004. Loss of moisture from harvested rice seeds on MRI. *Magnetic Resonance Imaging* 22(6): 871-875.

Jayas, D.S., and S. Sokhansanj. 1986. Thin-layer drying of wheat at low temperatures, 844-847. In: *Drying '86*. A.S. Mujumdar, ed. New York, NY: Hemisphere Publishing Corporation.

Jayas, D.S., S. Cenkowski, S. Pabis, and W.E. Muir. 1991. Review of thin-layer drying and wetting equations. *Drying Technology* 9(3):551-558.

Jenner, C.F., and G.P. Jones. 1990. Diffusion of water in the wheat grain: Nuclear magnetic resonance and radioisotopic methods provide complementary information. *Australian Journal of Plant Physiology* 17(2): 107-118.

Jenner, C.F., Y. Xia, C.D. Eccles, and P.T. Callaghan. 1988. Circulation of water within wheat grain revealed by nuclear magnetic resonance micro-imaging. *Nature* 336:6197, 399-402.

Jeyamkondan, S., D.S. Jayas, and R.A. Holley. 2001. Microbial growth modelling with artificial neural networks. *International Journal of Food Microbiology* 64(3): 343-354.

Jia, C.C., D.A. Sun, and C.W. Cao. 2000. Mathematical simulation of temperature and moisture fields within a grain kernel during drying. *Drying Technology* 18(6): 1305-1325.

Kang, S., and S.R. Delwiche. 1999. Moisture diffusion modeling of wheat kernels during soaking. *Transactions of the ASAE* 42(5): 1359-1365.

Karunakaran, C., D.S. Jayas, and N.D.G. White. 2004. Mass determination of wheat kernels from X-ray images. Paper No. 043120. St. Joseph, MI: ASAE.

Kasai, M, A. Lewis, F. Marica, S. Ayabe, K. Hatae, and C.A. Fyfe. 2005. NMR imaging investigation of rice cooking. *Food Research International* 38(4): 403-410.

Kovács, A.J., and M. Neményi. 1999. Moisture gradient vector calculation as a new method for evaluating NMR images of corn (*Zea mays* L.) kernels during drying. *Magnetic Resonance Imaging* 17(7):1077-1082.

MacMasters, M.M., D. Bradbury, and J.J.C. Hinton. 1964. Microscopic structure and composition of the wheat kernel. In *Wheat – Chemistry and Technology*, 55-110. I. Hlynka, ed. St. Paul, MN: Amercian Association of Cereal Chemists, Inc.

Manickavasagan, A., D.S. Jayas, and N.D.G. White. 2005. Thermal imaging to identify western Canadian wheat classes. Paper No. 056078. St. Joseph, MI: ASAE.

McEntyre, E., R. Ruan, and R.G. Fulcher. 1998. Comparison of water absorption patterns in two barley cultivars, using magnetic resonance imaging. *Cereal Chemistry* 75(6):792-795.

McEwen, E., W.H.C. Simmonds and G.T. Ward. 1954. The drying of wheat grain. Part III: Interpretation in terms of its biological structure. *Transactions of the Institution of Chemical Engineers* 32(3): 116-120.

Miketinac, M.J., S. Sokhansanj, and Z. Tutek. 1992. Determination of heat and mass transfer coefficients in thin layer drying of grain. *Transactions of the ASAE* 35(6): 1853-1858.

Miller, B.S., M.S. Lee, J.W. Hughes, and Y. Pomeranz. 1980. Measuring high moisture content of cereal grains by pulsed nuclear magnetic resonance. *Cereal Chemistry* 57(2): 126-129.

Mohorič, A., F. Vergeldt, E. Gerkema, A. Jager, J. Duynhoven, G. Dalen, and H.V. As. 2004. Magnetic resonance imaging of single rice kernels during cooking. *Journal of Magnetic Resonance* 171(1): 157-162.

Nellist, M.E., and D.M. Bruce. 1995. Heated-air grain drying. In *Stored-Grain Ecosystems*, 609-660. D.S. Jayas, N.D.G. White, W.E. Muir, eds. New York, NY: Marcel Dekker, Inc.

Neményi, M., I. Czaba, A. Kovacs, and T. Jani. 2000. Investigation of simultaneous heat and mass transfer within the maize kernels during drying. *Computers and Electronics in Agriculture* 26(2): 123-135.

Pabis, S., and S.M. Henderson. 1961. Grain drying theory –II. A critical analysis of the drying curve for shelled maize. *Journal of Agricultural Engineering Research* 6(4): 272-277.

Pabis, S., D.S. Jayas, and S. Cenkowski. 1998. *Grain Drying: Theory and Practice.* New York, NY: John Wiley & Sons, Inc.

Parde, S., D.S. Jayas, and N.D.G. White. 2003. Grain drying: a review. *Sciences des Aliments* 23(5-6):589-622.

Pomeranz, Y., and D.B. Bechtel. 1978. Structure of cereal grains as related to end-use properties. In *Cereals'78: Better nutrition for the world's millions*: Proc. Sixth International Cereal and Bread Congress, 85-104. Y. Pomeranz, ed. St. Paul, MN: American Association of Cereal Chemists, Inc.

Ranjan, R., J. Irudayaraj, and S. Jun. 2001. A three-dimensional control volume approach to modeling heat and mass transfer in food materials. *Transactions of the ASAE* 44(6): 1975-1982.

Ratković. S. 1987. Proton NMR of maize seed water: the relationship between spin-lattice relaxation time and water content. *Seed Science and Technology* 15: 147-154.

Ruan, R., and J.B. Litchfield. 1992. Determination of water distribution and mobility inside maize kernels during steeping using magnetic resonance imaging. *Cereal Chemistry* 69(1):13-17.

Ruan, R., J.B. Litchfield, and S.R. Eckhoff. 1992. Simultaneous and nondestructive measurement of transient moisture profiles and structural changes in corn kernels during steeping using microscopic nuclear magnetic resonance imaging. *Cereal Chemistry* 69(6):600-606.

Segerlind, L.J. 1984. *Applied Finite Element Analysis*. 2nd ed. New York, NY: John Wiley and Sons, Inc.

Simmonds, W.H.C., G.T. Ward, and E. McEwen. 1953. The drying of wheat grain. Part I: The mechanism of drying. *Transactions of the Institution of Chemical Engineers* 31: 265-278.

Sinico, R., W.E. Muir, D.S. Jayas, and S. Cenkowski. 1995. Thin-layer drying and wetting of wheat. *Postharvest Biology and Technology* 5(3): 261-275.

Smart, M.G., and T.P. O'Brien. 1983. The development of the wheat embryo in relation to the neighbouring tissues. *Protoplasma* 114(1-2): 1-13.

Sokhansanj, S, and R.J. Gustafson. 1980. Prediction of heat and mass transfer within a grain kernel – a finite element application. In: *Drying '80*, Vol. 2, 229-232. A.S. Majumdar ed. New York, NY: McGraw-Hill International Book Company.

Sokhansanj, S., and D.M. Bruce. 1987. A conduction model to predict grain temperature in grain drying simulation. *Transactions of the ASAE* 30(4): 1181-1184.

Song, H., and J.B. Litchfield. 1990. Nondestructive measurement of transient moisture profiles in ear corn during drying using NMR imaging. *Transactions of the ASAE* 33(4): 1286-1290.

Song, H.P., J.B. Litchfield, and H.D. Morris. 1992. Three dimensional microscopic MRI of maize kernels during drying. *Journal of Agricultural Engineering Research* 53(1): 51-69.

Song, H.P., S.R. Delwiche, and M.J. Line. 1998. Moisture distribution in a mature soft wheat grain by three-dimensional magnetic resonance imaging. *Journal of Cereal Science* 27(2): 191-197.

Stapley, A.G.F., M.H. Thomas, L.F. Gladden, and P.J. Fryer. 1997. NMR imaging of the wheat grain cooking process. *International Journal of Food Science and Technology* 32(5):355-375.

Stapley, A.G.F., P.J. Fryer, and L.F. Gladden. 1998. Diffusion and reaction in whole wheat grains during boiling. *AIChE Journal* 44(8): 1777-1789.

Steffe, J.F., and R.P. Singh. 1982. Diffusion coefficients for predicting rice drying behavior. *Journal of Agricultural Engineering Research* 27(6): 489-493.

Takeuchi, S., M. Fukuoka, Y. Gomi, M. Maeda, and H. Watanabe. 1997. An application of magnetic resonance imaging to the real time measurement of the change of moisture profile in a rice grain during boiling. *Journal of Food Engineering* 33(2):181-192.

Turhan, M., S. Gunasekaran, and B.P. Lamsal. 2001. Drying of gelatinized whole wheat. *Drying Technology* 19(2): 333-342.

Walton, L.R., G.M. White and I.J. Ross. 1988. A cellular diffusion-based drying model for corn. *Transactions of the ASAE* 31(1): 279-283.

Watson, E.L., and V.K. Bhargava. 1974. Thin layer drying studies on wheat. *Canadian Agricultural Engineering* 16(1): 18-22.

Wu, B., W. Yang, and C. Jia. 2004. A three-dimensional numerical simulation of transient heat and mass transfer inside a single rice kernel during the drying process. *Biosystems Engineering* 87(2): 191-200.

Yang, W. C.C. Jia, T.J. Siebenmorgen, T.A. Howell, and A.G. Cnossen. 2002. Intra-kernel moisture responses of rice to drying and tempering treatments by finite element simulation. *Transactions of the ASAE* 45(4): 1037-1044.

Zhilkin, P.A., and M.E. Alexander. 2000. 3D Image Registration using a fast noniterative algorithm. *Magnetic Resonance Imaging* 18(9): 1143-1150.

Zhilkin, P.A., and M.E. Alexander. 2005. Nonlinear registration using variational principle for normalized mutual information and AOS scheme. In *Proc. 13th International Society for Magnetic Resonance in Medicine*, p 1279, Miami, FL.

CONCLUSIONS

1. The Magnetic Resonance Imaging (MRI) technique was found to be a powerful tool to explain moisture movement in wheat drying.
2. The MR images showed that moisture was uniformly distributed in the pericarp region at an equilibrium state prior to drying in a single kernel of wheat. Inside the wheat kernel, the moisture was differentially distributed in the endosperm and germ regions. The transverse or spin-spin relaxation time (T_2) calculated for germ, pericarp, and endosperm of a wheat kernel indicated the non-uniform dynamics of moisture distribution in grain components by accurately measuring nuclei density in parts of kernels.
3. The MR images showed that the moisture removal pattern during drying of a wheat kernel was non-uniform. Water was removed faster from the pericarp than from the endosperm, and the moisture-loss rate during drying was the lowest in the germ.
4. Three physically different wheat kernels (intact kernels, mechanically scarified kernels with incisions in the pericarp, and kernels with the germ-removed) made it easy to visualize the underlying drying phenomena. Moisture appeared to move through the germ end of the wheat kernel from the endosperm after initial stages of drying whereas the pericarp dried faster and presumably acted as a moisture barrier. The results obtained from this study confirmed the general pattern of moisture distribution in grains during drying.

5. Gradient vector analysis of the MRI intensities provided a mathematical description of the real moisture loss from the kernel during drying.
6. The MRI images and the gradient vector analysis indicated that the moisture removal pattern was highly influenced by the grain structural components.
7. The drying curves between the MR image intensity ratio and drying time indicated no single exponential relationship, which indicated that water reduction not only depend on the water content of the kernels but also on the grain composition.
8. The following moisture calibration equation was developed between the Nuclear Magnetic Resonance (NMR) signal intensity and the wheat moisture content over the moisture content (M) range of 18.8 to 39.5% (dry mass basis) :

$$\text{NMR signal intensity} = 54.7 \times M + 90.7$$

9. Drying of intact, mechanically scarified, and germ removed wheat kernels was in the falling rate period.
10. Two falling rate periods were found for the drying of germ in which both liquid and vapor diffusion were assumed to be dominant factors for the moisture removal. However, the endosperm did not show variable falling rate of drying like the germ in which liquid diffusion was assumed to be predominant for the moisture removal.
11. The germ plays an important role in moisture migration during drying. In general, an initial higher drying rate from the germ than from the endosperm was observed in the case of intact and the scarified kernels because germ has high moisture

content. The endosperm has lower moisture which needs more time to be transferred from the interior of the grain.

12. A two-dimensional (2D) simultaneous heat and moisture transfer drying model for single wheat kernel was developed. The model assumed non-uniform initial moisture distribution in the germ and endosperm of a wheat kernel. The model was theoretically developed using 2D finite element method (FEM) and then was solved using COMSOL® Multiphysics™, a commercial finite element software package.
13. No predominant shrinkage of wheat kernels was found during drying from two-dimensional non-linear multimodal diffusion registration algorithm and therefore the effect of shrinkage was neglected in the development of the model.
14. Model simulated moisture data were validated by comparing the proton density MR images of wheat components that were converted into actual moisture contents using a moisture calibration equation, two published semi-empirical thin layer wheat drying models, and a published 2D heat and mass transfer model for single wheat kernel which assumed uniform initial moisture distribution within the whole kernel. The model prediction agreed well with observations obtained from the MR Imaging and from the published models.
15. Comparison of an intact kernel and a mechanically-scarified kernel showed that in scarified kernels, moisture removal was faster from the incised parts during the first 1.5 h of drying but in both cases moisture moved from the endosperm region to the germ during drying which was proven by the MRI experiments. Calculation of an activation energy of water removal process also confirmed the similar

pattern of moisture removal process. Germ-removed kernel showed almost a uniform pattern of moisture removal from the kernel.

16. A very high internal resistance to the moisture transfer was observed whereas the heat transfer was mainly controlled by external resistance with no internal temperature gradients.
17. Calculation of Lewis numbers for both endosperm and germ indicated an isothermal drying phenomenon in wheat kernels.
18. Sensitivity analysis of the model parameters to the closeness of moisture content values obtained from the MR imaging showed that values of water diffusivity in the germ and endosperm are the main parameters which control the overall grain drying process. It shows how important it is to get accurate values for these diffusivities.
19. The developed model has the potential to predict the actual moisture and temperature distribution inside any type or size of a grain kernel during drying considering non-uniform initial moisture distribution. Results of this model can be used to evaluate and maintain the grain quality particularly in the development of hydro-thermal stresses.

CHAPTER 8

RECOMMENDATIONS FOR FUTURE RESEARCH

1. Apply this model to the high-speed drying processes. This new model can provide a major contribution to the advancement of grain drying control if combined with a stochastic quality model.
2. Apply this model to simulate real size grain bin wheat drying situations where the entire grain bin can be considered as a deep bed consisting of several thin layers. Therefore develop a deep-bed drying model of wheat considering MRI predicted anisotropic and the non-uniform pattern of grain moisture movement. In this case, grain-air interface properties might be taken into consideration.
3. Assess the developed model to analyze both the thin-layer (single kernel) and the deep-bed drying kinetics for other cereal grains than wheat (for example, corn, rice, barley).
4. Determine the diffusion coefficients of the wheat components using Magnetic Resonance Imaging (MRI). Diffusivity of wheat germ is currently not available in the literature.
5. Explain the moisture movement in oilseeds (for example, sunflower, rapeseed, canola, soybean) during drying using Magnetic Resonance Imaging (MRI) and develop drying models.
6. Model certain grain quality parameters (for example, stress cracks, head rice yield, milling quality, seed germination percentage) affected by drying using Magnetic Resonance Imaging (MRI).

7. Develop moisture calibration curves for other cereal grains than wheat using Magnetic Resonance Imaging (MRI) for a non-destructive measurement of moisture content in the grain components.

REFERENCES

These are references for literature cited in chapters 1 and 2. For chapters 3-6, cited references are given at the end of each chapter.

Allen, J.R. 1960. Application of grain drying theory to the drying of maize and rice. *Journal of Agricultural Engineering Research* 5(4): 363-385.

Andaur, J.E., A.R. Guesalaga, E.E. Agosin, M.W. Guarini, and P. Irarrázaval. 2004. Magnetic resonance imaging for nondestructive analysis of wine grapes. *Journal of Agriculture and Food Chemistry* 52(2): 165-170.

Arora, V.K., S.M. Henderson, and T.H. Burkhardt. 1973. Rice drying and cracking versus thermal and mechanical properties. *Transactions of the ASAE* 16(2): 320-323.

ASAE. 1995. *ASAE Standards* D245.5. Moisture relationships of plant-based agricultural products. St. Joseph, MI: ASAE.

ASAE. 2003. *ASAE Standards* S352.2. Moisture measurement – unground grain and seeds. St. Joseph, MI: ASAE.

Babbit, J.D. 1949. Observation on the adsorption of water vapor by wheat. *Canadian Journal of Research* 27(F): 55-72.

Bačić, G., R. Srejić, G. Lahajnar, I. Zupančić, and S. Ratković. 1992. Water and lipids in maize seed embryos: a proton NMR relaxation and diffusion study. *Seed Science and Technology* 20: 233-240.

Baker-Arkema, F.W., A.A. Sokhansanj, and G. Green. 1977. High temperature wheat drying. Paper No. 77-3527. St. Joseph, MI: ASAE.

Barreiro, P., C. Ortiz, M. RuizAltisent, J. Ruiz-Cabello, M.E. Fernandez-Valle, I. Recasens, and A. Asensio. 2000. Mealiness assessment in apples and peaches using MRI techniques. *Magnetic Resonance Imaging* 18(9): 1175-1181.

Becker, H.A. 1959. A study of diffusion in solids of arbitrary shape, with application to the drying of the wheat kernel. *Journal of Applied Polymer Science* 1(2): 212-226.

Becker, H.A., and H.R. Sallans. 1955. A study of internal moisture movement in the drying of the wheat kernel. *Cereal Chemistry* 32(3): 212-226.

Brooker, D.B., F.W. Bakker-Arkema, and C.W. Hall. 1992. *Drying and storage of grains and oilseeds*. New York, NY: Van Nostrand Reinhold.

Bruce, D.M. 1985. Exposed-layer barley drying: three models fitted to new data up to 150°C. *Journal of Agricultural Engineering Research* 32(4): 337-347.

Brusewitz, G. H., and M. L. Stone. 1987. Wheat moisture and NMR. *Transactions of the ASAE* 30(3): 858-862.

Burdon, J., and C.J. Clark. 2001. Effect of postharvest water loss on 'Hayward' kiwifruit water status. *Postharvest Biology and Technology* 22(3): 215-225.

Bushong, S.C. 1988. *Magnetic Resonance Imaging: Physical and Biological Principles*. St. Louis, MO: Mosby-Year Book.

Callaghan, P.T., K.W. Jolley, and J. Lelievre. 1979. Diffusion of water in the endosperm tissue of wheat grains as studied by pulsed field gradient nuclear magnetic resonance. *Biophysics Journal* 28(1): 133-142.

Cenkowski, S., D.S. Jayas, and S. Pabis. 1993. Deep-bed grain drying – a review of particular theories. *Drying Technology* 11(7):1553-1581.

CGC. 1993. *Grain grading handbook for Western Canada*. Winnipeg, MB: Canadian Grain Commission.

Chambers, J., N. J. McKevitt, K. A. Scudamore, and C. E. Bowman. 1989. Nondestructive determination of the moisture content of individual wheat grains by nuclear magnetic resonance. *Journal of Food Science and Agriculture* 49(2): 211-224.

Chambers, J., N.J. McKevitt, and M.R. Stubbs. 1984. Nuclear magnetic resonance spectroscopy for studying the development and detection of the grain weevil, *Sitophilus granarius* (L.) (Coleoptera: Curculionidae), within wheat kernels. *Bulletin of Entomological Research* 74(4): 707-724.

Chen, P. M.J. McCarthy, and R. Kauten. 1989. NMR for quality evaluation of fruits and vegetables. *Transactions of the ASAE* 32(5): 1747-1753.

Chittenden, D.H., and A. Hustrulid. 1966. Determining drying constants for shelled corn. *Transactions of the ASAE* 9(1): 52-55.

Chu, S.T., and A. Hustrulid. 1968a. Numerical solution of diffusion equations. *Transactions of the ASAE* 11(5): 705-708.

Chu, S.T., and A. Hustrulid. 1968b. General characteristics of variable diffusivity process and the dynamic equilibrium moisture content. *Transactions of the ASAE* 11(5): 709-710,715.

Chua, H.S., M.D. Mantle, A.D. Haigh, F. Thompson, A.A.P. Gibson, and L.F. Gladden. 2004. Non-invasive measurement of lipid and water in single wheat grains using magnetic resonance imaging. In *9th IEEE High Frequency Postgraduate*

Colloquium, UMIST Manchester, Sept. 6-7, pp 199-204, IEEE Catelog No.: 04TH8740.

Clark C.J., and S.K. Forbes. 1994. Nuclear magnetic resonance imaging of the development of chilling injury in 'Fuyu' persimmon (*Diosyros kaki*). *New Zealand Journal of Crop and Horticultural Science* 22(2): 209-215.

Clark, C.J., and D.M. Burmeister. 1999. Magnetic resonance imaging of browning development in 'Braeburn' apple during controlled-atmosphere storage under high CO_2. *HortScience* 34(5): 915-919.

Clark, C.J., L.N. Drummond, and J.S. MacFall. 1998. Quantitative NMR imaging of kiwifruit (*Actinidia deliciosa*) during growth and ripening. *Journal of the Science of Food and Agriculture* 78(3): 349-358.

Cnossen, A.G., and T.J. Siebenmorgen. 2000. The glass transition temperature concept in rice drying and tempering: effect on milling quality. *Transactions of the ASAE* 43(6): 1661-1667.

Czaba, I., and M. Neményi. 1997. Investigation of simultaneous heat and mass transfer within the individual maize kernels during drying time. *Hungarian Agricultural Engineering* 10: 58-60.

Eccles, C.D., P.T. Callaghan, and C.F. Jenner. 1988. Measurement of the self-diffusion coefficient of water as a function of position in wheat grain using nuclear magnetic resonance imaging. *Biophysics Journal* 53(1): 77-81.

Eccles, C.D., P.T. Callaghan, and C.F. Jenner. 1988. Measurement of the self-diffusion coefficient of water as a function of position in wheat grain using nuclear magnetic resonance imaging. *Biophysics Journal* 53(1): 77-81.

Ekstrom, G.A., J.B. Liljedahl, and R.M. Peart. 1966. Thermal expansion and tensile properties of corn kernels and their relationships to cracking during drying. *Transactions of the ASAE* 9(4): 556-561.

Epp, D.A., D.S. Jayas, W.E. Muir, N.D.G. White, and D. St. George. 1997. Near-ambient drying of wheat using variable airflow - a simulation study. *Canadian Agricultural Engineering* 39(4): 297-302.

Evers, A.D., and D.B. Bechtel. 1988. Microscopic structure of the wheat grain. In *Wheat – Chemistry and Technology*, Vol. I, 47-96. Y. Pomeranz, ed. St. Paul, MN: Amercian Association of Cereal Chemists, Inc.

FAOSTAT. 2006. *FAOSTAT Classic – Crops primary*. Food and Agriculture Organization of the United Nations. Available at: http://faostat.fao.org/site/408/default.aspx. Accessed 25 October 2006.

Fortes, M., and M.R. Okos. 1978. A non-equilibrium thermodynamics approach to transport phenomena in capillary porous media. In *Proc. 1st International Symposium on Drying*, 100-109. A.S. Majumdar, ed. Princeton, NJ: Science Press.

Fortes, M., M.R. Okos, and J.R. Barrett. 1981. Heat and mass transfer analysis of intra-kernel wheat drying and rewetting. *Journal of Agricultural Engineering Research* 26(2): 109-125.

Frìas, J.M., L. Foucat, J.J. Bimbenet, and C. Bonazzi. 2002. Modelling of moisture profiles in paddy rice during drying mapped with magnetic resonance imaging. *Chemical Engineering Journal* 86(1-2): 173-178.

Friesen, O.H. 1980. *Heated-air grain dryers*. Manitoba Department of Agriculture Publication No. 1700. Ottawa, ON: Agriculture and Agri-Food Canada.

Fukuoka, M., T. Mihori, and H. Watanabe. 2000. MRI observation and mathematical model simulation of water migration in wheat flour during boiling. *Journal of Food Science* 65(8): 1343-1348.

Gamble, G.R. 1994. Non-invasive determination of freezing effects in blueberry fruit tissue by magnetic resonance imaging. *Journal of Food Science* 59(3):571-573, 610.

Ghosh, P.K., and D.S. Jayas. 2004. Magnetic resonance imaging: potential use for grain research. In *Proceedings of International Conference on Emerging Technologies in Agricultural Engineering*, Vol. Food and Bio Process Engineering, 130-136. New Delhi, India: Anamaya Publishers.

Ghosh, P.K., D.S. Jayas, M.L.H. Gruwel, and N.D.G. White. 2006. Magnetic resonance image analysis to explain moisture movement during wheat drying. *Transactions of the ASABE* 49(4): 1181-1191.

Ghosh, P.K., D.S. Jayas, and Y.C. Agrawal. 2004. Drying of oilseeds – a review. In *Recent Research Developments in Crop Science*, 71-96. S.G. Pandalai, ed. Kerala, India: Research Signpost.

Glidewell, S.M. 2006. NMR imaging of developing barley grains. *Journal of Cereal Science* 43(1): 70-78.

Gonzalez, J.J., R.C. Valle, S. Bobroff, W.V. Biasi, E.J. Mitcham, and M.J. McCarthy. 2001. Detection and monitoring of internal browning development in 'Fuji' apples using MRI. *Postharvest Biological Technology* 22(2):179-188.

Gonzalez, J.J., K.L. McCarthy, and M.J. McCarthy. 1998. MRI method to evaluate internal structural changes of tomato during compression. *Journal of Texture Studies* 29(5):537-551.

Gruwel, M.L.H., B. Chatson, X.S. Yin, and S. Abrams. 2001. A magnetic resonance study of water uptake in whole barley kernels. *International Journal of Food Science and Technology* 36(2): 161-168.

Gruwel, M.L.H., P. Latta, V. Volotovskyy, M. Šramek, and B. Tomanek. 2004. Magnetic resonance imaging of seeds by use of single point acquisition. *Journal of Agriculture and Food Chemistry* 52(16): 4979-4983.

Gruwel, M.L.H., X.S. Yin, M.J. Edney, S.W. Schroeder, A.W. MacGregor, and S. Abrams. 2002. Barley viability during storage: use of magnetic resonance as a potential tool to study viability loss. *Journal of Agriculture and Food Chemistry* 50(4): 667-676.

Haghighi, K, J. Irudayaraj, R.L. Stroshine, and S. Sokhansanj. 1990. Grain kernel drying simulation using the finite element method. *Transactions of the ASAE* 33(6): 1957-1965.

Haghighi, K. and L.J. Segerlind. 1988. Modeling simultaneous heat and mass transfer in an isotropic sphere – A finite element approach. *Transactions of the ASAE* 31(2):629-637.

Hahn, E.L. 1950. Spin echoes. *Physical Review* 80(4):580-594.

Hall, C.W., 1980. *Drying and storage of agricultural crops*. Westport, CT: AVI.

Hall, C.W., and J.H. Rodrigues-Aries. 1958. Applications of the Newton's equation to moisture removal from shelled corn at 40-140 F. *Journal of Agricultural Engineering Research* 3(4): 275-280.

Hills, B. 1995. Food processing: An MRI perspective. *Trends in Food Science and Technology* 6(4): 111-117.

Horigane, A.K., W.M.H.G. Engelaar, S. Maruyama, M. Yoshida, A. Okubo, and T. Nagata. 2001. Visualization of moisture distribution during development of rice caryopses (*Oryza sativa* L.) by nuclear magnetic resonance microimaging. *Journal of Cereal Science* 33(1): 105-114.

Hornak, J.P. 2006. The basics of MRI. Available at: http://www.cis.rit.edu/htbooks/mri/. Accessed 25 October 2006.

Hou, S. Q., E. J. Kendall, and G. M. Simpson. 1997. Water uptake and distribution in non-dormant and dormant wild oat (*Avena fatua* L.) caryopses. *Journal of Experimental Botany* 48(308): 683-692.

Hulbert, G.J., J. Bruce Litchfield, and S.J. Schmidt. 1995. Temperature mapping in carrot using T_1 weighted magnetic resonance imaging. *Journal of Food Science* 60(4): 780-785.

Hulbert, G.J., J. Bruce Litchfield, and S.J. Schmidt. 1997. Determination of convective heat transfer coefficients using a 2D MRI temperature mapping and finite element modeling. *Journal of Food Engineering* 34(2): 193-201.

Husain, A., C.S. Chen, and J.T. Clayton. 1973. Simultaneous heat and mass diffusion in biological materials. *Journal of Agricultural Engineering Research* 18(4):343-354.

Hustrulid, A., and A.M. Flikke. 1959. Theoretical drying curve for shelled corn. *Transactions of the ASAE* 2(1): 112-114.

Irudayaraj, J., K. Haghighi, and R.L. Sroshine. 1992. Finite element analysis of drying with application to cereal grains. *Journal of Agricultural Engineering Research* 53(3): 209-229.

Ishida, N., S. Naito, and H. Kano. 2004. Loss of moisture from harvested rice seeds on MRI. *Magnetic Resonance Imaging* 22(6): 871-875.

Ishida, N., T. Kibayashi, M. Koizumi and H. Kano. 1989. ^{1}H NMR imaging of tomato fruits. *Agricultural and Biological Chemistry* 53(9): 2363-2367.

Jayas, D.S., S. Cenkowski, S. Pabis, and W.E. Muir. 1991. Review of thin-layer drying and wetting equations. *Drying Technology* 9(3), 551-558.

Jayas, D.S., N.D.G. White, and W.E. Muir (Eds.). 1995. *Stored-Grain Ecosystems*. New York, NY: Marcel Dekker, Inc.

Jayas, D.S., and P.K. Ghosh. 2006. Preserving quality during grain drying and techniques for measuring grain quality. In *Proc. 9th International Working Conference on Stored Product Protection*, 969-981. I. Lorini, B. Bacaltchuk, H. Beckel, D. Deckers, E. Sunfeld, J.P. dos Santos, J.D. Biagi, J.C. Celaro, L.R. D'A. Faroni, L. de O.F. Bortolini, M.R. Sartori, M.C. Elias, R.N.C. Guedes, R.G. da Fonseca, and V.M. Scussel, eds. Campinas, Brazil: Brazilian Post-harvest Association.

Jenner, C.F., and G.P. Jones. 1990. Diffusion of water in the wheat grain: Nuclear magnetic resonance and radioisotopic methods provide complementary information. *Australian Journal of Plant Physiology* 17(2): 107-118.

Jenner, C.F., Y. Xia, C.D. Eccles, and P.T. Callaghan. 1988. Circulation of water within wheat grain revealed by nuclear magnetic resonance micro-imaging. *Nature* 336:6197, 399-402.

Jia, C.C., D.A. Sun, and C.W. Cao. 2000. Mathematical simulation of temperature and moisture fields within a grain kernel during drying. *Drying Technology* 18(6): 1305-1325.

Karunakaran, C., D.S. Jayas, and N.D.G. White. 2004. Mass determination of wheat kernels from X-ray images. Paper No. 043120. St. Joseph, MI: ASAE.

Kasai, M, A. Lewis, F. Marica, S. Ayabe, K. Hatae, and C.A. Fyfe. 2005. NMR imaging investigation of rice cooking. *Food Research International* 38(4): 403-410.

Koptyug, I.V., and R.Z. Sagdeev. 2002. Applications of NMR tomography to mass transfer studies. *Russian Chemical Reviews* 71(10): 789-835.

Kovács, A.J., and M. Neményi. 1999. Moisture gradient vector calculation as a new method for evaluating NMR images of corn (*Zea mays* L.) kernels during drying. *Magnetic Resonance Imaging* 17(7):1077-1082.

Lammertyn, J., T. Dresselaers, P. Van Hecke, P. Jancsók, M. Wevers, and B.M. Nicolaï. 2003. MRI and X-ray CT study of spatial distribution of core breakdown in 'Conference' pears. *Magnetic Resonance Imaging* 21(7): 805-815.

Lammertyn, J., T. Dresselaers, P. Van Hecke, P. Jancsók, M. Wevers, and B.M. Nicolaï. 2003. Analysis of the time course of core breakdown in 'Conference' pears by means of MRI and X-ray CT. *Postharvest Biology and Technology* 29(1): 19-28.

Liu, Q., and F.W. Bakker-Arkema. 2001. A model-predictive controller for grain drying. *Journal of Food Engineering* 49(4): 321-326.

Luikov, A.V. 1966. *Heat and mass transfer in capillary-porous bodies.* Oxford, UK: Pergammon Press.

MacMasters, M.M., D. Bradbury, and J.J.C. Hinton. 1964. Microscopic structure and composition of the wheat kernel. In *Wheat – Chemistry and Technology*, 55-110. I. Hlynka, ed. St. Paul, MN: Amercian Association of Cereal Chemists, Inc.

Manickavasagan, A., D.S. Jayas, and N.D.G. White. 2005. Thermal imaging to identify western Canadian wheat classes. Paper No. 056078. St. Joseph, MI: ASAE.

McCarthy, M.J., and K.L. McCarthy. 1994. Quantifying transport phenomena in food processing with nuclear magnetic resonance imaging. *Journal of the Science of Food and Agriculture* 65(3): 257-270.

McCarthy, M.J., and R.J. Kauten. 1990. Magnetic resonance imaging applications in food research. *Trends in Food Science and Technology* December: 134-139.

McCarthy, M.J., B. Zion, P. Chen, S. Ablett, A.H. Darke, and P.J. Lilliford. 1995. Diamagnetic susceptibility changes in apple tissue after bruising. *Journal of the Science of Food and Agriculture* 67(1): 13-20.

McCarthy, M.J., E. Perez, and M. Ozilgen. 1991. Model for transient moisture profiles of a drying apple slab using the data obtained with magnetic resonance imaging. *Biotechnology Progress* 7(6): 540-543.

McEntyre, E., R. Ruan, and R.G. Fulcher. 1998. Comparison of water absorption patterns in two barley cultivars, using magnetic resonance imaging. *Cereal Chemistry* 75(6):792-795.

Miketinac, M.J., S. Sokhansanj, and Z. Tutek. 1992. Determination of heat and mass transfer coefficients in thin layer drying of grain. *Transactions of the ASAE* 35(6): 1853-1858.

Miller, B. S., M. S. Lee, J. W. Hughes, and Y. Pomeranz. 1980. Measuring high moisture content of cereal grains by pulsed nuclear magnetic resonance. *Cereal Chemistry* 57(2): 126-129.

Misra, R.N., and J.H. Young. 1980. Numerical solution of simultaneous moisture diffusion and shrinkage during soybean drying. *Transactions of the ASAE* 23(5): 1277-1282.

Mohorič, A., F. Vergeldt, E. Gerkema, A. Jager, J. Duynhoven, G. Dalen, and H.V. As. 2004. Magnetic resonance imaging of single rice kernels during cooking. *Journal of Magnetic Resonance* 171(1): 157-162.

Montross, M.D., Bakker-Arkema, F.W., Hines, R.E., 1999. Moisture content variation and grain quality of corn dried in different high-temperature dryers. *Transactions of the ASAE* 42(2), 427-433.

Nellist, M.E., and D.M. Bruce. 1995. Heated-air grain drying. In *Stored-Grain Ecosystems*, 609-660. D.S. Jayas, N.D.G. White, W.E. Muir, eds. New York, NY: Marcel Dekker, Inc.

Neményi, M., I. Czaba, A. Kovacs, and T. Jani. 2000. Investigation of simultaneous heat and mass transfer within the maize kernels during drying. *Computers and Electronics in Agriculture* 26(2): 123-135.

Pabis, S., and S.M. Henderson. 1961. Grain drying theory –II. A critical analysis of the drying curve for shelled maize. *Journal of Agricultural Engineering Research* 6(4): 272-277.

Pabis, S., D.S. Jayas, and S. Cenkowski. 1998. *Grain Drying: Theory and Practice.* New York, NY: John Wiley & Sons, Inc.

Parde, S., D.S. Jayas, and N.D.G. White. 2003. Grain drying: a review. *Sciences des Aliments* 23(5-6):589-622.

Perez, E., R. Kauten, and M.J. McCarthy. 1989. Noninvasive measurement of moisture profiles during the drying of an apple. In: *Drying 89,* 149-156. A.S. Majumdar, ed. New York, NY: Hemisphere Publishing Co.

Pietrzak, L.N., J. Fregeau-Reid, B. Chatson, and B. Blackwell. 2002. Observations on water distribution in soybean seed during hydration processes using magnetic resonance imaging. *Canadian Journal of Plant Science* 82:513-519.

Pomeranz, Y., and D.B. Bechtel. 1978. Structure of cereal grains as related to end-use properties. In *Cereals'78: Better nutrition for the world's millions*: Proc. Sixth International Cereal and Bread Congress, 85-104. Y. Pomeranz, ed. St. Paul, MN: American Association of Cereal Chemists, Inc.

Pope, J.M., and V. Sarafis. 1990. NMR Microscopy. *Chemistry in Australia* July: 221-224.

Ranjan, R., J. Irudayaraj, and S. Jun. 2001. A three-dimensional control volume approach to modeling heat and mass transfer in food materials. *Transactions of the ASAE* 44(6): 1975-1982.

Ratković. S. 1987. Proton NMR of maize seed water: the relationship between spin-lattice relaxation time and water content. *Seed Science and Technology* 15: 147-154.

Ruan, R. R., and P. L. Chen. 1998. *Water in Foods and Biological Materials: A Nuclear Magnetic Resonance Approach*. Lancaster, PA: Technomic Publishing.

Ruan, R., and J.B. Litchfield. 1992. Determination of water distribution and mobility inside maize kernels during steeping using magnetic resonance imaging. *Cereal Chemistry* 69(1):13-17.

Ruan, R., J.B. Litchfield, and S.R. Eckhoff. 1992. Simultaneous and nondestructive measurement of transient moisture profiles and structural changes in corn kernels during steeping using microscopic nuclear magnetic resonance imaging. *Cereal Chemistry* 69(6):600-606.

Ruan, R., S.J. Schmidt, and A.R. Schimdt. 1991. Nondestructive measurement of transient moisture profiles and the moisture diffusion coefficient in a potato during drying and absorption by NMR imaging. *Journal of Food Process Engineering* 14(4): 297-313.

Ryniecki, A., D.S. Jayas, and W.E. Muir. 1993a. A generalized control-strategy for near-ambient drying of wheat under Canadian-prairie climate. *Transactions of the ASAE* 36(4): 1175-1183.

Ryniecki, A., W.E. Muir, and D.S. Jayas. 1993b. Optimization of control systems for near-ambient drying of wheat under maritime and continental climates. *Postharvest Biology and Technology* 2(3): 217-230.

Saito, K., T. Miki, S. Hayashi, H. Kajikawa, M. Shimada, Y. Kawate, T. Nishizawa, D. Ikegaya, N. Kimura, K. Takabatake, N. Sugiura, and M. Suzuki. 1996. Application of magnetic resonance imaging to non-destructive void detection in watermelon. *Cryogenics* 36(12): 1027-1031.

Schmidt, S.J., X. Sun, and J.B. Litchfield. 1996. Applications of magnetic resonance imaging in food science. *Critical Reviews in Food Science and Nutrition* 36(4):357-385.

Schrader, G.W., J.B. Litchfield, and S.J. Schimdt. 1992. Magnetic resonance imaging applications in the food industry. *Food Technology* Dec.77-83.

Segerlind, L.J. 1984. *Applied Finite Element Analysis*. 2nd ed. New York, NY: John Wiley and Sons, Inc.

Sharp, J.R. 1982. A review of low temperature drying simulation models. *Journal of Agricultural Engineering Research* 27(3): 169-190.

Simmonds, W.H.C., G.T. Ward, and E. McEwen. 1953. The drying of wheat grain. Part I: The mechanism of drying. *Transactions of the Institution of Chemical Engineers* 31: 265-278.

Simoneau, C., M.J. McCarthy, and J.B. German. 1993. Magnetic resonance imaging and spectroscopy for food systems. 1993. *Food Research International* 26(5): 387-398.

Sokhansanj, S., and R.J. Gustafson. 1980. Prediction of heat and mass transfer within a grain kernel – a finite element application. In: *Drying 80 vol. 2*, 229-232. A.S. Majumdar, ed. New York, NY: McGraw-Hill International Book Company.

Sokhansanj, S., and D.M. Bruce. 1987. A conduction model to predict grain temperature in grain drying simulation. *Transactions of the ASAE* 30(4): 1181-1184.

Sonego, L., R. Ben-Arie, J. Raynal, and J.C. Pech. 1995. Biochemical and physical evaluation of textural characteristics of nectarines exhibiting woolly breakdown: NMR imaging, X-ray computed tomography and pectin composition. *Postharvest Biology and Technology* 5(3): 187-198.

Song, H. and J.B. Litchfield. 1990. Nondestructive measurement of transient moisture profiles in ear corn during drying using NMR imaging. *Transactions of the ASAE* 33(4):1286-1290.

Song, H. P., J. B. Litchfield, and H. D. Morris. 1992. Three-dimensional microscopic MRI of maize kernels during drying. *Journal of Agricultural Engineering Research* 53(1): 51-69.

Song, H.P., S.R. Delwiche, and M.J. Line. 1998. Moisture distribution in a mature soft wheat grain by three-dimensional magnetic resonance imaging. *Journal of Cereal Science* 27(2): 191-197.

Stapley, A. G. F., P. J. Fryer, and L. F. Gladden. 1998. Diffusion and reaction in whole wheat grains during boiling. *AIChE Journal* 44(8): 1777-1789.

Stapley, A.G.F., M.H. Thomas, L.F. Gladden, and P.J. Fryer. 1997. NMR imaging of the wheat grain cooking process. *International Journal of Food Science and Technology* 32(5):355-375.

Stark, D. D., and W. G. Bradley. 1992. *Magnetic Resonance Imaging*. St. Louis, MO: Mosby-Year Book.

Steffe, J.F., and R.P. Singh. 1982. Diffusion coefficients for predicting rice drying behavior. *Journal of Agricultural Engineering Research* 27(6): 489-493.

Sun, D.W., and J.L. Woods. 1993. The moisture content/relative humidity equilibrium relationship of wheat – a review. *Drying Technology* 11(7): 1523-1551.

Sun, X., J.B. Litchfield and S.J. Schmidt. 1993. Temperature mapping in a model food gel using magnetic resonance imaging. *Journal of Food Science* 58(1): 168-172, 181.

Sun, X.Z., S.J. Schmidt and J.B. Litchfield. 1994. Temperature mapping in a potato using half Fourier transform MRI of diffusion. *Journal of Food Process Engineering* 17(4): 423-437.

Takeuchi, S., M. Fukuoka, Y. Gomi, M. Maeda, and H. Watanabe. 1997. An application of magnetic resonance imaging to the real-time measurement of the change of moisture profile in a rice grain during boiling. *Journal of Food Engineering* 33(1-2): 181-192.

Tollner, E. W., and Y. C. Hung. 1992. Low-resolution pulse magnetic resonance for measuring moisture in selected grains and kernels. *Journal of Agricultural Engineering Research* 53(3): 195-208.

Turhan, M., S. Gunasekaran, and B.P. Lamsal. 2001. Drying of gelatinized whole wheat. *Drying Technology* 19(2): 333-342.

Verstreken, E., P. Van Hecke, N. Scheerlinck, J. De Baerdemaeker, and B. Nicolai. 1998. Parameter estimation for moisture transport in apples with the aid of NMR imaging. *Magnetic Resonance in Chemistry* 36(3): 196-204.

Walde, S.G., K. Balaswamy, V. Velu, and D.G. Rao. 2002. Microwave drying and grinding characteristics of wheat (*Triticum aestivum*). *Journal of Food Engineering* 55(3): 271-276.

Walton, L.R., G.M. White, and I.J. Ross. 1988. A cellular diffusion-based drying model for corn. *Transactions of the ASAE* 31(1): 279-283.

Wang, C.Y., and P.C. Wang. 1992. Differences in nuclear magnetic resonance images between chilled and non-chilled zucchini squash. *Environmental Experimental Botany* 32(3): 213-219.

Wang, C.Y., and P.C. Wang. 1989. Nondestructive detection of core breakdown in 'Bartlett' pears with nuclear magnetic resonance imaging. *HortScience* 24(1): 106-109.

Wang, S.Y., P.C. Wang, and M. Faust. 1988. Non-destructive detection of watercore in apple with nuclear magnetic resonance imaging. *HortScience* 35(3-4): 227-234.

Watanabe, H., and M. Fukuoka. 1992. Measurement of moisture diffusion in foods using pulsed field gradient NMR. *Trends in Food Science and Technology* 3(August/September): 211-215.

Watson, E.L., and V.K. Bhargava. 1974. Thin layer drying studies on wheat. *Canadian Agricultural Engineering* 16(1): 18-22.

Williamson, B., A.B. Goodman, and J.A. Chudek. 1991. Nuclear magnetic resonance (NMR) microimaging of ripening red raspberry fruits. *New Phytologist* 120(1): 21-28.

Wu, B., W. Yang, and C. Jia. 2004. A three-dimensional numerical simulation of transient heat and mass transfer inside a single rice kernel during the drying process. *Biosystems Engineering* 87(2): 191-200.

Yang, W. C.C. Jia, T.J. Siebenmorgen, T.A. Howell, and A.G. Cnossen. 2002. Intra-kernel moisture responses of rice to drying and tempering treatments by finite element simulation. *Transactions of the ASAE* 45(4): 1037-1044.

Zeng, X.S., R.R. Ruan, R.G. Fulcher, and P. Chen. 1996. Evaluation of soybean seedcoat cracking during drying: Part II. Using MRI. *Drying Technology* 14(7 and 8): 1595-1623.

Zion, B., P. Chen, and M.J. McCarthy. 1995. Detection of bruises in magnetic resonance images of apples. *Computers and Electronics in Agriculture* 13(4):289-299.

MRI EXPERIMENTAL SET UP

Following figures show the MRI set up used in this study.

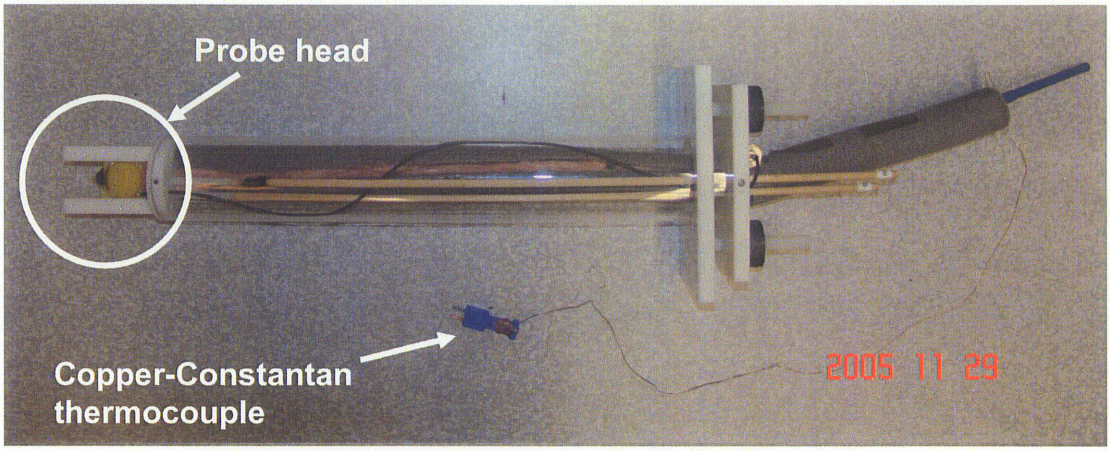

(a) The home built magnetic resonance imaging probe.

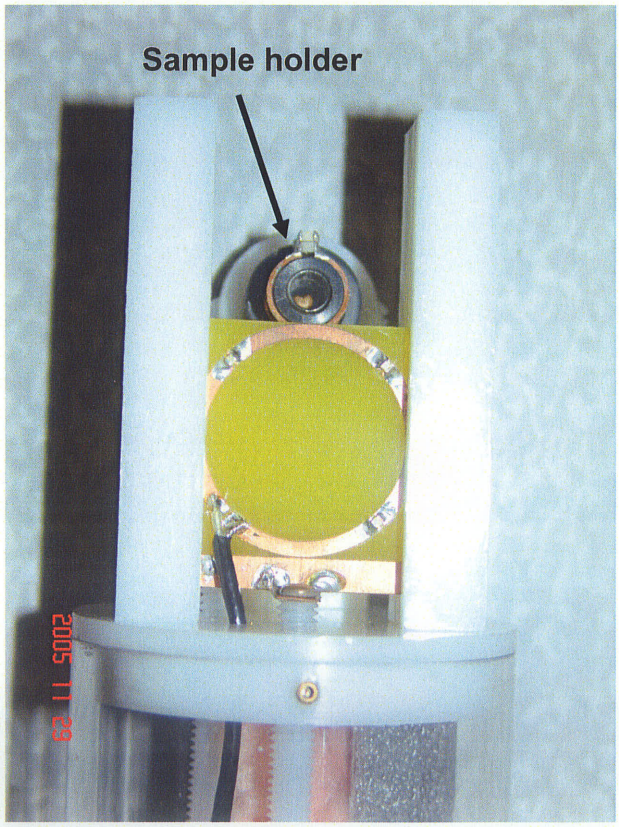

(b) Sample holder in the magnetic resonance imaging probe.

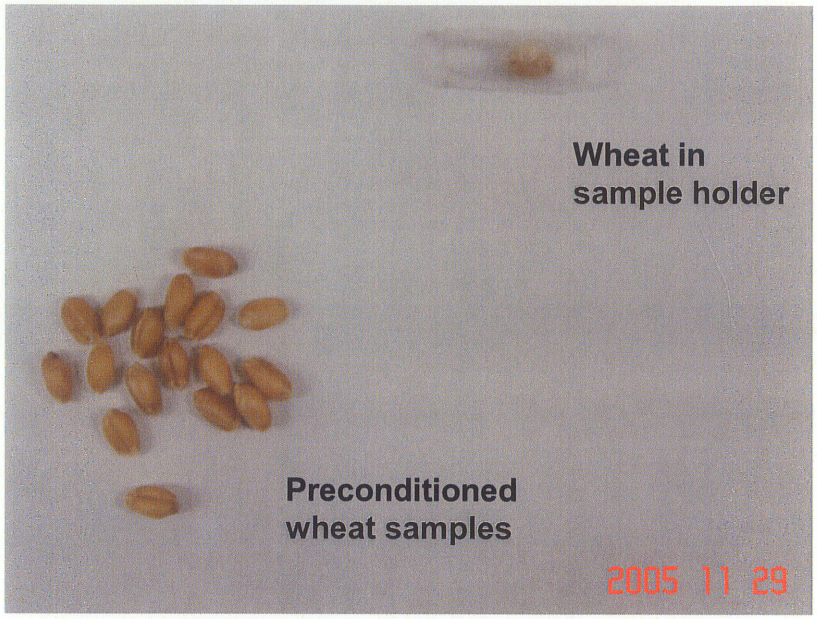

(c) Wheat samples prepared for the magnetic resonance imaging study.

(d) 11.7 T (500 Hz) Magnex (Magnex Scientific, Ltd., Yarnton, UK) vertical bore magnet used in this study.

(e) Drying apparatus.

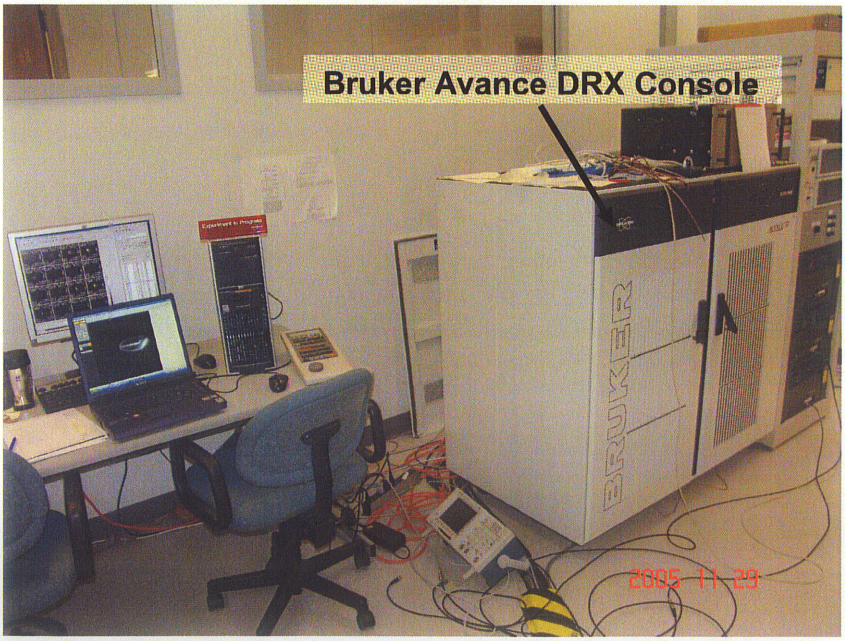

(f) Magnetic resonance image acquisition and analysis.

Figure A.1 Magnetic resonance imaging experimental set up.

BRUKER BVT-1000 VARIABLE TEMPERATURE AND FLOW CONTROLLER UNIT

Figure B.1 Bruker BVT-1000 variable temperature and flow controller unit.

Table B.1 Specifications of Bruker BVT-1000 variable temperature and flow controller unit.

Temperature sensor	Cu-Constantan
Temperature ranges	64-575 K
Temperature calibration	$\leq \pm$ 0.7 K for T 233 K
Accuracy	$\leq \pm$ 0.5 K for T 233 K
Temperature stability at sample	$\pm$ 0.1 K
Temperature control at sensor	$\pm$ 0.1 K
Temperature control at sample (in the range from 170 to 400 K)	$\leq \pm$ 0.3 K
Maximum settling time (for 10 K steps)	3 min
Overshoot (steps $\geq$ 10 K)	$\leq$ 8 K depending on: temperature, flow rate and probe head
Heat exchange gas	Air flow high temperatures N_2 for low temperatures
Flow rate	Air = 100 to 1600 l h^{-1} N_2 = 50 to 1300 l h^{-1}
Power of regulation heater	0-300 W
Power of liquid nitrogen heater	0-150 W
Power requirements	220 V/ 50-60 Hz, 400 VA
Dimensions	(150 × 320 × 480) mm
Weight	30 kg
Ambient temperature range	-30 °C to 60 °C

500 MHz VERTICAL VOLUME COIL SET-UP FOR GRAIN IMAGING

The probe for grain MR imaging incorporates holder including thermostat system, thermocouple and a Helmholtz RF coil. Total length of the set-up is about 650 mm, inner diameter of the resonator is approximately 7 mm. Sliding matching network is employed to connect resonator with TR switch. Precise tuning is achieved by another sliding paddle. Unloaded Q value is about 300.

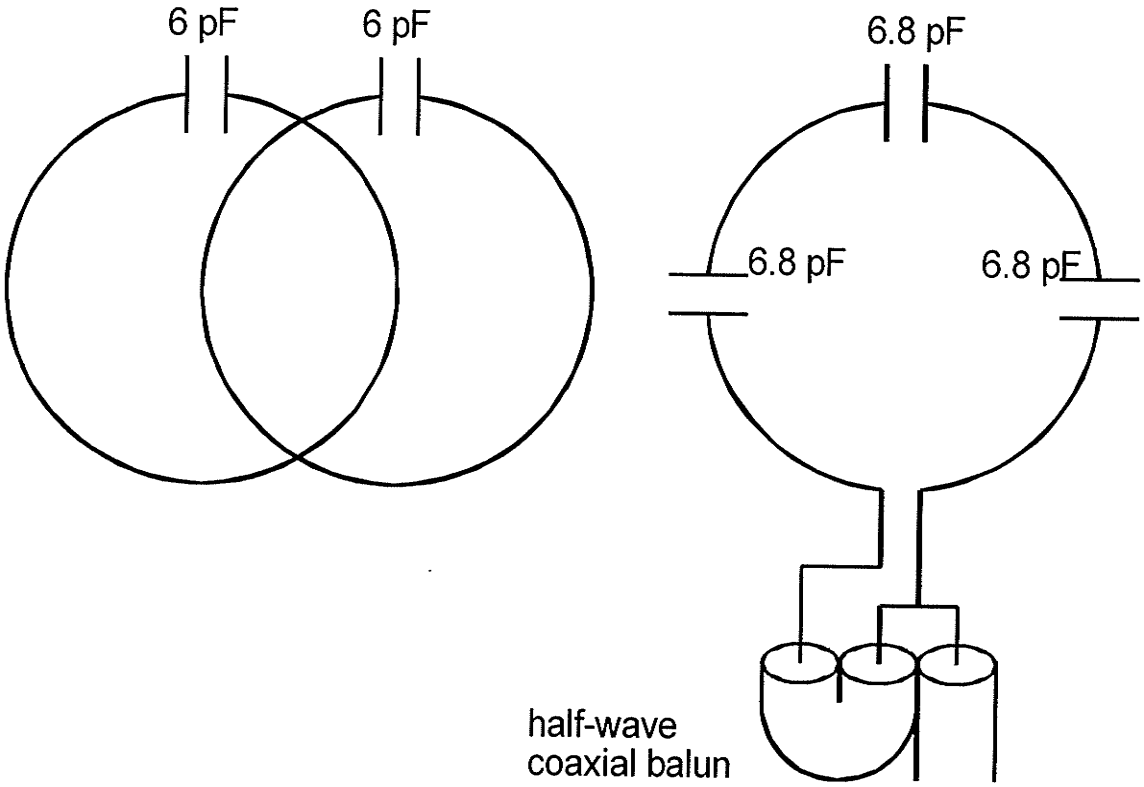

Figure C.1 Schematic of the radio-frequency (RF) coil.

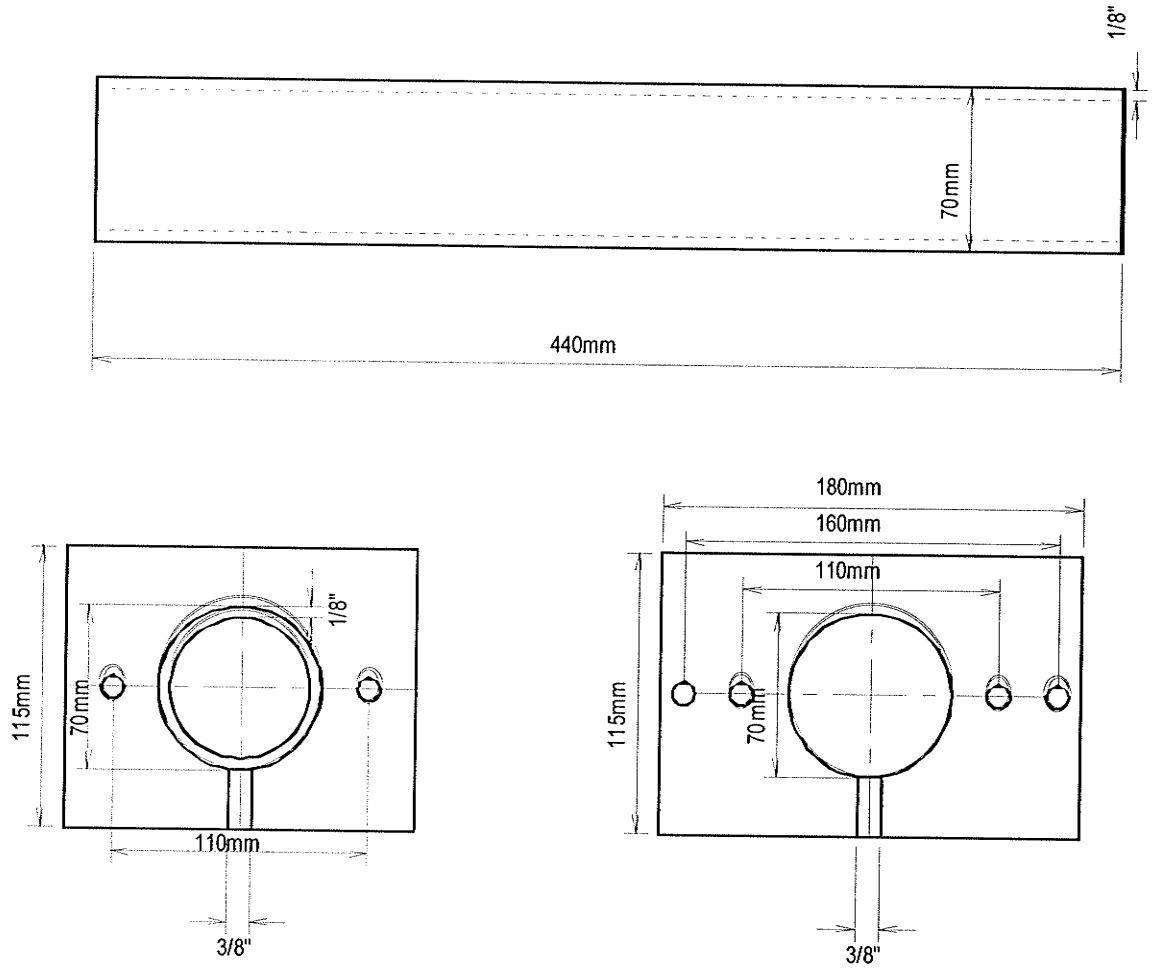

Figure C.2 Mechanical components of the holder.

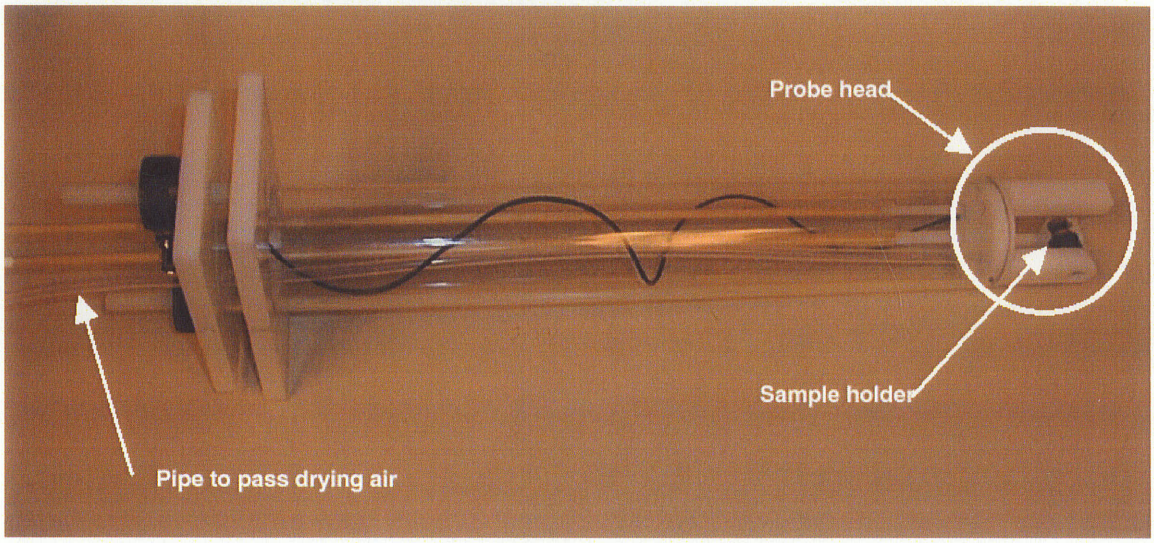

Figure C.3 Picture of the set-up.

IMAGE REGISTRATION DATA ANALYSIS

ImageReg50C

2D multimodal registration maximizing mutual information between test and reference images

multimodal method was used because images have different intensities.

images (128 × 64) were not zero-filled.

slice #5 was extracted from all 24 images, it was used for 2D registration

file slice5-series contains 24 images of this slice

image #8 in the above file (corresponding to slice #5 of 17.mar) was used as a reference

all other slices were registered against it

	mutual information	
image	initial	after diffusion registration
0	0.25048973	0.26854497
1	0.25182509	0.26488927
2	0.25148568	0.26642951
3	0.26345287	0.27660567
4	0.25928211	0.27233862
5	0.25660806	0.26561209
6	0.25041722	0.25338026
7	0.53399243	0.53399243
8	0.24401380	0.25289810
9	0.23402726	0.24394793
10	0.22162999	0.22807190
11	0.20714100	0.21079488
12	0.20614996	0.21114189
13	0.20131186	0.20834212
14	0.19077360	0.20032703
15	0.17458794	0.18334780
16	0.17101378	0.18031841
17	0.15939321	0.16646810
18	0.16467521	0.17450329
19	0.15358060	0.16544119
20	0.14561204	0.15732151
21	0.13979598	0.14960588
22	0.14413237	0.15211772
23	0.14023898	0.15034194

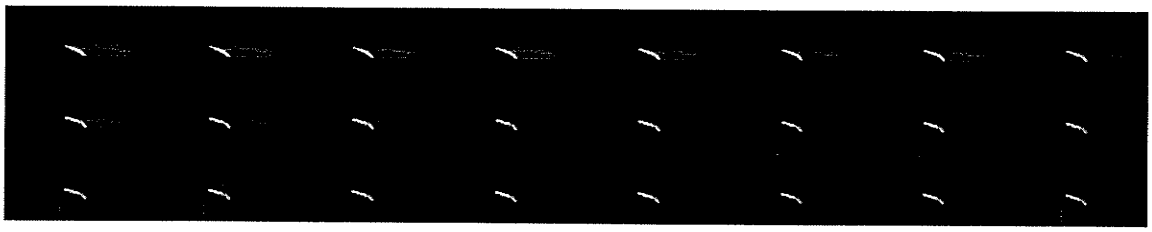

Figure C.4 Unregistered images, all images are in the same intensity scales.

Figure C.5 Unregistered images, all images are in the same intensity scales.

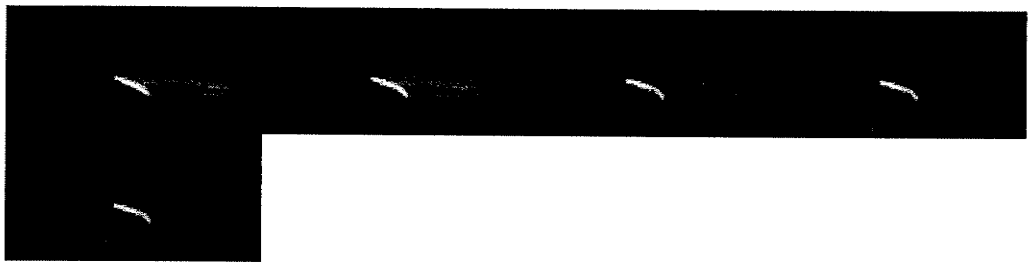

Figure C.6 Unregistered image slices of every 1h interval drying.

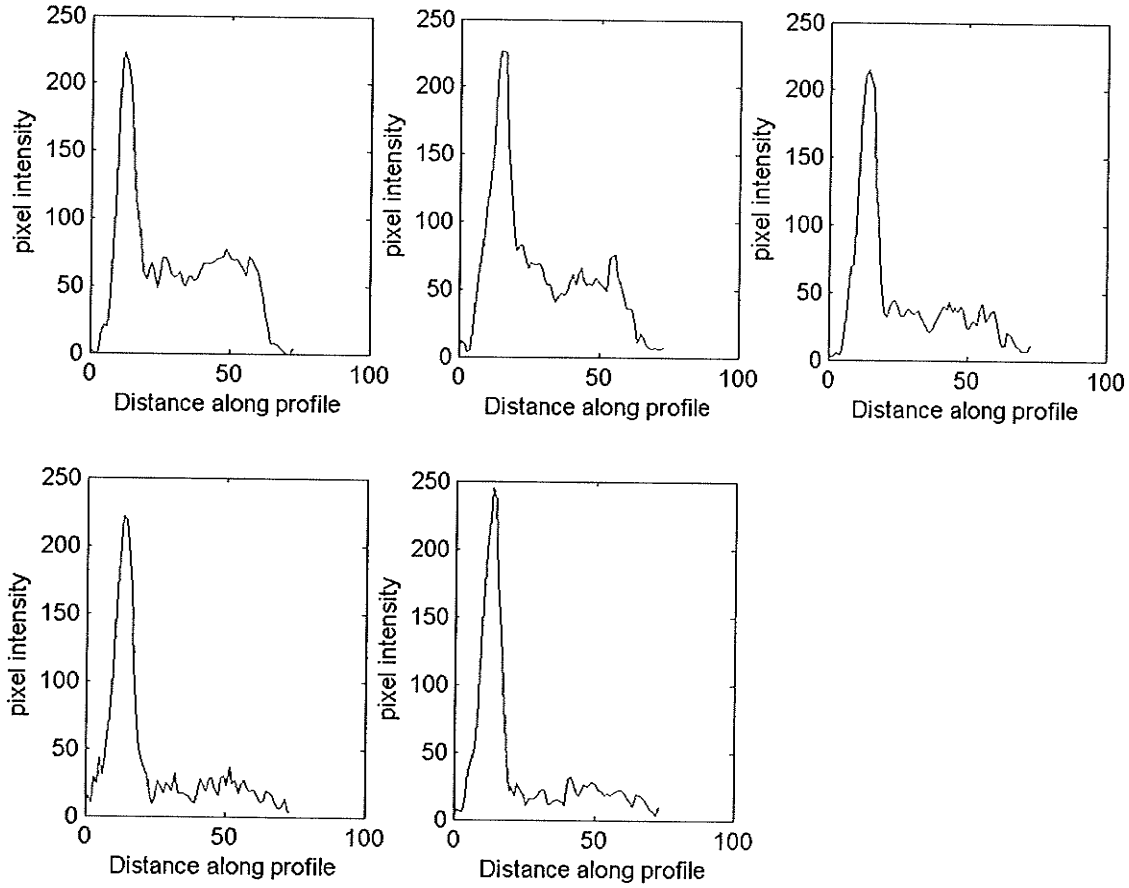

Figure C.7a Intensity profiles of the unregistered images of the wheat kernel at 1h drying interval data. Profiles along a chosen horizontal line segment [48.1616, 37.5272; 120.863, 40.2341].

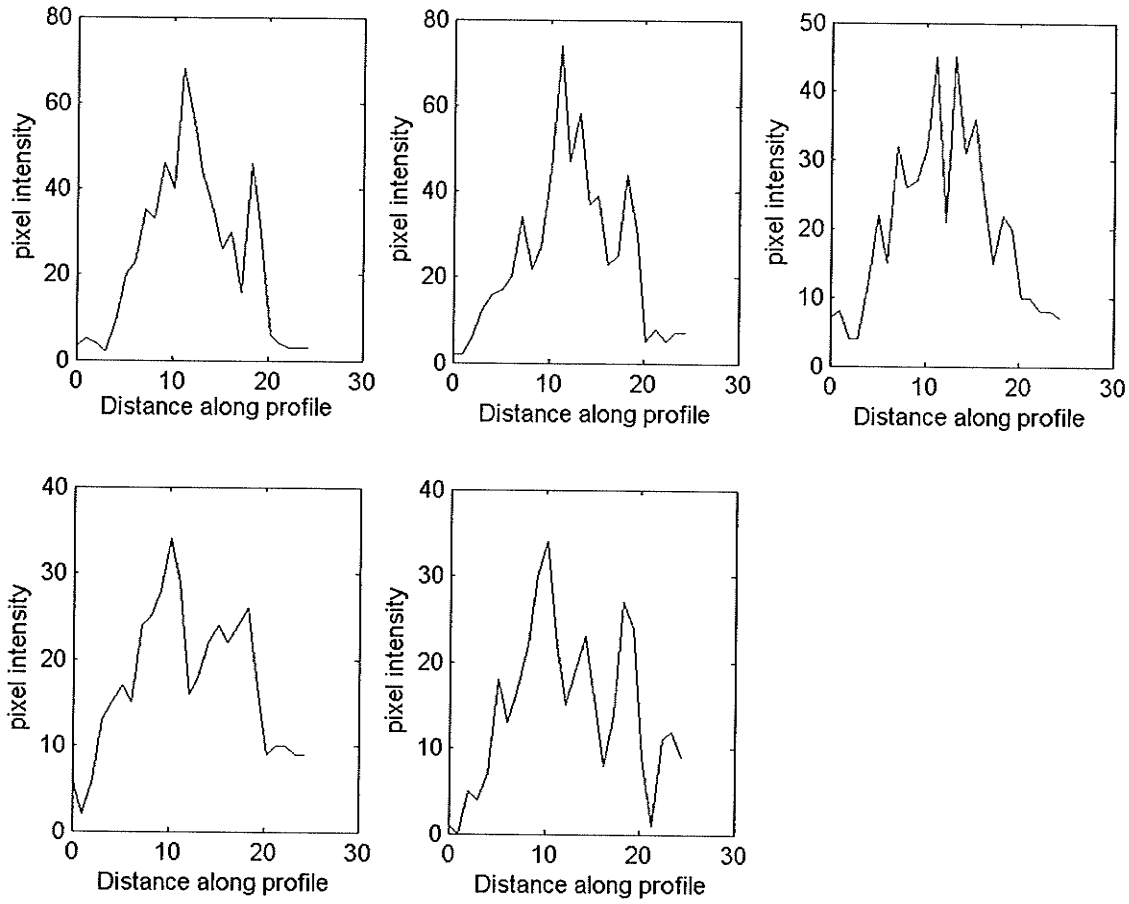

Figure C.7b Intensity profiles of the unregistered images of the wheat kernel at 1h drying interval data. Profiles along a chosen vertical line segment [83.352, 26.8927; 86.0589, 51.0619].

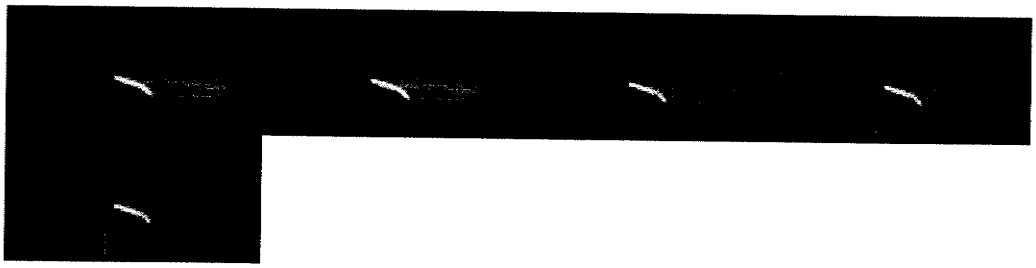

Figure C.8 Registered image slices of every 1h interval drying.

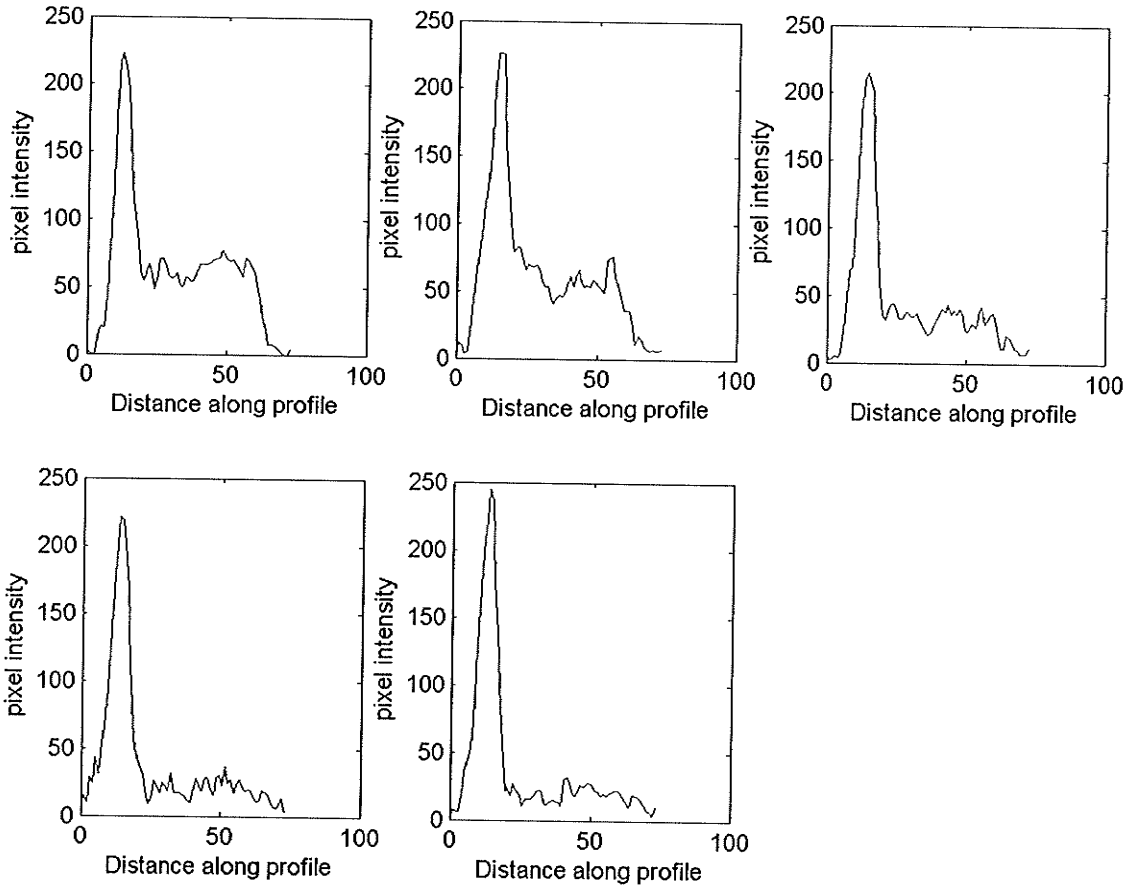

Figure C.8a Intensity profiles of the registered images of the wheat kernel at 1h drying interval data. Profiles along a chosen horizontal line segment [48.1616, 37.5272; 120.863, 40.2341].

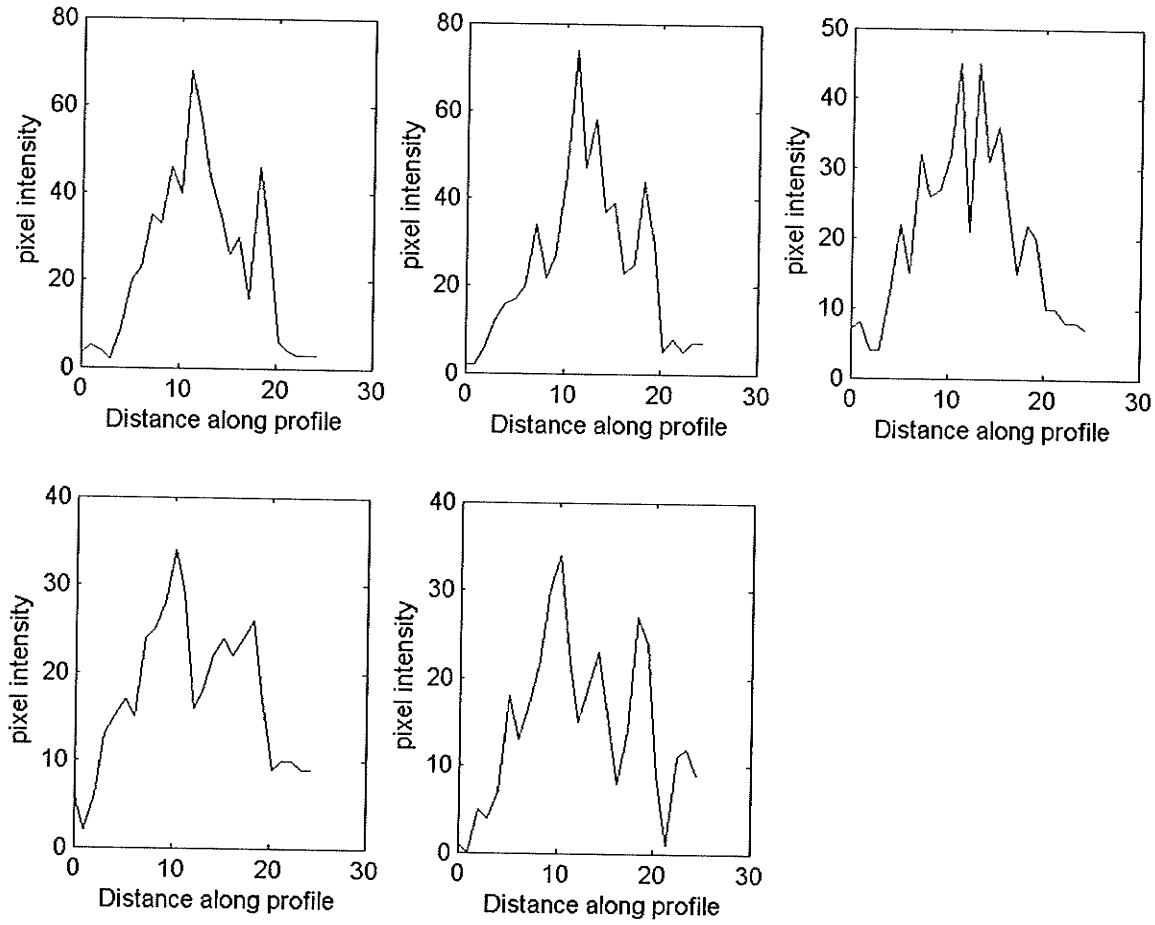

Figure C.8b Intensity profiles of the registered images of the wheat kernel at 1h drying interval data. Profiles along a chosen vertical line segment [83.352, 26.8927; 86.0589, 51.0619].

Table D.1 parameters used for T_2 determination (Fig. 3.3).

T_x-Attenuator - 0 (T_{xo})	37.2 dB
T_x-Attenuator – 1 (T_{x1})	31.2 dB
Spectral width	200 kHz
TR	1 s
TE	3.65 ms
Total experimental time	35 min 4 s
Excitation pulse	1000 µs
Ref pulse	1000 µs
Number of average	16
Number of echo images	8
Number of echoes/image	1
Number of echoes	8
Field-of-view (FOV)	1 cm
Number of slices	1
Slice thickness	5096 Hz
Basic frequency	500.5076967 MHz

Table D.2 Image intensities for developing Figure 3.3 for T_2 determination.

Wheat Components	TE (ms)	Pixel values (Observed)								Pixel values (Predicted)*
		Replications							Average	
		1	2	3	4	5	6	7		
Germ	0	--	--	--	--	--	--	--	--	238
	3.65	119	158	255	218	208	152	187	185	166
	7.3	44	74	118	104	96	65	87	84	116
	10.95	50	70	130	100	79	66	75	83	81
	14.6	27	43	79	63	52	45	46	52	57
	18.25	33	48	86	64	47	43	44	54	40
	21.9	23	30	48	37	29	29	25	33	28
	25.55	24	33	54	39	30	30	25	35	19
	29.2	14	19	27	20	17	19	12	19	13
Pericarp	0	--	--	--	--	--	--	--	--	184
	3.65	202	201	172	75	75	78	154	134	129
	7.3	69	104	58	32	44	42	58	58	90
	10.95	68	66	56	20	21	28	40	43	63
	14.6	34	42	26	16	18	21	22	26	44
	18.25	45	37	29	16	13	17	17	26	31
	21.9	23	35	14	9	12	13	12	18	21
	25.55	33	22	19	10	7	16	14	18	15
	29.2	17	22	13	11	8	11	10	14	10
Endosperm	0	--	--	--	--	--	--	--	--	166
	3.65	60	50	42	53	71	44	51	53	52
	7.3	16	13	10	10	15	7	13	12	16
	10.95	7	5	4	11	18	8	10	9	5
	14.6	4	3	2	6	10	8	9	6	2
	18.25	2	2	1	4	10	6	3	4	1
	21.9	2	2	1	4	9	6	1	4	0
	25.55	2	1	1	1	5	3	1	2	0
	29.2	1	1	1	3	3	2	2	2	0

*Germ: $I_i = 238.24 \exp(-0.0984 \cdot TE)$; Pericarp: $I_i = 184.33 \exp(-0.132 \cdot TE)$;
Endosperm: $I_i = 166.21 \exp(-0.3174 \cdot TE)$

PROTOCOLS AND STEPS IN PARAVISION V.2.1.1/V. 3.0.2 USED FOR MAGNETIC RESONANCE IMAGING

1. POSITION

FOV = 2 cm

T_{xo} = ~ 36.0 dB

2. ONE PULSE

Offset = 2500

2.1 ACQ. → Auto SHIM

2.2 Set off Freq01 = 0.0

ACQ. → Auto SF

Lock off

Write Config. Freq.

Set basic Freq.

3. Clone Scan → Load Scan protocol

Protocol: GEFI

T_{xo} = 46.0 dB

Click 'GSP'

Digitizer filling = ~ 40% (Receiver Gain)

Click 'GOP'

4. Clone Scan → Load Scan Protocol

Protocol: GEFI_AXIAL

Click 'GSP'

Digitizer filling = ~ 40% (Receiver Gain)

Click 'GOP'

5. Clone Scan → Load Scan Protocol

Protocol: MSME_MOD

Load Reference: GEFI_AXIAL

T_{xo} = 46.4 or 43.0 dB

T_{x1} = 40.4 or 37.0 dB

Click 'GSP'

Digitizer filling = ~ 60% (Receiver Gain)

Click 'GOP'

6. Clone Scan → Load Scan Protocol

Protocol: BLIP_MOD

Load Reference: GEFI_AXIAL

T_{xo} = 36.4 or 33.8 dB

T_{x1} = 36.4 or 33.8 dB

Average = 6

Number of Echoes per image = 1

Image acquisition time = 10 min 18 s

Click 'GSP'

Digitizer filling = ~ 60% (Receiver Gain)

Click 'GOP'

7. Clone Scan 24 times

8. Plug in the dryer assembly and wait until the BVT-1000 Unit indicates the desired temperature

9. Enable Macro

Other associated parameters for the MR imaging can be found in any of the Chapters 3 to 6.

RAW DATA USED IN CHAPTER 3

Table F.1 Data for drying curves in terms of magnetic resonance image signal amplitude vs. drying time obtained from a series of two-dimensional magnetic resonance image slices (slice 6) of a whole wheat kernel (average moisture content approximately 20% w.b.) at 40°C drying temperature (Fig. 3.7a).

Wheat components	Drying time (min)	MRI signal amplitude (arbitrary units) Collected at randomly selected pixels on the wheat components (Replications)											Average
Germ	0	180	242	255	234	182	151	155	--	--	--	--	200
	30	172	215	215	218	157	--	--	--	--	--	--	195
	60	204	238	216	171	213	115	--	--	--	--	--	193
	90	190	206	214	210	186	122	--	--	--	--	--	188
	120	176	233	150	172	196	--	--	--	--	--	--	185
	150	181	207	172	240	235	123	135	--	--	--	--	185
	180	191	185	206	216	160	141	--	--	--	--	--	183
	210	180	201	216	226	137	146	--	--	--	--	--	184
	240	185	167	219	174	212	126	--	--	--	--	--	181
Endosperm	0	74	88	80	101	96	93	86	111	90	--	--	91
	30	76	64	60	84	81	91	92	100	76	91	--	82
	60	86	87	76	63	67	67	75	--	--	--	--	74
	90	65	47	51	46	43	51	81	64	81	69	73	61
	120	49	42	44	49	55	49	62	69	56	--	--	53
	150	49	31	44	45	33	40	43	48	44	--	--	42
	180	33	34	45	38	44	37	42	44	51	44	37	41
	210	38	20	34	36	24	42	35	38	33	47	--	35
	240	35	35	36	32	22	34	35	32	26	19	--	31

Table F.2 Data for drying curves in terms of magnetic resonance image signal amplitude vs. drying time obtained from a series of two-dimensional magnetic resonance image slices (slice 6) of a whole (intact) wheat kernel (average moisture content approximately 20% w.b.) at 50°C drying temperature (Fig. 3.7b).

Wheat components	Drying time (min)	MRI signal amplitude (arbitrary units)											
		Collected at randomly selected pixels on the wheat components (Replications)											Average
Germ	0	214	240	205	203	--	--	--	--	--	--	--	216
	30	244	173	238	227	196	176	--	--	--	--	--	209
	60	217	210	216	182	180	--	--	--	--	--	--	201
	90	197	168	194	237	215	162	173	--	--	--	--	192
	120	180	161	245	214	150	--	--	--	--	--	--	190
	150	170	211	209	177	182	--	--	--	--	--	--	190
	180	143	141	237	232	202	177	144	--	--	--	--	182
	210	143	224	157	180	188	--	--	--	--	--	--	178
	240	149	221	170	158	--	--	--	--	--	--	--	175
Endosperm	0	35	40	35	36	26	27	23	24	24	--	--	30
	30	36	29	23	25	27	34	31	27	--	--	--	29
	60	25	28	26	28	30	27	26	29	--	--	--	27
	90	26	26	27	26	22	14	24	21	24	18	--	23
	120	21	24	18	14	24	24	24	28	--	--	--	22
	150	24	16	20	14	20	24	20	16	7	--	--	18
	180	16	19	18	20	14	18	13	16	20	23	16	18
	210	15	18	25	18	17	12	17	12	18	16	--	17
	240	17	17	14	20	20	15	7	16	16	--	--	16

Table F.3 Data for drying curves in terms of magnetic resonance image signal amplitude vs. drying time obtained from a series of two-dimensional magnetic resonance image slices (slice 5) of a mechanically scarified wheat kernel (average moisture content approximately 64% w.b.) at 40°C drying temperature (Fig. 3.12a).

Wheat components	Drying time (min)	MRI signal amplitude (arbitrary units)													
		Collected at randomly selected pixels on the wheat components (Replications)													Average
Germ	0	230	232	181	159	241	--	--	--	--	--	--	--	--	216
	30	222	200	245	161	221	--	--	--	--	--	--	--	--	209
	60	183	101	169	255	--	--	--	--	--	--	--	--	--	201
	90	225	180	118	85	64	105	--	--	--	--	--	--	--	192
	120	217	235	195	185	149	133	--	--	--	--	--	--	--	190
	150	205	237	235	187	105	--	--	--	--	--	--	--	--	190
	180	199	177	223	235	99	162	--	--	--	--	--	--	--	182
	210	198	223	212	99	121	--	--	--	--	--	--	--	--	178
	240	209	239	239	124	196	132	--	--	--	--	--	--	--	175
Endosperm	0	38	22	18	24	30	43	28	29	40	37	31	41	42	33
	30	53	17	22	36	63	36	--	--	--	--	--	--	--	38
	60	32	14	32	27	40	30	42	--	--	--	--	--	--	31
	90	42	18	36	33	60	75	--	--	--	--	--	--	--	44
	120	31	47	71	57	75	83	--	--	--	--	--	--	--	61
	150	57	17	42	55	60	55	--	--	--	--	--	--	--	48
	180	31	17	46	41	38	53	46	--	--	--	--	--	--	39
	210	18	18	27	29	40	24	29	--	--	--	--	--	--	26
	240	38	15	28	28	25	25	17	--	--	--	--	--	--	25

Table F.4 Data for drying curves in terms of magnetic resonance image signal amplitude vs. drying time obtained from a series of two-dimensional magnetic resonance image slices (slice 6) of a mechanically scarified wheat kernel (average moisture content approximately 64% w.b.) at 50°C drying temperature (Fig. 3.12b).

Wheat components	Drying time (min)	MRI signal amplitude (arbitrary units)											
		Collected at randomly selected pixels on the wheat components (Replications)											Average
Germ	0	204	234	181	238	248	--	--	--	--	--	--	216
	30	255	165	124	193	125	--	--	--	--	--	--	209
	60	167	165	154	144	171	--	--	--	--	--	--	201
	90	188	128	149	169	--	--	--	--	--	--	--	192
	120	144	158	182	194	--	--	--	--	--	--	--	190
	150	147	158	121	250	167	--	--	--	--	--	--	190
	180	197	208	204	221	218	224	206	--	--	--	--	182
	210	165	176	155	204	255	187	--	--	--	--	--	178
	240	195	170	222	168	195	233	235	178	--	--	--	175
Endosperm	0	35	40	35	36	26	27	23	24	24	--	--	30
	30	36	29	23	25	27	34	31	27	--	--	--	29
	60	25	28	26	28	30	27	26	29	--	--	--	27
	90	26	26	27	26	22	14	24	21	24	18	--	23
	120	21	24	18	14	24	24	24	28	--	--	--	22
	150	24	16	20	14	20	24	20	16	7	--	--	18
	180	16	19	18	20	14	18	13	16	20	23	16	18
	210	15	18	25	18	17	12	17	12	18	16	--	17
	240	17	17	14	20	20	15	7	16	16	--	--	16

Table F.5 Data for drying curves in terms of magnetic resonance image signal amplitude vs. drying time obtained from a series of two-dimensional magnetic resonance image slices (slice 6) of a germ-removed wheat kernel (average moisture content approximately 37% w.b.) at 40 and 50°C drying temperature (Fig. 3.13).

Drying temperature (°C)	Drying time (min)	MRI signal amplitude (arbitrary units)												
		Collected at randomly selected pixels on the wheat components (Replications)												Average
40	0	160	179	185	173	162	147	148	179	194	--	--	--	171
	30	107	139	210	198	157	116	146	203	194	--	--	--	170
	60	71	173	207	218	156	166	129	235	106	--	--	--	174
	90	101	136	140	195	137	148	166	210	164	156	--	--	161
	120	167	157	151	146	137	141	--	--	--	--	--	--	146
	150	70	108	149	174	149	136	184	171	172	129	--	--	152
	180	77	147	177	149	118	154	174	144	57	158	--	--	142
	210	82	138	179	174	156	150	152	129	122	91	95	--	139
	240	71	159	168	106	156	149	77	140	148	49	163	99	129
50	0	64	129	118	108	110	131	149	--	--	--	--	--	124
	30	34	40	49	112	120	131	--	--	--	--	--	--	90
	60	40	51	46	76	135	105	99	--	--	--	--	--	85
	90	23	31	46	59	56	117	109	168	--	--	--	--	84
	120	43	41	38	13	161	25	115	--	--	--	--	--	66
	150	27	139	41	14	8	76	25	48	--	--	--	--	50
	180	46	10	27	41	24	45	--	--	--	--	--	--	29
	210	27	38	27	24	26	17	29	--	--	--	--	--	27
	240	17	16	5	24	5	17	23	--	--	--	--	--	15

RAW DATA USED IN CHAPTER 5

Table G.1a Data for drying curves of intact wheat kernels during drying at 30°C obtained from the magnetic resonance images (Fig. 5.8).

Wheat components	Drying time (min)	Averaged local normalized image intensity (I)			Intensity ratio (I/I_o)			ln (I/I_o)			
		Rep. 1	Rep. 2	Rep. 3	Rep. 1	Rep. 2	Rep. 3	Rep. 1	Rep. 2	Rep. 3	Average
Endosperm	0	14.30	5.69	22.60	1.00	1.00	1.00	0.00	0.00	0.00	0.00
	30	13.60	5.85	21.80	0.95	1.03	0.96	-0.05	0.03	-0.04	-0.02
	60	13.10	4.53	19.80	0.92	0.80	0.88	-0.09	-0.23	-0.13	-0.15
	90	12.80	4.10	16.10	0.90	0.72	0.71	-0.11	-0.33	-0.34	-0.26
	120	10.90	3.04	13.20	0.76	0.53	0.58	-0.27	-0.63	-0.54	-0.48
	150	8.80	2.59	10.30	0.62	0.46	0.46	-0.49	-0.79	-0.79	-0.69
	180	7.57	1.81	7.90	0.53	0.32	0.35	-0.64	-1.15	-1.05	-0.94
	210	5.98	1.42	6.68	0.42	0.25	0.30	-0.87	-1.39	-1.22	-1.16
	240	5.05	1.13	5.37	0.35	0.20	0.24	-1.04	-1.62	-1.44	-1.36
Embryo	0	65.20	18.40	73.20	1.00	1.00	1.00	0.00	0.00	0.00	0.00
	30	66.30	19.80	65.80	1.02	1.08	0.90	0.02	0.07	-0.11	-0.01
	60	56.40	20.30	49.00	0.87	1.10	0.67	-0.14	0.10	-0.40	-0.15
	90	56.00	17.60	34.60	0.86	0.96	0.47	-0.15	-0.04	-0.75	-0.32
	120	50.10	17.20	29.00	0.77	0.93	0.40	-0.26	-0.07	-0.93	-0.42
	150	42.50	17.50	25.60	0.65	0.95	0.35	-0.43	-0.05	-1.05	-0.51
	180	37.00	15.60	26.00	0.57	0.85	0.36	-0.57	-0.17	-1.04	-0.59
	210	32.10	16.30	23.40	0.49	0.89	0.32	-0.71	-0.12	-1.14	-0.66
	240	28.70	14.60	22.70	0.44	0.79	0.31	-0.82	-0.23	-1.17	-0.74

Table G.1b Data for drying curves of intact wheat kernels during drying at 40°C obtained from the magnetic resonance images (Fig. 5.8).

Wheat components	Drying time (min)	Averaged local normalized image intensity (I)			Intensity ratio (I/I_o)			ln (I/I_o)			
		Rep. 1	Rep. 2	Rep. 3	Rep. 1	Rep. 2	Rep. 3	Rep. 1	Rep. 2	Rep. 3	Average
Endosperm	0	4.48	9.06	20.90	1.00	1.00	1.00	0.00	0.00	0.00	0.00
	30	3.43	8.05	18.00	0.77	0.89	0.86	-0.27	-0.12	-0.15	-0.18
	60	2.42	8.50	12.40	0.54	0.94	0.59	-0.62	-0.06	-0.52	-0.40
	90	1.99	6.05	8.15	0.44	0.67	0.39	-0.81	-0.40	-0.94	-0.72
	120	1.34	3.57	6.36	0.30	0.39	0.30	-1.21	-0.93	-1.19	-1.11
	150	1.03	2.49	4.35	0.23	0.27	0.21	-1.47	-1.29	-1.57	-1.44
	180	0.74	1.69	3.03	0.17	0.19	0.14	-1.80	-1.68	-1.93	-1.80
	210	0.60	1.49	2.13	0.13	0.16	0.10	-2.01	-1.81	-2.28	-2.03
	240	0.58	1.33	1.81	0.13	0.15	0.09	-2.04	-1.92	-2.45	-2.14
Embryo	0	17.60	41.60	64.30	1.00	1.00	1.00	0.00	0.00	0.00	0.00
	30	12.20	29.50	46.10	0.69	0.71	0.72	-0.37	-0.34	-0.33	-0.35
	60	10.20	25.00	23.10	0.58	0.60	0.36	-0.55	-0.51	-1.02	-0.69
	90	11.40	18.90	22.50	0.65	0.45	0.35	-0.43	-0.79	-1.05	-0.76
	120	11.50	16.40	14.60	0.65	0.39	0.23	-0.43	-0.93	-1.48	-0.95
	150	11.90	15.40	16.30	0.68	0.37	0.25	-0.39	-0.99	-1.37	-0.92
	180	9.86	15.50	14.70	0.56	0.37	0.23	-0.58	-0.99	-1.48	-1.01
	210	9.23	15.10	16.30	0.52	0.36	0.25	-0.65	-1.01	-1.37	-1.01
	240	10.70	16.40	15.60	0.61	0.39	0.24	-0.50	-0.93	-1.42	-0.95

Table G.1c Data for drying curves of intact wheat kernels during drying at 50°C obtained from the magnetic resonance images (Fig. 5.8).

Wheat components	Drying time (min)	Averaged local normalized image intensity (I)			Intensity ratio (I/I_o)			ln (I/I_o)			
		Rep. 1	Rep. 2	Rep. 3	Rep. 1	Rep. 2	Rep. 3	Rep. 1	Rep. 2	Rep. 3	Average
Endosperm	0	3.49	4.68	20.40	1.00	1.00	1.00	0.00	0.00	0.00	0.00
	30	2.37	2.79	14.00	0.68	0.60	0.69	-0.39	-0.52	-0.38	-0.43
	60	1.36	1.49	10.50	0.39	0.32	0.51	-0.94	-1.14	-0.66	-0.92
	90	0.77	1.06	5.94	0.22	0.23	0.29	-1.51	-1.49	-1.23	-1.41
	120	0.55	0.70	3.48	0.16	0.15	0.17	-1.85	-1.90	-1.77	-1.84
	150	0.42	0.60	2.42	0.12	0.13	0.12	-2.11	-2.05	-2.13	-2.10
	180	0.34	0.51	1.56	0.10	0.11	0.08	-2.32	-2.21	-2.57	-2.37
	210	0.31	0.45	1.13	0.09	0.10	0.06	-2.42	-2.34	-2.89	-2.55
	240	0.27	0.49	0.98	0.08	0.11	0.05	-2.56	-2.25	-3.03	-2.62
Embryo	0	20.40	24.70	67.90	1.00	1.00	1.00	0.00	0.00	0.00	0.00
	30	13.70	16.70	35.90	0.67	0.68	0.53	-0.40	-0.39	-0.64	-0.48
	60	11.80	12.70	20.50	0.58	0.51	0.30	-0.55	-0.67	-1.20	-0.80
	90	11.10	9.82	16.90	0.54	0.40	0.25	-0.61	-0.92	-1.39	-0.97
	120	10.60	9.18	13.00	0.52	0.37	0.19	-0.65	-0.99	-1.65	-1.10
	150	10.10	10.50	14.50	0.50	0.43	0.21	-0.70	-0.86	-1.54	-1.03
	180	9.00	14.30	13.30	0.44	0.58	0.20	-0.82	-0.55	-1.63	-1.00
	210	8.54	14.00	11.80	0.42	0.57	0.17	-0.87	-0.57	-1.75	-1.06
	240	9.21	12.30	13.60	0.45	0.50	0.20	-0.80	-0.70	-1.61	-1.03

Table G.2a Data for drying curves of mechanically scarified wheat kernels during drying at 30°C obtained from the magnetic resonance images (Fig. 5.9).

Wheat components	Drying time (min)	Averaged local normalized image intensity (I)			Intensity ratio (I/I_o)			ln (I/I_o)			
		Rep. 1	Rep. 2	Rep. 3	Rep. 1	Rep. 2	Rep. 3	Rep. 1	Rep. 2	Rep. 3	Average
Endosperm	0	3.37	19.20	11.20	1.00	1.00	1.00	0.00	0.00	0.00	0.00
	30	1.80	18.10	10.80	0.53	0.94	0.96	-0.63	-0.06	-0.04	-0.24
	60	1.37	16.90	10.10	0.41	0.88	0.90	-0.90	-0.13	-0.10	-0.38
	90	1.09	15.70	7.58	0.32	0.82	0.68	-1.13	-0.20	-0.39	-0.57
	120	0.88	13.10	6.28	0.26	0.68	0.56	-1.35	-0.38	-0.58	-0.77
	150	0.68	11.70	4.87	0.20	0.61	0.43	-1.61	-0.50	-0.83	-0.98
	180	0.65	10.20	3.45	0.19	0.53	0.31	-1.65	-0.63	-1.18	-1.15
	210	0.38	8.41	2.77	0.11	0.44	0.25	-2.17	-0.83	-1.40	-1.47
	240	0.34	6.96	2.30	0.10	0.36	0.21	-2.29	-1.01	-1.58	-1.63
Embryo	0	19.90	92.80	59.60	1.00	1.00	1.00	0.00	0.00	0.00	0.00
	30	11.60	80.40	55.50	0.58	0.87	0.93	-0.54	-0.14	-0.07	-0.25
	60	9.07	85.80	50.60	0.46	0.92	0.85	-0.79	-0.08	-0.16	-0.34
	90	6.22	55.80	40.60	0.31	0.60	0.68	-1.16	-0.51	-0.38	-0.69
	120	6.17	39.90	33.40	0.31	0.43	0.56	-1.17	-0.84	-0.58	-0.86
	150	4.60	30.80	29.20	0.23	0.33	0.49	-1.46	-1.10	-0.71	-1.09
	180	6.70	30.20	27.00	0.34	0.33	0.45	-1.09	-1.12	-0.79	-1.00
	210	5.08	25.90	26.10	0.26	0.28	0.44	-1.37	-1.28	-0.83	-1.16
	240	5.26	24.70	26.40	0.26	0.27	0.44	-1.33	-1.32	-0.81	-1.16

Table G.2b Data for drying curves of mechanically scarified wheat kernels during drying at 40°C obtained from the magnetic resonance images (Fig. 5.9).

Wheat components	Drying time (min)	Averaged local normalized image intensity (I)			Intensity ratio (I/I_o)			ln (I/I_o)			
		Rep. 1	Rep. 2	Rep. 3	Rep. 1	Rep. 2	Rep. 3	Rep. 1	Rep. 2	Rep. 3	Average
Endosperm	0	31.10	4.13	5.77	1.00	1.00	1.00	0.00	0.00	0.00	0.00
	30	26.80	3.19	6.42	0.86	0.77	1.11	-0.15	-0.26	0.11	-0.10
	60	19.00	2.17	4.41	0.61	0.53	0.76	-0.49	-0.64	-0.27	-0.47
	90	10.70	1.29	2.35	0.34	0.31	0.41	-1.07	-1.16	-0.90	-1.04
	120	5.01	0.87	1.38	0.16	0.21	0.24	-1.83	-1.56	-1.43	-1.60
	150	2.90	0.64	1.22	0.09	0.16	0.21	-2.37	-1.86	-1.55	-1.93
	180	1.93	0.45	0.90	0.06	0.11	0.16	-2.78	-2.21	-1.86	-2.28
	210	1.39	0.30	0.85	0.04	0.07	0.15	-3.11	-2.61	-1.92	-2.55
	240	0.90	0.41	0.85	0.03	0.10	0.15	-3.54	-2.32	-1.92	-2.59
Embryo	0	155.00	27.00	24.60	1.00	1.00	1.00	0.00	0.00	0.00	0.00
	30	93.40	18.60	17.60	0.60	0.69	0.72	-0.51	-0.37	-0.33	-0.40
	60	41.80	14.60	16.90	0.27	0.54	0.69	-1.31	-0.61	-0.38	-0.77
	90	17.50	14.90	14.20	0.11	0.55	0.58	-2.18	-0.59	-0.55	-1.11
	120	10.20	12.60	12.00	0.07	0.47	0.49	-2.72	-0.76	-0.72	-1.40
	150	9.17	13.80	12.50	0.06	0.51	0.51	-2.83	-0.67	-0.68	-1.39
	180	7.75	13.20	10.60	0.05	0.49	0.43	-3.00	-0.72	-0.84	-1.52
	210	7.57	10.00	9.33	0.05	0.37	0.38	-3.02	-0.99	-0.97	-1.66
	240	9.88	13.30	8.63	0.06	0.49	0.35	-2.75	-0.71	-1.05	-1.50

Table G.2c Data for drying curves of mechanically scarified wheat kernels during drying at 50°C obtained from the magnetic resonance images (Fig. 5.9).

Wheat components	Drying time (min)	Averaged local normalized image intensity (I)			Intensity ratio (I/I_o)			ln (I/I_o)			
		Rep. 1	Rep. 2	Rep. 3	Rep. 1	Rep. 2	Rep. 3	Rep. 1	Rep. 2	Rep. 3	Average
Endosperm	0	26.40	9.66	9.38	1.00	1.00	1.00	0.00	0.00	0.00	0.00
	30	16.60	6.28	6.00	0.63	0.65	0.64	-0.46	-0.43	-0.45	-0.45
	60	9.97	3.90	4.33	0.38	0.40	0.46	-0.97	-0.91	-0.77	-0.88
	90	4.87	2.16	2.93	0.18	0.22	0.31	-1.69	-1.50	-1.16	-1.45
	120	3.23	1.36	1.75	0.12	0.14	0.19	-2.10	-1.96	-1.68	-1.91
	150	1.65	0.83	1.20	0.06	0.09	0.13	-2.77	-2.46	-2.06	-2.43
	180	1.31	0.78	0.74	0.05	0.08	0.08	-3.00	-2.51	-2.54	-2.68
	210	0.88	0.38	0.53	0.03	0.04	0.06	-3.40	-3.24	-2.87	-3.17
	240	0.73	0.39	0.43	0.03	0.04	0.05	-3.59	-3.22	-3.08	-3.30
Embryo	0	71.70	39.50	47.00	1.00	1.00	1.00	0.00	0.00	0.00	0.00
	30	35.50	25.00	29.90	0.50	0.63	0.64	-0.70	-0.46	-0.45	-0.54
	60	11.20	17.40	16.90	0.16	0.44	0.36	-1.86	-0.82	-1.02	-1.23
	90	6.59	15.70	10.70	0.09	0.40	0.23	-2.39	-0.92	-1.48	-1.60
	120	5.64	14.90	11.80	0.08	0.38	0.25	-2.54	-0.97	-1.38	-1.63
	150	4.56	15.40	9.59	0.06	0.39	0.20	-2.76	-0.94	-1.59	-1.76
	180	4.97	16.70	10.30	0.07	0.42	0.22	-2.67	-0.86	-1.52	-1.68
	210	4.29	17.10	9.72	0.06	0.43	0.21	-2.82	-0.84	-1.58	-1.74
	240	5.14	15.40	9.43	0.07	0.39	0.20	-2.64	-0.94	-1.61	-1.73

Table G.3 Data for drying curves of embryo-removed wheat kernels during drying at different temperatures obtained from the magnetic resonance images (Fig. 5.10).

Drying Temp. (°C)	Drying time (min)	Averaged local normalized image intensity (I)			Intensity ratio (I/I_o)			ln (I/I_o)			
		Rep. 1	Rep. 2	Rep. 3	Rep. 1	Rep. 2	Rep. 3	Rep. 1	Rep. 2	Rep. 3	Average
30	0	12.00	6.62	7.38	1.00	1.00	1.00	0.00	0.00	0.00	0.00
	30	11.00	5.99	6.43	0.92	0.90	0.87	-0.09	-0.10	-0.14	-0.11
	60	9.68	5.48	5.76	0.81	0.83	0.78	-0.21	-0.19	-0.25	-0.22
	90	7.44	4.56	4.74	0.62	0.69	0.64	-0.48	-0.37	-0.44	-0.43
	120	6.01	4.23	4.14	0.50	0.64	0.56	-0.69	-0.45	-0.58	-0.57
	150	4.76	3.66	3.20	0.40	0.55	0.43	-0.92	-0.59	-0.84	-0.78
	180	3.92	3.24	2.62	0.33	0.49	0.36	-1.12	-0.71	-1.04	-0.96
	210	3.36	2.85	2.30	0.28	0.43	0.31	-1.27	-0.84	-1.17	-1.09
	240	2.91	2.62	1.92	0.24	0.40	0.26	-1.42	-0.93	-1.35	-1.23
40	0	37.80	4.86	23.20	1.00	1.00	1.00	0.00	0.00	0.00	0.00
	30	35.00	3.47	19.70	0.93	0.71	0.85	-0.08	-0.34	-0.16	-0.19
	60	23.20	2.35	16.20	0.61	0.48	0.70	-0.49	-0.73	-0.36	-0.52
	90	13.50	1.33	11.00	0.36	0.27	0.47	-1.03	-1.30	-0.75	-1.02
	120	9.19	1.17	7.65	0.24	0.24	0.33	-1.41	-1.42	-1.11	-1.32
	150	6.01	0.62	4.58	0.16	0.13	0.20	-1.84	-2.06	-1.62	-1.84
	180	3.69	0.63	3.41	0.10	0.13	0.15	-2.33	-2.05	-1.92	-2.10
	210	2.55	0.44	2.11	0.07	0.09	0.09	-2.70	-2.40	-2.40	-2.50
	240	1.94	0.50	1.70	0.05	0.10	0.07	-2.97	-2.27	-2.61	-2.62
50	0	18.10	6.84	23.70	1.00	1.00	1.00	0.00	0.00	0.00	0.00
	30	10.50	3.98	14.20	0.58	0.58	0.60	-0.54	-0.54	-0.51	-0.53
	60	5.22	1.68	7.32	0.29	0.25	0.31	-1.24	-1.40	-1.17	-1.27
	90	1.70	1.35	4.04	0.09	0.20	0.17	-2.37	-1.62	-1.77	-1.92
	120	0.97	0.80	2.66	0.05	0.12	0.11	-2.93	-2.15	-2.19	-2.42
	150	0.40	0.78	1.44	0.02	0.11	0.06	-3.81	-2.17	-2.80	-2.93
	180	0.20	0.46	1.14	0.01	0.07	0.05	-4.52	-2.71	-3.03	-3.42
	210	0.00	0.72	1.00	0.00	0.11	0.04	-9.10	-2.25	-3.17	-4.84
	240	0.01	0.65	0.93	0.00	0.09	0.04	-7.52	-2.36	-3.24	-4.37

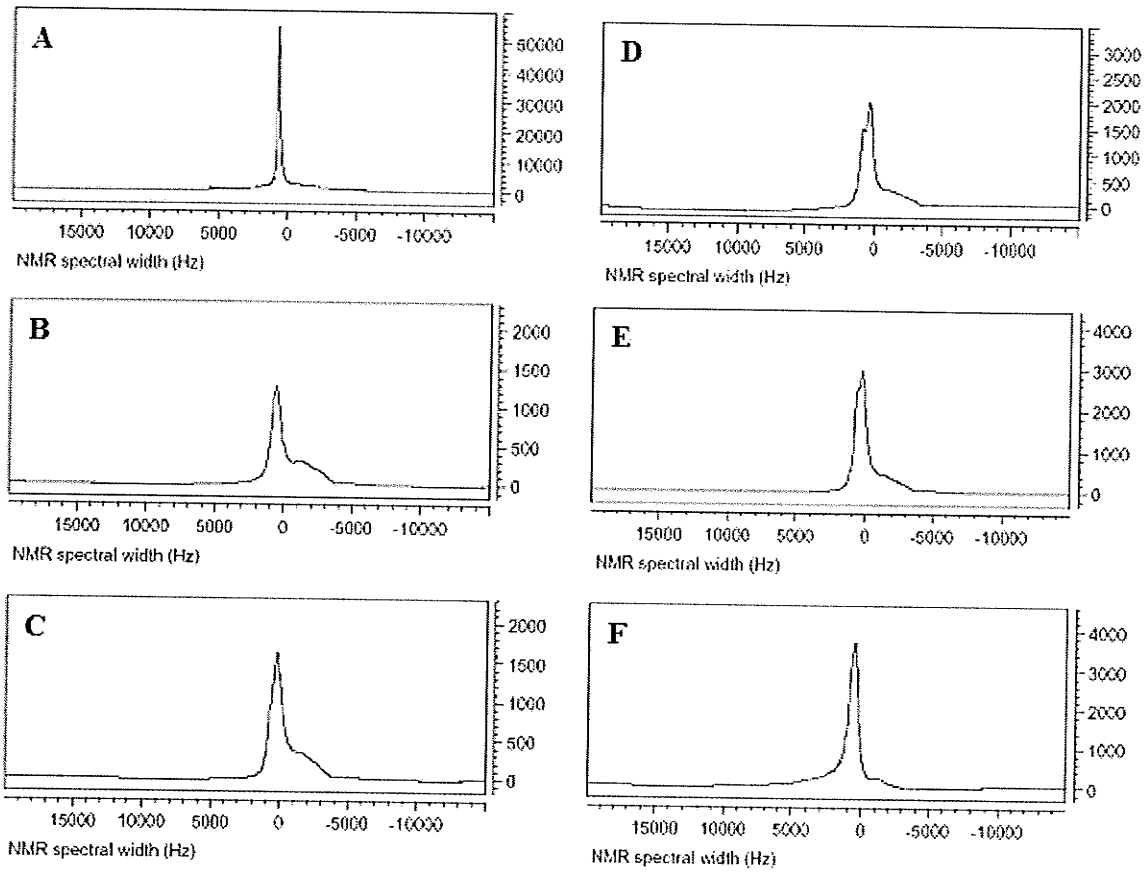

Figure G.1 Representative proton nuclear magnetic resonance (NMR) spectra of wheat kernels at different moisture contents: A – water phantom, B – 18.8% d.b., C – 23.6% d.b., D – 29.0% d.b., E – 34.6% d.b., F – 39.4% d.b.

Table G.4 Data for developing the calibration curve between wheat nuclear magnetic resonance (NMR) integrated spectral intensity and gravimetric moisture content (Fig. 5.11).

Moisture content, % d.b.						Integrated NMR signal amplitude, arbitrary units											
Replications					Mean	Replications											Mean
I	II	III	IV	V	±S.D.*	I	II	III	IV	V	VI	VII	VIII	IX	X	XI	±S.D.
19.40	19.09	19.47	17.50	18.19	18.72 ±0.86	939.02	985.65	1210.2	1085.4	1207.2	1161.6	1074.5	1121.7	1021.7	1242.8	1098.9	1104.42 ±96.99
23.50	24.22	24.39	23.15	22.94	23.64 ±0.64	1170.8	1409	1372.7	1355.1	1401.2	1317.6	1309.2	1579.1	1263	1270.6	1630.9	1370.84 ±134.89
30.11	29.63	29.37	28.30	28.09	29.09 ±0.87	1401.9	1468.6	1790.3	1715	1645.9	1963.8	1830.1	1899.4	1511.4	1626.6	1948.5	1709.23 ±195.39
35.56	35.06	35.54	33.32	33.64	34.61 ±1.07	1813.6	2114.5	1869	2041	1886	1988.9	2222.8	2204.9	2000.7	1935.7	2083.9	2014.64 ±134.26
39.43	39.41	39.68	39.28	39.78	39.51 ±0.21	2244.1	2151.5	1970.8	2300.1	2450.6	2099.4	2266.4	2036.8	2127.7	2444.3	2317	2218.97 ±156.67

*S.D. – Standard Deviation.

Table G.5a Data for developing the drying rate curves of intact kernels obtained from the moisture calibration equation (Eq. 5.3) (Fig. 5.12).

Drying Temp. (°C)	Drying time (min)	Endosperm			Embryo		
		Moisture content, d.b., decimal (M)	Average moisture content	Drying rate, dM/dt	Moisture content, d.b., decimal (M)	Average moisture content	Drying rate, dM/dt
30	0	0.413	--	--	1.566	--	--
	30	0.401	0.41	0.0004	1.515	1.54	0.0017
	60	0.362	0.38	0.0013	1.251	1.38	0.0088
	90	0.316	0.34	0.0015	1.076	1.16	0.0058
	120	0.256	0.29	0.0020	0.955	1.02	0.0040
	150	0.201	0.23	0.0018	0.846	0.90	0.0036
	180	0.159	0.18	0.0014	0.776	0.81	0.0023
	210	0.126	0.14	0.0011	0.707	0.74	0.0023
	240	0.101	0.11	0.0008	0.649	0.68	0.0019
40	0	0.413	--	--	1.523	--	--
	30	0.350	0.38	0.0021	1.078	1.30	0.0148
	60	0.275	0.31	0.0025	0.708	0.89	0.0123
	90	0.185	0.23	0.0030	0.641	0.67	0.0022
	120	0.125	0.16	0.0020	0.514	0.58	0.0042
	150	0.081	0.10	0.0015	0.525	0.52	-0.0004
	180	0.051	0.07	0.0010	0.484	0.50	0.0014
	210	0.036	0.04	0.0005	0.488	0.49	-0.0001
	240	0.028	0.03	0.0003	0.514	0.50	-0.0009
50	0	0.420	--	--	1.716	--	--
	30	0.278	0.35	0.0047	0.999	1.36	0.0239
	60	0.190	0.23	0.0029	0.673	0.84	0.0109
	90	0.103	0.15	0.0029	0.562	0.62	0.0037
	120	0.057	0.08	0.0015	0.484	0.52	0.0026
	150	0.034	0.05	0.0008	0.521	0.50	-0.0012
	180	0.020	0.03	0.0005	0.544	0.53	-0.0008
	210	0.011	0.02	0.0003	0.507	0.53	0.0012
	240	0.011	0.01	0.0000	0.521	0.51	-0.0005

Table G.5b Data for developing the drying rate curves of mechanically scarified kernels obtained from the moisture calibration equation (Eq. 5.3) (Fig. 5.13).

Drying Temp. (°C)	Drying time (min)	Endosperm			Embryo		
		Moisture content, d.b., decimal (M)	Average moisture content	Drying rate, dM/dt	Moisture content, d.b., decimal (M)	Average moisture content	Drying rate, dM/dt
30	0	0.319	--	--	1.687	--	--
	30	0.286	0.30	0.0011	1.444	1.57	0.0081
	60	0.265	0.28	0.0007	1.423	1.43	0.0007
	90	0.224	0.24	0.0014	0.999	1.21	0.0141
	120	0.185	0.20	0.0013	0.770	0.88	0.0076
	150	0.153	0.17	0.0011	0.622	0.70	0.0049
	180	0.126	0.14	0.0009	0.616	0.62	0.0002
	210	0.099	0.11	0.0009	0.547	0.58	0.0023
	240	0.078	0.09	0.0007	0.541	0.54	0.0002
40	0	0.402	--	--	2.089	--	--
	30	0.353	0.38	0.0016	1.304	1.70	0.0262
	60	0.243	0.30	0.0037	0.729	1.02	0.0192
	90	0.130	0.19	0.0038	0.457	0.59	0.0091
	120	0.057	0.09	0.0024	0.338	0.40	0.0040
	150	0.032	0.04	0.0008	0.344	0.34	-0.0002
	180	0.017	0.02	0.0005	0.304	0.32	0.0013
	210	0.008	0.01	0.0003	0.258	0.28	0.0015
	240	0.005	0.01	0.0001	0.307	0.28	-0.0016
50	0	0.528	--	--	1.884	--	--
	30	0.330	0.43	0.0066	1.059	1.47	0.0275
	60	0.203	0.27	0.0042	0.532	0.80	0.0176
	90	0.102	0.15	0.0034	0.380	0.46	0.0051
	120	0.059	0.08	0.0014	0.373	0.38	0.0002
	150	0.027	0.04	0.0011	0.341	0.36	0.0011
	180	0.016	0.02	0.0004	0.369	0.36	-0.0009
	210	0.005	0.01	0.0004	0.359	0.36	0.0003
	240	0.001	0.00	0.0001	0.344	0.35	0.0005

Table G.5c Data for developing the drying rate curves of embryo-removed kernels obtained from the moisture calibration equation (Eq. 5.3) (Fig. 5.14).

Drying Temp. (°C)	Drying time (min)	Endosperm		
		Moisture content, d.b., decimal (M)	Average moisture content	Drying rate, dM/dt
30	0	0.503	--	--
	30	0.449	0.48	0.0018
	60	0.401	0.43	0.0016
	90	0.318	0.36	0.0028
	120	0.270	0.29	0.0016
	150	0.216	0.24	0.0018
	180	0.180	0.20	0.0012
	210	0.151	0.17	0.0010
	240	0.133	0.14	0.0006
40	0	0.514	--	--
	30	0.451	0.48	0.0021
	60	0.318	0.38	0.0044
	90	0.191	0.25	0.0042
	120	0.128	0.16	0.0021
	150	0.073	0.10	0.0018
	180	0.046	0.06	0.0009
	210	0.024	0.04	0.0007
	240	0.017	0.02	0.0002
50	0	0.506	--	--
	30	0.293	0.40	0.0071
	60	0.135	0.21	0.0053
	90	0.061	0.10	0.0025
	120	0.032	0.05	0.0010
	150	0.012	0.02	0.0007
	180	0.003	0.01	0.0003
	210	0.003	0.00	0.0000
	240	0.000	0.00	0.0001

RAW DATA USED IN CHAPTER 6

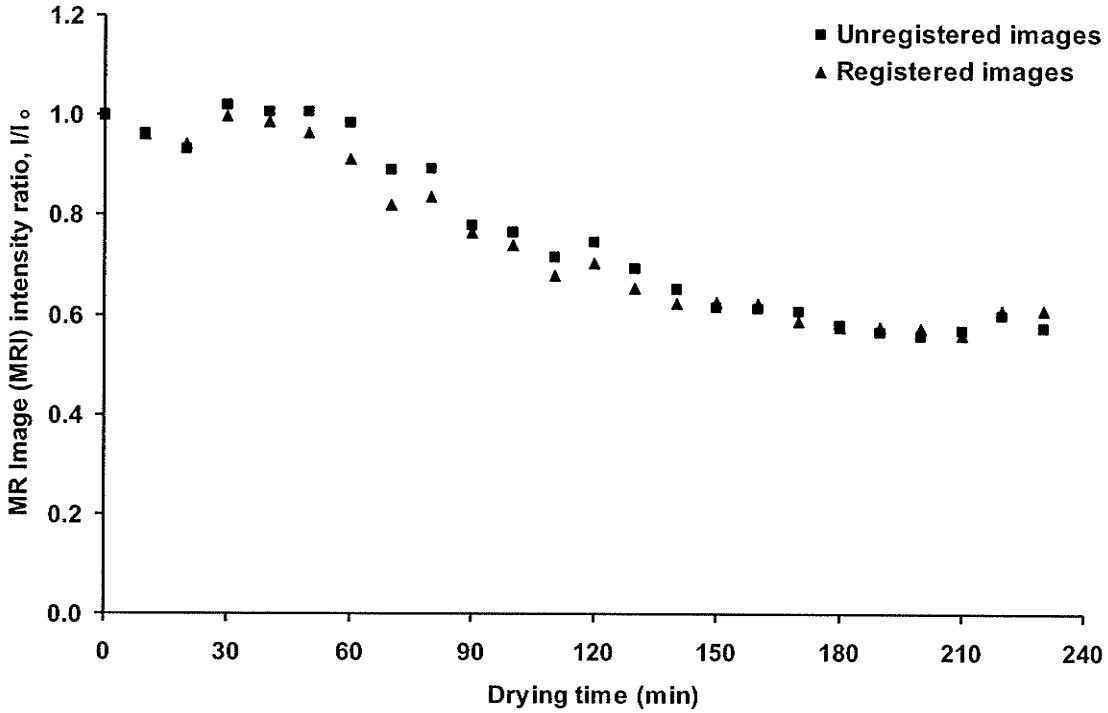

Figure H.1 Time plot for the intensity ratio of both unregistered and registered images for a specific region of interest (ROI).

Table H.1 Data used to create Fig. 6.1 and Fig. H.1.

Time (min)	Unregistered images					Registered images				
	Area of ROI	Mean intensity (I)	Minimum intensity	Maximum intensity	Intensity ratio (I/I_o)	Area of ROI	Mean intensity (I)	Minimum intensity	Maximum intensity	Intensity ratio (I/I_o)
0	330	57.448 (I_o)	19	253	1.000	330	62.264 (I_o)	19	254	1.000
10	330	55.185	19	255	0.961	330	59.830	20	249	0.961
20	330	53.515	18	244	0.932	330	58.700	14	250	0.943
30	330	58.624	15	254	1.020	330	62.115	17	250	0.998
40	330	57.758	17	254	1.005	330	61.415	22	242	0.986
50	330	57.733	22	255	1.005	330	60.058	19	255	0.965
60	330	56.509	17	255	0.984	330	56.809	18	255	0.912
70	330	51.067	9	218	0.889	330	51.067	9	218	0.820
80	330	51.273	17	255	0.893	330	52.027	17	237	0.836
90	330	44.733	17	239	0.779	330	47.673	15	225	0.766
100	330	43.985	15	231	0.766	330	46.027	13	237	0.739
110	330	41.121	11	220	0.716	330	42.300	13	224	0.679
120	330	42.797	13	229	0.745	330	43.879	12	222	0.705
130	330	39.821	12	240	0.693	330	40.803	13	236	0.655
140	330	37.473	4	240	0.652	330	38.845	5	235	0.624
150	330	35.400	8	228	0.616	330	39.000	11	240	0.626
160	330	35.118	7	216	0.611	330	38.803	0	234	0.623
170	330	34.842	4	220	0.606	330	36.597	8	221	0.588
180	330	33.227	4	233	0.578	330	35.870	9	224	0.576
190	330	32.545	2	255	0.567	330	35.870	9	224	0.576
200	330	32.024	6	243	0.557	330	35.785	4	232	0.575
210	330	32.621	2	236	0.568	330	34.918	5	229	0.561
220	330	34.373	6	251	0.598	330	37.915	8	232	0.609
230	330	32.945	6	245	0.573	330	37.958	12	239	0.610

THEORETICAL ANALYSIS OF THE MODEL

Finite element method was used to solve the system of 2D heat and mass transfer equations in (Eqs. 6.2 through 6.9) because it can provided solution for irregular geometries. The cross-section of the wheat kernel was discreatized into small straight-sided quadratic triangular elements (6 nodes) and Galerkin's weighted residual method was adopted to obtain approximate simple continuous functions for temperature and moisture distributions over each element. The assembly of these continuous functions provide the temperature and moisture distributions over the entire domain. The typical trial functions considered are:

$$\tilde{U}_1^{(e)}(x,y,M) = \sum_{j=1}^{6} M_j \phi_j^{(e)}(x,y) \tag{H.1}$$

$$\text{and } \tilde{U}_2^{(e)}(x,y,T) = \sum_{j=1}^{6} T_j \phi_j^{(e)}(x,y) \tag{H.2}$$

where n is the number of degrees of freedom (DOF) in the element (e) and $\phi_j^{(e)}(x,y)$ is the interpolation or shape function. M_j and T_j are the function of time indicating that the trial solution is a function of both coordinate (x,y) and time (t). The Galerkin's residuals for a general element for Eqs. 6.2 and 6.6 are:

$$R_1^{(e)}(x,y,M) = \frac{\partial \tilde{U}_1^{(e)}(x,y,M)}{\partial t} - \frac{\partial}{\partial x}\left\{D_x \frac{\partial \tilde{U}_1^{(e)}(x,y,M)}{\partial x}\right\} - \frac{\partial}{\partial y}\left\{D_y \frac{\partial \tilde{U}_1^{(e)}(x,y,M)}{\partial y}\right\} + h_m \tilde{U}_1^{(e)}(x,y,M) - h_m M_e \tag{H.3}$$

and

$$R_2^{(e)}(x,y,T) = \rho_g C_g \frac{\partial \tilde{U}_2^{(e)}(x,y,T)}{\partial t} - \frac{\partial}{\partial x}\left\{K_x \frac{\partial \tilde{U}_2^{(e)}(x,y,T)}{\partial x}\right\}$$
$$- \frac{\partial}{\partial y}\left\{K_y \frac{\partial \tilde{U}_2^{(e)}(x,y,T)}{\partial y}\right\} - L\,\rho_g \frac{\tilde{U}_2^{(e)}(x,y,T)}{\partial t} + h_t \tilde{U}_2^{(e)}(x,y,T) - h_t T_a \qquad \text{(H.4)}$$

The weighted residual equation for each DOF in Eqs. H.1 and H.2 are:

$$\iint R_1^{(e)}(x,y,M)\ \phi_i^{(e)}(x,y)\ dx\ dy = 0 \qquad \text{(H.5)}$$

and

$$\iint R_2^{(e)}(x,y,T)\ \phi_i^{(e)}(x,y)\ dx\ dy = 0 \qquad \text{(H.6)}$$

$i = 1, 2, ..., 6.$

Substituting Eq. H.3 into Eq. H.5 and Eq. H.4 into Eq. H.6 yield the desired residual equations:

$$\iint \left[\begin{array}{l} \dfrac{\partial \tilde{U}_1^{(e)}(x,y,M)}{\partial t} - \dfrac{\partial}{\partial x}\left\{D_x \dfrac{\partial \tilde{U}_1^{(e)}(x,y,M)}{\partial x}\right\} \\ - \dfrac{\partial}{\partial y}\left\{D_y \dfrac{\partial \tilde{U}_1^{(e)}(x,y,M)}{\partial y}\right\} + h_m \tilde{U}_1^{(e)}(x,y,M) - h_m M_e \end{array}\right] \phi_i^{(e)}(x,y)\,dx\,dy = 0 \qquad \text{(H.7)}$$

and

$$\iint \left[\begin{array}{l} \rho_g C_g \dfrac{\partial \tilde{U}_2^{(e)}(x,y,T)}{\partial t} - \dfrac{\partial}{\partial x}\left\{K_x \dfrac{\partial \tilde{U}_2^{(e)}(x,y,T)}{\partial x}\right\} \\ - \dfrac{\partial}{\partial y}\left\{K_y \dfrac{\partial \tilde{U}_2^{(e)}(x,y,T)}{\partial y}\right\} - L\,\rho_g \dfrac{\tilde{U}_2^{(e)}(x,y,T)}{\partial t} \\ + h_t \tilde{U}_2^{(e)}(x,y,T) - h_t T_a \end{array}\right] \phi_i^{(e)}(x,y)\,dx\,dy = 0 \qquad \text{(H.8)}$$

where $i = 1, 2, ..., 6$

After integrating by parts:

$$\iint \frac{\partial \tilde{U}_1^{(e)}(x,y,M)}{\partial t}\,\phi_i^{(e)}(x,y)\,dx\,dy - \iint \left[\begin{array}{l} \dfrac{\partial}{\partial x}\left\{D_x \dfrac{\partial \tilde{U}_1^{(e)}(x,y,M)}{\partial x}\,\phi_i^{(e)}(x,y)\right\} \\ + \dfrac{\partial}{\partial y}\left\{D_y \dfrac{\partial \tilde{U}_1^{(e)}(x,y,M)}{\partial y}\,\phi_i^{(e)}(x,y)\right\} \end{array}\right] dx\,dy +$$

$$\iint \left[\left\{D_x \frac{\partial \tilde{U}_1^{(e)}(x,y,M)}{\partial x}\right\}\frac{\partial \phi_i^{(e)}(x,y)}{\partial x} + \left\{D_y \frac{\partial \tilde{U}_1^{(e)}(x,y,M)}{\partial y}\right\}\frac{\partial \phi_i^{(e)}(x,y)}{\partial y}\right] dx\,dy$$

$$+ \iint h_m \tilde{U}_1^{(e)}(x,y,M)\,\phi_i^{(e)}(x,y)\,dx\,dy$$

$$- \iint h_m M_e \phi_i^{(e)}(x,y)\,dx\,dy = 0$$

(H.9)

and

$$\iint \rho_g C_g \frac{\partial \tilde{U}_2^{(e)}(x,y,T)}{\partial t}\,\phi_i^{(e)}(x,y)\,dx\,dy - \iint \left[\begin{array}{l} \dfrac{\partial}{\partial x}\left\{K_x \dfrac{\partial \tilde{U}_2^{(e)}(x,y,T)}{\partial x}\,\phi_i^{(e)}(x,y)\right\} \\ + \dfrac{\partial}{\partial y}\left\{K_y \dfrac{\partial \tilde{U}_2^{(e)}(x,y,T)}{\partial y}\,\phi_i^{(e)}(x,y)\right\} \end{array}\right] dx\,dy +$$

$$\iint \left[\left\{K_x \frac{\partial \tilde{U}_2^{(e)}(x,y,T)}{\partial x}\right\}\frac{\partial \phi_i^{(e)}(x,y)}{\partial x} + \left\{K_y \frac{\partial \tilde{U}_2^{(e)}(x,y,T)}{\partial y}\right\}\frac{\partial \phi_i^{(e)}(x,y)}{\partial y}\right] dx\,dy$$

$$- \iint L \rho_g \frac{\partial \tilde{U}_2^{(e)}(x,y,T)}{\partial t}\,\phi_i^{(e)}(x,y)\,dx\,dy + \iint h_t \tilde{U}_2^{(e)}(x,y,T)\,\phi_i^{(e)}(x,y)\,dx\,dy$$

$$- \iint h_t T_a\,\phi_i^{(e)}(x,y)\,dx\,dy = 0$$

(H.10)

where i = 1, 2, ... 6

The second integral in both Eqs. H.9 and H.10 is the 2D version of a perfect differential in 1D i.e., it can be reduced to an integral over the boundary of the area. Using Green's theorem the second integral of both Eqs. H.9 and H.10 can be written as:

$$\iint\left[\frac{\partial}{\partial x}\left\{D_x\frac{\partial\tilde{U}_1^{(e)}(x,y,M)}{\partial x}\phi_i^{(e)}(x,y)\right\}+\frac{\partial}{\partial y}\left\{D_y\frac{\partial\tilde{U}_1^{(e)}(x,y,M)}{\partial y}\phi_i^{(e)}(x,y)\right\}\right]dx\,dy$$
$$=\oint_{S_2}\left\{D_x\frac{\partial\tilde{U}_1^{(e)}(x,y,M)}{\partial x}\phi_i^{(e)}(x,y)\,l_x^{(e)}+D_y\frac{\partial\tilde{U}_1^{(e)}(x,y,M)}{\partial y}\phi_i^{(e)}(x,y)\,l_y^{(e)}\right\}dS_2 \qquad (H.11)$$

and

$$\iint\left[\frac{\partial}{\partial x}\left\{K_x\frac{\partial\tilde{U}_2^{(e)}(x,y,T)}{\partial x}\phi_i^{(e)}(x,y)\right\}+\frac{\partial}{\partial y}\left\{K_y\frac{\partial\tilde{U}_2^{(e)}(x,y,T)}{\partial y}\phi_i^{(e)}(x,y)\right\}\right]dx\,dy$$
$$=\oint_{S_2}\left\{K_x\frac{\partial\tilde{U}_2^{(e)}(x,y,T)}{\partial x}\phi_i^{(e)}(x,y)\,l_x^{(e)}+K_y\frac{\partial\tilde{U}_2^{(e)}(x,y,T)}{\partial y}\phi_i^{(e)}(x,y)\,l_y^{(e)}\right\}dS_2 \qquad (H.12)$$

where $l_x^{(e)}$ and $l_y^{(e)}$ are the direction cosines, outward unit normal to the element boundary, and S_2 is a coordinate along the boundary.

Eqs. H.11 and H.12 were further simplified by using expressions for the x and y components of outward-normal flux:

$$\tilde{\tau}_M^{(e)}=\tilde{\tau}_x^{(e)}\,l_x^{(e)}+\tilde{\tau}_y^{(e)}\,l_y^{(e)}=D_x\frac{\partial\tilde{U}_1^{(e)}(x,y,M)}{\partial x}l_x+D_y\frac{\partial\tilde{U}_1^{(e)}(x,y,M)}{\partial y}l_y \qquad (H.13)$$

and

$$\tilde{\tau}_T^{(e)}=\tilde{\tau}_x^{(e)}\,l_x^{(e)}+\tilde{\tau}_y^{(e)}\,l_y^{(e)}=K_x\frac{\partial\tilde{U}_2^{(e)}(x,y,T)}{\partial x}l_x+K_y\frac{\partial\tilde{U}_2^{(e)}(x,y,T)}{\partial y}l_y \qquad (H.14)$$

Replacing the second integral in both Eqs. H.9 and H.10 and placing all load terms in the right hand side of the equations, the respective residual equations become:

$$\iint \frac{\partial \tilde{U}_1^{(e)}(x,y,M)}{\partial t}\,\phi_i^{(e)}(x,y)\,dx\,dy +$$
$$\iint\left[\left\{D_x\,\frac{\partial \tilde{U}_1^{(e)}(x,y,M)}{\partial x}\right\}\frac{\partial \phi_i^{(e)}(x,y)}{\partial x}+\left\{D_y\,\frac{\partial \tilde{U}_1^{(e)}(x,y,M)}{\partial y}\right\}\frac{\partial \phi_i^{(e)}(x,y)}{\partial y}\right]dx\,dy$$
$$+\iint h_m \tilde{U}_1^{(e)}(x,y,M)\,\phi_i^{(e)}(x,y)\,dx\,dy \qquad \text{(H.15)}$$
$$=\iint h_m M_e\,\phi_i^{(e)}(x,y)\,dx\,dy+\oint_{S_2}\tilde{\tau}_M^{(e)}\,\phi_i^{(e)}(x,y)\,dS_2$$

and

$$\iint \rho_g\,C_g\,\frac{\partial \tilde{U}_2^{(e)}(x,y,T)}{\partial t}\,\phi_i^{(e)}(x,y)\,dx\,dy +$$
$$\iint\left[\left\{K_x\,\frac{\partial \tilde{U}_2^{(e)}(x,y,T)}{\partial x}\right\}\frac{\partial \phi_i^{(e)}(x,y)}{\partial x}+\left\{K_y\,\frac{\partial \tilde{U}_2^{(e)}(x,y,T)}{\partial y}\right\}\frac{\partial \phi_i^{(e)}(x,y)}{\partial y}\right]dx\,dy$$
$$-\iint L\,\rho_g\,\frac{\partial \tilde{U}_2^{(e)}(x,y,T)}{\partial t}\,\phi_i^{(e)}(x,y)\,dx\,dy+\iint h_t \tilde{U}_2^{(e)}(x,y,T)\,\phi_i^{(e)}(x,y)\,dx\,dy \qquad \text{(H.16)}$$
$$=\iint h_t T_a\,\phi_i^{(e)}(x,y)\,dx\,dy-\oint_{S_2}\tilde{\tau}_T^{(e)}\,\phi_i^{(e)}(x,y)\,dS_2$$

Note that $\tilde{\tau}_M^{(e)}$ is positive in Eq. H.15 which is the outward-normal component of diffusive flux and thus represents moisture is lost from the grain and $\tilde{\tau}_T^{(e)}$ is negative in Eq. H.16 which is the inward-normal component of heat flux which represents heat is being added to the grain.

Applying Eq. H.1 in Eq. H.15 and Eq. H.2 in Eq. H.16, we get

$$\sum_{j=1}^{6}\left\{\iint \phi_i^{(e)}(x,y)\,\phi_j^{(e)}(x,y)\,dx\,dy\right\}\frac{\partial M}{\partial t}+\sum_{j=1}^{6}\left\{\iint\left[D_x\,\frac{\partial \phi_i^{(e)}(x,y)}{\partial x}\right]\frac{\partial \phi_j^{(e)}(x,y)}{\partial x}dx\,dy+\iint\left[D_y\,\frac{\partial \phi_i^{(e)}(x,y)}{\partial y}\right]\frac{\partial \phi_j^{(e)}(x,y)}{\partial y}dx\,dy\right\}\{M\}$$
$$+\iint h_m\,\phi_i^{(e)}(x,y)\,\phi_j^{(e)}(x,y)\,dx\,dy\{M\}=\iint h_m M_e\,\phi_i^{(e)}(x,y)\,dx\,dy+\oint_{S_2}\tilde{\tau}_M^{(e)}\,\phi_i^{(e)}(x,y)\,dS_2$$

(H.17)

and

$$\sum_{j=1}^{6}\left\{\iint \rho_g C_g \phi_i^{(e)}(x,y)\,\phi_j^{(e)}(x,y)\,dx\,dy\right\}\frac{\partial T}{\partial t}+\sum_{j=1}^{6}\left\{\begin{array}{l}\iint\left[K_x\dfrac{\partial \phi_i^{(e)}(x,y)}{\partial x}\right]\dfrac{\partial \phi_j^{(e)}(x,y)}{\partial x}dx\,dy \\ +\iint\left[K_y\dfrac{\partial \phi_i^{(e)}(x,y)}{\partial y}\right]\dfrac{\partial \phi_j^{(e)}(x,y)}{\partial y}dx\,dy\end{array}\right\}\{T\}$$

$$-\sum_{j=1}^{6}\left\{\iint L\rho_g \phi_i^{(e)}(x,y)\,\phi_j^{(e)}(x,y)\,dx\,dy\right\}\frac{\partial M}{\partial t}+\iint h_t\,\phi_i^{(e)}(x,y)\,\phi_j^{(e)}(x,y)\,dx\,dy\{T\}$$

$$=\iint h_t\,T_a\,\phi_i^{(e)}(x,y)\,dx\,dy-\oint_{S_2}\tilde{\tau}_T^{(e)}\,\phi_i^{(e)}(x,y)\,dS_2 \qquad \text{(H.18)}$$

Eqs. H.17 and H.18 can be put in the form of Eqs. 6.10 and 6.11.

MAGNETIC RESONANCE IMAGES USED TO OBTAIN THE GEOMETRY OBJECTS (FIGURES 6.3-6.5) FOR MODEL SIMULATION

(a) Intact wheat kernel

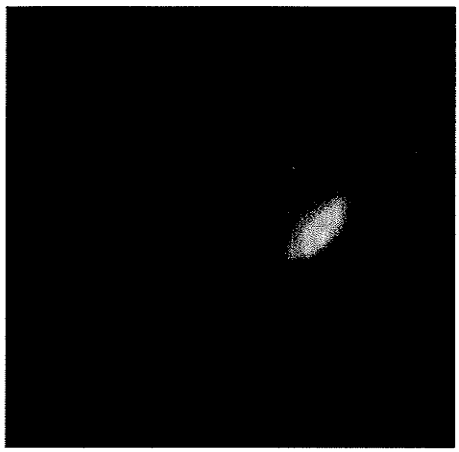

(b)Mechanically scarified kernel

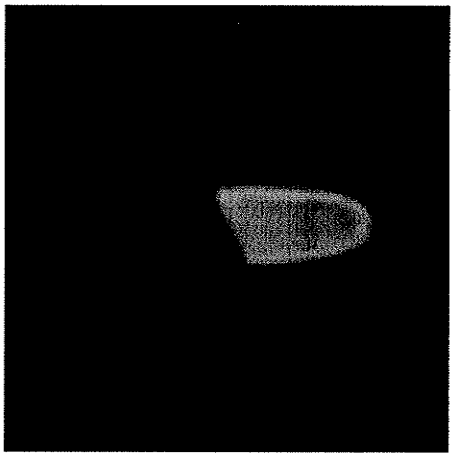

(c) Germ-removed kernel

Figure H.2 Selected magnetic resonance images of three physically different types of wheat kernels to use in MATLAB-COMSOL environment to obtain geometry objects for the model simulation.

IMPORTING MAGNETIC RESONANCE IMAGE INTO COMSOL (WORKING WITH COMSOL-MATLAB INTERFACE)

In MATLAB Command Window:

```
I=imread('fig.bmp');
Imahsow(I);
h=ones(5,5)/25;
I2=imfilter(I,h);
figure, imshow(I2);
imwrite(I2, 'filtered_image.bmp');
pic = imread('filtered_image.bmp')
image(pic)
v = axis;
[c2,r] = flim2curve(pic,{[],1:10:150},'KeepFrac',0.07);
figure
geomplot(c2,'Pointmode','off');
for j = 1:length(r)
 hold on
 geomplot(r{j},'Pointmode','off','edgecolor','g')
end
axis(v)
axis ij

g = geomcsg({rect2(70,200,70,140)},{c2});% create geometery object g from intact MR image
%g2 = geomcsg({rect2(60,180,70,140)},{c2});% create geometery object g2 from scarified MR
image
%g3 = geomcsg({rect2(100,200,80,140)},{c2});% create geometery object g2 from germ-removed
MR image
s2 = solid2(g2);% creates a solid 2D Geometry Object
% In COMSOL :- File>Import>Geometry Object then s is the name of the
% object.
% Draw>Split object : creates separate objects for each contour
% To merge objects : shift-click on the objects and use Union
%                  : Draw>Delete interior boundaries
%
% Meshing: Mesh>Mesh parameters>Subdomain>max element size = 1/15 max
% dimension ~10 (try 1 for very small elements)
%
% Export Image : File>export image (jpeg and bmp are good; tiff is not so
% good)
figure
geomplot(s2,'pointmode','off','sublabels','on');
axis(v)
axis ij
```

Import the solid object 's2' into COMSOL using **File>Import>Geometry Objects**

MODELING USING GRAPHICAL USER INTERFACE OF COMSOL

Following steps were followed to model the drying of an intact wheat kernel at 30°C.

First, import the 2D geometry object of an intact wheat kernel using MATLAB-COMSOL interface (procedure mentioned in the earlier section).

MODEL NAVIGATOR

1 Open the **Model Navigator**. In the **Space dimension** list select **2D**.

2 From the list of application modes select
Comsol Multiphysics > Heat Transfer > Conduction > Transient Analysis.

3 Click the **Multiphysics** button, then click **Add.**

4 Similarly select application mode:
Comsol Multiohysics > Convection and Diffusion > Diffusion > Transient Analysis.

5 Click **OK.**

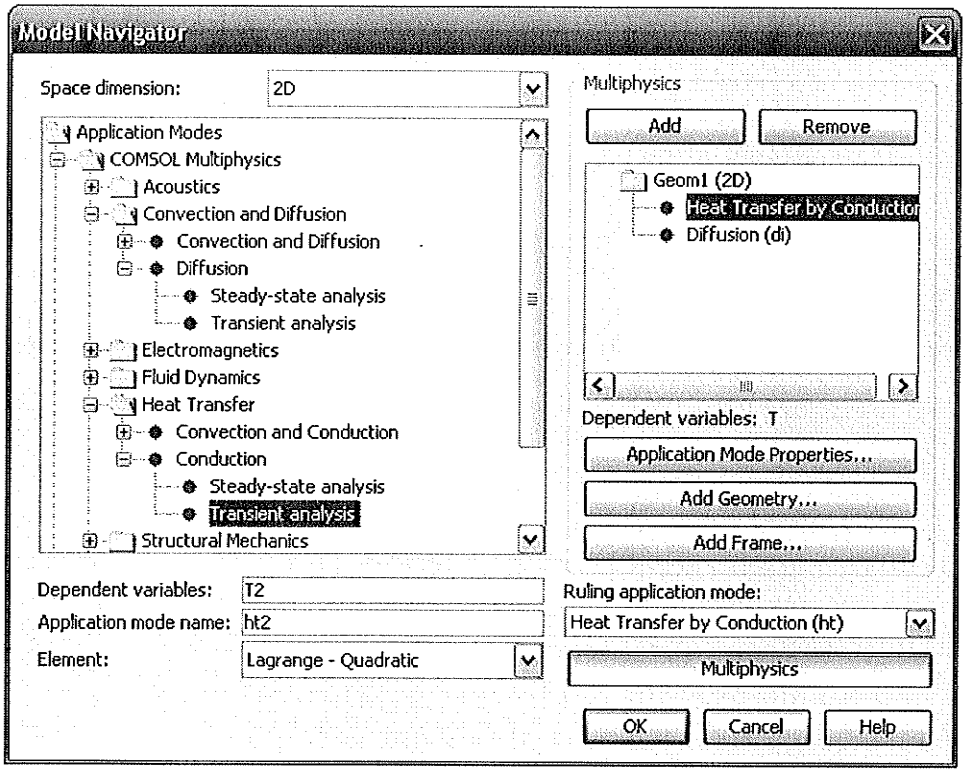

OPTIONS AND SETTINGS

From the **Options** menu select **Constants**. Enter the following names and expressions; when done, click **OK**:

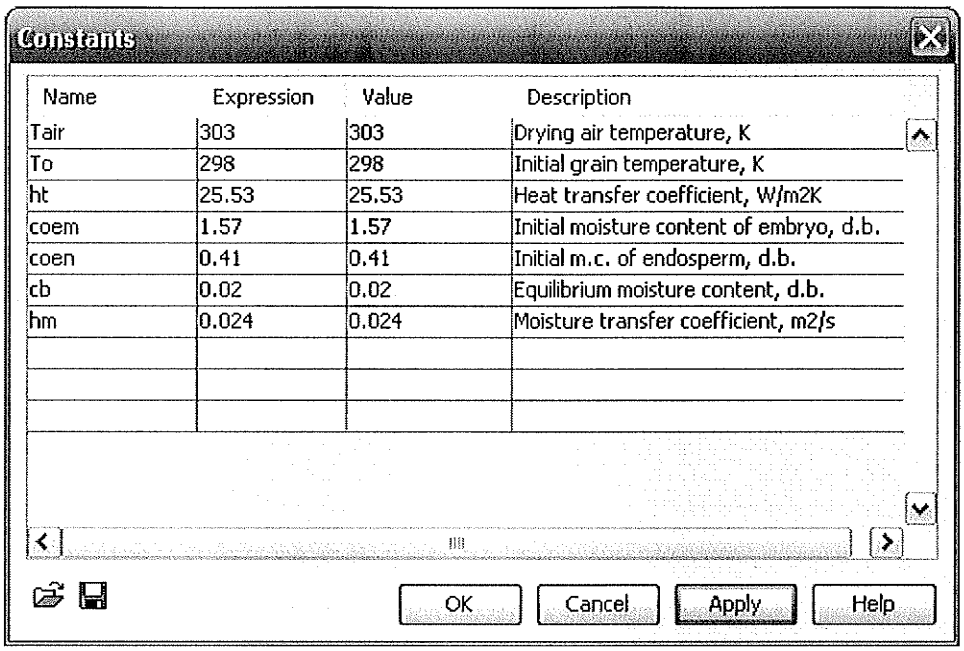

Again, from the **Options** menu select **Scalar Expressions**. Enter the following names and expressions; when done, click **OK**:

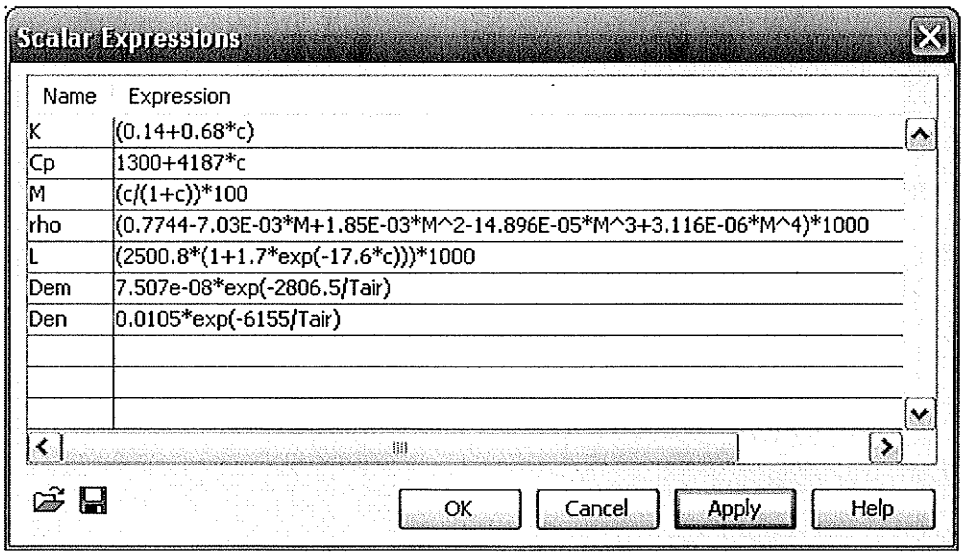

c – moisture content, decimal, d.b.; M – moisture content, %, w.b.; rho – grain density; Dem – diffusivity of embryo or germ; Den – diffusivity of endosperm (all in SI units).

PHYSICS SETTINGS

Subdomain Settings – Heat Transfer by Conduction

1 From the **Multiphysics** menu select **1 Heat Transfer by Conduction (ht)**.

2 From the **Physics** menu select **Subdomain Settings**.

3 Select the subdomains **2** (refers to embryo or germ), **3** (endosperm), and **4** (attachment layer between embryo and endosperm) and enter the following settings from the figures; when done, click **OK**.

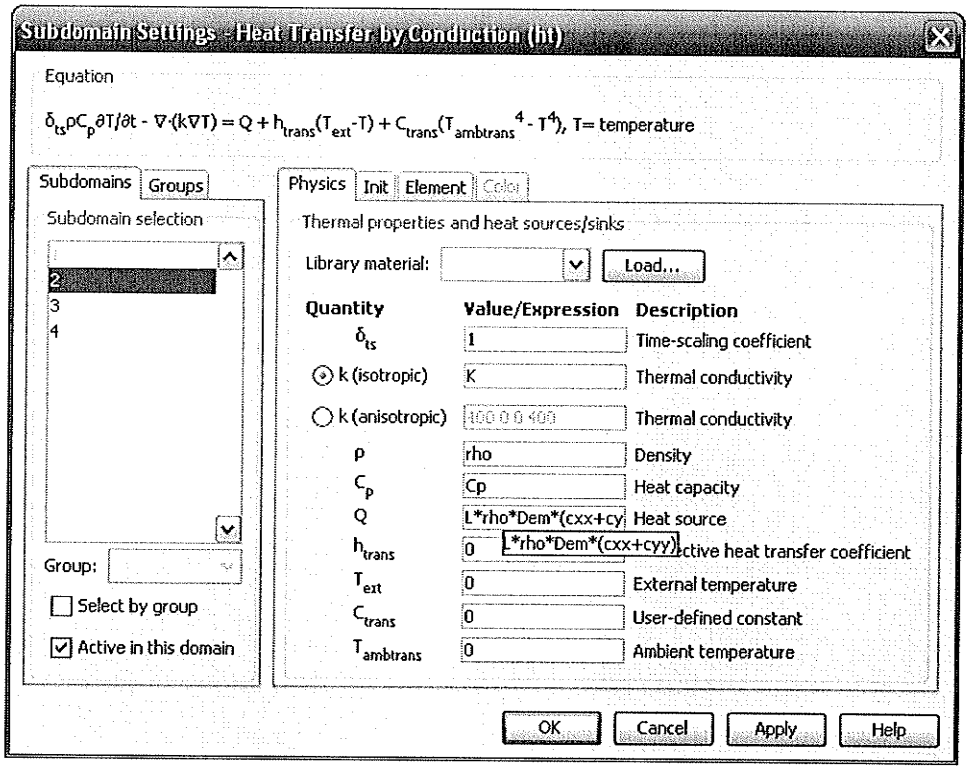

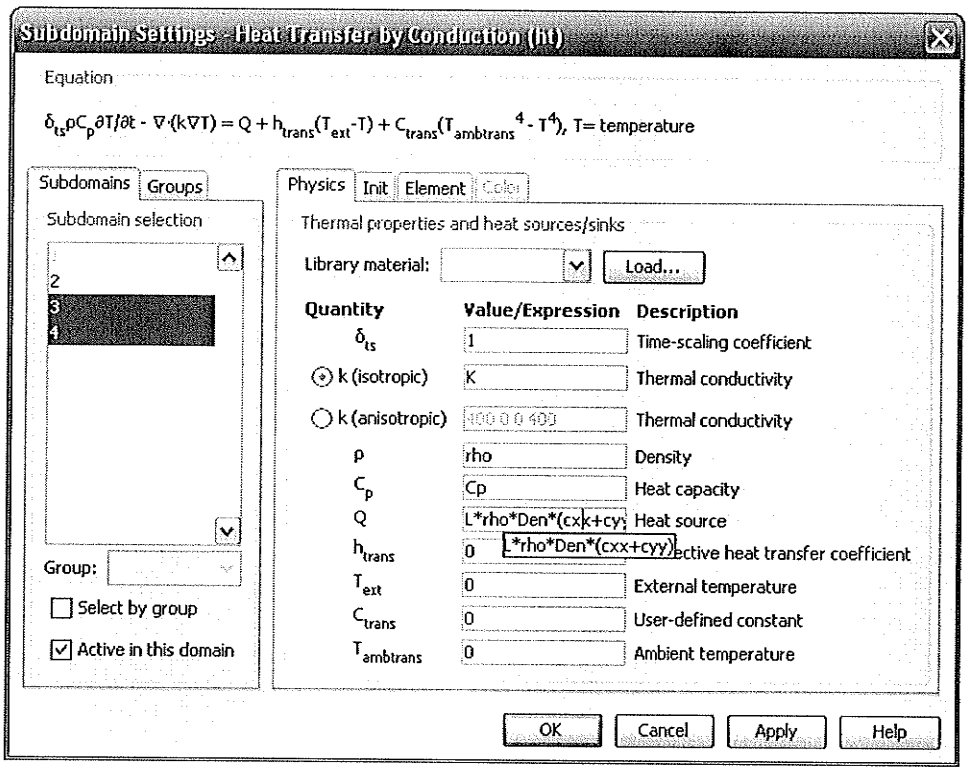
Subdomain Settings - Heat Transfer by Conduction (ht)
Equation
$\delta_{ts}\rho C_p \partial T/\partial t - \nabla\cdot(k\nabla T) = Q + h_{trans}(T_{ext}-T) + C_{trans}(T_{ambtrans}^4 - T^4)$, T= temperature
Subdomains
Groups
Subdomain selection
2
3
4
Group:
Select by group
Active in this domain
Physics
Init
Element
Color
Thermal properties and heat sources/sinks
Library material:
Load...
Quantity
Value/Expression
Description
δ_{ts}
1
Time-scaling coefficient
k (isotropic)
K
Thermal conductivity
k (anisotropic)
Thermal conductivity
ρ
rho
Density
C_p
Cp
Heat capacity
Q
L*rho*Den*(cxx+cy
Heat source
h_{trans}
0
L*rho*Den*(cxx+cyy)
ective heat transfer coefficient
T_{ext}
0
External temperature
C_{trans}
0
User-defined constant
$T_{ambtrans}$
0
Ambient temperature
OK
Cancel
Apply
Help

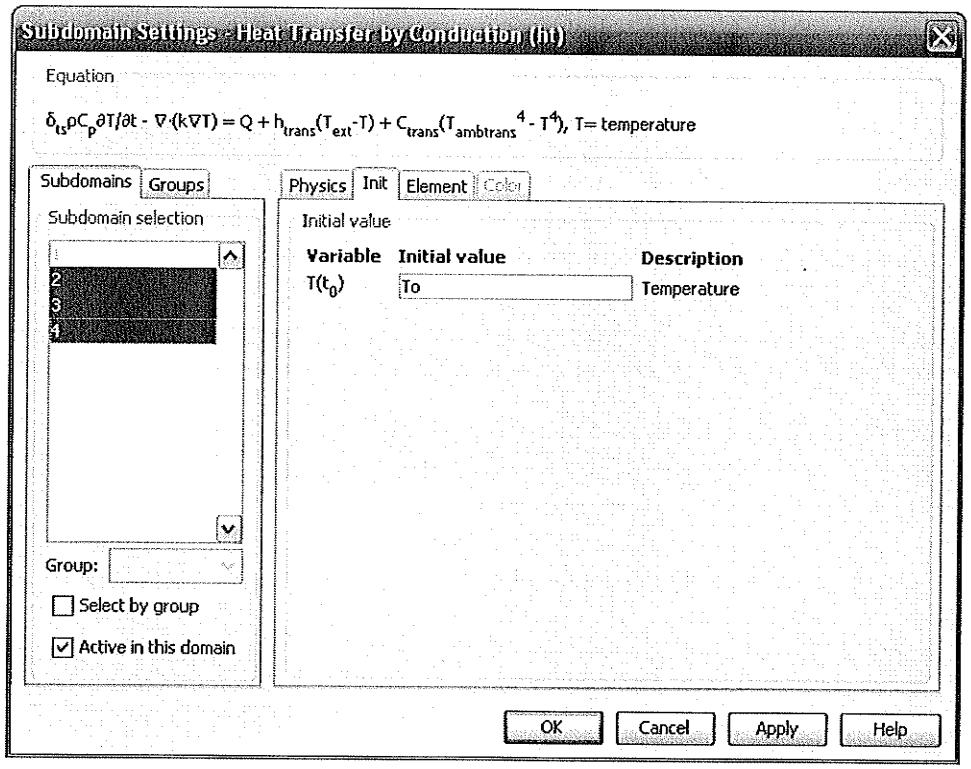
Subdomain Settings - Heat Transfer by Conduction (ht)
Equation
$\delta_{ts}\rho C_p \partial T/\partial t - \nabla\cdot(k\nabla T) = Q + h_{trans}(T_{ext}-T) + C_{trans}(T_{ambtrans}^4 - T^4)$, T= temperature
Subdomains
Groups
Subdomain selection
2
3
4
Group:
Select by group
Active in this domain
Physics
Init
Element
Color
Initial value
Variable
Initial value
Description
$T(t_0)$
To
Temperature
OK
Cancel
Apply
Help

Boundary Settings – Heat Transfer by Conduction

1 From the **Physics** menu select **Boundary Settings**.

2 Enter the settings as follows; when done, click **OK**:

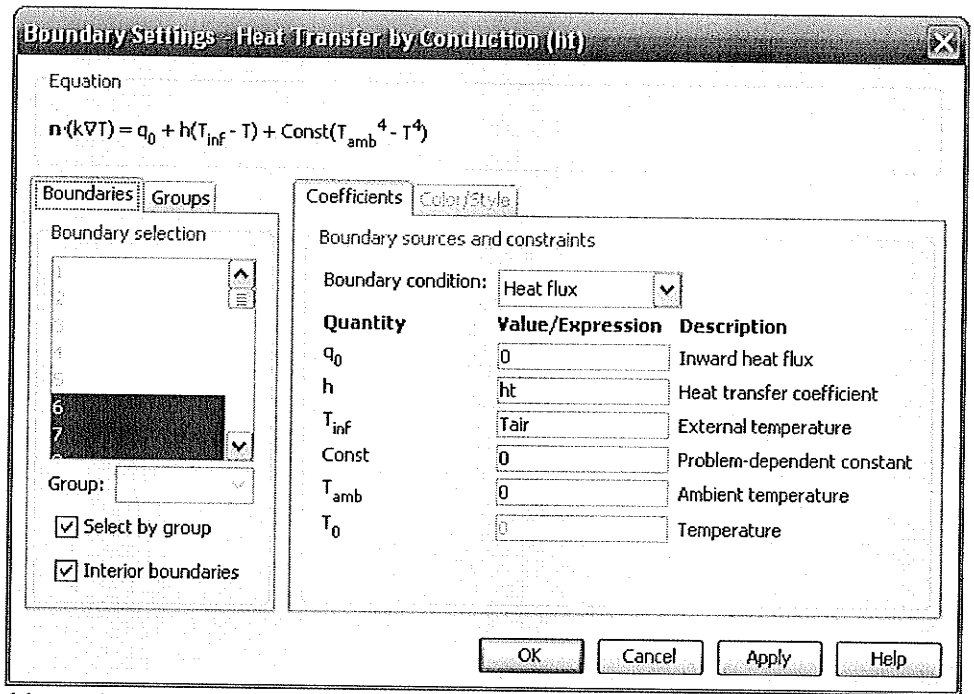

Selected boundaries: 6-8, 11-12, 15-16, 20-21, 27, 29, 32, 35-36, 39-40, 43-44, 47-49.

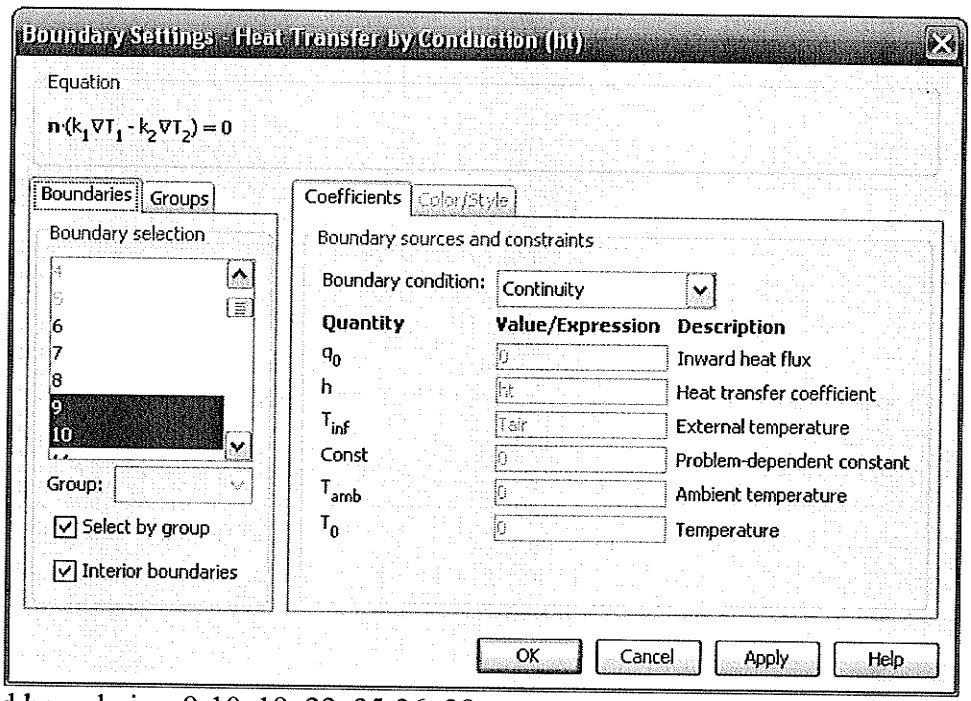

Selected boundaries: 9-10, 19, 22, 25-26, 28.

Subdomain Settings – Diffusion

1 From the **Multiphysics** menu select **2 Diffusion (di)**.

2 From the **Physics** menu select **Subdomain Settings**.

3 Select the subdomains **2** (refers to embryo or germ), **3** (endosperm), and **4** (attachment layer between embryo and endosperm) and enter the following settings from the figures; when done, click **OK**:

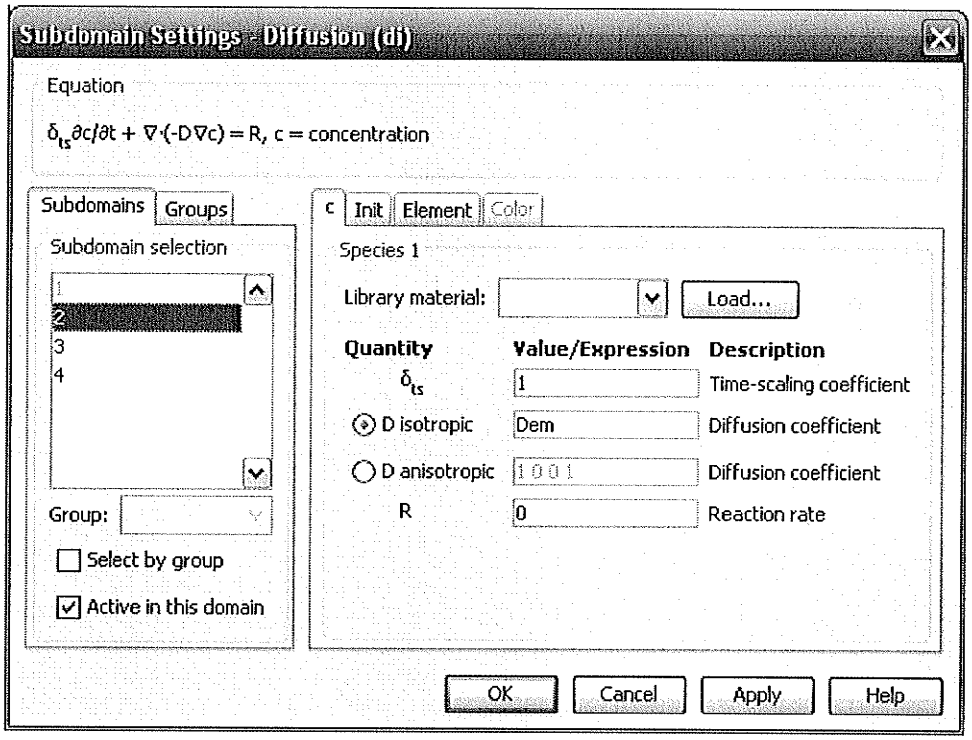

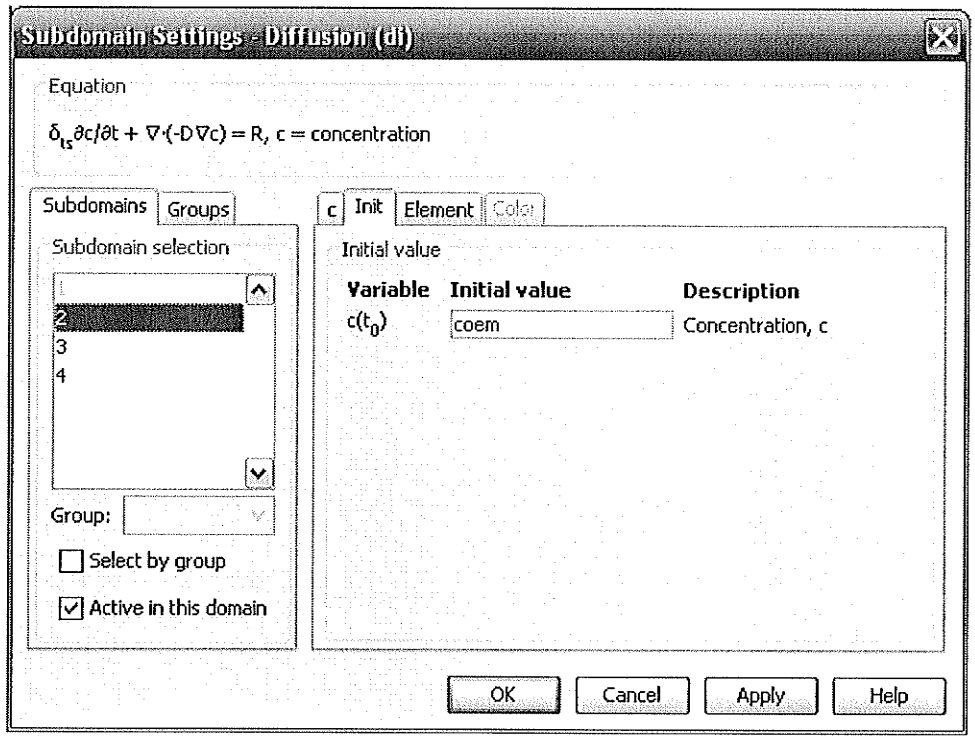
Subdomain Settings - Diffusion (di)
Equation
$\delta_{ts}\partial c/\partial t + \nabla\cdot(-D\nabla c) = R$, c = concentration
Subdomains
Groups
Subdomain selection
1
2
3
4
Group:
Select by group
Active in this domain
c
Init
Element
Color
Initial value
Variable
Initial value
Description
$c(t_0)$
coem
Concentration, c
OK
Cancel
Apply
Help

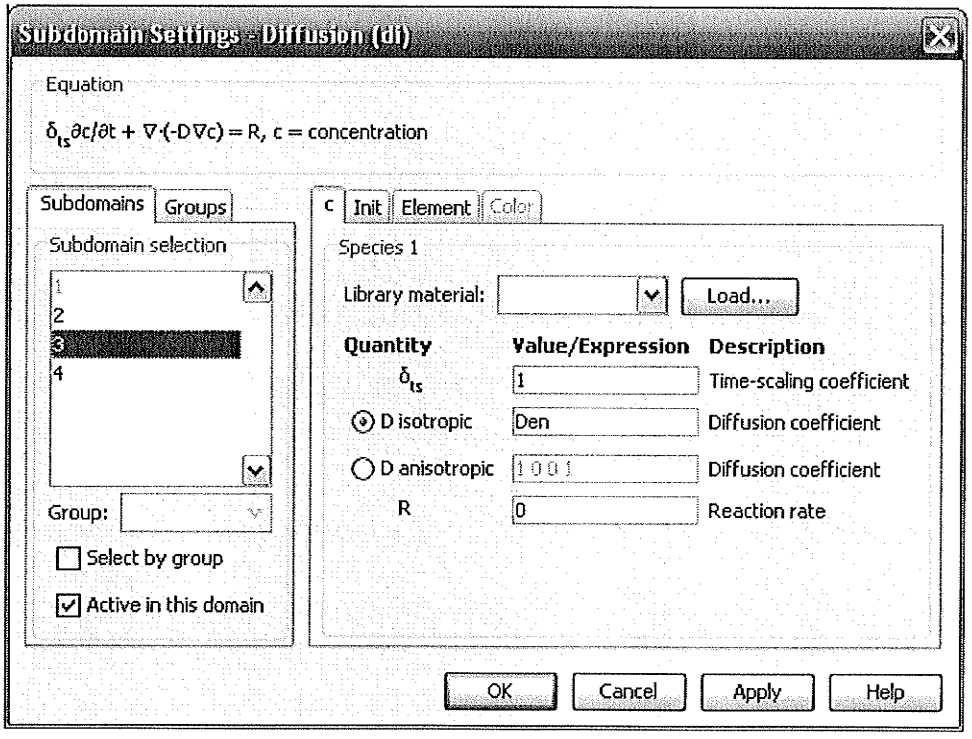
Subdomain Settings - Diffusion (di)
Equation
$\delta_{ts}\partial c/\partial t + \nabla\cdot(-D\nabla c) = R$, c = concentration
Subdomains
Groups
Subdomain selection
1
2
3
4
Group:
Select by group
Active in this domain
c
Init
Element
Color
Species 1
Library material:
Load...
Quantity
Value/Expression
Description
δ_{ts}
1
Time-scaling coefficient
D isotropic
Den
Diffusion coefficient
D anisotropic
1 0 0 1
Diffusion coefficient
R
0
Reaction rate
OK
Cancel
Apply
Help

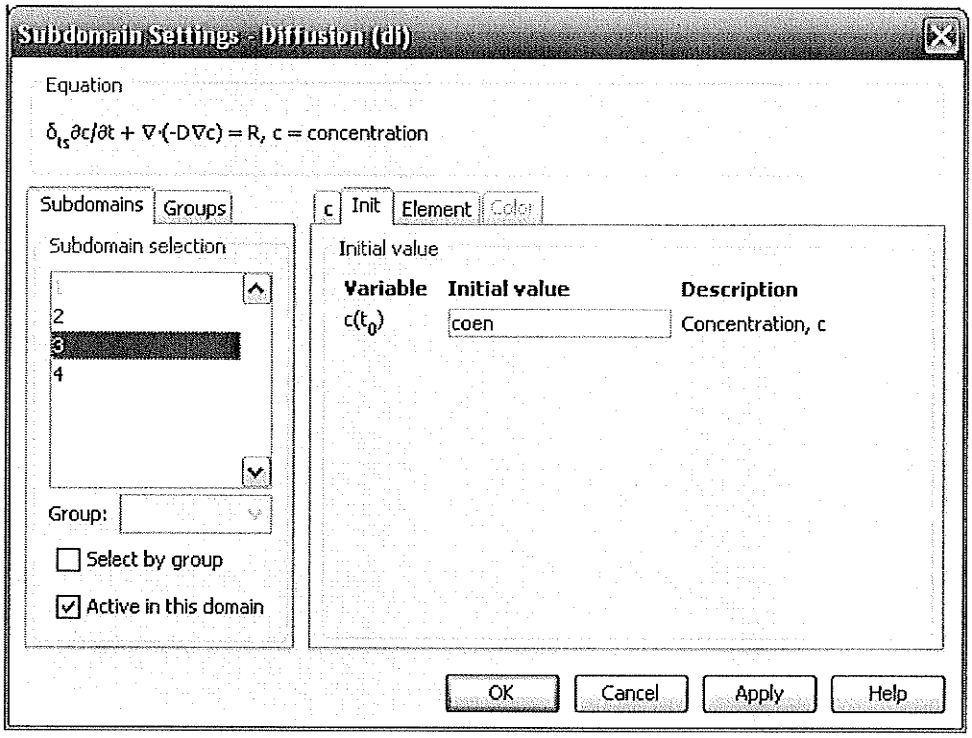
Subdomain Settings - Diffusion (di)
Equation
$\delta_{ts}\partial c/\partial t + \nabla\cdot(-D\nabla c) = R$, c = concentration
Subdomains
Groups
Subdomain selection
2
3
4
Group:
Select by group
Active in this domain
c
Init
Element
Color
Initial value
Variable
Initial value
Description
$c(t_0)$
coen
Concentration, c
OK
Cancel
Apply
Help

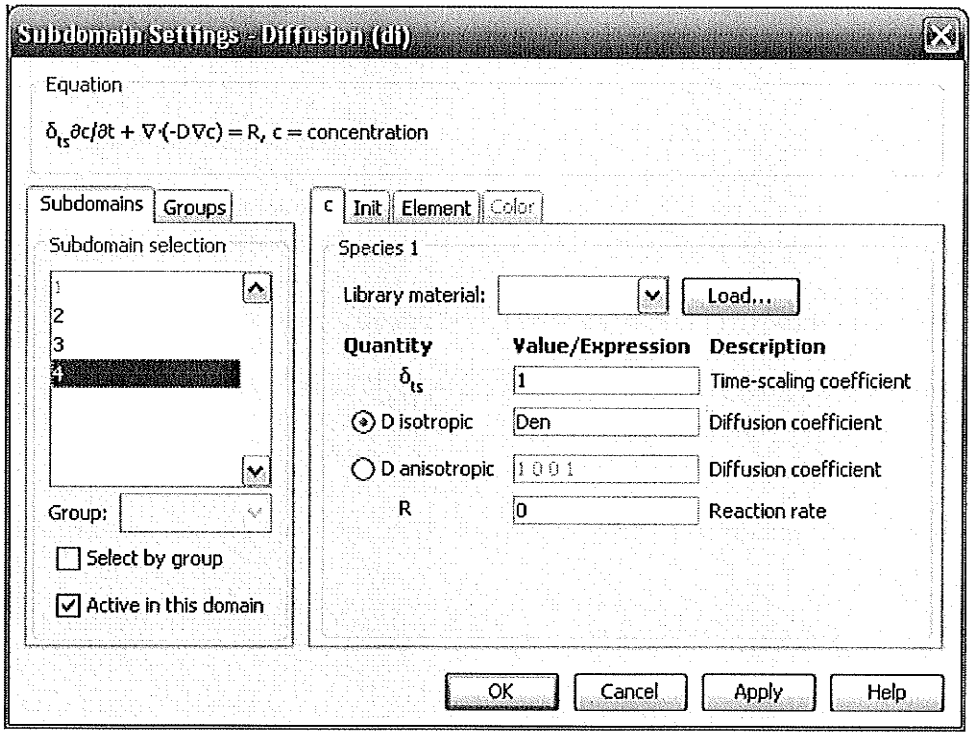
Subdomain Settings - Diffusion (di)
Equation
$\delta_{ts}\partial c/\partial t + \nabla\cdot(-D\nabla c) = R$, c = concentration
Subdomains
Groups
Subdomain selection
1
2
3
4
Group:
Select by group
Active in this domain
c
Init
Element
Color
Species 1
Library material:
Load...
Quantity
Value/Expression
Description
δ_{ts}
1
Time-scaling coefficient
D isotropic
Den
Diffusion coefficient
D anisotropic
1 0 0 1
Diffusion coefficient
R
0
Reaction rate
OK
Cancel
Apply
Help

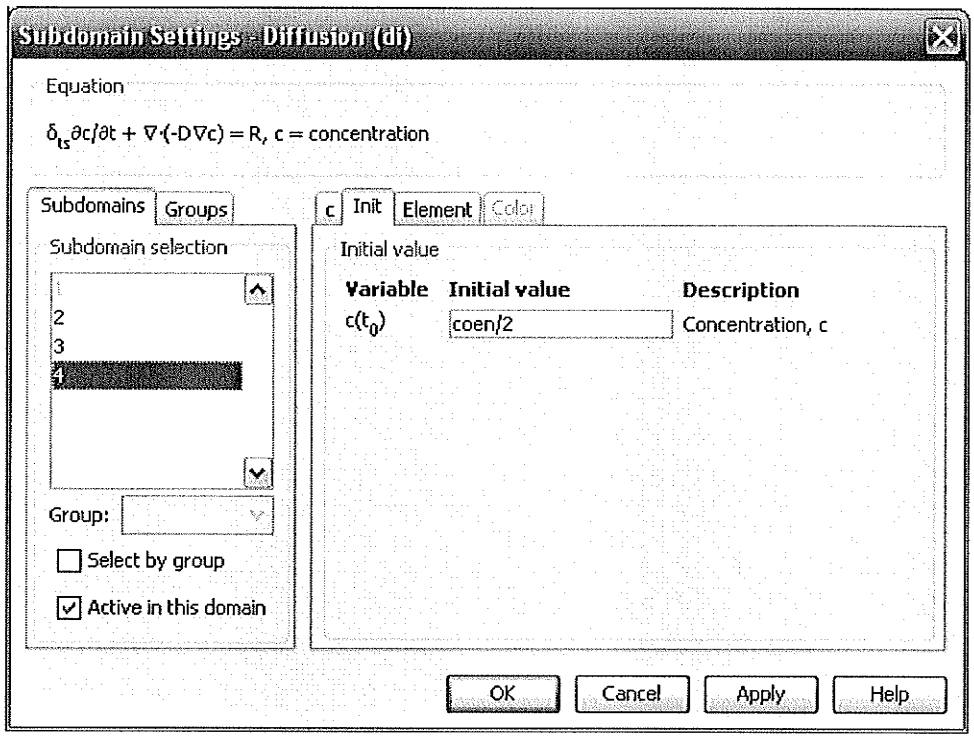

Boundary Settings – Heat Transfer by Conduction

1 From the **Physics** menu select **Boundary Settings**.

2 Enter the settings as follows; when done, click **OK**:

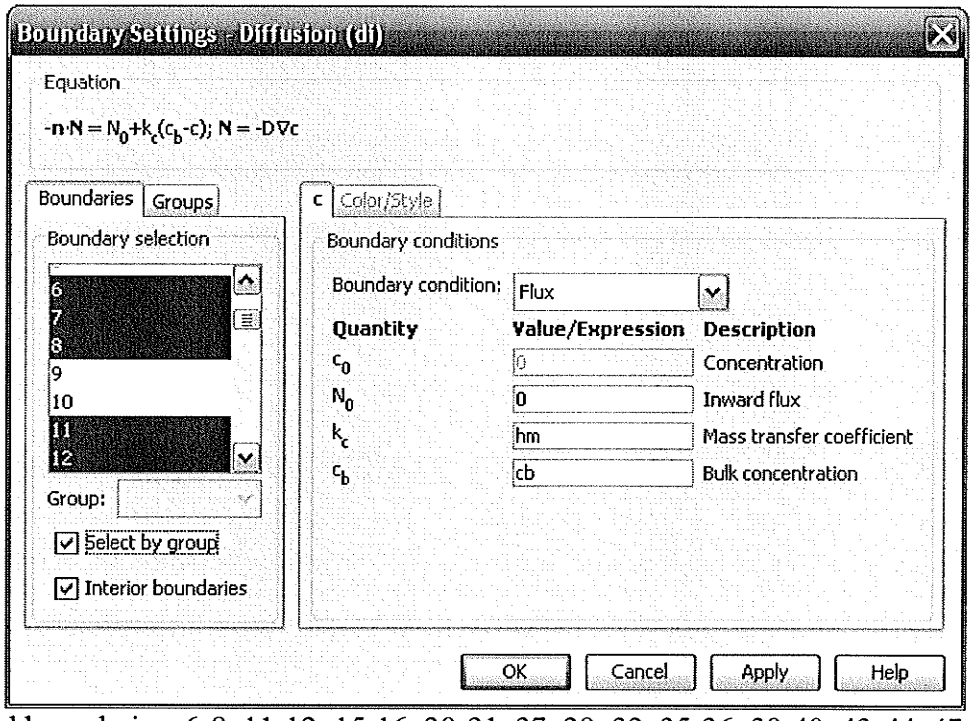

Selected boundaries: 6-8, 11-12, 15-16, 20-21, 27, 29, 32, 35-36, 39-40, 43-44, 47-49.

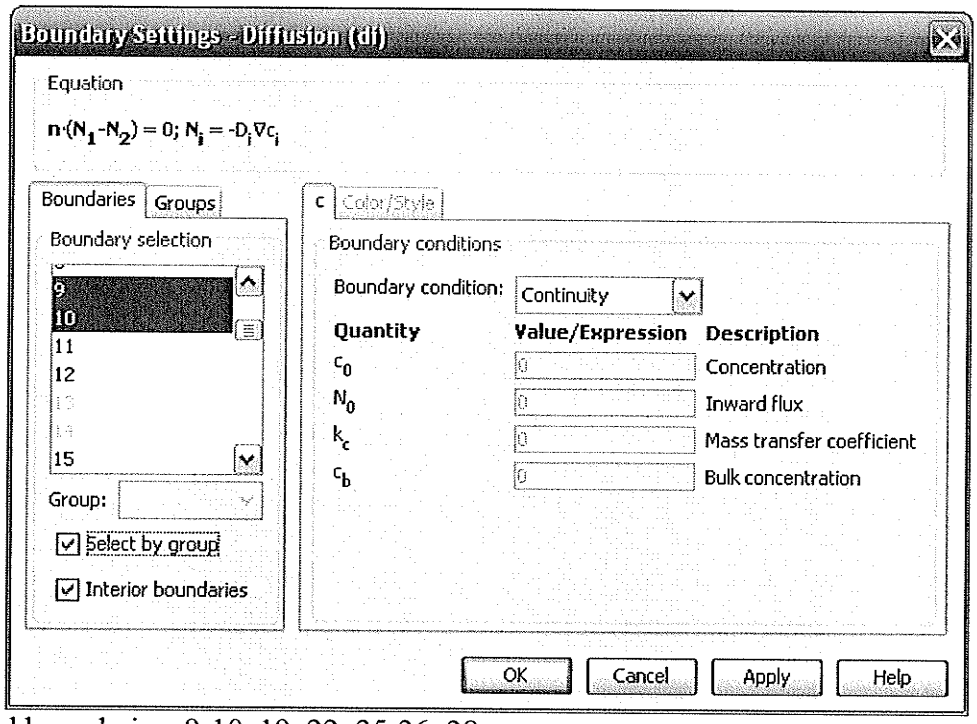

Selected boundaries: 9-10, 19, 22, 25-26, 28.

MESH GENERATION

1 From the **Mesh** menu select **Initialize Mesh**.

COMPUTING THE SOLUTION

1 From the **Solve** menu open the **Solver Parameters** dialog box.

2 In the **General** page enter 0:600:14400 in the **Times** field. Click **OK**.

3 From the **Solve** menu select **Solve Problem**.

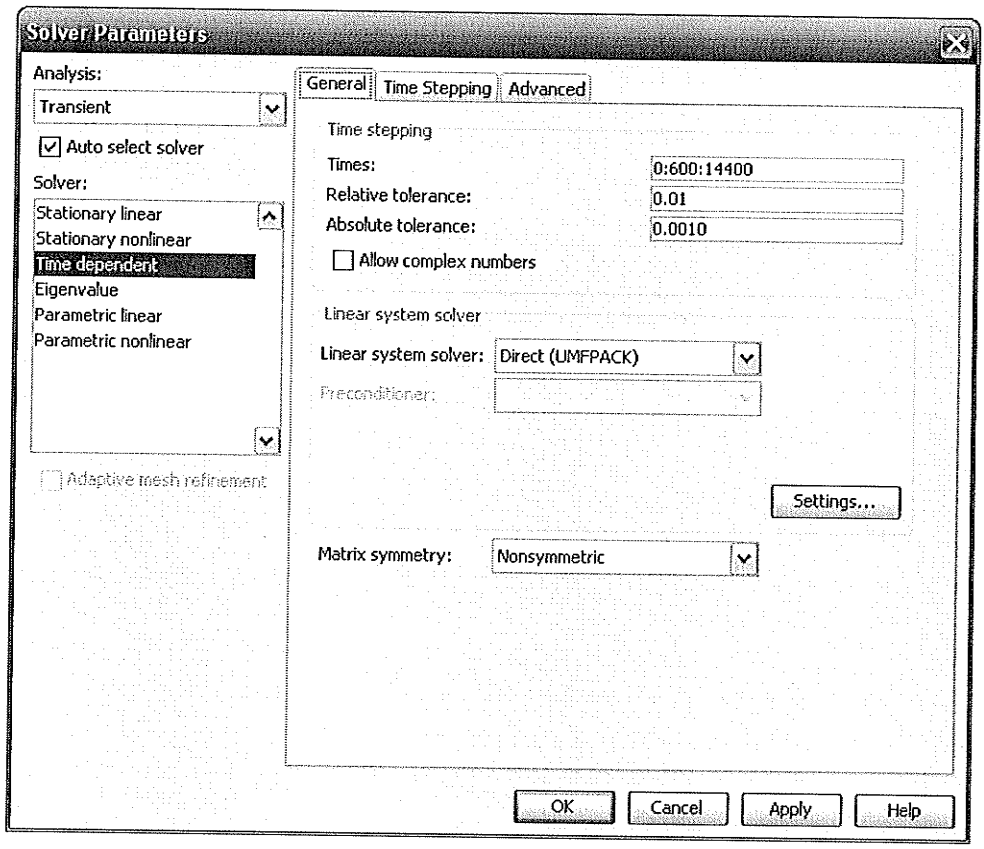

POSTPROCESSING AND VISUALIZATION

1 From the **Postprocessing** menu open the **Plot Parameters** dialog box.

2 Go to the **General** page and choose the way of viewing the plot as mentioned below:

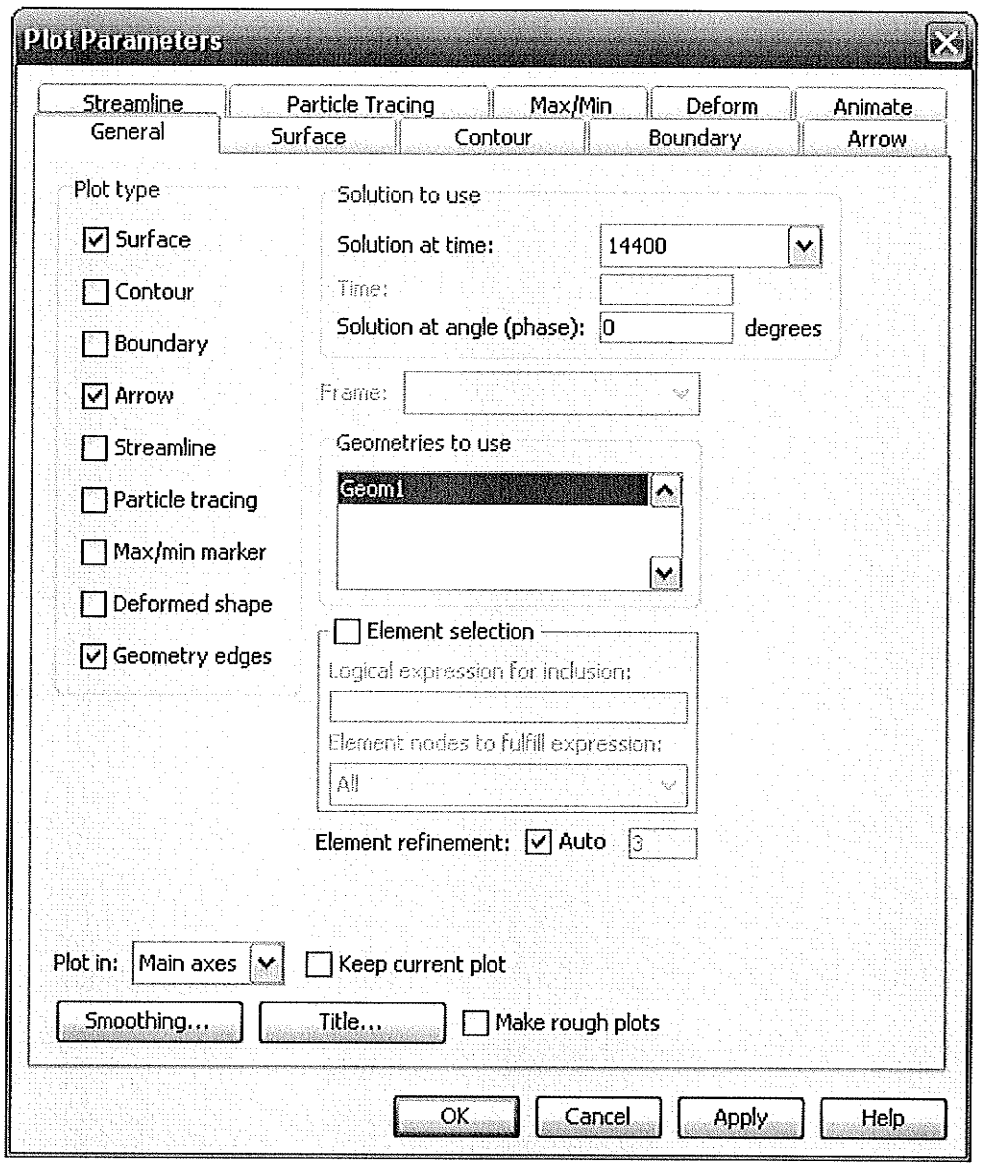

The following steps describe how to compute the moisture content:

1 From the **Postprocessing** menu open the **Subdomain Integration** dialog box.

2 Go to **Predefined quantities** and select Concentration, c (di).

3 Select subdomain 1, then in the **Expression** edit field enter 1. Click **Apply**. The value of the selected area appears in the message bar at the bottom of the user interface.

4 Again follow steps 1 and 2.

5 Select subdomain 1, then in the **Expression** edit field enter [(c/value obtained from Step 3)*100]. Click **Apply**. The value of the moisture content (in percentage) appears in the message bar at the bottom of the user interface.

Table H.2 Various model simulated wheat drying data (initial moisture content 17% w.b., drying temperature 35°C) used in Fig. 6.7.

Drying time (min)	Moisture content, % d.b.			
	Jayas and Sokhansanj (1986)	Sinico et al. (1995)	Present study	Jia et al. (2000)
0	20.45	20.45	19.83	19.99
30	18.05	18.21	17.26	18.94
60	16.23	17.12	16.16	18.54
90	14.85	16.33	15.37	18.24
120	13.80	15.70	14.75	17.99
150	13.01	15.19	14.24	17.77
180	12.40	14.76	13.80	17.58
210	11.95	14.39	13.43	17.40
240	11.60	14.07	13.10	17.25

Table H.3 Model simulated drying data for wheat components (initial moisture content 17% w.b., drying temperature 35°C) used in Fig. 6.8.

Drying time (min)	Moisture content, % d.b.	
	Germ	Endosperm
0	57.35	13.93
30	43.41	13.15
60	37.48	12.80
90	33.28	12.55
120	29.97	12.36
150	27.25	12.19
180	24.99	12.04
210	23.06	11.91
240	21.40	11.80

Table H.4 Model simulated mass average moisture data for wheat drying (initial moisture content 17.4% w.b., drying temperature 47°C) used in Fig. 6.9.

Drying time (min)	Moisture content, % w.b.	
	Jia et al. (2000)	Present study
0	17.42	17.31
5	17.12	16.83
10	17.01	16.61
15	16.92	16.45
20	16.85	16.32
25	16.78	16.20
30	16.72	16.09
35	16.66	15.99
40	16.61	15.90
45	16.57	15.81
50	16.52	15.73
55	16.49	15.65
60	16.44	15.58
65	16.41	15.52
70	16.37	15.45

Table H.5a Data for magnetic resonance image data trends and predicted drying curves for endosperm of intact wheat kernels during drying at 30, 40, and 50°C (Fig. 6.10a).

Drying Temperature (°C)	Drying time (min)	Average MR image (MRI) intensity ratio $(I/I_o)^*$	Model derived moisture content, M, d.b. (decimal)	Moisture ratio, $MR = \frac{M - M_e}{M_o - M_e}$ §
30	0	1.00	0.4079	1.00
	30	0.98	0.3358	0.81
	60	0.86	0.3077	0.74
	90	0.78	0.2873	0.69
	120	0.63	0.2704	0.65
	150	0.51	0.2560	0.61
	180	0.40	0.2434	0.58
	210	0.32	0.2322	0.55
	240	0.26	0.2219	0.52
40	0	1.00	0.4078	1.00
	30	0.84	0.3095	0.75
	60	0.69	0.2728	0.65
	90	0.50	0.2465	0.58
	120	0.33	0.2251	0.53
	150	0.24	0.2071	0.48
	180	0.17	0.1916	0.44
	210	0.13	0.1780	0.41
	240	0.12	0.1658	0.38
50	0	1.00	0.4179	1.00
	30	0.65	0.2844	0.66
	60	0.41	0.2370	0.55
	90	0.25	0.2033	0.46
	120	0.16	0.1771	0.39
	150	0.12	0.1559	0.34
	180	0.09	0.1381	0.30
	210	0.08	0.1229	0.26
	240	0.08	0.1098	0.23

* Data obtained from Table G.1a-c. § M_e is the equilibrium moisture content = 0.02 (d.b.).

Table H.5b Data for magnetic resonance image data trends and predicted drying curves for germ of intact wheat kernels during drying at 30, 40, and 50°C (Fig. 6.10b).

Drying Temperature (°C)	Drying time (min)	Average MR image (MRI) intensity ratio $(I/I_o)^*$	Model derived moisture content, M, d.b. (decimal)	Moisture ratio, $MR = \frac{M - M_e}{M_o - M_e}$ §
30	0	1.00	1.5525	1.00
	30	1.00	1.1397	0.73
	60	0.88	0.9620	0.61
	90	0.76	0.8339	0.53
	120	0.70	0.7309	0.46
	150	0.65	0.6454	0.41
	180	0.59	0.5729	0.36
	210	0.57	0.5105	0.32
	240	0.51	0.4560	0.28
40	0	1.00	1.5031	1.00
	30	0.71	1.0238	0.68
	60	0.51	0.8289	0.55
	90	0.48	0.6925	0.45
	120	0.42	0.5854	0.38
	150	0.43	0.4983	0.32
	180	0.39	0.4268	0.27
	210	0.38	0.3671	0.23
	240	0.41	0.3168	0.20
50	0	1.00	1.7006	1.00
	30	0.63	1.0654	0.62
	60	0.46	0.8231	0.48
	90	0.40	0.6543	0.38
	120	0.36	0.5283	0.30
	150	0.38	0.4306	0.24
	180	0.41	0.3531	0.20
	210	0.39	0.2907	0.16
	240	0.38	0.2403	0.13

* Data obtained from Table G.1a-c. § M_e is the equilibrium moisture content = 0.02 (d.b.).

Table H.6a Data for magnetic resonance image data trends and predicted drying curves for endosperm of mechanically scarified wheat kernels during drying at 30, 40, and 50°C (Fig. 6.11a).

Drying Temperature (°C)	Drying time (min)	Average MR image (MRI) intensity ratio $(I/I_o)^*$	Model derived moisture content, M, d.b. (decimal)	Moisture ratio, $MR = \frac{M - M_e}{M_o - M_e}$ §
30	0	1.00	0.2921	1.00
	30	0.81	0.2407	0.81
	60	0.73	0.2179	0.73
	90	0.61	0.2007	0.66
	120	0.50	0.1868	0.61
	150	0.41	0.1749	0.57
	180	0.34	0.1645	0.53
	210	0.27	0.1553	0.50
	240	0.22	0.1470	0.47
40	0	1.00	0.3979	1.00
	30	0.92	0.2825	0.69
	60	0.63	0.2407	0.58
	90	0.35	0.2113	0.51
	120	0.20	0.1882	0.45
	150	0.15	0.1693	0.40
	180	0.11	0.1535	0.35
	210	0.09	0.1400	0.32
	240	0.09	0.1284	0.29
50	0	1.00	0.5261	1.00
	30	0.64	0.3226	0.60
	60	0.41	0.2544	0.46
	90	0.24	0.2089	0.37
	120	0.15	0.1753	0.31
	150	0.09	0.1491	0.26
	180	0.07	0.1281	0.21
	210	0.04	0.1108	0.18
	240	0.04	0.0965	0.15

* Data obtained from Table G.2a-c. § M_e is the equilibrium moisture content = 0.02 (d.b.).

Table H.6b Data for magnetic resonance image data trends and predicted drying curves for germ of mechanically scarified wheat kernels during drying at 30, 40, and 50°C (Fig. 6.11b).

Drying Temperature (°C)	Drying time (min)	Average MR image (MRI) intensity ratio (I/I_o)*	Model derived moisture content, M, d.b. (decimal)	Moisture ratio, $MR = \frac{M - M_e}{M_o - M_e}$ §
30	0	1.00	1.6760	1.00
	30	0.79	1.2870	0.77
	60	0.74	1.1146	0.66
	90	0.53	0.9858	0.58
	120	0.43	0.8826	0.52
	150	0.35	0.7955	0.47
	180	0.37	0.7203	0.42
	210	0.32	0.6540	0.38
	240	0.32	0.5950	0.35
40	0	1.00	2.0728	1.00
	30	0.67	1.4904	0.72
	60	0.50	1.2462	0.60
	90	0.41	1.0697	0.51
	120	0.34	0.9277	0.44
	150	0.36	0.8098	0.38
	180	0.32	0.7103	0.34
	210	0.27	0.6252	0.29
	240	0.30	0.5515	0.26
50	0	1.00	1.8653	1.00
	30	0.59	1.2494	0.67
	60	0.32	1.0038	0.53
	90	0.24	0.8293	0.44
	120	0.24	0.6935	0.36
	150	0.22	0.5840	0.31
	180	0.24	0.4937	0.26
	210	0.23	0.4188	0.22
	240	0.22	0.3552	0.18

* Data obtained from Table G.2a-c. § M_e is the equilibrium moisture content = 0.02 (d.b.).

Table H.7 Data for magnetic resonance image data trends and predicted drying curves for endosperm of germ-removed wheat kernels during drying at 30, 40, and 50°C (Fig. 6.12).

Drying Temperature (°C)	Drying time (min)	Average MR image (MRI) intensity ratio (I/I_o)*	Model derived moisture content, M, d.b. (decimal)	Moisture ratio, $MR = \frac{M - M_e}{M_o - M_e}$ §
30	0	1.00	0.4999	1.00
	30	0.90	0.3870	0.76
	60	0.80	0.3431	0.67
	90	0.65	0.3110	0.61
	120	0.57	0.2851	0.55
	150	0.46	0.2627	0.51
	180	0.39	0.2432	0.47
	210	0.34	0.2259	0.43
	240	0.30	0.2104	0.40
40	0	1.00	0.5099	1.00
	30	0.83	0.3534	0.68
	60	0.60	0.2949	0.56
	90	0.37	0.2530	0.48
	120	0.27	0.2199	0.41
	150	0.16	0.1927	0.35
	180	0.12	0.1696	0.31
	210	0.08	0.1500	0.27
	240	0.08	0.1331	0.23
50	0	1.00	0.5099	1.00
	30	0.59	0.3030	0.58
	60	0.28	0.2297	0.43
	90	0.15	0.1800	0.33
	120	0.09	0.1438	0.25
	150	0.07	0.1161	0.20
	180	0.04	0.0948	0.15
	210	0.05	0.0783	0.12
	240	0.04	0.0655	0.09

* Data obtained from Table G.3. § M_e is the equilibrium moisture content = 0.02 (d.b.).

Table H.8a Calculation of Biot number for heat transfer and Lewis number for intact wheat kernel during drying at 30°C for 4 h (Figs. 6.18 and 6.20).

Wheat components	Model derived moisture content, d.b.	Thermal conductivity (K)* W m^{-1} K^{-1}	Specific heat (C_g)* J kg^{-1} K^{-1}	Density (ρ_g)* kg m^{-3}	Biot number for heat transfer[a]	Lewis number[b]
Endosperm	0.41	0.417	3007.88	696.50	0.245	12609.19
	0.34	0.368	2705.99	644.76	0.277	13361.99
	0.31	0.349	2588.34	647.84	0.292	13181.74
	0.29	0.335	2502.93	656.14	0.305	12924.52
	0.27	0.324	2432.16	666.04	0.315	12653.85
	0.26	0.314	2371.87	676.13	0.325	12395.43
	0.24	0.306	2319.12	685.87	0.334	12156.48
	0.23	0.298	2272.22	695.00	0.343	11939.09
	0.22	0.291	2229.10	703.62	0.351	11738.38
Germ	1.55	1.196	7800.32	16317.84	0.085	1317.52
	1.14	0.915	6071.92	8219.41	0.112	2571.36
	0.96	0.794	5327.89	5327.87	0.129	3923.82
	0.83	0.707	4791.54	3596.26	0.144	5754.87
	0.73	0.637	4360.28	2467.50	0.160	8303.97
	0.65	0.579	4002.29	1731.46	0.176	11715.77
	0.57	0.530	3698.73	1258.93	0.193	15950.76
	0.51	0.487	3437.46	964.91	0.210	20598.73
	0.46	0.450	3209.27	790.74	0.227	24874.73

*Values are derived using the equations in Table 6.2; [a]Refer to Eq. 6.30; [b]Refer to Eq. 6.31.

Moisture diffusivities of Endosperm at 30, 40, and 50°C are: 1.58e-11, 3.03e-11, and 5.56e-11 m^2 s^{-1}, respectively.

Moisture diffusivities of Germ at 30, 40, and 50°C are: 7.13e-12, 9.58e-12, and 1.26e-11 m^2 s^{-1}, respectively.

Table H.8b Calculation of Biot number for heat transfer and Lewis number for intact wheat kernel during drying at 40°C for 4 h (Figs. 6.18 and 6.20).

Wheat components	Model derived moisture content, d.b.	Thermal conductivity (K)* W m^{-1} K^{-1}	Specific heat (C_g)* J kg^{-1} K^{-1}	Density (ρ_g)* kg m^{-3}	Biot number for heat transfer[a]	Lewis number[b]
Endosperm	0.41	0.417	3007.46	696.35	0.244	6576.28
	0.31	0.350	2595.88	647.33	0.290	6883.11
	0.27	0.326	2442.21	664.49	0.312	6619.71
	0.25	0.308	2332.10	683.41	0.331	6370.07
	0.23	0.293	2242.49	700.93	0.347	6153.47
	0.21	0.281	2167.13	716.05	0.362	5972.65
	0.19	0.270	2102.23	728.70	0.376	5823.10
	0.18	0.261	2045.29	739.09	0.390	5699.15
	0.17	0.253	1994.20	747.59	0.402	5595.07
Germ	1.50	1.162	7593.48	15285.03	0.087	1045.14
	1.02	0.836	5586.65	6275.91	0.122	2489.48
	0.83	0.704	4770.60	3535.73	0.145	4354.52
	0.69	0.611	4199.50	2113.47	0.166	7184.76
	0.59	0.538	3751.07	1330.33	0.189	11255.42
	0.50	0.479	3386.38	919.39	0.212	16054.43
	0.43	0.430	3087.01	727.25	0.236	20003.54
	0.37	0.390	2837.05	655.47	0.261	21870.78
	0.32	0.355	2626.44	645.68	0.286	21877.31

*Values are derived using the equations in Table 6.2; [a]Refer to Eq. 6.30; [b]Refer to Eq. 6.31.

Moisture diffusivities of Endosperm at 30, 40, and 50°C are: 1.58e-11, 3.03e-11, and 5.56e-11 m^2 s^{-1}, respectively.

Moisture diffusivities of Germ at 30, 40, and 50°C are: 7.13e-12, 9.58e-12, and 1.26e-11 m^2 s^{-1}, respectively.

Table H.8c Calculation of Biot number for heat transfer and Lewis number for intact wheat kernel during drying at 50°C for 4 h (Figs. 6.18 and 6.20).

Wheat components	Model derived moisture content, d.b.	Thermal conductivity (K)* W m^{-1} K^{-1}	Specific heat (C_g)* J kg^{-1} K^{-1}	Density (ρ_g)* kg m^{-3}	Biot number for heat transfer[a]	Lewis number[b]
Endosperm	0.42	0.424	3049.75	711.79	0.239	3514.41
	0.28	0.333	2490.78	657.66	0.305	3660.49
	0.24	0.301	2292.32	691.05	0.337	3419.33
	0.20	0.278	2151.22	719.21	0.365	3234.53
	0.18	0.260	2041.52	739.75	0.390	3101.52
	0.16	0.246	1952.75	753.76	0.413	3006.09
	0.14	0.234	1878.22	762.90	0.434	2935.97
	0.12	0.224	1814.58	768.48	0.454	2883.58
	0.11	0.215	1759.73	771.53	0.473	2843.70
Germ	1.70	1.296	8420.41	19468.23	0.078	627.64
	1.07	0.864	5760.83	6950.24	0.117	1713.54
	0.82	0.700	4746.32	3466.21	0.145	3375.47
	0.65	0.585	4039.55	1799.17	0.174	6387.40
	0.53	0.499	3511.99	1038.27	0.203	10866.22
	0.43	0.433	3102.92	734.39	0.235	15073.86
	0.35	0.380	2778.43	648.65	0.267	16738.88
	0.29	0.338	2517.16	654.46	0.301	16268.17
	0.24	0.303	2306.14	688.36	0.335	15168.75

*Values are derived using the equations in Table 6.2; [a]Refer to Eq. 6.30; [b]Refer to Eq. 6.31.

Moisture diffusivities of Endosperm at 30, 40, and 50°C are: 1.58e-11, 3.03e-11, and 5.56e-11 m^2 s^{-1}, respectively.

Moisture diffusivities of Germ at 30, 40, and 50°C are: 7.13e-12, 9.58e-12, and 1.26e-11 m^2 s^{-1}, respectively.

Table H.9 Model derived center and surface temperatures in the wheat kernel during drying at 50°C (Fig. 6.19).

Drying time (s)	Center temperature (°C)	Surface temperature (°C)
0	25.9	25.9
5	26.3	28.5
10	27.0	29.9
15	27.7	31.1
20	28.5	32.1
25	29.2	33.1
30	29.9	33.8
40	31.2	35.3
50	32.5	36.5
60	33.6	37.5
70	34.6	38.4
80	35.7	39.2
90	36.6	39.9
100	37.4	40.6
110	38.2	41.2
120	38.8	41.7
130	39.5	42.2
140	40.1	42.7
150	40.7	43.2
180	42.2	44.3
210	43.4	45.3
240	44.5	46.0
270	45.3	46.6
300	46.0	47.2
360	47.1	48.0
420	47.8	48.6
480	48.3	48.9
540	48.6	49.2
600	48.8	49.4
660	48.9	49.4
720	49.0	49.5
840	49.2	49.6
900	49.3	49.7

Table H.10a Model predicted data for deriving the scale factors needed for calculating activation energies of water removal process from intact wheat kernel components (Fig. 6.21a) and for developing the normalized drying curves (Fig. 6.22).

Wheat components	Drying time (min)	Drying temperature (°C)								
		30		40		50		30	40	50
Col. 1	Col. 2	Col. 3	Col. 4	Col. 5	Col. 6	Col. 7	Col. 8	Col. 9	Col. 10	Col. 11
		MR	ln (MR)	MR	ln (MR)	MR	ln (MR)	ln (MR) × Scale factor*§		
Endosperm	0	1.00	0.00	1.00	0.00	1.00	0.00	0.00	0.00	0.00
	30	0.81	-0.21	0.75	-0.29	0.66	-0.41	-0.21	-0.20	-0.19
	60	0.74	-0.30	0.65	-0.43	0.55	-0.61	-0.30	-0.30	-0.28
	90	0.69	-0.37	0.58	-0.54	0.46	-0.78	-0.37	-0.37	-0.36
	120	0.65	-0.44	0.53	-0.64	0.39	-0.93	-0.44	-0.44	-0.43
	150	0.61	-0.50	0.48	-0.73	0.34	-1.07	-0.50	-0.51	-0.50
	180	0.58	-0.55	0.44	-0.82	0.30	-1.21	-0.55	-0.57	-0.57
	210	0.55	-0.60	0.41	-0.90	0.26	-1.35	-0.60	-0.62	-0.63
	240	0.52	-0.65	0.38	-0.98	0.23	-1.49	-0.65	-0.68	-0.70
Germ	0	1.00	0.00	1.00	0.00	1.00	0.00	0.00	0.00	0.00
	30	0.73	-0.31	0.68	-0.39	0.62	-0.47	-0.31	-0.32	-0.30
	60	0.61	-0.49	0.55	-0.61	0.48	-0.74	-0.49	-0.50	-0.46
	90	0.53	-0.63	0.45	-0.79	0.38	-0.97	-0.63	-0.65	-0.61
	120	0.46	-0.77	0.38	-0.96	0.30	-1.20	-0.77	-0.80	-0.75
	150	0.41	-0.90	0.32	-1.13	0.24	-1.41	-0.90	-0.94	-0.88
	180	0.36	-1.02	0.27	-1.29	0.20	-1.62	-1.02	-1.07	-1.01
	210	0.32	-1.14	0.23	-1.45	0.16	-1.83	-1.14	-1.20	-1.14
	240	0.28	-1.26	0.20	-1.61	0.13	-2.03	-1.26	-1.33	-1.27

*Scale factors (Table 6.9) were calculated based on the following third-order polynomial regression curves:

$$\text{Endosperm}_{30^\circ C}: \ln(MR) = -6e-08 \cdot t^3 + 3e-05 \cdot t^2 - 0.0063 \cdot t - 0.0144 \quad \text{(H.19)}$$

$$\text{Endosperm}_{40^\circ C}: \ln(MR) = -8e-08 \cdot t^3 + 4e-05 \cdot t^2 - 0.0089 \cdot t - 0.0202 \quad \text{(H.20)}$$

$$\text{Endosperm}_{50^\circ C}: \ln(MR) = -1e-07 \cdot t^3 + 5e-05 \cdot t^2 - 0.0125 \cdot t - 0.0271 \quad \text{(H.21)}$$

$$\text{Germ}_{30^\circ C}: \ln(MR) = -8e-08 \cdot t^3 + 4e-05 \cdot t^2 - 0.0098 \cdot t - 0.018 \quad \text{(H.22)}$$

$$\text{Germ}_{40^\circ C}: \ln(MR) = -1e-07 \cdot t^3 + 5e-05 \cdot t^2 - 0.0121 \cdot t - 0.0227 \quad \text{(H.23)}$$

$$\text{Germ}_{50^\circ C}: \ln(MR) = -1e-07 \cdot t^3 + 5e-05 \cdot t^2 - 0.0146 \cdot t - 0.0272 \quad \text{(H.24)}$$

§Columns 2 vs. 4, 6, and 8 were plotted in Fig. 6.21a; and columns 2 vs. 9, 10, and 11 were plotted in Fig. 6.22.

Table H.10b Model predicted data for deriving the scale factors needed for calculating activation energies of water removal process from mechanically scarified wheat kernel components (Fig. 6.21b) and for developing the normalized drying curves (Fig. H.3).

Wheat components	Drying time (min)	Drying temperature (°C)								
		30		40		50		30	40	50
Col. 1	Col. 2	Col. 3	Col. 4	Col. 5	Col. 6	Col. 7	Col. 8	Col. 9	Col. 10	Col. 11
		MR	ln (MR)	MR	ln (MR)	MR	ln (MR)	ln (MR) × Scale factor*§		
Endosperm	0	1.00	0.00	1.00	0.00	1.00	0.00	0.00	0.00	0.00
	30	0.81	-0.21	0.69	-0.36	0.60	-0.51	-0.21	-0.27	-0.28
	60	0.73	-0.32	0.58	-0.54	0.46	-0.77	-0.32	-0.40	-0.42
	90	0.66	-0.41	0.51	-0.68	0.37	-0.99	-0.41	-0.51	-0.54
	120	0.61	-0.49	0.45	-0.81	0.31	-1.18	-0.49	-0.60	-0.64
	150	0.57	-0.56	0.40	-0.93	0.26	-1.37	-0.56	-0.69	-0.74
	180	0.53	-0.63	0.35	-1.04	0.21	-1.54	-0.63	-0.77	-0.84
	210	0.50	-0.70	0.32	-1.15	0.18	-1.72	-0.70	-0.85	-0.93
	240	0.47	-0.76	0.29	-1.25	0.15	-1.89	-0.76	-0.93	-1.03
Germ	0	1.00	0.00	1.00	0.00	1.00	0.00	0.00	0.00	0.00
	30	0.77	-0.27	0.72	-0.33	0.67	-0.41	-0.27	-0.28	-0.28
	60	0.66	-0.41	0.60	-0.52	0.53	-0.63	-0.41	-0.43	-0.44
	90	0.58	-0.54	0.51	-0.67	0.44	-0.82	-0.54	-0.56	-0.58
	120	0.52	-0.65	0.44	-0.82	0.36	-1.01	-0.65	-0.68	-0.71
	150	0.47	-0.76	0.38	-0.96	0.31	-1.19	-0.76	-0.80	-0.83
	180	0.42	-0.86	0.34	-1.09	0.26	-1.36	-0.86	-0.91	-0.95
	210	0.38	-0.96	0.29	-1.22	0.22	-1.53	-0.96	-1.02	-1.07
	240	0.35	-1.06	0.26	-1.35	0.18	-1.71	-1.06	-1.13	-1.19

*Scale factors (Table 6.9) were calculated based on the following third-order polynomial regression curves:

$$\text{Endosperm}_{30^\circ C} : \ln(MR) = -6e-08 \cdot t^3 + 3e-05 \cdot t^2 - 0.0065 \cdot t - 0.0124 \quad \text{(H.25)}$$

$$\text{Endosperm}_{40^\circ C} : \ln(MR) = -1e-07 \cdot t^3 + 5e-05 \cdot t^2 - 0.0111 \cdot t - 0.0246 \quad \text{(H.26)}$$

$$\text{Endosperm}_{50^\circ C} : \ln(MR) = -1e-07 \cdot t^3 + 7e-05 \cdot t^2 - 0.0158 \cdot t - 0.033 \quad \text{(H.27)}$$

$$\text{Germ}_{30^\circ C} : \ln(MR) = -7e-08 \cdot t^3 + 3e-05 \cdot t^2 - 0.0084 \cdot t - 0.0151 \quad \text{(H.28)}$$

$$\text{Germ}_{40^\circ C} : \ln(MR) = -8e-08 \cdot t^3 + 4e-05 \cdot t^2 - 0.0103 \cdot t - 0.0197 \quad \text{(H.29)}$$

$$\text{Germ}_{50^\circ C} : \ln(MR) = -1e-07 \cdot t^3 + 5e-05 \cdot t^2 - 0.0125 \cdot t - 0.0237 \quad \text{(H.30)}$$

§Columns 2 vs. 4, 6, and 8 were plotted in Fig. 6.21b; and columns 2 vs. 9, 10, and 11 were plotted in Fig. H.3.

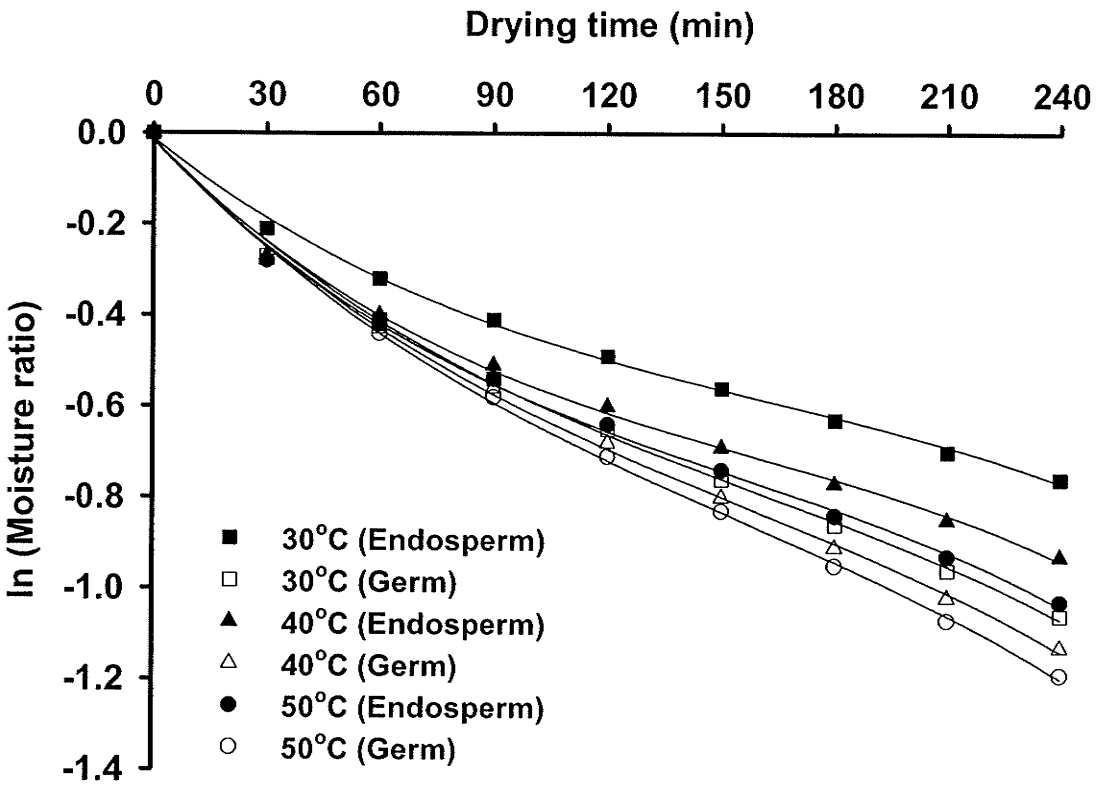

Figure H.3 Normalized drying curves of mechanically scarified kernel at different temperatures; normalization was done with respect to 30°C.

Table H.10c Model predicted data for deriving the scale factors needed for calculating activation energies of water removal process from germ-removed wheat kernel components (Fig. 6.21c) and for developing the normalized drying curves (Fig. H.4).

Wheat components	Drying time (min)	Drying temperature (°C)								
		30		40		50		30	40	50
Col. 1	Col. 2	Col. 3	Col. 4	Col. 5	Col. 6	Col. 7	Col. 8	Col. 9	Col. 10	Col. 11
		MR	ln (MR)	MR	ln (MR)	MR	ln (MR)	ln (MR) × Scale factor*§		
Endosperm	0	1.00	0.00	1.00	0.00	1.00	0.00	0.00	0.00	0.00
	30	0.76	-0.27	0.68	-0.38	0.58	-0.55	-0.27	-0.24	-0.23
	60	0.67	-0.40	0.56	-0.58	0.43	-0.85	-0.40	-0.36	-0.36
	90	0.61	-0.50	0.48	-0.74	0.33	-1.12	-0.50	-0.47	-0.48
	120	0.55	-0.59	0.41	-0.90	0.25	-1.38	-0.59	-0.56	-0.58
	150	0.51	-0.68	0.35	-1.04	0.20	-1.63	-0.68	-0.66	-0.69
	180	0.47	-0.77	0.31	-1.19	0.15	-1.88	-0.77	-0.75	-0.80
	210	0.43	-0.85	0.27	-1.33	0.12	-2.13	-0.85	-0.83	-0.90
	240	0.40	-0.92	0.23	-1.47	0.09	-2.38	-0.92	-0.92	-1.01

*Scale factors (Table 6.9) were calculated based on the following third-order polynomial regression curves:

$$\text{Endosperm}_{30^\circ C} : \ln(MR) = -8e-08 \cdot t^3 + 4e-05 \cdot t^2 - 0.0082 \cdot t - 0.0182 \quad \text{(H.31)}$$

$$\text{Endosperm}_{40^\circ C} : \ln(MR) = -1e-07 \cdot t^3 + 5e-05 \cdot t^2 - 0.0118 \cdot t - 0.025 \quad \text{(H.32)}$$

$$\text{Endosperm}_{50^\circ C} : \ln(MR) = -1e-07 \cdot t^3 + 6e-05 \cdot t^2 - 0.0167 \cdot t - 0.0332 \quad \text{(H.33)}$$

§Columns 2 vs. 4, 6, and 8 were plotted in Fig. 6.21c; and columns 2 vs. 9, 10, and 11 were plotted in Fig. H.4.

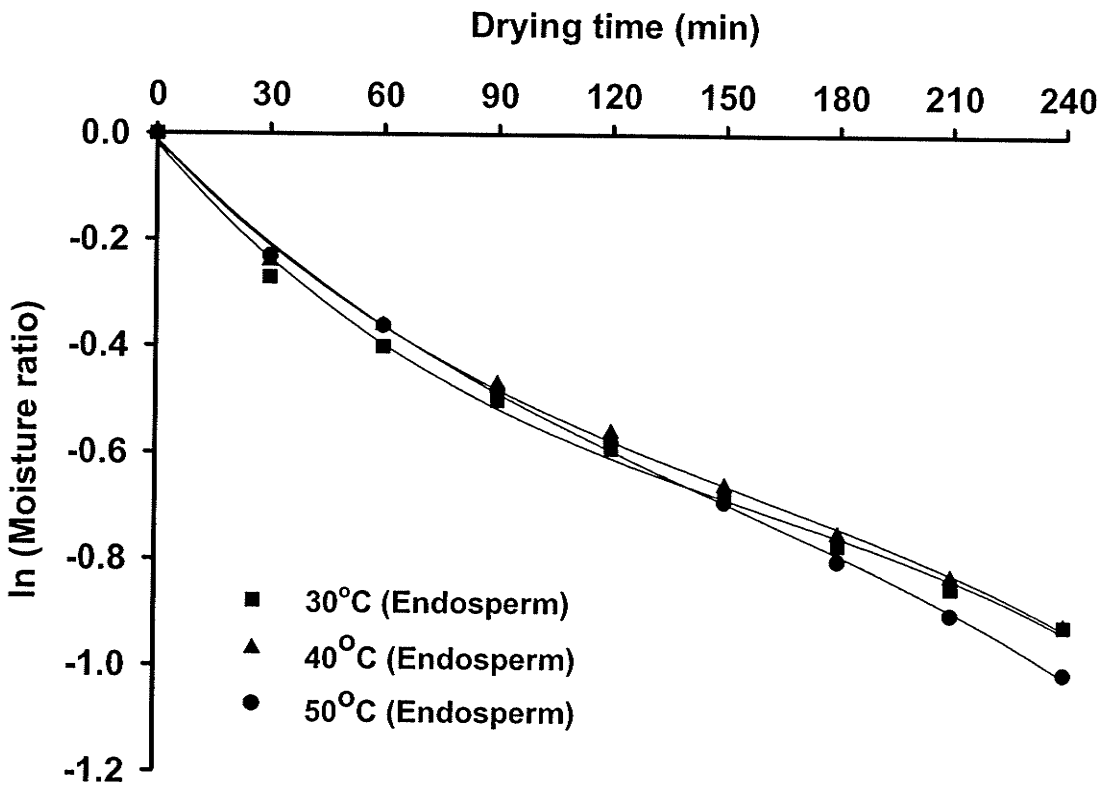

Figure H.4 Normalized drying curves of germ removed kernel at different temperatures; normalization was done with respect to 30°C.

Table H.11 Data for Fig. 6.23.

Physical kinds of wheat	Wheat components	Drying temp. (°C)	1/T (K^{-1})	Scale factor (k)	ln (k)
Col. 1	Col. 2	Col. 3	Col. 4	Col. 5	Col. 6
Intact	Endosperm	30	0.00330	1.000	0.000
		40	0.00319	0.695	-0.364
		50	0.00310	0.468	-0.759
	Germ	30	0.00330	1.000	0.000
		40	0.00319	0.828	-0.189
		50	0.00310	0.626	-0.468
Mechanically scarified	Endosperm	30	0.00330	1.000	0.000
		40	0.00319	0.742	-0.298
		50	0.00310	0.543	-0.611
	Germ	30	0.00330	1.000	0.000
		40	0.00319	0.838	-0.177
		50	0.00310	0.700	-0.357
Germ removed	Endosperm	30	0.00330	1.000	0.000
		40	0.00319	0.629	-0.464
		50	0.00310	0.425	-0.856

Figure 6.23 was plotted with columns 4 and 6. Linear regression was performed on the plotted data to obtain the activation energy from the slope of the following equations:

$$\text{Endosperm}_{\text{Intact}} : \ln(k) = 3712.6 \cdot \left(\frac{1}{T}\right) - 12.244 \quad \text{(H.34)}$$

$$\text{Endosperm}_{\text{Scarified}} : \ln(k) = 2986.4 \cdot \left(\frac{1}{T}\right) - 9.8508 \quad \text{(H.35)}$$

$$\text{Endosperm}_{\text{Germ-removed}} : \ln(k) = 4189.5 \cdot \left(\frac{1}{T}\right) - 13.834 \quad \text{(H.36)}$$

$$\text{Germ}_{\text{Intact}} : \ln(k) = 2286.6 \cdot \left(\frac{1}{T}\right) - 7.5295 \quad \text{(H.37)}$$

$$\text{Germ}_{\text{Scarified}} : \ln(k) = 1744.6 \cdot \left(\frac{1}{T}\right) - 5.7554 \quad \text{(H.38)}$$

Table H.12a Magnetic resonance imaging data for deriving the scale factors needed for calculating activation energies of water removal process from intact wheat kernel components (Fig. H.5a) and for developing the normalized drying curves (Fig. H.5b).

Wheat components	Drying time (min)	Drying temperature (°C)								
		30		40		50		30	40	50
Col. 1	Col. 2	Col. 3	Col. 4	Col. 5	Col. 6	Col. 7	Col. 8	Col. 9	Col. 10	Col. 11
		I/I_o	$\ln(I/I_o)$	I/I_o	$\ln(I/I_o)$	I/I_o	$\ln(I/I_o)$	$\ln(I/I_o) \times$ Scale factor*§		
Endosperm	0	1.00	0.00	1.00	0.00	1.00	0.00	0.00	0.00	0.00
	30	0.98	-0.02	0.84	-0.17	0.65	-0.43	-0.02	-0.04	-0.03
	60	0.86	-0.15	0.69	-0.37	0.41	-0.89	-0.15	-0.09	-0.06
	90	0.78	-0.25	0.50	-0.69	0.25	-1.39	-0.25	-0.16	-0.10
	120	0.63	-0.46	0.33	-1.11	0.16	-1.83	-0.46	-0.26	-0.13
	150	0.51	-0.67	0.24	-1.43	0.12	-2.12	-0.67	-0.34	-0.15
	180	0.40	-0.92	0.17	-1.77	0.09	-2.41	-0.92	-0.42	-0.17
	210	0.32	-1.14	0.13	-2.04	0.08	-2.53	-1.14	-0.48	-0.18
	240	0.26	-1.35	0.12	-2.12	0.08	-2.53	-1.35	-0.50	-0.18
Germ	0	1.00	0.00	1.00	0.00	1.00	0.00	0.00	0.00	0.00
	30	1.00	0.00	0.71	-0.34	0.63	-0.46	0.00	-0.05	-0.05
	60	0.88	-0.13	0.51	-0.67	0.46	-0.78	-0.13	-0.09	-0.08
	90	0.76	-0.27	0.48	-0.73	0.4	-0.92	-0.27	-0.10	-0.09
	120	0.70	-0.36	0.42	-0.87	0.36	-1.02	-0.36	-0.12	-0.10
	150	0.65	-0.43	0.43	-0.84	0.38	-0.97	-0.43	-0.12	-0.09
	180	0.59	-0.53	0.39	-0.94	0.41	-0.89	-0.53	-0.13	-0.09
	210	0.57	-0.56	0.38	-0.97	0.39	-0.94	-0.56	-0.13	-0.09
	240	0.51	-0.67	0.41	-0.89	0.38	-0.97	-0.67	-0.12	-0.09

*Scale factors (Table 6.9) were calculated based on the following third-order polynomial regression curves:

$$\text{Endosperm}_{30^\circ C}: \ln(I/I_o) = 9e-08 \cdot t^3 - 5e-05 \cdot t^2 + 0.0004 \cdot t - 0.014 \quad \text{(H.39)}$$

$$\text{Endosperm}_{40^\circ C}: \ln(I/I_o) = 3e-07 \cdot t^3 - 9e-05 \cdot t^2 - 0.0016 \cdot t - 0.0151 \quad \text{(H.40)}$$

$$\text{Endosperm}_{50^\circ C}: \ln(I/I_o) = 2e-07 \cdot t^3 - 3e-05 \cdot t^2 - 0.0145 \cdot t + 0.0107 \quad \text{(H.41)}$$

$$\text{Germ}_{30^\circ C}: \ln(I/I_o) = 3e-08 \cdot t^3 - 1e-05 \cdot t^2 - 0.0023 \cdot t + 0.0278 \quad \text{(H.42)}$$

$$\text{Germ}_{40^\circ C}: \ln(I/I_o) = -1e-07 \cdot t^3 + 7e-05 \cdot t^2 - 0.0137 \cdot t - 0.0067 \quad \text{(H.43)}$$

$$\text{Germ}_{50^\circ C}: \ln(I/I_o) = -3e-07 \cdot t^3 + 0.0001 \cdot t^2 - 0.0198 \cdot t + 0.0092 \quad \text{(H.44)}$$

§Columns 2 vs. 4, 6, and 8 were plotted in Fig. H.5a; and columns 2 vs. 9, 10, and 11 were plotted in Fig. H.5b.

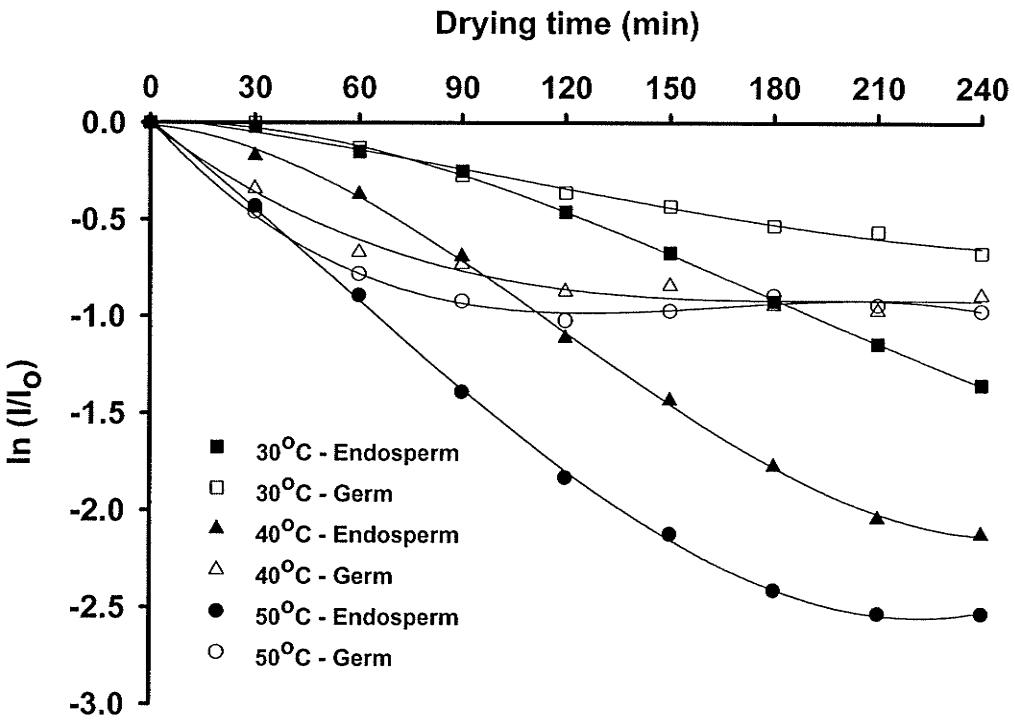

Figure H.5a Magnetic resonance imaging derived drying curves of the intact kernel components at different temperatures.

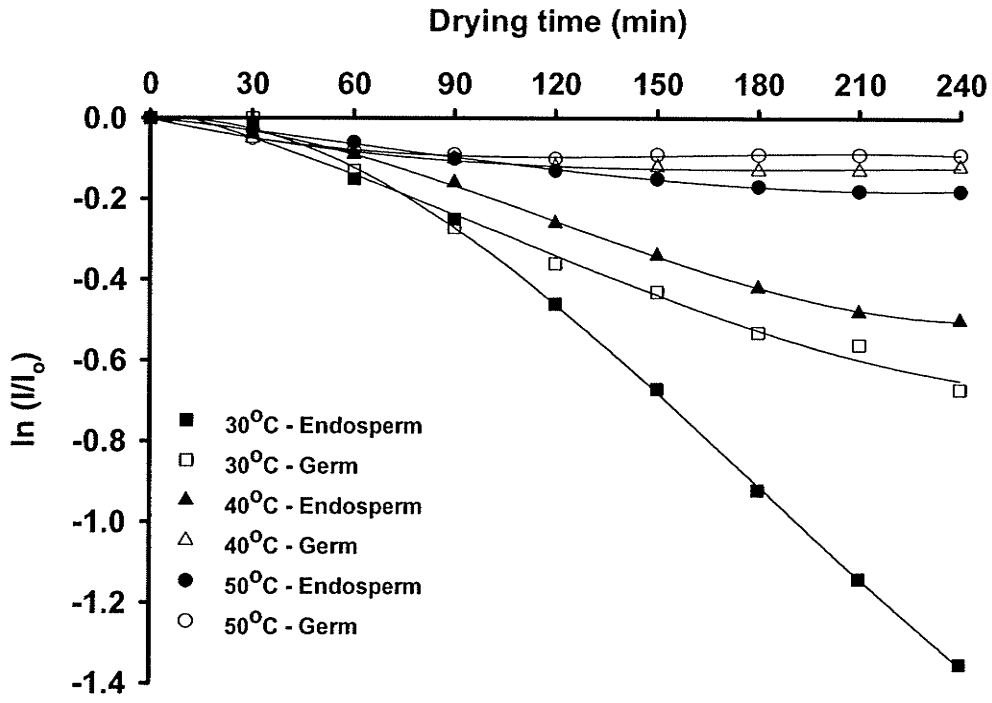

Figure H.5b Magnetic resonance imaging derived normalized drying curves of the intact kernel components at different temperatures; normalization was done with respect to 30°C.

Table H.12b Magnetic resonance imaging data for deriving the scale factors needed for calculating activation energies of water removal process from mechanically scarified wheat kernel components (Fig. H.5c) and for developing the normalized drying curves (Fig. H.5d).

Wheat components	Drying time (min)	Drying temperature (°C)								
		30		40		50		30	40	50
Col. 1	Col. 2	Col. 3	Col. 4	Col. 5	Col. 6	Col. 7	Col. 8	Col. 9	Col. 10	Col. 11
		I/I_o	$\ln(I/I_o)$	I/I_o	$\ln(I/I_o)$	I/I_o	$\ln(I/I_o)$	$\ln(I/I_o) \times$ Scale factor*§		
Endosperm	0	1.00	0.00	1.00	0.00	1.00	0.00	0.00	0.00	0.00
	30	0.81	-0.21	0.92	-0.09	0.64	-0.45	-0.21	-0.11	-0.17
	60	0.73	-0.32	0.63	-0.46	0.41	-0.88	-0.32	-0.59	-0.34
	90	0.61	-0.50	0.35	-1.04	0.24	-1.43	-0.50	-1.33	-0.55
	120	0.50	-0.69	0.20	-1.59	0.15	-1.90	-0.69	-2.05	-0.74
	150	0.41	-0.88	0.15	-1.87	0.09	-2.39	-0.88	-2.41	-0.93
	180	0.34	-1.07	0.11	-2.21	0.07	-2.66	-1.07	-2.85	-1.03
	210	0.27	-1.32	0.09	-2.43	0.04	-3.14	-1.32	-3.12	-1.22
	240	0.22	-1.50	0.09	-2.39	0.04	-3.28	-1.50	-3.08	-1.27
Germ	0	1.00	0.00	1.00	0.00	1.00	0.00	0.00	0.00	0.00
	30	0.79	-0.23	0.67	-0.40	0.59	-0.53	-0.23	-0.20	-0.16
	60	0.74	-0.30	0.50	-0.69	0.32	-1.14	-0.30	-0.34	-0.35
	90	0.53	-0.63	0.41	-0.88	0.24	-1.43	-0.63	-0.43	-0.44
	120	0.43	-0.84	0.34	-1.08	0.24	-1.45	-0.84	-0.52	-0.45
	150	0.35	-1.05	0.36	-1.02	0.22	-1.52	-1.05	-0.50	-0.47
	180	0.37	-0.99	0.32	-1.13	0.24	-1.44	-0.99	-0.55	-0.44
	210	0.32	-1.13	0.27	-1.32	0.23	-1.46	-1.13	-0.64	-0.45
	240	0.32	-1.13	0.30	-1.20	0.22	-1.51	-1.13	-0.58	-0.47

*Scale factors (Table 6.9) were calculated based on the following third-order polynomial regression curves:

$$\text{Endosperm}_{30^\circ C}: \ln(I/I_o) = 3e-10 \cdot t^3 - 5e-06 \cdot t^2 + 0.005 \cdot t - 0.0156 \quad \text{(H.45)}$$

$$\text{Endosperm}_{40^\circ C}: \ln(I/I_o) = 4e-07 \cdot t^3 - 0.0001 \cdot t^2 - 0.0034 \cdot t - 0.0489 \quad \text{(H.46)}$$

$$\text{Endosperm}_{50^\circ C}: \ln(I/I_o) = 1e-07 \cdot t^3 - 4e-05 \cdot t^2 - 0.0135 \cdot t + 0.0005 \quad \text{(H.47)}$$

$$\text{Germ}_{30^\circ C}: \ln(I/I_o) = 1e-07 \cdot t^3 - 2e-05 \cdot t^2 - 0.0059 \cdot t + 0.0017 \quad \text{(H.48)}$$

$$\text{Germ}_{40^\circ C}: \ln(I/I_o) = -1e-07 \cdot t^3 + 7e-05 \cdot t^2 - 0.0148 \cdot t - 0.0084 \quad \text{(H.49)}$$

$$\text{Germ}_{50^\circ C}: \ln(I/I_o) = -3e-07 \cdot t^3 + 0.0002 \cdot t^2 - 0.028 \cdot t + 0.0507 \quad \text{(H.50)}$$

§Columns 2 vs. 4, 6, and 8 were plotted in Fig. H.5c; and columns 2 vs. 9, 10, and 11 were plotted in Fig. H.5d.

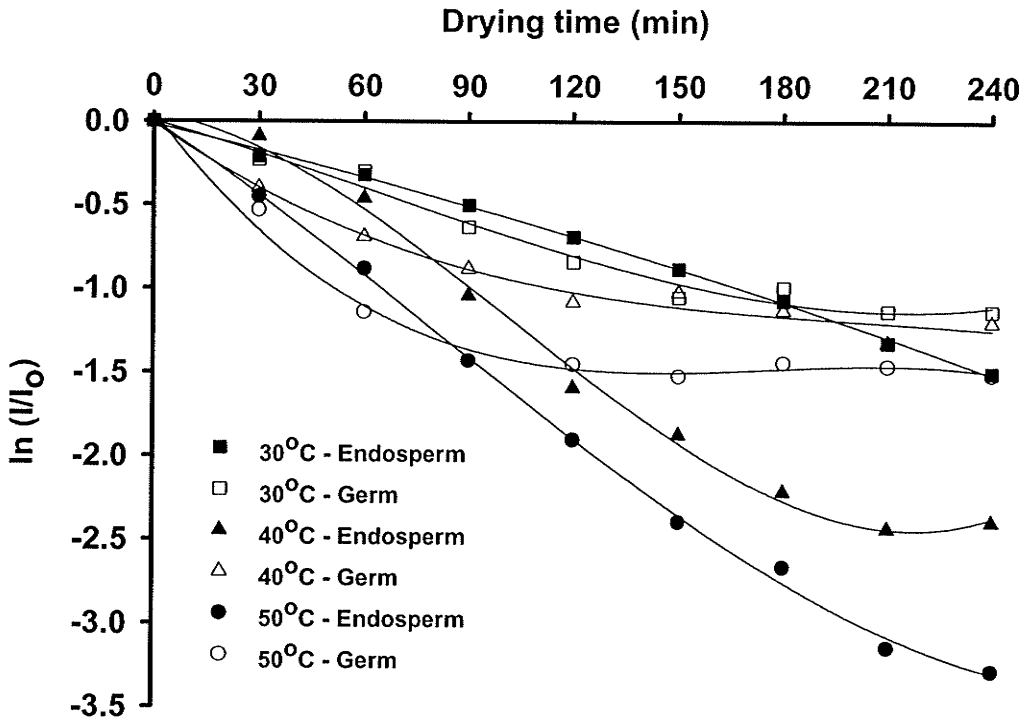

Figure H.5c Magnetic resonance imaging derived drying curves of the mechanically scarified kernel components at different temperatures.

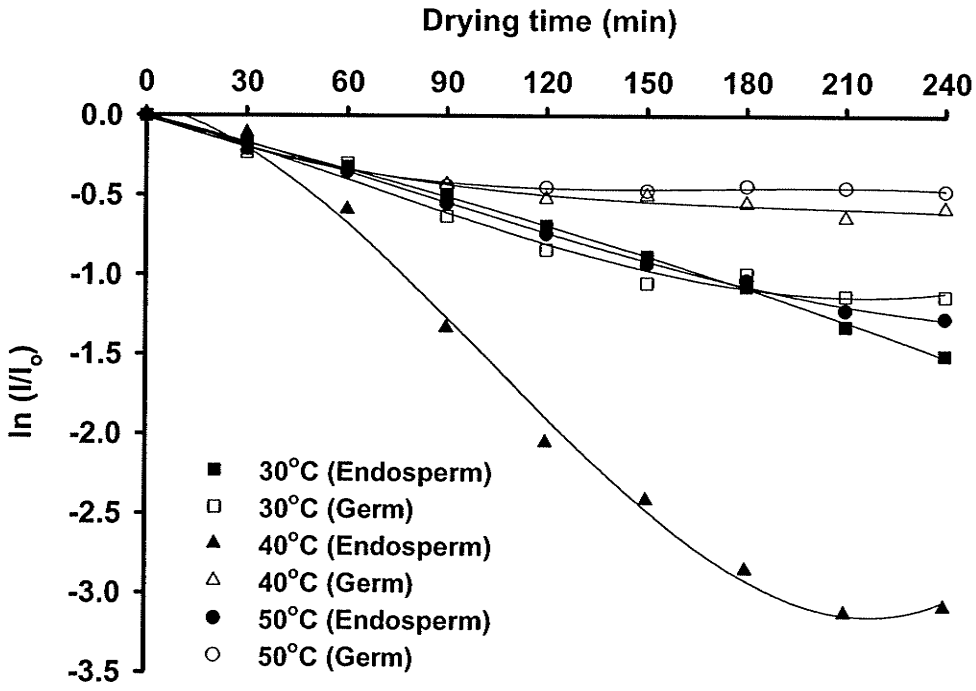

Figure H.5d Magnetic resonance imaging derived normalized drying curves of the mechanically scarified kernel components at different temperatures; normalization was done with respect to 30°C.

Table H.12c Magnetic resonance imaging data for deriving the scale factors needed for calculating activation energies of water removal process from germ-removed wheat kernel components (Fig. H.5e) and for developing the normalized drying curves (Fig. H.5f).

Wheat components	Drying time (min)	Drying temperature (°C)								
		30		40		50		30	40	50
Col. 1	Col. 2	Col. 3	Col. 4	Col. 5	Col. 6	Col. 7	Col. 8	Col. 9	Col. 10	Col. 11
		I/I_o	$\ln(I/I_o)$	I/I_o	$\ln(I/I_o)$	I/I_o	$\ln(I/I_o)$	$\ln(I/I_o) \times$ Scale factor*§		
Endosperm	0	1.00	0.00	1.00	0.00	1.00	0.00	0.00	0.00	0.00
	30	0.90	-0.11	0.83	-0.19	0.59	-0.53	-0.11	-0.11	-0.09
	60	0.80	-0.22	0.60	-0.51	0.28	-1.27	-0.22	-0.29	-0.22
	90	0.65	-0.43	0.37	-1.00	0.15	-1.87	-0.43	-0.57	-0.32
	120	0.57	-0.57	0.27	-1.30	0.09	-2.36	-0.57	-0.74	-0.40
	150	0.46	-0.77	0.16	-1.82	0.07	-2.72	-0.77	-1.04	-0.46
	180	0.39	-0.94	0.12	-2.08	0.04	-3.17	-0.94	-1.19	-0.54
	210	0.34	-1.08	0.08	-2.49	0.05	-3.01	-1.08	-1.42	-0.51
	240	0.30	-1.21	0.08	-2.58	0.04	-3.11	-1.21	-1.47	-0.53

*Scale factors (Table 6.9) were calculated based on the following third-order polynomial regression curves:

$$\text{Endosperm}_{30^\circ C}: \ln(I/I_o) = 7e-08 \cdot t^3 - 3e-05 \cdot t^2 + 0.0026 \cdot t - 0.0002 \quad \text{(H.51)}$$

$$\text{Endosperm}_{40^\circ C}: \ln(I/I_o) = 2e-07 \cdot t^3 - 8e-05 \cdot t^2 - 0.0049 \cdot t - 0.0099 \quad \text{(H.52)}$$

$$\text{Endosperm}_{50^\circ C}: \ln(I/I_o) = 2e-07 \cdot t^3 - 1e-05 \cdot t^2 - 0.0214 \cdot t + 0.0367 \quad \text{(H.53)}$$

§Columns 2 vs. 4, 6, and 8 were plotted in Fig. H.5e; and columns 2 vs. 9, 10, and 11 were plotted in Fig. H.5f.

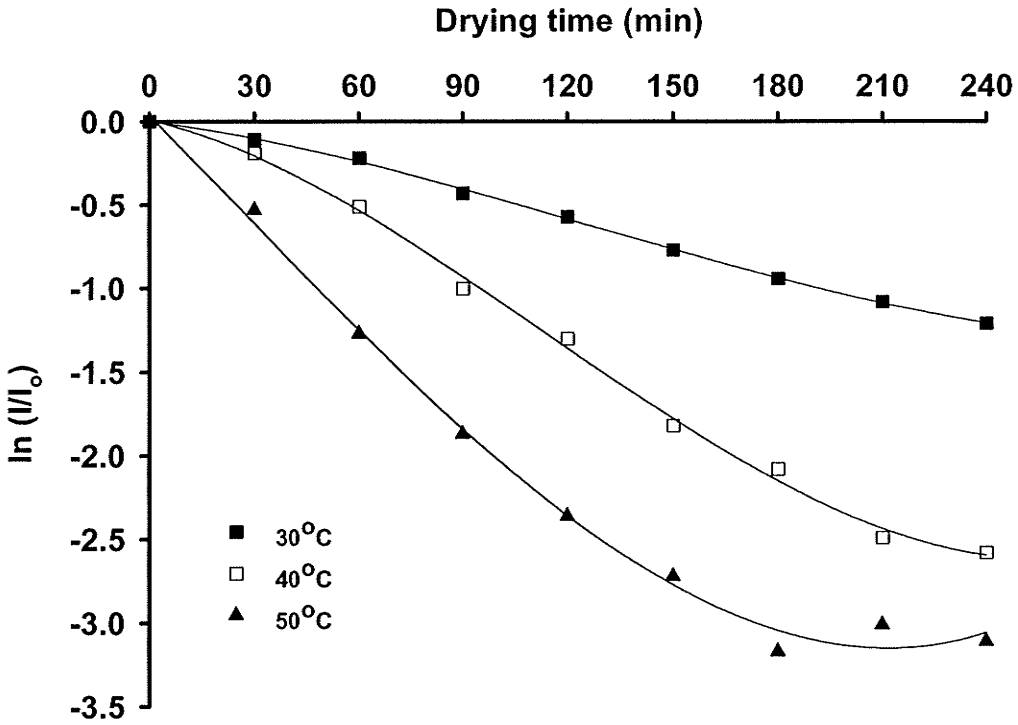

Figure H.5e Magnetic resonance imaging derived drying curves of the germ-removed kernel components at different temperatures.

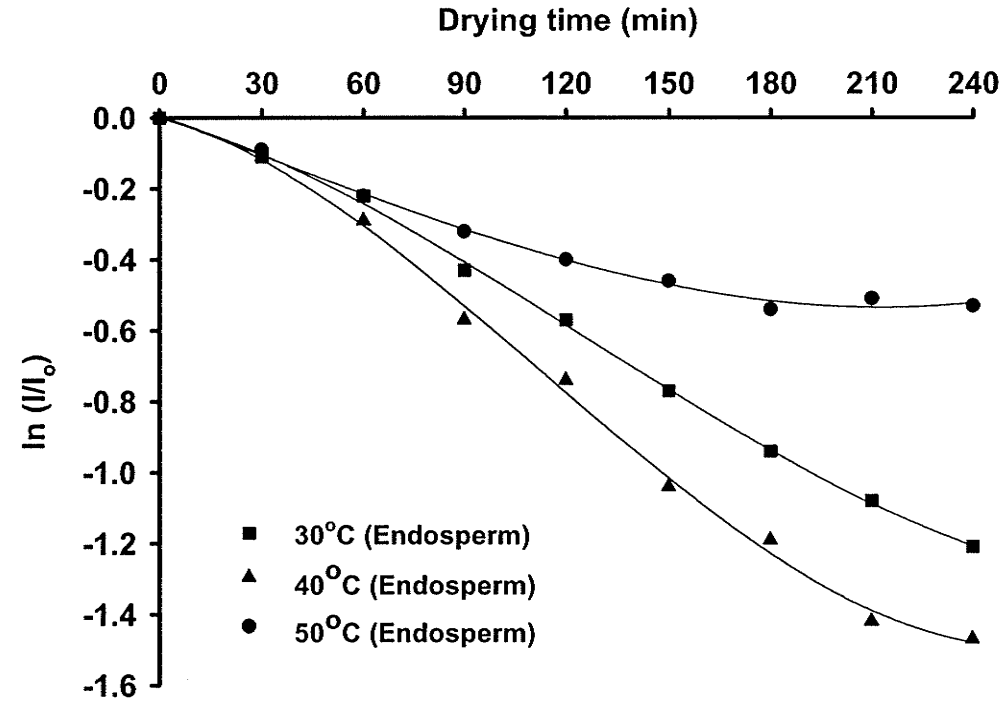

Figure H.5f Magnetic resonance imaging derived normalized drying curves of the germ-removed kernel components at different temperatures; normalization was done with respect to 30°C.

Table H.13 Data for Fig. 6.24.

Physical kinds of wheat	Wheat components	Drying temp. (°C)	1/T (K^{-1})	Scale factor (k)	ln (k)
Col. 1	Col. 2	Col. 3	Col. 4	Col. 5	Col. 6
Intact	Endosperm	30	0.00330	1.000	0.00
		40	0.00319	0.235	-1.45
		50	0.00310	0.072	-2.63
	Germ	30	0.00330	1.000	0.00
		40	0.00319	0.138	-1.98
		50	0.00310	0.098	-2.32
Mechanically scarified	Endosperm	30	0.00330	1.000	0.00
		40	0.00319	1.286	0.25
		50	0.00310	0.388	-0.95
	Germ	30	0.00330	1.000	0.00
		40	0.00319	0.486	-0.72
		50	0.00310	0.309	-1.17
Germ removed	Endosperm	30	0.00330	1.000	0.00
		40	0.00319	0.570	-0.56
		50	0.00310	0.170	-1.77

Figure 6.24 was plotted with columns 4 and 6. Linear regression was performed on the plotted data to obtain the activation energy from the slope of the following equations except for the data for endosperm of mechanically scarified kernel due to high non-linearity:

$$\text{Endosperm}_{\text{Intact}} : \ln(k) = 13151 \cdot \left(\frac{1}{T}\right) - 43.4 \tag{H.54}$$

$$\text{Endosperm}_{\text{Germ-removed}} : \ln(k) = 8712.6 \cdot \left(\frac{1}{T}\right) - 28.628 \tag{H.55}$$

$$\text{Germ}_{\text{Intact}} : \ln(k) = 11834 \cdot \left(\frac{1}{T}\right) - 39.26 \tag{H.56}$$

$$\text{Germ}_{\text{Scarified}} : \ln(k) = 5875.4 \cdot \left(\frac{1}{T}\right) - 19.412 \tag{H.57}$$

A strong correlation of the water removal process to the drying temperature was observed in case of the endosperm of an intact kernel, mechanically scarified kernel and an

embryo-removed kernel. However, for the endosperm the activation energy of the water removal process was the highest in an intact kernel (activation energy of 109 kJ mol^{-1}) compared to a germ-removed kernel and a mechanically scarified kernel, respectively. In case of the scarified kernel, the pericarp started offering a water resistance due to closely adhered thick-walled cells after initial stages of drying. Therefore, the moisture removal from this part became slower. However, the rate of decrease of factor k was slower after 40°C for the germ in both the intact and mechanically scarified kernels, which indicated that the drying did not depend on temperatures above 40°C (Ghosh et al. 2006b in Chapter 6). Furthermore, the activation energy of the water removal process in the germ was higher in an intact kernel than that in a scarified kernel (activation energy 49 kJ mol^{-1}). Since water was released relatively faster from the scarified regions of the endosperm-pericarp boundary at the initial stages of drying, less "free" water was available in the germ in the case of the scarified kernels.

Table H.14 Transient moisture content data used for the sensitivity analysis in Table 6.10.

Drying time (min)	Present model derived moisture content , % d.b.																	Jayas and Sokhansanj (1986)	Sinico et al. (1995)
	Original parameters	Moisture content data for percentage change in parameter values																	
		$M_o$layer -75 (M_{oE})	$M_o$layer -25 (M_{oE})	h_t +25	h_t -25	h_m +25	h_m -25	K +25	K -25	C_g +25	C_g -25	ρ_g +25	ρ_g -25	D_G +25	D_G -25	D_E +25	D_E -25		
0	19.83	19.78	19.89	19.83	19.83	19.83	19.83	19.83	19.83	19.83	19.83	19.83	19.83	19.83	19.83	19.83	19.83	20.45	20.45
30	17.26	17.24	17.26	17.26	17.26	17.25	17.24	17.26	17.26	17.26	17.26	17.26	17.26	17.05	17.49	17.14	17.41	18.05	18.21
60	16.16	16.16	16.16	16.16	16.16	16.16	16.16	16.16	16.16	16.16	16.16	16.16	16.16	15.89	16.47	16.01	16.34	16.23	17.12
90	15.37	15.38	15.37	15.37	15.37	15.38	15.38	15.37	15.37	15.37	15.37	15.37	15.37	15.07	15.74	15.21	15.58	14.85	16.33
120	14.75	14.76	14.75	14.75	14.75	14.76	14.76	14.75	14.75	14.75	14.75	14.75	14.75	14.43	15.16	14.57	14.97	13.80	15.70
150	14.24	14.25	14.24	14.24	14.24	14.24	14.24	14.24	14.24	14.24	14.24	14.24	14.24	13.89	14.67	14.05	14.47	13.01	15.19
180	13.8	13.81	13.8	13.8	13.8	13.8	13.81	13.8	13.8	13.8	13.8	13.8	13.8	13.45	14.25	13.61	14.05	12.40	14.76
210	13.43	13.44	13.43	13.43	13.43	13.43	13.43	13.43	13.43	13.43	13.43	13.43	13.43	13.08	13.89	13.23	13.68	11.95	14.39
240	13.1	13.11	13.1	13.1	13.1	13.1	13.1	13.1	13.1	13.1	13.1	13.1	13.1	12.76	13.56	12.9	13.35	11.60	14.07

Table H.14a Transient moisture content data used for the sensitivity analysis for intact wheat kernels during drying at 30°C in Table 6.11a.

Wheat components	Drying time (min)	Present model derived moisture content , % d.b.							
		Original parameters	Moisture content data for percentage change in D_E				Moisture content data for percentage change in D_G		
			+25	+100	+150	+200	+25	-25	-50
Endosperm	0	40.79	40.79	40.79	40.79	40.79	40.79	40.79	40.79
	30	33.60	32.74	30.73	29.63	28.66	33.60	33.54	33.54
	60	30.79	29.69	27.01	25.55	24.33	30.79	30.73	30.73
	90	28.72	27.38	24.33	22.68	21.22	28.72	28.66	28.66
	120	27.01	25.61	22.13	20.36	18.72	27.07	27.01	27.01
	150	25.61	24.02	20.36	18.41	16.71	25.61	25.61	25.61
	180	24.33	22.68	18.78	16.77	15.06	24.33	24.33	24.33
	210	23.23	21.46	17.38	15.30	13.60	23.23	23.23	23.23
	240	22.19	20.36	16.16	14.02	12.25	22.19	22.19	22.19
Germ	0	155.43	155.43	155.43	155.43	155.43	155.43	155.43	155.43
	30	113.95	113.18	111.63	111.24	110.85	109.69	118.99	124.81
	60	96.12	95.35	93.80	93.41	93.02	90.31	103.1	111.63
	90	83.33	82.17	81.01	80.62	80.23	76.74	91.47	101.94
	120	73.25	72.09	70.93	70.54	70.15	65.50	82.17	93.80
	150	64.73	63.56	62.40	62.01	61.63	59.59	74.42	87.21
	180	57.36	56.59	55.04	54.65	54.65	49.22	67.44	81.01
	210	51.16	50.39	48.84	48.45	48.45	42.63	61.63	75.58
	240	45.74	44.96	43.80	43.41	43.02	37.40	56.20	70.93

Table H.14b Transient moisture content data used for the sensitivity analysis for intact wheat kernels during drying at 40°C in Table 6.11a.

Wheat components	Drying time (min)	Present model derived moisture content , % d.b.							
		Original parameters	Moisture content data for percentage change in D_E				Moisture content data for percentage change in D_G		
			+25	+100	+150	+200	+25	-25	-50
Endosperm	0	40.79	40.79	40.79	40.79	40.79	40.79	40.79	40.79
	30	30.97	29.88	27.26	25.85	24.63	30.97	30.91	30.91
	60	27.26	25.91	22.50	20.67	19.15	27.32	27.26	27.26
	90	24.63	22.99	19.15	17.13	15.43	24.63	24.63	24.63
	120	22.5	20.67	16.52	14.45	12.74	22.50	22.50	22.50
	150	20.73	18.78	14.45	12.32	10.55	20.73	20.73	20.73
	180	19.15	17.13	12.68	10.55	8.84	19.15	19.15	19.15
	210	17.80	15.73	11.22	9.15	7.50	17.80	17.80	17.80
	240	16.58	14.45	9.94	7.93	6.40	16.58	16.58	16.58
Germ	0	150.39	150.39	150.39	150.39	150.39	150.39	150.39	150.39
	30	102.32	101.94	100.77	100.39	100.00	97.67	108.14	115.5
	60	82.94	82.56	81.39	81.01	80.62	76.36	90.70	100.77
	90	69.38	68.6	67.44	67.44	67.05	61.63	78.29	89.92
	120	58.53	57.75	56.98	56.98	56.59	50.39	68.6	81.39
	150	50.00	49.22	48.45	48.06	48.06	41.47	60.08	74.03
	180	42.63	42.25	41.47	41.08	41.08	34.61	53.10	67.83
	210	36.74	36.28	35.54	35.35	35.12	28.87	47.29	62.01
	240	31.70	31.28	30.58	30.39	30.15	24.19	42.25	59.98

Table H.14c Transient moisture content data used for the sensitivity analysis for intact wheat kernels during drying at 50°C in Table 6.11a.

Wheat components	Drying time (min)	Present model derived moisture content , % d.b.							
		Original parameters	Moisture content data for percentage change in D_E				Moisture content data for percentage change in D_G		
			+25	+100	+150	+200	+25	-25	-50
Endosperm	0	41.77	41.77	41.77	41.77	41.77	41.77	41.77	41.77
	30	28.41	27.07	23.66	21.89	20.30	28.47	28.41	28.41
	60	23.72	21.89	17.68	15.55	13.84	23.72	23.72	23.66
	90	20.30	18.35	13.78	11.58	9.82	2.30	20.30	20.30
	120	17.68	15.61	10.97	8.84	7.26	17.74	17.68	17.68
	150	15.61	13.41	8.84	6.89	5.54	15.61	15.61	15.61
	180	13.78	11.58	7.26	5.52	4.39	13.78	13.78	13.78
	210	12.32	10.12	6.03	4.53	3.61	12.32	12.32	12.32
	240	10.97	8.84	5.10	3.82	3.08	10.97	10.97	10.97
Germ	0	170.15	170.15	170.15	170.15	170.15	170.15	170.15	170.15
	30	106.59	106.20	105.43	105.04	104.65	100.00	114.34	123.64
	60	82.17	81.78	81.01	80.62	80.62	74.03	92.63	105.43
	90	65.50	65.12	64.34	63.95	63.95	56.2	76.74	91.47
	120	52.71	52.71	51.94	51.55	51.55	43.41	64.73	81.01
	150	43.02	42.663	42.25	41.86	41.86	33.95	55.04	72.09
	180	35.31	34.96	34.42	34.26	34.19	26.74	47.29	64.34
	210	29.07	28.72	28.29	28.10	28.02	21.20	40.70	57.75
	240	24.03	23.72	23.33	23.18	23.10	16.90	34.92	51.94

Table H.15a Transient moisture content data used for the sensitivity analysis for mechanically scarified wheat kernels during drying at 30°C in Table 6.11b.

Wheat components	Drying time (min)	Present model derived moisture content , % d.b.							
		Original parameters	Moisture content data for percentage change in D_E				Moisture content data for percentage change in D_G		
			+25	+100	+150	+200	+25	-25	-50
Endosperm	0	31.89	31.89	31.89	31.89	31.89	31.89	31.89	31.89
	30	25.20	24.39	22.57	21.55	20.67	25.20	25.20	25.13
	60	22.57	21.55	19.19	17.90	16.76	22.63	22.57	22.57
	90	20.74	19.53	16.82	15.4	14.19	20.74	20.67	20.67
	120	19.19	17.90	15.00	13.44	12.23	19.19	19.19	19.19
	150	17.90	16.55	13.51	11.96	10.74	17.97	17.90	17.90
	180	16.82	15.40	12.23	10.67	9.46	16.82	16.82	16.82
	210	15.88	14.39	11.15	9.66	8.38	15.88	15.88	15.88
	240	15.00	13.51	10.27	8.72	7.50	15.00	15.00	15.00
Germ	0	167.86	167.86	167.86	167.86	167.86	167.86	167.86	167.86
	30	128.57	127.92	126.3	125.97	125.32	124.67	133.44	139.28
	60	111.36	110.39	108.77	108.12	107.79	105.84	118.18	126.3
	90	98.70	97.73	96.10	95.45	95.13	91.88	106.82	116.56
	120	88.31	87.34	85.71	85.39	84.74	80.84	97.08	108.77
	150	79.54	78.57	76.95	76.62	76.30	71.43	89.28	101.95
	180	72.08	71.10	69.48	69.15	68.83	63.31	82.47	96.10
	210	65.26	64.28	62.99	62.34	62.01	56.49	76.30	90.58
	240	59.41	58.44	57.14	56.49	56.17	50.32	70.78	85.71

Table H.15b Transient moisture content data used for the sensitivity analysis for mechanically scarified wheat kernels during drying at 40°C in Table 6.11b.

Wheat components	Drying time (min)	Present model derived moisture content , % d.b.							
		Original parameters	Moisture content data for percentage change in D_E				Moisture content data for percentage change in D_G		
			+25	+100	+150	+200	+25	-25	-50
Endosperm	0	39.8	39.80	39.80	39.80	39.80	39.80	39.80	39.80
	30	28.31	27.03	23.99	22.43	21.08	28.31	28.24	28.24
	60	24.05	22.50	18.78	16.96	15.34	24.05	24.05	23.99
	90	21.15	19.32	15.34	13.38	11.76	21.15	21.15	21.08
	120	18.85	16.96	12.84	10.88	9.32	18.85	18.85	18.85
	150	16.96	15.00	10.88	8.99	7.50	16.96	16.96	16.96
	180	15.34	13.44	9.32	7.57	6.20	15.34	15.34	15.34
	210	13.99	12.09	8.11	6.41	5.21	13.99	13.99	13.99
	240	12.84	10.88	7.03	5.51	4.44	12.84	12.84	12.84
Germ	0	207.47	207.47	207.47	207.47	207.47	207.47	207.47	207.47
	30	149.02	148.05	146.43	146.1	145.78	142.86	156.17	164.93
	60	124.35	123.38	122.08	121.75	121.43	116.23	134.41	146.43
	90	106.82	105.84	104.22	103.9	103.57	97.08	118.51	133.12
	120	92.86	91.88	90.26	89.93	89.61	82.14	105.84	122.08
	150	80.84	80.19	78.90	78.25	77.92	69.8	94.8	112.66
	180	71.7	70.13	68.83	68.51	68.18	59.41	85.39	104.54
	210	62.34	61.69	60.39	60.06	59.74	50.97	77.27	97.08
	240	55.19	54.54	53.25	52.92	52.60	43.83	70.13	90.58

Table H.15c Transient moisture content data used for the sensitivity analysis for mechanically scarified wheat kernels during drying at 50°C in Table 6.11b.

Wheat components	Drying time (min)	Present model derived moisture content , % d.b.							
		Original parameters	Moisture content data for percentage change in D_E				Moisture content data for percentage change in D_G		
			+25	+100	+150	+200	+25	-25	-50
Endosperm	0	39.79	39.79	39.79	39.79	39.79	39.79	39.79	39.79
	30	24.59	30.27	25.40	22.97	20.88	32.30	32.30	32.23
	60	19.53	22.9	17.43	14.86	12.77	25.4	25.4	25.4
	90	16.08	18.24	12.77	10.34	8.44	20.88	20.88	20.81
	120	13.58	14.93	9.66	7.43	5.91	17.57	17.5	17.43
	150	11.62	12.36	7.43	5.51	4.39	14.93	14.93	14.86
	180	10.07	10.34	5.86	4.29	3.46	12.77	12.77	12.77
	210	8.78	8.72	4.75	3.50	2.90	11.08	11.08	11.08
	240	7.70	7.43	3.97	2.99	2.55	9.59	9.59	9.59
Germ	0	207.47	207.47	207.47	207.47	207.47	207.47	207.47	207.47
	30	138.64	124.35	123.38	123.05	122.73	118.51	132.47	141.56
	60	111.36	99.67	98.7	98.38	98.05	91.56	110.39	123.38
	90	91.88	82.14	81.17	80.84	80.84	73.05	94.48	109.74
	120	76.62	68.83	67.86	67.53	67.21	59.09	82.14	98.70
	150	64.61	57.79	56.82	56.49	56.49	48.05	71.75	89.28
	180	54.54	48.7	48.05	47.72	47.72	38.96	62.66	81.17
	210	46.43	41.23	40.58	40.26	40.26	32.01	55.19	74.35
	240	39.28	35.06	34.41	34.09	34.09	26.30	48.70	67.86

Table H.16 Transient moisture content data used for the sensitivity analysis for germ-removed wheat kernels in Table 6.11c.

Drying Temperature (°C)	Drying time (min)	Present model derived moisture content , % d.b.				
		Original parameters	Moisture content data for percentage change in D_E			
			+25	+100	+150	+200
30	0	50.00	50.00	50.00	50.00	50.00
	30	38.71	37.39	34.32	32.56	31.14
	60	34.32	32.56	28.51	26.31	24.34
	90	31.14	29.06	24.34	21.82	19.63
	120	28.51	26.31	20.94	18.31	16.12
	150	26.21	23.90	18.31	15.57	13.38
	180	24.34	21.82	16.01	13.27	11.07
	210	22.59	19.96	14.14	11.40	9.37
	240	21.05	18.31	12.50	9.88	7.96
40	0	50.99	50.99	50.99	50.99	50.99
	30	35.31	33.66	29.38	27.19	25.33
	60	29.49	27.19	21.93	19.19	16.88
	90	25.33	22.70	16.88	14.03	11.73
	120	21.93	19.19	13.27	10.57	8.42
	150	19.30	16.34	10.60	8.09	6.26
	180	16.99	14.03	8.55	6.35	4.86
	210	15.02	12.17	7.01	5.11	3.91
	240	13.27	10.57	5.82	4.23	3.28
50	0	50.99	50.99	50.99	50.99	50.99
	30	30.37	28.07	22.92	20.28	17.98
	60	22.92	20.17	14.36	11.51	9.41
	90	17.98	15.13	9.47	7.03	5.43
	120	14.36	11.62	6.56	4.68	3.62
	150	11.62	8.99	4.8	3.47	2.81
	180	9.47	7.13	3.73	2.82	2.41
	210	7.83	5.77	3.06	2.43	2.18
	240	6.55	4.77	2.65	2.21	2.06